Structural and Functional Studies on AcrB, a Bacterial Multidrug Efflux Pump and Homologue of Niemann-Pick C1 Protein

Dissertation

zur

Erlangung der naturwissenschaftlichen Doktorwürde
(Dr. sc. nat.)

vorgelegt der

Mathematisch-naturwissenschaftlichen Fakultät

der

Universität Zürich

von

Thomas Eicher

von

Goldingen SG

Promotionskomitee

Prof. Dr. François Verrey
Prof. Dr. Klaas Martinus Pos
Prof. Dr. Raimund Dutzler

Zürich, 2009

Table of Contents

1. Summary

Antibiotic resistance of pathogenic bacteria is an emerging threat to global public health. The increased tolerance to antimicrobial drugs is mainly due to the efflux of these substrates out of bacterial cells mediated by multidrug resistance (MDR) transporters.

In Gram-negative bacteria such as *Escherichia coli* or *Pseudomonas aeruginosa*, highly effective tripartite multidrug efflux systems extrude a large variety of noxious substrates from the cell interior or the inner membrane directly into the medium.

In *E. coli*, the major multidrug efflux pump is the tripartite AcrA/AcrB/TolC complex, which extrudes structurally and functionally diverse chemical compounds. This complex is composed of the outer membrane factor (OMF) TolC spanning the outer membrane and protruding 100 Å into the periplasmic space. The membrane fusion protein (MFP) AcrA links the proximal end of TolC with the periplasmic domain of the inner membrane component AcrB. The latter protein belongs to the resistance-nodulation-cell division (RND) superfamily of transport proteins and is both the substrate specificity determinant and the energy module of the AcrA/AcrB/TolC efflux system. While in prokaryotes the main physiological function of RND proteins is associated with extrusion of noxious substrates, they seem to be involved in lipid homeostasis and cell morphogenesis in eukaryotic cells. One of the most intensively studied human RND proteins is Niemann-Pick C1, which is engaged in salvage of lipids from the endosomal/lysosomal pathway.

Recently, an asymmetric structure of AcrB in which the monomers adopt the three different conformations called loose, tight and open was determined. Binding of the substrates minocyclin and doxorubicin to a hydrophobic pocket in the periplasmic domain of the tight conformer was observed. In the loose and tight state, tunnels lead from a lateral periplasmic entrance towards the location of the binding pocket, while in the open conformer, this pocket is exclusively connected *via* another tunnel to a funnel at the centre of the AcrB trimer ultimately leading towards the TolC channel. The current hypothesis states that transport of substrate is accomplished by functional rotation, meaning that each monomer cycles in a connected and concerted fashion from the loose to tight to open conformation and back to the loose conformation in analogy to the functional rotation of the catalytic β-subunit observed in the F_1F_o

ATPase. Since AcrB is driven by the proton motive force, the energy conversion to drive the large conformational changes observed in the periplasmic domain is considered to be generated by protonation and deprotonation of essential charged residues residing in the transmembrane domain.

In my PhD thesis, the focus was on the binding of substrate to the hydrophobic pocket and on the translocation of protons through the transmembrane domain, which was analyzed by structural and functional experiments with wild-type and mutant AcrB.

Substitution of the binding pocket residue F610 with alanine resulted in *E. coli* mutants with an impaired phenotype for all the substrate tested, whereas the binding pocket residue V612 to phenylalanine conversion changed the substrate specificity of the V612F mutant including an increased resistance towards linezolid. Crystallization of the V612F variant in the presence and absence of Designed Ankyrin Repeat Proteins (DARPins) and subsequent X-ray crystallography revealed that AcrB_V612F comprises a novel conformation in which each of the monomers were present in the tight state. The “all-tight” conformation observed for AcrB_V612F is postulated to be adopted by wild-type AcrB during functional rotation as well, for example when the concentration of substrate is high.

To shed light on the protonation and deprotonation events in the transmembrane domain, four essential charged residues D407, D408, K940 and R971 - also referred to as proton relay network - as well as the important polar residue T978 were substituted with asparagine (D407, D408) or with alanine (K940, R971, T978) and the structures of both wild-type and mutant AcrB/DARPin complexes were determined at a resolution of 2.0-3.0 Å. The most prominent differences between wild-type and mutant protein were observed in the tight conformation near the proton relay network. Here, the AcrB_D407N and AcrB_R971A mutant exhibited structural features that are typical for the open conformer, implying that the structure of these mutant proteins might resemble intermediate conformations at different steps during the transition from tight to the open state. Additionally, we identified water molecules in the transmembrane domain that exhibit distinct positions in the three monomers. Based on these high resolution structural information, a putative pathway for protons through the transmembrane domain from the periplasm to the cytoplasm is proposed, and a detailed model for protonation and deprotonation events during functional rotation is presented.

1. Zusammenfassung

Die Verbreitung von antibiotikaresistenten pathogenen Bakterien ist eine zunehmende Gefahr für die weltweite Gesundheit. Erhöhte Toleranz gegenüber multiplen antibakteriellen Substanzen wird hauptsächlich durch sogenannte „multidrug resistance“ Transportproteine verursacht, welche verschiedenste toxische Stoffe aus der bakteriellen Zelle befördern. In Gram-negativen Bakterien wie zum Beispiel *Escherichia coli* oder *Pseudomonas aeruginosa* transportieren dreiteilige Effluxsysteme äusserst effektiv eine Vielzahl von schädlichen Substanzen entweder aus dem Zellinnern oder von der inneren Membran direkt ins umgebende Medium.

Das wichtigste „multidrug“ Transportsystem in *E. coli* ist der dreiteilige AcrA/AcrB/TolC-Komplex, welcher strukturell und funktionell verschiedenste Chemikalien transportiert. Dieser Komplex besteht aus dem „Outer Membrane Factor (OMF)“ TolC, welcher die äussere Membran durchdringt und 100 Å weit ins Periplasma ragt; der inneren Membrankomponente AcrB, ein trimeres Transportprotein der „Resistance-Nodulation-cell Division (RND)“ Superfamilie, welches die Substratsdeterminante und das Energiemodul des gesamten AcrA/AcrB/TolC-Komplexes darstellt; und des „Membrane Fusion Protein (MFP)“ AcrA, welches das proximale Ende von TolC mit der periplasmatischen Domäne von AcrB verbindet. Während die RND Proteine in Prokaryoten hauptsächlich mit dem Export von schädlichen Stoffen in Verbindung gebracht werden, scheinen sie in Eukaryoten in Lipid-Homöostase und Zellmorphogenese involviert zu sein. Eines der am intensivsten untersuchten menschlichen RND Proteine ist Niemann-Pick C1, welches am „salvage-pathway“ von Lipiden aus dem endosomal/lysosomalen System beteiligt ist.

Kürzlich wurde eine asymmetrische Struktur von trimerem AcrB bestimmt, in welchem die Monomere die drei Konformationen „loose“, „tight“ und „open“ einnehmen. Des weiteren konnte die Bindung der Substrate Minocyclin und Doxorubicin in einer hydrophoben Bindungstasche in der periplasmatischen Domäne des „tight“ Konformers nachgewiesen werden. Im „loose“ und „tight“ Zustand führen Tunnel von einem periplasmatisch lokalisierten lateralen Eingang zur Position der Bindungstasche, während im „open“ Konformer ein neuer Tunnel diese Stelle mit einem Ausgangstrichter verbindet, welcher sich in der Mitte der drei Monomere

befindet und zum TolC Kanal führt. Gemäss der aktuellen Hypothese wird der Transport von Substraten durch funktionelle Rotation bewerkstelligt: analog zur funktionellen Rotation der katalytischen β-Untereinheit der F_1F_o-ATPase nimmt jeder der drei Monomere in einer abgestimmten Art und Weise nacheinander die Zustände „loose", „tight" und „open" an. Es wird angenommen, dass in AcrB, welches durch die protonenmotorische Kraft angetrieben wird, titrierbare Aminosäurereste in der Transmembrandomäne protoniert und deprotoniert werden. Dadurch würden die grossen konformationellen Änderungen in der periplasmatischen Domäne energetisiert, welche zu Substrattransport führten.

Der Fokus meiner Doktorarbeit war auf die Bindung von Substraten in der periplasmatischen AcrB-Bindungstasche und auf die Translokation von Protonen durch die Transmembrandomäne gerichtet. Dafür wurde wildtyp und mutiertes AcrB funktionell und strukturell untersucht.

Die Alanin-Substitution von F610, welches sich in der Bindungstasche befindet, führte zu einem eingeschränkten Transport für alle getesteten Substrate, während die V612F Punktmutation spezifisch die Substratspezifität von AcrB veränderte: gegenüber den meisten Substraten wurde die in *E. coli* gemessene Resistenz zwar erniedrigt, die Toleranz gegenüber Linezolid jedoch spezifisch erhöht. Röntgenstruktur-Analysen der AcrB Variante V612F mit und ohne „Designed Ankyrin Repeat Proteins" (DARPins) zeigten das Transportprotein in einer neuen Konformation, in welcher alle Monomere den „tight" Zustand einnahmen. Es wird postuliert, dass während der funktionellen Rotation die „all-tight" Konformation auch in wildtyp AcrB vorkommt, zum Beispiel bei hoher Substratkonzentration.

Um Protonierungs- und Deprotonierungsereignisse in der Transmembrandomäne zu untersuchen, wurde das sogenannte „proton relay network", bestehend aus den vier essentiellen und titrierbaren Aminosäureresten D407, D408, K940 und R971, und der funktionell wichtige polare Aminosäurerest T978 durch Asparagin (D407, D408) oder durch Alanin (K940, R971, T978) ersetzt und die Strukturen von wildtyp und mutanten AcrB/DARPin-Komplexen bei einer Auflösung von 2.0 bis 3.0 Å bestimmt. Die auffallendste Unterschiede zwischen dem Wildtyp und den mutierten AcrB Varianten wurden im „tight" Konformer nahe des „proton relay network" beobachtet: AcrB_D407N und AcrB_R971A wiesen strukturelle Eigenschaften sowohl des „tight" wie auch des „open" Monomers auf. Möglicherweise repräsentieren diese Strukturen

unterschiedlich weit fortgeschrittene Intermediate während der Konversion vom „tight“ zum „open“ Konformer. Zusätzlich identifizierten wir in der Transmembrandomäne Wassermolekülen, welche in den drei Konformationen unterschiedliche Positionen aufwiesen. Basierend auf diesen hochauflösenden Strukturinformationen wird ein möglicher Weg der Protonen durch die Transmembrandomäne vom Periplasma ins Zytoplasma vorgeschlagen und ein detailliertes Modell der Protonierungs- und Deprotonierungsereignisse während der funktionellen Rotation präsentiert.

2. Introduction

2.1 Antibiotic resistance

In the late 1960´s, the US Surgeon General William H. Stewart declared "...that we had essentially defeated infectious diseases and could close the book on them [infectious diseases]..." (1). This statement, however, turned out to be incorrect, since during the upcoming decades many infections reemerged to become the second most cause of death worldwide (2).

The main reason for failure in the fight against pathogenic organisms causing infectious disease is the emergence of antibiotic resistance. Consequently, our existing arsenal of antibiotics is failing ever often due to the increasing numbers of multiple drug resistant organisms. In 1993, the World Health Organization (WHO) declared *Mycobacterium tuberculosis*, formerly believed to be defeated with the help of antibiotics, to be a global emergency, the first such designation ever made by the organization (3).

The intrinsic development of resistance to antibiotics as soon as the drug is deployed urges the design and production of new antibiotics. However, the trend goes in the opposite direction: over the past 20 years, there has been a 56% decline in the number of antibiotics approved annually by the American Food and Drug Administration (FDA) and over the last decade, only 22 new antibacterial drugs have been launched (4). In fact, many large pharmaceutical companies have reprioritized their research and development (R&D) efforts to either de-emphasize or to no longer include antibacterials (5-9). The most likely reason for disinterest to develop new antibiotics is their low monetary value in the marketplace: they are administered in predominantly acute situations to reduce infection and prevent mortality. Because of their effectiveness, the number of patients-days[1] is small and revenue low. In contrast, drugs prescribed for chronic diseases are more attractive since patients most likely are prescribed these drugs over a long period of time or even life-long (e.g. obesity, pain relief, asthma treatment, erectile dysfunction). To reduce the expenses of R&D of antibiotics, the remaining antibiotic developing companies mainly focus on modifying the safe and proven classes of antibiotics and high through-put screening (HTS) of pre-existing synthetic libraries of compounds made primarily for other purposes. As a

[1] total number of days an individual patient is on drug therapy

consequence of the former approach no new classes of antibiotics are developed (**Figure 1**), with the notable exception of the oxazolidinones (e.g. linezolid). Despite the fact that excellent *in vitro* target inhibitors could be identified using HTS, restricted permeation of the bacterial cell membranes rendered those ineffective against bacteria (10).

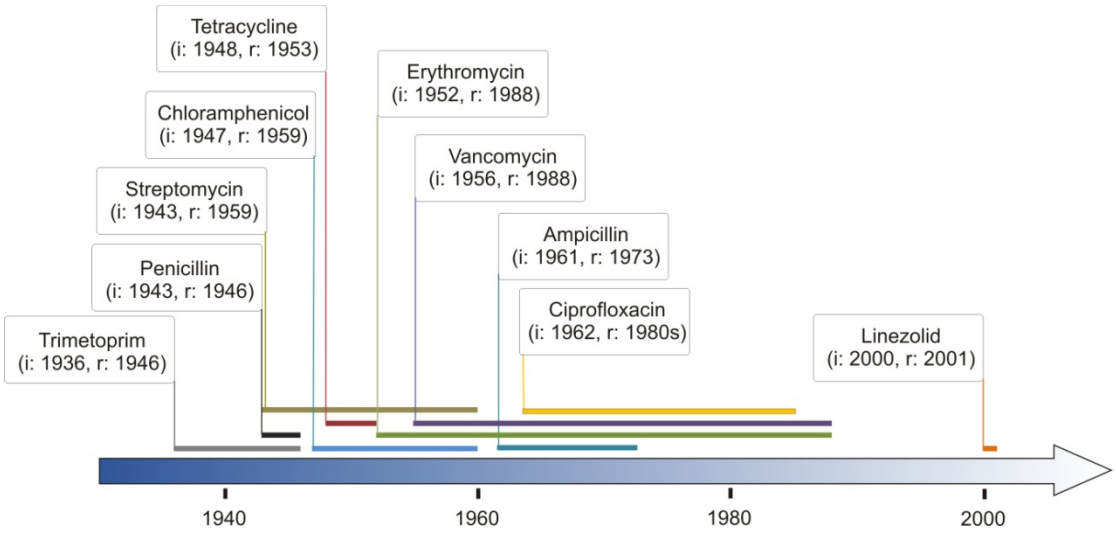

Figure 1: Deployment of new classes of antibiotics and development of resistance. Between the 1930s and 1960s, many new classes of antibiotics were introduced into clinical practice. There is an innovation gap of 38 years between deployment of ciprofloxacin (1962) and linezolid (2000). Development of resistance was observed within one year (linezolid) and 36 years (erythromycin) after deployment (see horizontal bar). One name of a representative antibiotic of a chemical class is displayed (trimetoprim for sulfonamides, penicillin for β-lactams, streptomycin for aminoglycosides, tetracycline for polyketitedes, erythromycin for macrolides, vancomycin for glycopeptides, ampicillin for aminopenicillins, ciprofloxacin for fluoroquinolones, and linezolid for oxazolidinones). Year of introduction into clinical practice (i) and of observation of resistance (r) is indicated. (11-13)

The reason for the inevitable development of antibiotic resistance in bacteria is the combination of short replication time and spontaneous mutation events. Already in a *Escherichia coli* population of $1.3*10^5$ cells (corresponding to 13µl of a culture at OD_{600} = 1.0), each of the 4500 genes carries at least one mutation after one replication cycle given the typical error frequency of the bacterial DNA polymerase of 10^{-7} and

the genome size of 4.6 million nucleotides[2]. If one of these mutations confers some degree of resistance, the mutants have a selective advantage and will prevail.

Resistance of bacteria towards antibiotics are known to be evoked by at least three different mechanisms: (i) target modification (e.g. resistance against macrolides mediated by methylation of the ribosome (14-16) or resistance against fluoroquinolones by mutations in DNA gyrase, (17,18), (ii) antibiotic modification (e.g. hydrolysis of β-lactam ring by β-lactamase (19) or acetylation of aminoglycosides, (20)) and (iii) reduced uptake of antibiotics in the target compartment (periplasm, cytoplasm) through suppression of porin synthesis (21) and/or overproduction of efflux pumps (22-27).

Resistance conferred by antibiotic and target modification is often restricted to a single class of antibiotics or even a single compound. In contrast, multidrug resistance (MDR) transporters enable the bacteria to efflux a broad range of substances and hence confer resistance to unrelated compounds. The central role of MDR transporters was highlighted by Lomovskaya *et al*. by analyzing resistance of *Pseudomonas aeruginosa* towards the antibiotic levofloxacin. Their findings suggested that (i) overexpression of MDR transporters is the first resistance mechanism that can be observed when the cells are exposed to antibiotics, that (ii) the probability of other resistance mechanism to develop is significantly higher when MDR transporters are present and that (iii) MDR transporters increase the resistance conferred by other mechanisms (23).

2.2 Multidrug resistance transporters

Based on a systematic genome-wide analysis of membrane transport systems (28), solute transporters were identified and classified into about 550 families and superfamilies (Transport Classification Database (tcdb), http://www.tcdb.org/). According to this transporter classification system, all the MDRs known belong to five superfamilies. These are the ATP binding cassette (ABC) superfamily (TC#3.A.1), the major facilitator superfamily (MFS) (TC#2.A.1), the drug/metabolite transporter (DMT) superfamily (TC#2.A.7), the multidrug/oligosaccharidyl-

[2] $\left(1-\left(1-f\right)^{l*x}\right)^{g}=0.99$, where 0.99 is the statistical probability, *f* the error frequency of the DNA polymerase, *l* the average gene lenght, *x* the number of cells an *g* the number of genes in the genome.

lipid/polysaccharide (MOP) flippase superfamily (TC#2.A.66) and the resistance-nodulation-cell division (RND) superfamily (TC#2.A.6). It has to be stated that not all the proteins assigned to these families are actual multidrug efflux transporters but are rather involved in transport of pivotal substrates (e.g. lipids, nutrients, signalling molecules) or have hitherto unknown function.

The primary active MDR ABC transporters are typical for eukaryotes where they play a major role in exporting noxious substrates out of the cell. Among these substrates are also chemotherapeutics and therefore members of the superfamily of ABC transporters such as the human P-glycoprotein negatively affect the effectiveness of cancer therapy. It is estimated that around 40% of human tumors develop resistance to chemotherapeutic drugs (29).
The minimal requirements for ABC transporters are two transmembrane domains (TMDs) and two nucleotide binding domains (NBDs). In mammalian ABC transporters these domains are located on a single polypeptide, whereas in bacteria most commonly two monomers comprising one TMD and one NBD form a functional homodimer. Besides mammalian P-glycoprotein (30), prominent members of the ABC superfamily are the human multidrug exporter MRP1 (31,32), the cystic fibrosis transmembrane conductance regulator CFTR (33), LmrA of *Lactococcus lactis* (34) and Sav1866 of *Staphylococcus aureus*, the first ABC transporter whose structure was determined at high resolution (35).

The drug-translocating members of the other four subfamilies belong to the class of secondary active transporters and hence utilize the electrochemical gradient of ions (mostly protons) across the membrane.

Members of the MFS typically consist of a single polypeptide with 12 or 14 transmembrane helices. X-ray structural data are available for the *E. coli* proteins EmrD (Yin 2006), LacY (36,37) and GlpT (38). Whereas EmrD is an MDR with broad substrate specificity, LacY and GlpT exhibit narrow substrate specificity.
The structures of all three proteins resemble a membrane embedded bowl with two linings of transmembrane α-helices. Whereas the α-helices of the outer lining adopt a similar configuration in all three proteins, the arrangement of the inner layer is quite

distinct, forming a larger internal cavity in EmrD compared to LacY and GlpT. Although no bound substrate could be detected in EmrD, mutational analysis in its homologues LmrP and MdfA imply that residues located at the surface of this large internal cavity are involved in substrate recognition and translocation. Furthermore, whereas the interior of LacY and GlpT is rather hydrophilic, the residues lining the internal cavity of EmrD are aliphatic or aromatic, a common feature for MDR proteins transporting charged amphipathic compounds (39-41). Thus, the voluminous internal cavity may accommodate several binding sites or a single, large and flexible binding site, both of which would account for the broad substrate specificity of EmrD (29).

Whereas the other four superfamilies of MDRs are present in all phyla, small multidrug resistance (SMR) transporters (TC#2.A.7.1), a subdivision of the DMT superfamily, are only found in prokaryotes. With only four transmembrane α-helices per monomer and no significant extramembrane domain, these are considered as the smallest MDRs up to date. The most probable functional unit is a bundle of eight transmembrane helices, formed either by homodimerization (EmrE) or by a heterodimerization (YdfEF). The topological orientation of the two monomers in the membrane is still controversial: crosslink studies performed by Schuldiner and colleagues suggest a parallel arrangement with cytoplasmic N- and C-termini (42,43), whereas a genome wide screen with C-terminal tagged membrane proteins (44,45), manipulation of the K+R bias of EmrE (46) as well as structure determination by X-ray crystallography (47) support an antiparallel orientation of the two monomers.
Like the structurally characterized MFS transporters, the SMR transporters appear to have an overlapping binding site for the substrate and the coupling ion suggesting a common transport pathway. In EmrE, this pathway involves the essential residue E14 (48,49).

The multi antimicrobial extrusion (MATE) family (TC#2.A.66.1), a subdivision of the MOP flippase superfamily, is the most recently classified and least characterized class of MDRs. Members of this family consist of twelve transmembrane α-helices and are energized either by the influx of Na^+ (50) or by protons (51). Prominent members of

this family are NorM of *Vibrio paraphaemolyticus* and *Neisseria gonorrhoeae* and YdhE of *E. coli*.

Proteins of the RND superfamily are ubiquitous in all phyla. In prokaryotes their main physiological function seems to be associated with the extrusion of noxious substrates and hence function as a typical MDR transporter, with notable exceptions like the secretory accessory proteins SecDF (52,53), lipid exporter MmpL7 (54,55) and the putative lipooligosaccharide nodulation factor exporter NolG (56). In eukarya, however, the functionally characterized RND proteins seem to be involved in lipid homeostasis (57-59) and cell morphogenesis (60,61). For the proteobacterial heavy metal (HM) efflux pump CzcA (*Ralstonia* sp. CH34), it was shown that the transport of Zn^{2+} ions is coupled to the antiport of protons (62). As phylogenetic analyses suggest, energization *via* the proton motive force might be a common feature for all RND transporters (28).
Most members of the RND superfamily are located in the inner-membrane of proteobacteria. They typically assemble with two accessory proteins, a membrane fusion protein (MFP; TC#8.A.1) and an outer membrane factor (OMF; TC#1.B.17). The so formed tripartite complex spans the outer membrane, the periplasm as well as the inner membrane of the Gram-negative bacterium. The outer membrane, besides the tripartite efflux pumps, is considered to be the main barrier for drugs on their way to the inside of the cell (63,64) The combination of the intrinsic impermeability of the outer membrane, the reduction of the number of outer membrane pores and the upregulation of tripartite MDRs enables effective synergistic drug resistance (65).

Within the phylogentic tree (**Figure 2**), the clustering pattern of proteobacterial RND protein mirrors their substrate specificity with the heavy metal efflux (HME; TC#2.A.6.1) family catalyzing export of heavy metal ions, the hydrophobe/amphiphile efflux-1 (HAE1; TC#2.A.6.2) family catalyzing export of multiple drugs and the putative nodulation factor exporter (NFE; TC#2.A.6.3) family exporting lipooligosaccharides involved in plant nodulation. The remaining families comprise also proteins of firmicutes (HAE2; TC#2.A.6.5), archaea (HAE3; TC#2.A.6.7) and eukaryotes (EST; TC#2.A.6.6 and Dispatched; TC#2.A.6.9). It was not until 2000 that the first mammalian RND protein – Niemann-Pick Type C1 – was detected and characterized (66).

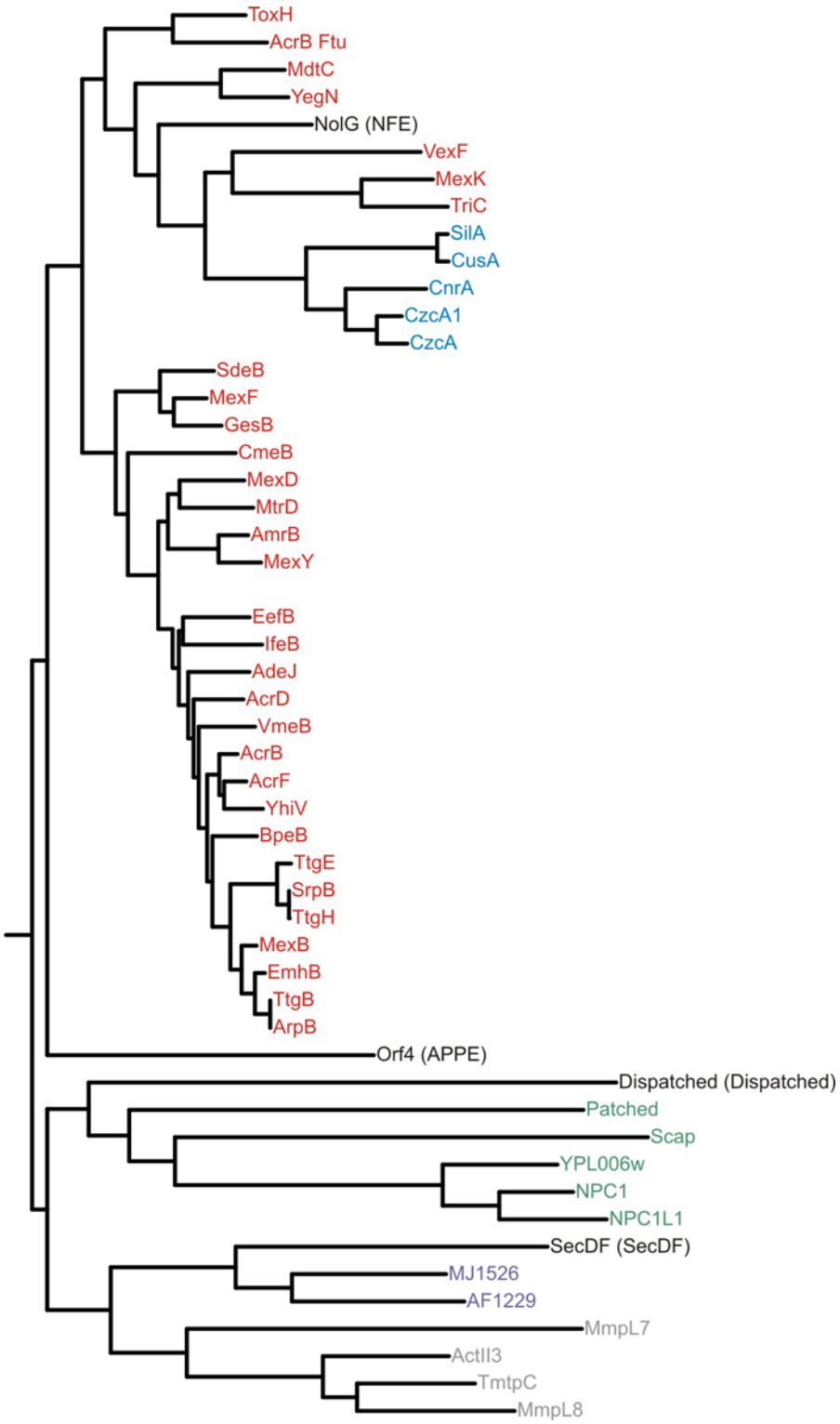

Figure 2: Maximum-likelihood phylogenetic tree of proteins of the RND superfamily. Proteins of the proteobacterial HME and HAE1 family are depicted in blue and red, respectively. Members of the eukaryotic EST, the archeal HAE3 family and proteins of HAE2 in firmicutes are shown in green, violet and grey, respectively. Note that, with the exception of the proteobacterial SecDF transporter, the clustering of the proteins mirrors their phylogenetic origin. Orf4 is a proteobacterial protein and the only member of the Brominated, Aryl Polyene Pigment Exporter (APPE) family. Protein families that are represented by only one member in the Transport Classification Database (NFE, APPE, Dispatched SecDF) are shown in black. 3-hydroxy-3-methylglutaryl (HMG)-CoA reductase, a human protein of the EST family, is not shown. For construction of the tree, a multiple sequence alignment was built using Mafft (67) with default settings. The tree was inferred using PHYML (68) with the JTT matrix (69)

2.3 Niemann-Pick C1 and homologous eukaryotic RND proteins

The Niemann-Pick C1 transporter is localized in the lysosomal membrane of eukaryotic cells (66,70). Mutations in this protein have been shown to cause the fatal neurodegenerative Niemann-Pick disease that is characterized by accumulation of lipids in endosomal/lysosomal (E/L) pathway causing death in early childhood (71,72). Human and murine NPC1 as well as drosophila NPC1a seem to be ubiquitously expressed housekeeping proteins located on the membrane of late endosomes (73) and are indispensable for proper lipid turnover. In 5% of patients showing Niemann-Pick C phenotype, another protein, designated NPC2 (formerly known as HE1) is mutated. NPC2 is a small soluble lysosomal glycoprotein (74) that binds cholesterol and other sterols (75) and transfers cholesterol to phospholipid membranes (58). The structure of the NPC2/cholesterol sulfate comples was solved by X-ray crystallography and showed the iso-octyl side chain deeply buried in a hydrophobic pocket, whereas the A ring is exposed to the solvent (76). This is in accordance with the observation that binding of cholesterol derivatives having modifications at the iso-octyl side chain (for example 25-hydroxycholesterol) by NPC2 is inhibited, whereas the ligand/protein interaction is not affected when the A ring of cholesterol (for example epicholesterol) is modified (59).

Unlike conventional RND proteins which are composed of twelve transmembrane helices (TM) and two large hydrophilic loops, NPC1 exhibits at its N-terminus an extended luminal loop plus an additional transmembrane helix (66,70) (**Figure 3**). It was recently shown that cholesterol is bound by this additional N-terminal domain (NTD). In direct contrast to the findings with NPC2, binding of sterol to NPC1(NTD) is not inhibited by hydroxylation of the iso-octyl side chain, but rather by modification of the A ring (59).

In mice, $NPC1^{-/-}$, $NPC2^{-/-}$ and the double mutant showed essentially the same phenotype, suggesting nonredundant functions in the same pathway at different steps (57). In an *in vitro* assays using NPC2 and soluble NPC1(NTD), binding and release of substrate by both proteins, protein-protein transfer of cholesterol and substrate transfer between protein and liposomes were analyzed (58). These experiments revealed that the on- and off-rate of NPC2 is much faster than the one of

NPC1(NTD). Interestingly, binding and release of cholesterol by NPC1(NTD) was accelerated by a factor of approximately 100 in the presence of NPC2, suggesting that NPC2 shuttles cholesterol to and/or from NPC1(NTD) and promotes binding and release by NPC1(NTD). Based on these findings, two models were proposed in which unidirectional egress of unesterified cholesterol out of the E/L system is dependent on the cooperation of NPC1 and NPC2. In the first model, cholesterol is bound by NPC1 and then transferred *via* NPC2 to a yet unidentified lysosomal cholesterol transporter which would insert the substrate into the endosomal membrane. According to the second model, it is rather NPC2 that binds cholesterol first and mediates its transfer to NPC1, which would integrate the substrate into the membrane. Membrane bound cholesterol would then be transported to the ER for further processing (58).

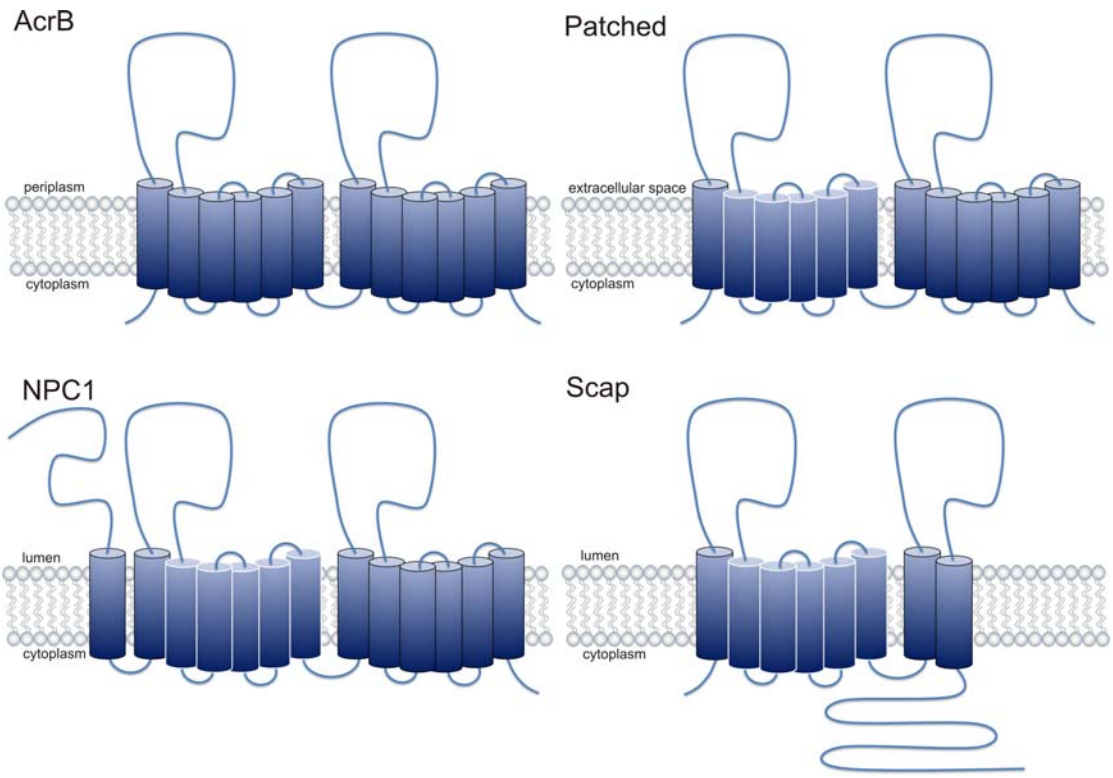

Figure 3: Topology of AcrB, NPC1, Patched and Scap. The transmembrane helices forming the sterol sensing domain (SSD) are framed in white. The extensive loops connecting TM1 with TM2 and TM7 with TM8 (for NPC1: TM2 with TM3 and TM8 with TM9) are all localized extracellularly or luminally. See text for details and references.

Besides in mammalian cells, orthologues of NPC1 were identified in the yeast *Saccharomyces cerevisiae*, the nematode *Caenorhabditis elegans* and the fruit fly

Drosophila melanogaster, where they all seem to be involved in trafficking of lipids and derivatives (77,78).

The closest homolog of NPC1 is NPC1 like protein 1 (NPC1L1). The localization of murine NPC1L1 and drosophila NPC1b is restricted to the plasma membrane (PM) of small intestine. Human and primate NPC1L1 is found in the PM of small intestine and the liver. They accomplish the absorption of food administered cholesterol and can be specifically inhibited by the anti-hyperlipidemic drug ezetimibe (79-81).

The transmembrane helices 3 to 7 of NPC1 bear sequence homology to a sterol sensing domain (SSD) found in other RND proteins like the sterol regulatory element binding protein (SREBP) cleavage activating protein (Scap), the HMG-CoA reductase and Patched (Ptc) (**Figure 3**) (70,82). However, binding of cholesterol by the SSD was only shown for Scap (83,84).

Scap is predicted to have eight transmembrane helices, from which TM2 to 6 form the SSD (85-87) (**Figure 3**). Scap and SREBP are present as a complex in the membrane of the endoplasmatic reticulum (ER). When the cell is deprived of sterols, the Scap/SREBP complex is moved *via* COPII-coated vesicles to the Golgi apparatus. There, SREBP is cleaved by the proteases S1P and S2P, releasing the soluble N-terminus. Processed SREBP enters the nucleus and acts as a transcription factor by binding to the sterol regulatory element (SRE), which promotes transcription of genes involved in cholesterol uptake (for example low-density lipoprotein (LDL) receptors) and biosynthesis (for example HMG-CoA reductase). In the presence of cholesterol, the SSD of Scap binds to the transmembrane protein Insig (88,89), which inhibits movement of the Scap/SREBP complex to the Golgi apparatus and processing of nuclear SREBP (90,91).

HMG-CoA reductase resides in the membrane of the ER and is the rate controlling enzyme in the mevalonate pathway, with cholesterol and other isoprenoids as products. Since both substrate (HMG-CoA) and product (mevalonic acid) of the reaction catalyzed by HMG-CoA reductase are water soluble, the reason for membrane attachment appears to be purely regulatory (92). HMG-CoA reductase has seven (93) or eight (94) transmembrane helices, TM2 to 6 form the SSD (85,87,94,95) and the catalytic activity is restricted to the cytosolic C-terminus (93). Upon accumulation of cholesterol and its precursors, HMG-CoA reductase binds to Insig, is then targeted for ubiquitinylation and subsequently degraded by the proteasome (96).

The Patched (Ptc) protein is located at the plasma membrane, where it acts as a receptor for the morphogenetic signaling peptide Hedgehog (Hh) (reviewed in (97,98). Ptc has twelve predicted transmembrane helices, the SSD is formed by TM2 to TM6 (85,99) (**Figure 3**). Interestingly, oxysterol derivatives have been suggested to influence Ptc activity (100). When Hh is absent, Ptc catalytically inhibits activity of its target protein Smoothened (Smo) (60). In the presence of Hh, Smo starts a complex signaling cascade ultimately leading to activation of the Ci/GLI family of transcription factors (101-103), which control morphogenesis of a variety of tissues and organs (97) and proliferation of stem cells in adult tissues (104).

2.4 Tripartite MFP/RND/OMF complexes

The inner membrane located proteobacterial RND proteins associate with two accessory proteins for their function *in vivo*, namely the periplasmic membrane fusion proteins (MFPs) and the outer membrane factors (OMFs). They form a tripartite complex which allows the effective transport from the outer leaflet of the inner membrane directly into the medium (**Figure 4**). The *E. coli* genome codes for four MFPs (AcrA, AcrE (EnvC), MdtE (YhiU), MdtA (YegM)) and six RNDs (AcrB, AcrD, AcrF (EnvD), MdtF (YhiV), MdtB (YegN), MdtC (YegO), MdtBC). Most of the MFP and RND components are encoded on the same operon, whereas *acrD* is found isolated on the chromosome. TolC is the only OMF in *E. coli*, whereas in *P. aeruginosa*, there are five OMFs for nine MFPs and eight RNDs[3]. Systematic deletion of seven known and nine predicted MDR transporters in *E. coli* demonstrated that the tripartite AcrA/AcrB/TolC efflux system is solely responsible for the observed intrinsic antibiotic resistance of *E. coli* wild-type (wt) strains (105). The AcrA/AcrB/TolC system is constitutively expressed at a low level. For the other *E. coli* MFP/RND/OMF complexes, increased resistance towards some toxic compounds was only detected when the proteins were overexpressed (106).

[3] These make up the following tripartite systems: MexA/MexB/OprM, MexC/MexD/OprJ, MexE/MexF/OprN, MexX/MexY/OprM, MexJ/MexK/OprM, MexH/I/OpmD, MexV/MexW/OprM, TriA/TriB/TriC/OpmH.

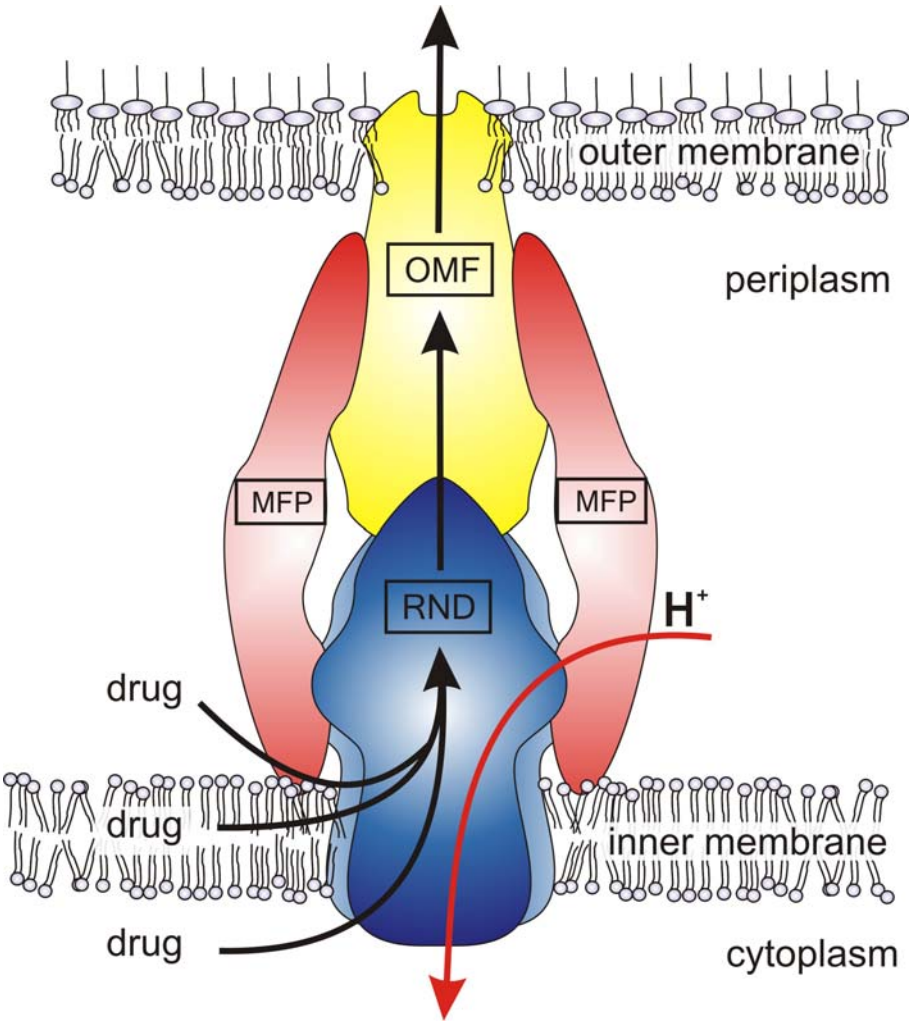

Figure 4: Schematic representation of tripartite MFP/RND/OMF multidrug efflux system in proteobacteria. For proper function *in vivo*, all three component are needed. The RND protein resides in the inner membrane and is the energy module and the substrate specificity determinant coupling the influx of protons to the export of noxious compounds. Whether the substrate is garnered from the cytoplasm, the inner membrane or the periplasm may depend on the transporter and the chemical properties of the substrate. Suggestions for MFP:RND ratio varies between one and four. The drug:proton stoichiometry is as yet unknown (based on the original drawing of Andrea Eberle).

2.5 Outer membrane factors (OMFs) - TolC

The *tolC* locus in *E. coli* was identified *via* a mutation causing a phenotype that was resistant against the colicin family of bacteriocins (*tol*erance to *C*olicins) (107), suggesting that TolC acts as an entry pore. Furthermore, TolC deficient strains were shown to be highly susceptible to bile salts and dyes. TolC belongs to the family of OMF (TC #1.B.17), which spans the outer membrane and protrudes into the

periplasm in proteobacteria putatively allowing transport from the periplasm into the medium and *vice versa*.

TolC is known to interact with other proteins located in the periplasm and inner membrane and behaves very promiscuous. In addition to the formation of complexes with the RND proteins and the MFPs mentioned above, it has been shown to also form complexes with the type I secretion system HlyBD, the primary active (ABC-type) MDR MacAB and the MFS member EmrAB (108).

Structures of OMFs of *E. coli* (TolC) (109), *P. aeruginosa* (OprM) (110) and *Vibirio cholerae* (VceC) (111) have been solved by X-ray crystallography. OMFs are homotrimeric proteins spanning the outer membrane and protruding 100 Å into the periplasm. The proteins display a β-sheet domain forming a β-barrel, a periplasmic α-helical domain, and an equatorial domain. In the β-sheet domain, twelve β-sheets form a pore that is inserted into the outer membrane. The equatorial domain divides the periplasmic α-helical domain into two sections of approximately equal lengths: an outer membrane proximal subdomain in which twelve helices pack to form a hollow cylinder, and a distal subdomain where twelve helices form conventional coiled coils. Recent crystallographic structures of TolC in space groups lacking threefold symmetry revealed that by modulating the curvature of the coiled coils, TolC can switch between the open and closed state in a fashion that is reminiscent of the iris mechanism of a camera (112) (**Figure 5**).

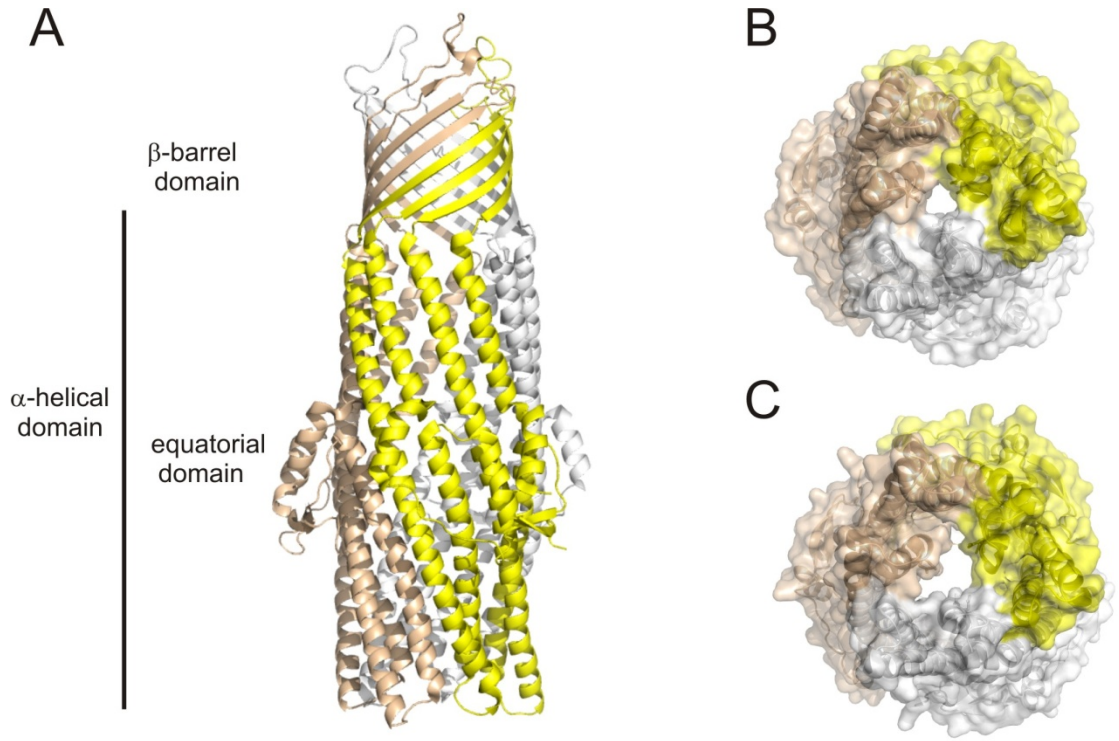

Figure 5: Crystal structure of TolC. **A)** Side view of trimeric TolC. The β-barrel domain, which resides in the outer membrane, and the two periplasmic α-helical and equatorial domains are depicted. **B)** and **C)** Top view of the proximal end TolC of the closed (B) and the (partially) open (C) state. Pictures were made using pdb coordinate files 1EK9 for (A) and (B) and 2VDD for (C), respectively.

The diameter of the closing aperture varies from 8.5 Å in the closed conformation (pdb-ID: 1EK9, (109)) to 20 Å in the open conformation (pdb-ID: 2VDD, (112)). Opening and closing of the channel was already suggested by Thanabalu *et al.*, who observed that TolC in the HlyB/HlyD/TolC complex is more susceptible to proteolytic cleavage when the substrate HlyA was present, implying a substrate induced conformational change (113). The opening mechanism of TolC was further analyzed by disruption of salt bridges and hydrogen bonds at the very distal ends between the coiled coils (114). As a result, TolC was locked in constitutively open state, allowing passive influx of the large antibiotic vancomycin (112,115). Furthermore, conductance was increased when single channels composed of this particular open TolC mutant protein were integrated in black lipid membranes, whereas HlyA export and thus assembly with the ABC transporter HlyB and the MFP HlyD was unaffected (114).

2.6 Membrane Fusion Proteins (MFPs) - AcrA

The membrane fusion protein (MFP, TC #8.A.1.) family was given its name because its members are homologous to the paramyxovirus membrane fusion protein involved in fusion of the viral envelope and the cell membrane (116). Similarly, MFPs were thought to fuse the outer and the inner membrane in proteobacteria, possibly by bridging the inner membrane protein with the outer membrane factor (65,116-118). This perception has been changed over the years, as more structural information on in particular the MFP proteins AcrA and MexA became available.

The structures of *E. coli* MFP AcrA and *P. aeruginosa* MexA have been solved (110,119-121). For AcrA deletion of amino acids 313 to 397 was essential to obtain crystals (119). The first two MexA structures did not include the N-terminal 27 (120) and 24 (110) amino acids and a long C-terminal stretch stretch (283 to 383 (120) and 302 to 383 (110) in unprocessed MexA, respectively) due to disorder in the crystal structure. Very recently, Symmons *et al.* revealed the missing structural information by further analysis of the crystallographic data and averaging of the rigid body movement in MexA. MexA and supposedly also AcrA are composed of a β-barrel domain, a lipoyl domain, an α-helical hairpin domain and a membrane proximal (MP) domain (121) (**Figure 6**). The N-terminal signal sequence (amino acids 1 to 24) is responsible for the translocation of AcrA and MexA into the periplasm and is subsequently cleaved producing the mature protein (25 to 397 and 24 to 383 for AcrA and MexA, respectively). Both AcrA and MexA are attached to the inner membrane *via* a lipid (palmitoyl-) anchor, which is post-translationally coupled to Cys25 and Cys24, respectively. However, since mutants coding for soluble, non-palmitoylated AcrA and MexA exhibit a normal resistance phenotype (118,122), the lipid anchor appears not to be essential.

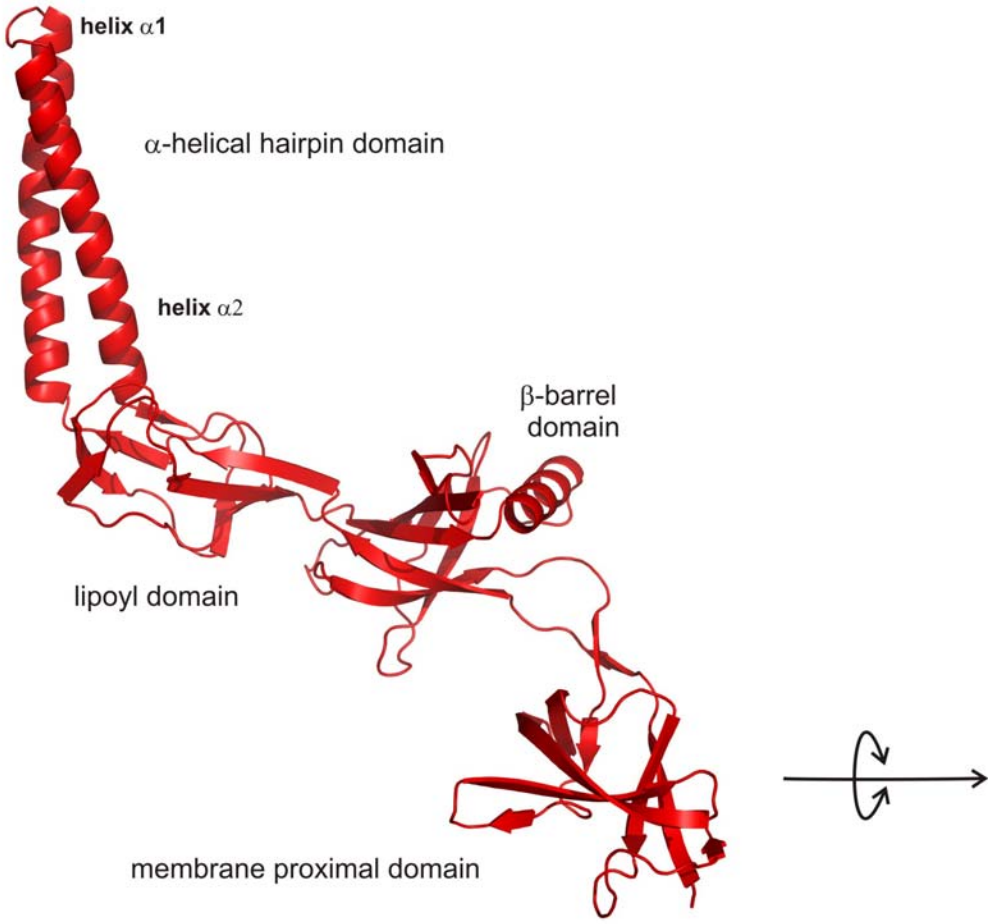

Figure 6: Crystal structure of MexA. Different domains of MexA are indicated. Due to their homology, the structure of the MP domain in AcrA is supposed to be similar. MexA crystallizes as a 13-mer in which the MP domain of five monomers exhibit the orientation depicted above. In six momomers, the MP domain is rotated by approximately 85° along the indicated axis whereas in two monomers, this domain is not resolved due to disorder. Picture was made using pdb coordinate file 2V4D.

In proteobacteria, transporters of the MF-superfamily (EmrAB, (65,123); FarA, (124), VceA, (125)) and the ABC family form complexes with MFPs and OMFs. The MFP-dependent ABC family includes the type I secretion transporter complexes CvaAB-TolC and HlyBD-TolC (113,126), and the MDR transporter MacAB-TolC (106,127). It was shown that upon reconstitution of MacB into proteoliposomes, ATPase activity was strictly dependent on the presence of MacA. As Thikonova *et al.* stated (127), this stimulatory effect of MacA is reminiscent of the activity stimulation of loaded periplasmic ligand-binding proteins on their cognate transporters. Examples of the latter include the maltose- (MalE) and histidine-binding (HisJ) proteins (128). Besides

stimulating the ATPase activity of the transporters, periplasmic ligand-binding proteins are also responsible for the high-affinity binding of substrates (129,130).
In firmicutes, the MFPs cannot have the function of connecting the inner membrane protein with the OMF, so their role is still elusive. Nevertheless, MFPs have been found to be essential factors for ABC transporters in these bacteria. The Gram positive MFPs appear to exist in two sizes, full length proteins and internally shortened proteins lacking the central 270 residue α-helical region (131).
Additionally, experiments performed by Elkins and Krishnamoorthy suggest that in proteobacteria, MFPs influence substrate specificity: the *E. coli* MFP AcrE is able to substitute AcrA in AcrB-mediated transport for some antibiotics, but not for all (132). Similarly, mutations on AcrA affected the substrate specificity of the chimeric complex AcrA/MexB/TolC and hence affect growth of cells differentially: A D111N and S249N amino acid exchange enhanced resistance towards all drugs tested which can be explained by an improved interaction between the non-cognate components of the transport complex. Interestingly, substitution of G240 by serine showed unchanged MIC values for SDS and erythromycin, but a 16-fold increase towards nalidixic acid. A V244M exchange lowered the MIC for SDS, whereas the value for nalidixic acid and lincomycin was increased (133). These findings strongly suggest that MFPs are functionally more than just a physical linker between the inner membrane protein and the outer membrane factor.

2.7 AcrB as a paradigm for Resistance-Nodulation-cell Division (RND) superfamily proteins

RND proteins represent the energy module and the substrate specificity determinant of the tripartite RND/MFP/OMF efflux system. The most extensively studied RND proteins are MexB of *P. aeruginosa* and AcrB of *E. coli*. In 1965, the locus coding for *acrA* and *acrB* was identified (134). Upon mutation of one of these genes, susceptibility towards acriflavine was increased (*acr*iflavine resistance protein *A* and *B*). The inner membrane protein AcrB confers resistance to a variety of chemical unrelated compounds. The substrate specificity of AcrB compared to the many other MDR proteins is staggering. It includes dyes, bile salts, organic solvents and antibiotics of different chemical classes; molecules that are anionic, cationic, zwitterionic, aromatic or just aliphatic; chemicals of bulky or planar geometry. Some

of the restrictive features might be the size and the hydrophobicity, since to our knowledge there has been no report of an AcrB substrate with a molecular weight larger than 1000 Da and to be more hydrophilic than $logP_{OW}$* of -0.3[4]. However, since export of membrane lipids and cofactors such as flavonoids is expected to be lethal for bacterial cells, additional criteria to discriminate between noxious compounds and vital cell constituents must exist, a matter of ongoing research. Like most proteobacterial RND proteins, AcrB consists of twelve transmembrane α-helices and two extensive periplasmic loops which account for approximately half of the protein's 1049 amino acids. The loops connect TM1 with TM2 and TM7 with TM8, respectively. The topology of the transmembrane domain – five-plus-one-transmembrane helices, repeated twice – is also referred to as RND signature (135). The repetition of the motif suggests that RND transporters arose as a result of an intragenic tandem duplication event (136,137). Indeed, the archaeal RND transporter MJ1562 from *Methanococcus jannaschii* codes for a protein comprising only 372 amino acids, corresponding to six TMs and one extensive extracellular loop that connects TM1 with TM2. Moreover, MexB from *P. aeruginosa* remains active when its N- and C-terminal halves are expressed as two separate proteins (138).

It appears that the substrate specificity determination is residing in the periplasmic loops, which was shown by designing chimeric proteins. Specifically, the two extracellular loops of AcrD were replaced by the periplasmic loops of AcrB (139). The resulting transporter exhibited a resistance pattern that was typical for AcrB. Conversely, when the periplasmic loops of AcrB were replaced by the corresponding domains of AcrD, the chimeric protein lost the ability to confer resistance towards substrates of AcrB, but the resistance towards aminoglycosides – which are substrates of AcrD – was enhanced.

Domain swapping experiments between MexB and MexY led to similar results (140). Here, the periplasmic loops of MexB were combined with the transmembrane domain of MexY. Again, the resulting protein conferred resistance towards typical MexB substrates, while the cells where susceptible towards MexY specific drugs.

Additional evidence on the role of the periplasmic domain in substrate specificity determination came from a study where six single site mutations causing altered substrate specificity were all found to be located on the extracellular loops (141).

[4] P is the partition coefficient of a given solvent in an equimolar octanol-water mixture. $logP_{OW}$ of -0.3 is the experimental partition coefficient of tetracycline (http://www.drugbank.ca/)

Crystallographic studies provided further insights on the role of the periplasmic loops in substrate recognition and transport (40,41,142).

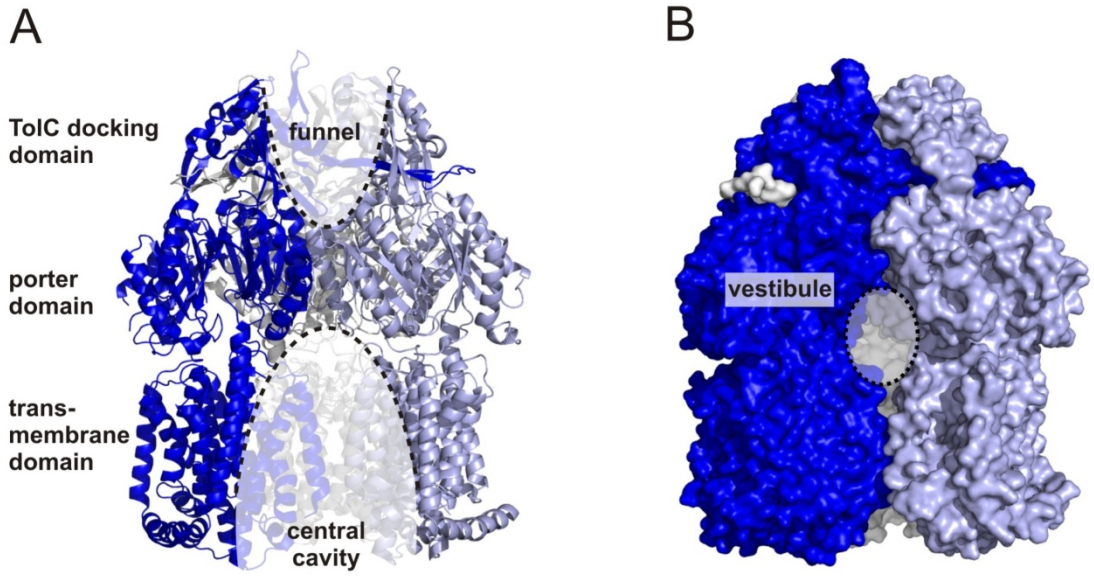

Figure 7: Side view of trimeric AcrB. The monomers are colored in different shades of blue. **A)** Three pore helices located in the central part of the porter domain separate the funnel from the central cavity. The different domains are indicated. **B)** The central cavity is accessible to solvent *via* vestibules formed at the interface of two monomers. Pictures were made using the pdb coordinate file 1IWG.

The first AcrB structure ((143), PDB entry: 1IWG) was based on 3.5 Å X-ray diffraction data from crystals containing one unliganded AcrB monomer in the asymmetric unit. The trimer therefore contains due to the crystallographic symmetry three monomers with exactly the same conformation. Each monomer includes a transmembrane domain with twelve TM helices which form a bundle with two central helices (TM4 and TM10) in its topological core. On these central α-helices, three titratable residues, the D407/D408/K940 triad, were found to be essential for protein function (144-146) (**Figure 8**).

The periplasmic part – formed by the periplasmic loops described above - extends 70 Å into the periplasm. It can be further divided into a TolC docking domain which is most distal from the membrane plane and a porter domain, formerly known as pore domain (**Figure 7**).

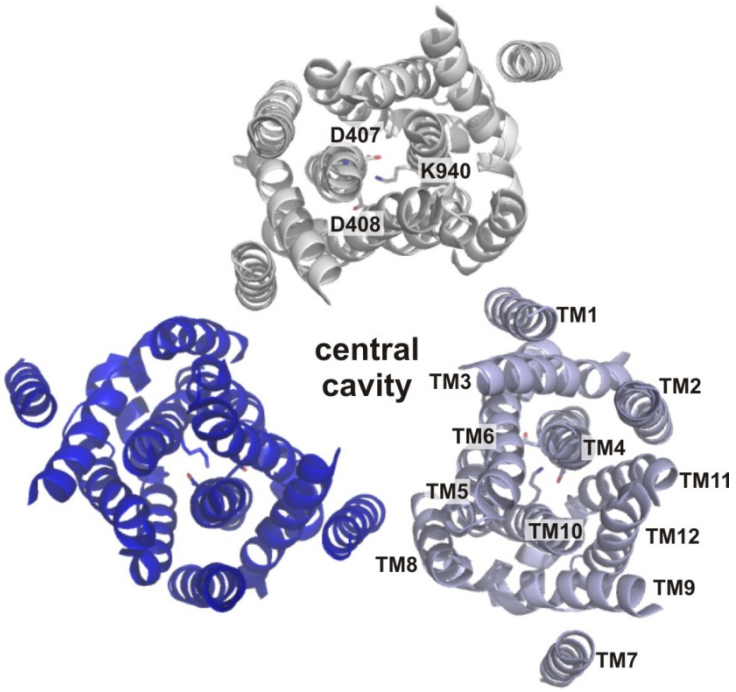

Figure 8: Transmembrane domain of trimeric AcrB viewed from the periplasm. D407, D408 and K940, three of the four essential charged residues (the fourth being R971 on TM11) of the transmembrane domain are depicted. They are located on TM4 and TM10, which are surrounded by the remaining helices of the monomer and are referred to as triad. Picture was made using pdb coordinate files 1IWG.

The TolC-docking domain is the expected interaction site of the outer membrane channel TolC (112,147-149). The TolC docking domain of each monomer furthermore exhibits a hairpin-like loop that protrudes into the neighboring monomer, which appears to be the main stabilizing factor for the trimeric AcrB complex.

The porter domain is divided in subdomains PN1, PN2, PC1 and PC2, which are coupled by sequential proximity (PN1-PN2, PC1-PC2) or by sharing β-strands to form common β-sheets (PN2-PC1, PC2-PN1). The PN1 subdomains are located in the centre of the trimer, surrounded by the PN2, PC1 and PC2 subdomains towards the periphery. Between the PC1 and PC2 subdomains a cleft is apparent which is approximately perpendicular to the membrane plane. In the centre of the trimer, the TolC docking domain exhibits a funnel-like structure narrowing to a central pore, defined by α-helices (designated pore helices) of the PN1 subdomains of each monomer. This pore has a small diameter and therefore does not allow drug passage in this conformation (**Figure 9**). Towards the membrane plane, the central pore leads to a central cavity and further to a 30 to 35 Å wide, presumably lipid-filled

transmembrane hole defined by the ring-like arrangement of the TM helices of the trimer (**Figure 8**). Three vestibules at the monomer interface located just above the membrane plane lead towards the central cavity. It is postulated that substrate might access the central cavity *via* these vestibules (143) (**Figure 7**). Indeed, there have been several reports on AcrB/substrate co-crystals with positive densities in the electron density maps derived from (symmetric) R32 crystals that have been interpreted as substrate molecules bound to the inner wall of the AcrB central cavity. (150-154). From there, large synchronous conformational rearrangements were suggested to occur in order to open the central pore, through which substrate would be transported into the funnel (153). This mode of action was called elevator mechanism since substrate was envisioned to be lifted perpendicular to the membrane plane directly from the central cavity *via* TolC into the media.

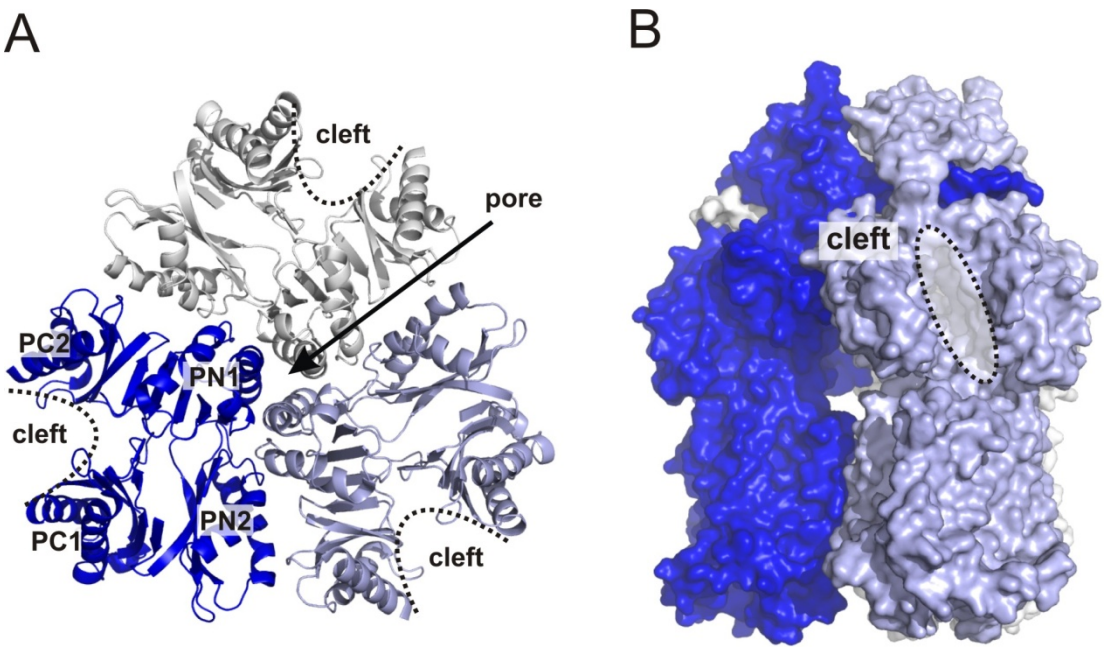

Figure 9: Porter domain of trimeric AcrB. **A)** The porter domain viewed from the periplasm. The PN1, PN2, PC1 and PC2 subdomains are indicated. Three α-helices donated by the PN1 domain of each monomer define the central pore. At the periphery, a cleft is formed at the interface of the PC1 and PC2 subdomains. **B)** Side view of trimeric AcrB. Pictures were made using pdb coordinate files 1IWG.

In 2006, three groups independently published an asymmetric structure of AcrB grown in the monoclinic space group C2 (40,41,142) (2.8 to 2.9 Å), the triclinic space group P1 (41) (3.0 Å) and an AcrB structure including bound designed ankyrin repeat proteins (DARPins) grown in the orthorhombic space group $P2_12_12_1$ (142) (2.5 Å).

The DARPin bound AcrB structure was almost identical to the AcrB structures crystallized without binder with root mean square deviation (rmsd) of the superimposed trimeric structures ≤ 1 Å. The DARPin molecules only bind to the loose and the tight conformers, resulting in a ratio of two DARPin molecules per AcrB trimer. This stoichiometry was verified by sedimentation velocity experiments, suggesting that in solution and probably also *in vivo* AcrB adopts mainly the asymmetric conformation (142).

Within the AcrB trimer, each monomer has a different conformation denoted as loose, tight and open (access, binding and extrusion, respectively) (40,41), while the loose state is closest to the conformation of the monomers in the symmetric structure (143). Compared to the conformation of the symmetric structure, the tight protomer has an up-shifted PN1 subdomain, the transmembrane helices are elevated up to 3 Å towards the periplasmic part and at the interface of the PN2/PC1 subdomains, a hydrophobic pocket is present that is not apparent in the other two conformers (**Figure 12**).
Hallmarks of the open monomer are a coil-to-helix transition at the N-terminal part of TM8, tilting of the PN1 subdomain including the pore helices towards the neighbouring protomer and the PC2 subdomain approaching the membrane plane by 6.5 Å (**Figure 10**). Although the pore helices are differently oriented in the asymmetric structure as compared to the symmetric structure, the pore diameter is similar and hence there does not appear to be an opening of the central pore. Instead, conformer specific cavities and tunnels could be identified in the porter domain. In the loose conformer, a tunnel (tunnel 2) starts in the PC1/PC2 subdomain cleft approximately 15 Å above the membrane plane and protrudes in the direction of the pore. In the tight conformer, an additional tunnel (tunnel 1) with an entrance situated in a groove formed by TM8 and TM9 at the height of the membrane plane is apparent (**Figure 11**).

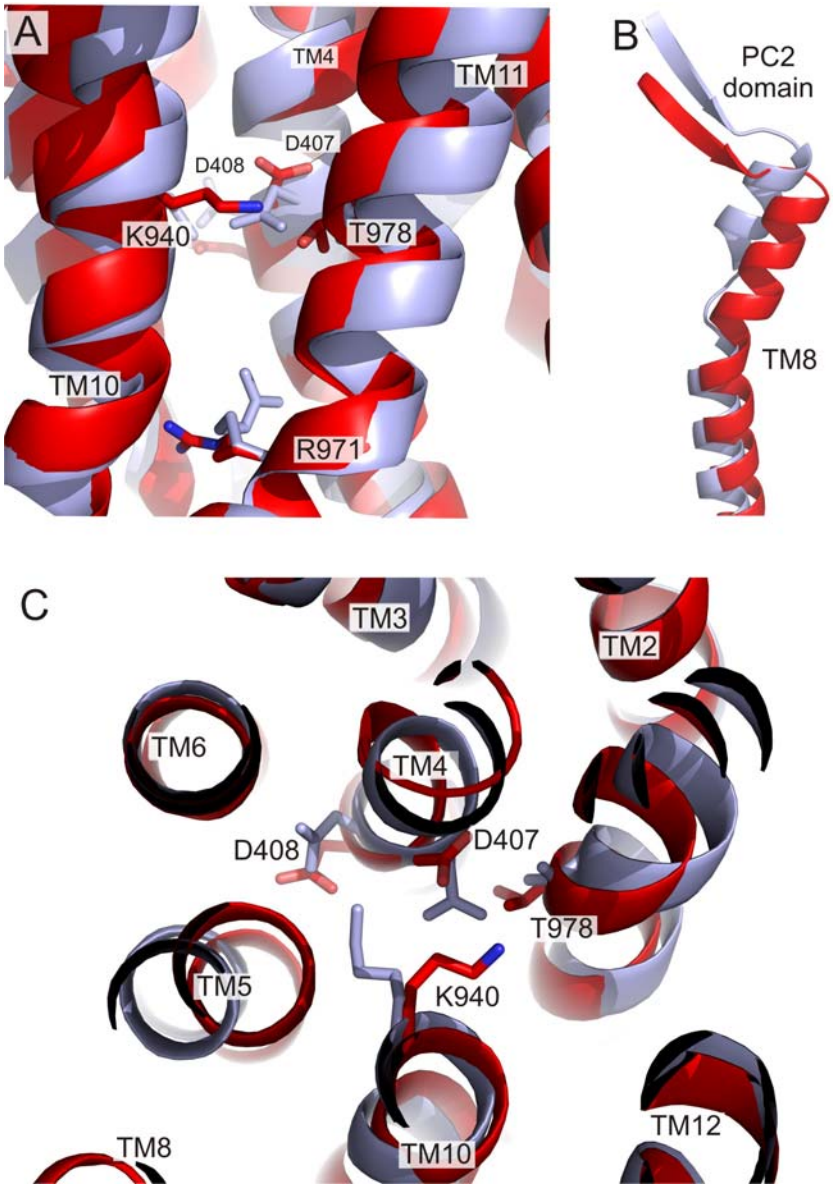

Figure 10: Main structural differences between the AcrB monomers loose, tight (both in light blue) and open (red). **A)** Side view of the proton relay. In the loose and tight state, D408 and D407 sandwich K940 and R971 is oriented towards the triad. The polar side chains of D407, D408, K940 and T978 are forming a continuous hydrogen bonded network. Upon transition to the open state, this network gets disrupted: K940 bends towards T978 and D407 reorients towards the periplasm. Additionally, R971 relocates in the direction of the cytoplasm. **B)** During the transition from tight to open state, there is a coil-to-helix transition at the N-terminal end of TM8. As a consequence, the PC2 subdomain is repositioned and approaches the membrane plane by 6.5 Å. The N-terminal end of helix 8 and the C-terminal β-strand of the PC2 subdomain are shown. **C)** Top view of the triad from the cytoplasm. In addition to the drastic reorientation of K940 (as discussed in (A)), a bulging of TM5 towards TM4 and TM10 can be observed. The open and the loose monomer are colored in red and blue, respectively. The corresponding structural details of the tight momomer are very similar to the loose monomer. The pictures were generated by superimposition of the loose and the open monomer. The pdb coordinate file 2GIF was used for figures A) and B), and 2J8S for figure C).

Due to reorientation of the PN2 subdomain in the tight monomer, a hydrophobic pocket at the interface of PN2 and PC1 subdomains is created. This pocket is situated close to the end of the tunnel in the tight conformer (defined by the PN1 subdomain of the adjacent open monomer) and is rich in aromatic amino acids, a feature that is often observed for binding pockets of MDR proteins (39,155-157) (**Figure 12**). Indeed, Murakami *et al.* detected electron densities for the AcrB substrates minocycline and doxorubicin in the hydrophobic pocket. By using a brominated derivative of the former compound (9-bromo-minocycline), they unambiguously could assign the position of this substrate within the binding pocket (40) due to the anomalous signal produced by the bromine atom in the X-ray diffraction experiment.

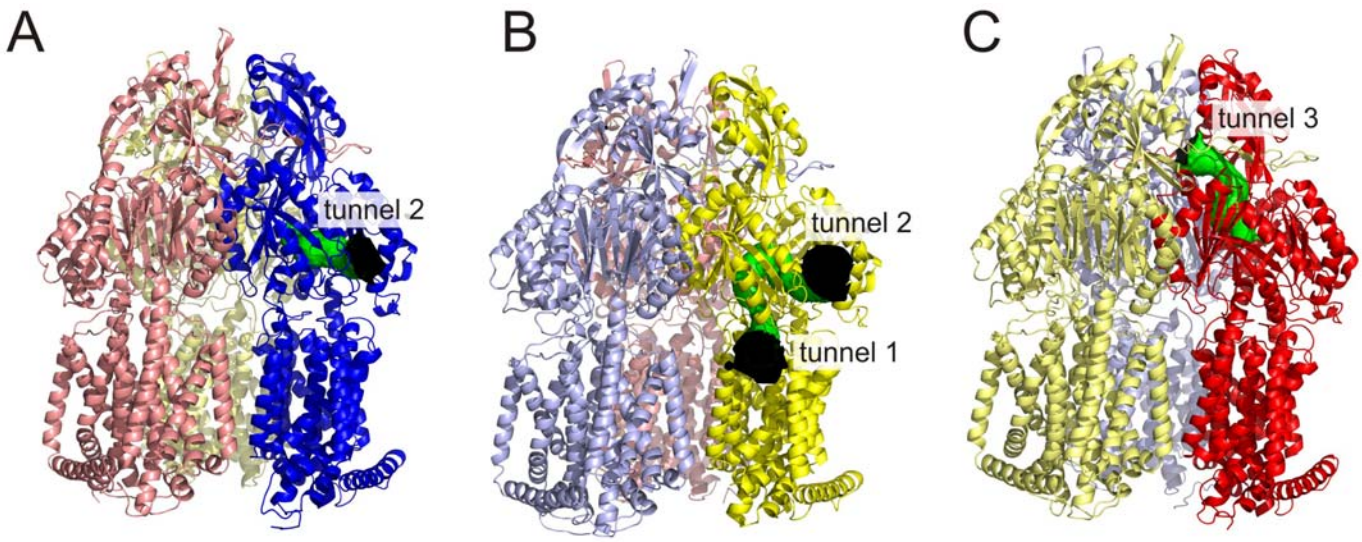

Figure 11: Visualization of tunnels in the porter domain of the different monomers. **A)** In the loose monomer, tunnel 2 leads from the entry situated in the cleft about 15 Å above the membrane plane towards the centre of the periplasmic porter domain. **B)** An additional tunnel (tunnel 1) is apparent in the tight conformer. This tunnel starts at the height of the membrane plane and joins tunnel 2 near the binding pocket, which is open in the tight conformer. **C)** Due to dramatic reorientation of the subdomains and the coil-to-helix transition at the N-terminal end of TM8, both lateral tunnels are closed in the open conformer. Instead there is a new tunnel (tunnel 3) which leads from the collapsed binding pocket to the funnel in the centre of trimer. The figures were made using pdb coordinate file 2J8S. Tunnels were calculated by the program Mole (158).

In the open monomer, the lateral periplasmic entrance of the tunnels observed in the loose and tight conformations are closed due to the coil-to-helix transition of TM8,

whereas another tunnel (tunnel 3) is created due to tilting of the pore helix (PN1 subdomain). The latter tunnel leads from the now collapsed binding pocket to the funnel located in the centre of the AcrB trimer.

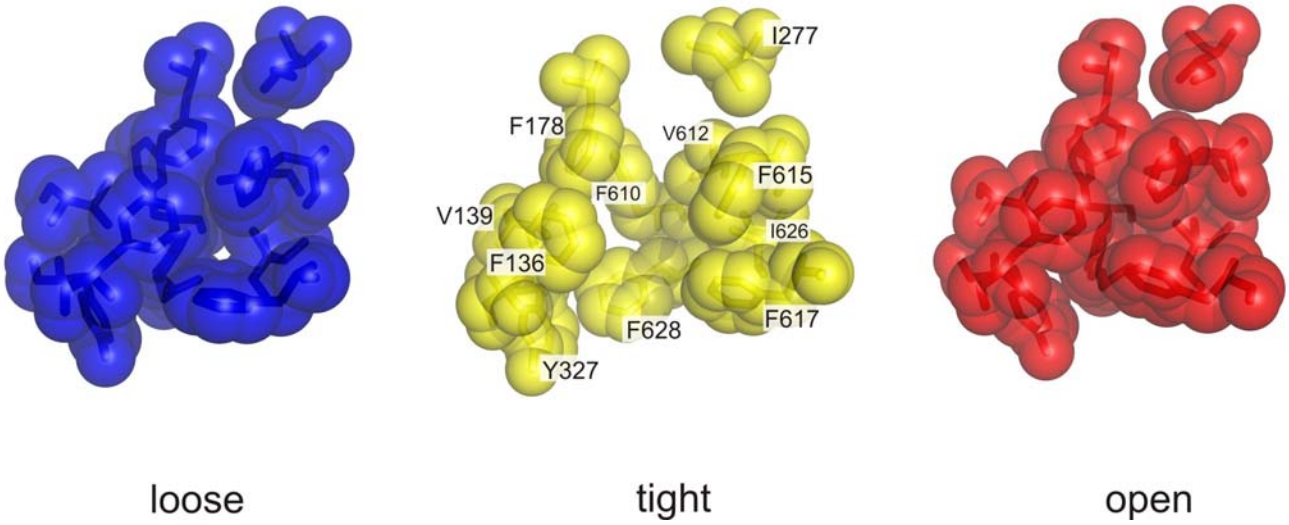

Figure 12: Binding pocket in different monomers of the AcrB trimer. At the interface of the subdomains PN2 and PC1, a hydrophobic binding pocket is located close to the end of tunnel 1 and 2. The binding pocket is open only in the tight monomer. Picture was made by using pdb coordinate file 2GIF.

Substrate transport by AcrB was postulated to be accomplished *via* functional rotation in which each monomer changes its conformation in a concerted fashion (40,41). One transport hypothesis assumes the substrate to be garnered from the outer leaflet of the inner membrane. It might enter the loose monomer *via* the TM8/TM9 groove or *via* tunnel 2 approximately 15 Å above the membrane plane. While it is not clear how hydrophobic compounds might enter tunnel 2 once these have been partitioned in the inner membrane, several groups provided structural data of symmetric AcrB (where all the monomers adopt the loose conformation) based on 3.2-3.8 Å data with presumably bound AcrB substrates in the tunnel 2 region (151,159). High resolution (2.5 Å) data describing the asymmetric trimer show clear densities in the TM8/TM9 groove of the loose monomer, which has been attributed to the highly concentrated detergent and AcrB substrate n-dodecyl-β-D-maltoside (142). Upon conformational change from the loose to the tight state, tunnel 1 appears and might provide one of the pathways for substrates towards the hydrophobic pocket which accommodates the substrate molecule. Structural flexibility within the trimer (160,161) suggests that the

loose and even tight conformational states might be adoptable in the absence of substrates and that substrate binding to the hydrophobic pocket specifically stabilizes the tight conformation. This might also present an alternative role for tunnel 2 in these conformations as an exit pathway for compounds which are not substrates of the pump (**Figure 11**). In analogy with the binding change mechanism (162), the conversion of the tight monomer to the open monomer is energy consuming and subject to bi-site activation i.e. only occurs upon binding of substrate to the neighboring monomer (163).

Upon transition from the tight to the open state, the binding pocket closes again; substrate is squeezed out and follows a newly formed tunnel (tunnel 3) to the funnel, and is from there finally extruded into the media *via* TolC.

In summary, upon conformational change from loose to tight to open and back to loose, an alternating access tunnel is formed through which substrates are transported from the outer leaflet of the inner-membrane towards the outside medium. The mode of action is suggested to be based on occlusions migrating from the lateral entrance(s) to the central funnel and is reminiscent of a peristaltic pump.

To test the proposed conformational cycling *in vivo*, subdomains that undergo substantial rearrangement during cycling were locked by the introduction of disulfide bonds (160,161). As could be demonstrated by tracing the efflux of a fluorescent substrate, formation of disulfide bonds significantly decreased AcrB mediated transport. When the disulfide bonds were broken by the addition of the reducing reagent dithiothreitol (DTT), transport activity was restored, which was in strong support of the functional rotation mechanism (160). Even more convincing, Takatsuka and Nikaido designed a functional covalently linked AcrB trimer, which could be inactivated by the introduction of a mutation in the proton relay network (D407A) or by disulfide formation in only *one* of the protomers (164). These results are in accordance with the proposed functional rotation mechanism.

As a secondary active transporter, AcrB couples the efflux of substrate to the influx of protons from the periplasm to the cytoplasm. Besides the four essential charged residues D407, D408, K940 and R971, T978 is also thought to be involved in mediating passage of the proton through the transmembrane domain (145). Therefore, these five residues are denoted as proton relay. Indeed, the observed alterations in the orientation of these residues in the different states of the functional rotation might be indicative for protonation and deprotonation events: K940 is sandwiched between

D407 and D408 in the loose and tight states, but gets reoriented towards T978 in the open state; R971 is oriented towards D407 in the loose and tight state, but points in the cytoplasmic direction in the open monomer; D407 is oriented towards the cytoplasm in the loose and tight state, but bends towards the periplasm in the open state. Furthermore, the N-terminal end of TM8 in the loose and tight monomers is marked by Pro874, but gets elongated by four full turns in the open monomer and a bulging of TM5 towards TM4 and TM10 in the open conformation can be observed. How these conformational changes are levered to the porter domain and cause the large conformational changes observed there is subject to ongoing research.

2.8 Tripartite AcrA/AcrB/TolC complex

To date, there is no structure of the complete assembled AcrA/AcrB/TolC complex or of its homologues available. However, models have been described on the interaction between the components of the tripartite complex which are based on biochemical studies including co-purification, crosslink studies, the design of chimeric proteins, isothermal titration calorimetry (ITC) and crystallographic structure-driven *in silico* docking.

In one study, the interaction between the components of the tripartite MexA/MexB/OprM complex in *P. aeruginosa* was analyzed by a pull-down assay tagging only one of the subunits (165). In the presence of all three components, MexA, MexB and OprM could be co-purified independent of which subunit was tagged, suggesting tight association of the components in the trimeric complex. Additionally the bi-partite MFP/OMF complex MexA/OprM could be co-purified in the absence of MexB (165), whereas co-purification of the bi-partite RND/MFP and RND/OMF complexes failed. In another study the physical proximity between AcrA and AcrB in absence of TolC (149,166,167) and between AcrB and TolC in absence of AcrA (148,166) was shown *in vivo* by using the crosslinker dithio(succinimidylpropionate) (DSP). Physical interaction between AcrA and TolC as well as between AcrA and AcrB was demonstrated by ITC, whereas there appeared to be no measurable interaction between AcrB and TolC (166).

To locate the interaction sites of the MFP MexE with its cognate RND and OMF, a chimeric MexE/MexA fusion protein was designed where the α-helical hairpin domain originated from MexA (168). This mosaic protein could be shown to form a functional complex with MexF and OprM, the cognate OMF of MexA, but lost its ability to interact with OprN, the cognate OMF of MexE. Similarly, the complex AcrA/AcrB/OprM is functional when the α-helical hairpin domain of AcrA is replaced by the corresponding domain of MexA (169).

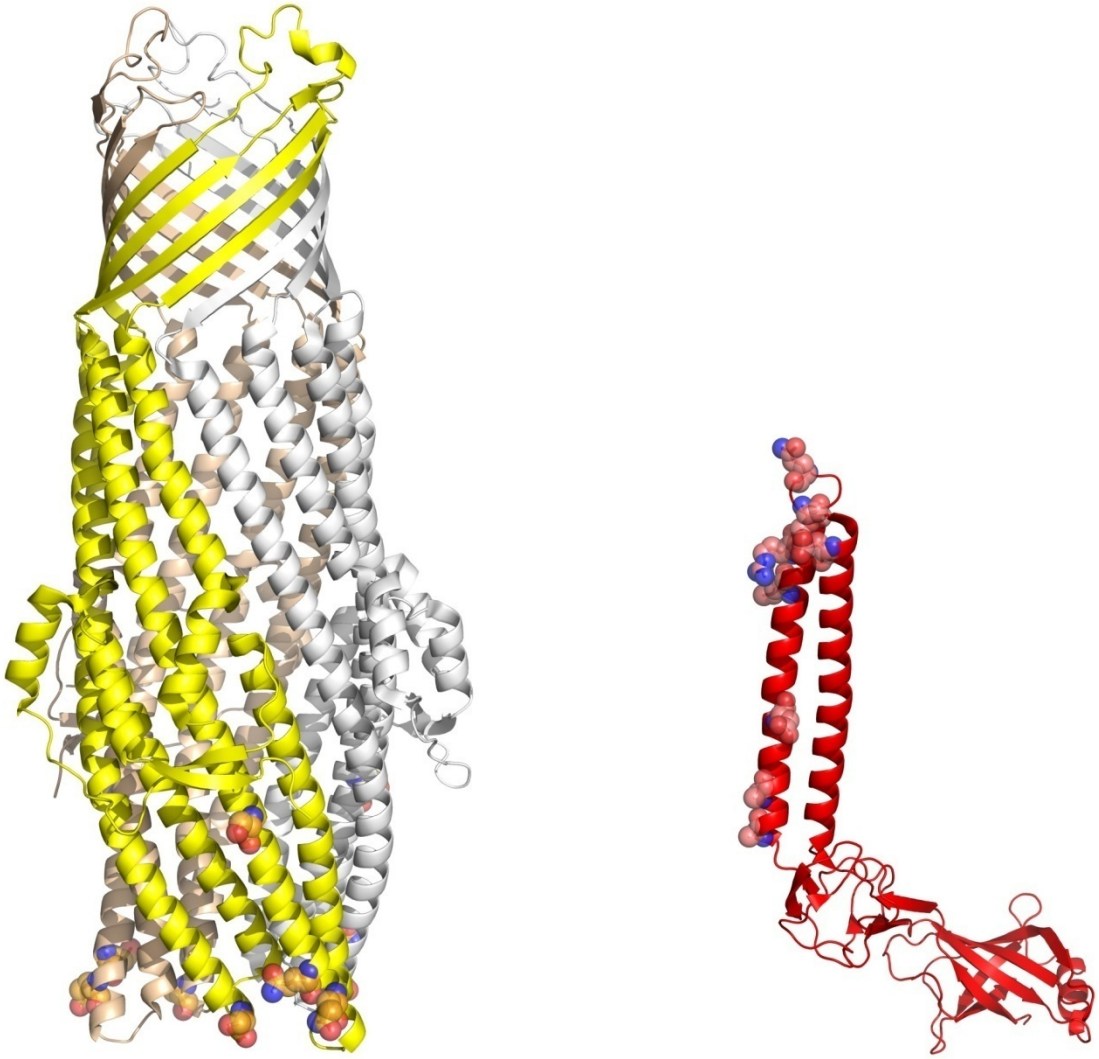

Figure 13: Interaction surface between TolC and AcrA. Four single cysteine mutants of TolC could be cross-linked to wt AcrA by using bi-functional cross-linking agents. Reciprocally, eight single cysteine mutants of AcrA could be cross-linked to TolC. The positions of the mutated residues are indicated with spheres in the wt structure of the two proteins. The monomers of trimeric TolC are colored in different shades of yellow. Coordinate file of TolC: 2VDD, Coordinate file of AcrA: 2F1M.

The interaction surface between AcrA and TolC was investigated in detail by cysteine scanning of both proteins (170). Crosslink experiments followed by co-purification revealed that AcrA contacts TolC at the outer surface of the channel between the tip of the closing aperture and the equatorial domain. For AcrA, residues of the helix α1 of the α-helical hairpin domain exhibiting appropriate orientation are involved in contact formation (**Figure 13**).

The interaction between the RND and MFP component was analyzed by construction of chimeric proteins, ITC and crosslink studies. Domains of AcrA were replaced by the corresponding domains of the AcrA paralogue YhiU, which is unable to form a functional complex with AcrB (132). Minimal Inhibitory Concentration (MIC) assays allowed to distinguish between active and non-active chimeras and revealed that interaction between AcrA and AcrB is mediated by the protease sensitive domain (119) between residues 290 and 357. This stretch roughly corresponds to the MP domain of MexA (121) and had to be removed in AcrA to allow crystal formation (110,119,120). CD spectroscopy revealed that the C-terminal part of AcrA is largely unordered (but not unfolded). However, ITC analysis indicated strong association with AcrB, whereas no interaction between the AcrB and the N-terminal half of AcrA could be detected (166).

The lack of structural information on the C-terminal domain of MFPs (i.e. AcrA and MexA) was for long time the main obstacle in building an assembled model of a trimeric MFP/RNF/OMF complex. Different stoichiometric ratios between MFP:RND:OMF were proposed, i.e. 4:1:1 (110), 3:1:1 (120), 2:1:1 ((110,169)) and 1:1:1 (170). The latter suggestion was found by two molecular docking approaches to be the only ratio that satisfies the restriction revealed by cysteine scanning experiments (121,170) (**Figure 14**). Furthermore, a leaky mutant of TolC was crystallized exhibiting a novel asymmetric conformation in a partly open state (112). In each TolC monomer, a shallow external groove extending from the closing aperture to the equatorial domain was identified. Since this area interacts with AcrA as was shown by crosslink studies (170), Bavro *et al.* suggested that three grooves of trimeric TolC accommodate one AcrA molecule each. Unlike previous suggestions, crosslink studies between AcrA and AcrB revealed that the contact surface of the two proteins is located on the PN2 subdomain of AcrB rather than in the cleft situated between the PC1 and PC2 subdomain.

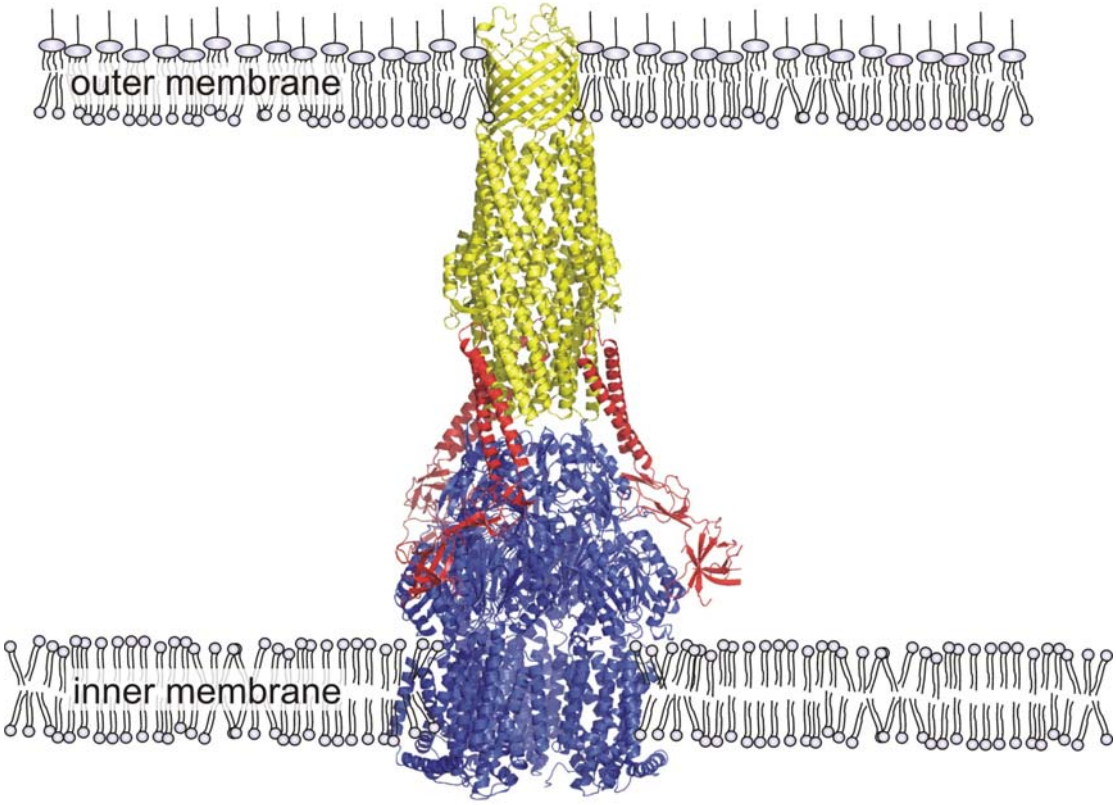

Figure 14: Putative assembly of the AcrA/AcrB/TolC complex. AcrB and TolC reside in the inner and outer membrane of Gram-negative bacteria, respectively. AcrA (red) functions as an adapter and connects AcrB (blue) with TolC (yellow). A ratio of 1:1:1 of the three proteins was found to be the most probable stoichiometry based on two molecular docking approaches considering the results from cysteine crosslink studies (121,170). AcrA might control opening and closing of the distal end of TolC and transduce the energy generated by AcrB to the OMF. This would allow TolC to convey substrate unidirectionally into the outer space.

Since AcrB is postulated to undergo a functional rotation (40,41,160), the interaction between each AcrB monomer and its affiliated AcrA molecule would be nonequivalent. Hence, the subtle conformational changes observed in TolC would be caused by induced fit interactions between AcrA and TolC. Rather than just being an rigid adapter, AcrA would actively transduce the energy generated by AcrB and induce the coordinated substrate transport through TolC. Similar to the tunnels observed in a single AcrB protomer during functional rotation (40,41), TolC is probably not a rigid hollow cylinder but changes its diameter by conformational change of each monomer, thereby pushing substrate unidirectionally from the closing aperture into the media (163,171,172).

2.9 Multispecificity

AcrB is known to transport a plethora of structurally and functionally unrelated compounds. This broad substrate specificity, a common feature for MDR transporters, contrasts dramatically with the narrow chemical specificity of the vast majority of ligand-binding proteins and the tight interaction between enzymes and their cognate substrates. Therefore, alternative transport mechanisms as how to expel drugs from the cell interior without an intermediate binding step were discussed, including formation of discontinuities in the lipid bilayer and „slippery" protein-lipid interfaces (29).

The first structural data available for a multidrug binding protein in complex with one of its multiple substrate was from a truncated version of BmrR (BRC) binding tetraphenylphosphonium (TPP) (155). BmrR is a soluble *B. subtilis* regulator of the MerR family that activates transcription of Bmr, an MDR transporter of the MF superfamily (173). BmrR is known to be induced by the same chemical compounds that the transporter Bmr confers resistance to. Binding of substrate by BmrR was shown to take place in a pocket that is partly solvent-inaccessible in the apo form. Binding is mediated by stacking interactions with aromatic residues, van der Waals contacts with multiple hydrophobic side chains and neutralization of the positive charge by a glutamate.

In 2001, the crystal structures of six QacR/drug complexes were published by Schumacher *et al.* (QacR in complex with rhodamine 6G (R6G), ethidium, dequalinium, crystal violet, malachite green and berberine, respectively) (39). QacR of *Staphylococcus aureus* regulates the transcription of the MFS transporter QacA and is a repressor of the TetR family (174). Like BmrR, QacR is induced by the same chemical compounds that its target gene (*qacA*) confers resistance to. QacR consists of nine α-helices, three of which form the DNA binding domain, the remaining six form a binding/dimerization domain. The structures were in agreement with the stoichiometry obtained by biochemical experiments of one drug molecule per QacR dimer. In the drug free monomer, an internal cavity of 400 $Å^3$ was detected. Y92 plays an essential role in formation of the protein hydrophobic core. This residue is located on a coil and its aromatic side chain protrudes into the pocket, filling the space

of the collapsed cavity together with two structured waters. In the substrate loaded monomer, the Y92 containing coil undergoes a coil-to-helix transition. As a result, Y92 is expelled from the pocket and accommodates a position towards the solvent region. Additional conformational rearrangements lead to a triplication of the volume of the cavity. These events are thought to be the trigger for the conformational changes in the DNA-binding domain necessary for the dissociation of the dimer from the DNA.

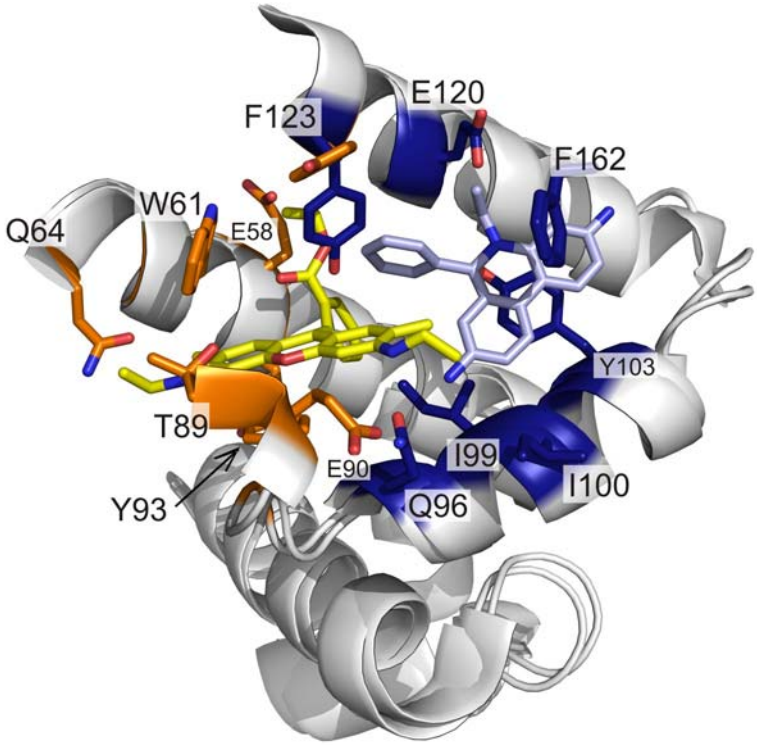

Figure 15: R6G- and ethidium binding pocket in QacR. The two substrates R6G (yellow) and ethidium (blue) interact with distinct residues of the QacR binding pocket (colored orange and blue, respectively). The residues involved in the formation of polar, stacking and van der Waals interaction are depicted. The positive charge of the two substrate molecules is compensated by acidic glutamates E90 and E120. Picture was made by using the pdb coordinate files 1JUS (QacR/R6G) and 1JTY (QacR/ethidium).

The monovalent substrates R6G and ethidium were found to occupy different areas within the binding pocket. The large internal cavity was therefore interpreted as two separate binding pockets, termed ethidium- and R6G pocket. They are partially overlapping yet distinct (**Figure 15**). Key residues in the R6G pocket are the aromatic residues W61 and Y93, in between of which R6G is stacked with the shortest

interatomic distance (SID) between the residues and the drug being 3.5 Å. The polar residues Q64, Q96 and T89 also interact with R6G, with an SID of 3.9, 3.4 and 3.9 Å, respectively. E90 neutralizes the positive charge of R6G, the carboxilic oxygen being 4 Å away from the formal positive charge of R6G. The acidic residues E57 and E58 are also part of the R6G pocket, but do not interact with the drug.

Hallmark of the ethidium pocket are the aromatic residues Y103 and F162 which sandwich ethidium with an SID of 3.3 and 3.7 Å, respectively. I99 and I100 make van der Waals contacts with the drug (SID = 3.4 and 3.7 Å, respectively), the acidic E120 compensates for the formal positive charge of the phenanthridinium ring (SID = 4.0 Å) and Q96 is within hydrogen bonding distance (SID = 2.9 Å) to one of the amine groups of the ethidium ring system. Upon rotation of the side chain, Y123 can make stacking interactions with ligands bound by either the R6G- or the ethidium binding pocket.

Berberine is a planar monovalent cationic drug and gets bound in the R6G pocket. The anthracene ring is stacked in between W61 and Y93 with an SID of 3.6 and 3.1 Å, respectively. The positive charge gets compensated by E57 and E58 (SID = 5.6 and 4.9 Å, respectively). At the other end of the drug molecule, Y123 undergoes stacking interactions (SID = 3.4 Å) and N157 is within hydrogen bonding distance (SID = 3.1 Å) to the dioxolane ring.

The bivalent substrate dequanilium consists of two positively charged aminomehtylquinolinium groups that are linked by a 20.6 Å long decamethylene linker. Consequently, this molecule spans the entire internal cavity and its two positive charges are neutralized by glutamates of both the ethidium- and the R6G pockets. Crystal violet and malachite green, two molecules with propeller-like geometry, are bound in between the two pockets. Hence, QacR is flexible enough to bind mono- and bivalent cationic drugs and can cope with planar chemicals as well as with bulky propeller-like substances (**Figure 19**).

In 2004, Schumacher *et al*. published the structure of the binary complex QacR/proflavine and the ternary complex QacR/ethidium/proflavine. Additionally, the binding affinities of QacR for ethidium and proflavine were determined to be 42 ± 11 and 186 ± 25 μM (156).When both substrates were added simultaneously, the binding affinity for proflavine was not affected (K_D = 35 ± 4 μM) whereas the affinity for ethidium decreased (K_D = approx. 1000 μM). This observation was reflected by

comparing the crystal structure of the ternary QacR/ethidium/proflavine complex with the corresponding binary complexes: whereas proflavine maintained its location in the R6G binding pocket, the position of ethidium was shifted but still accomplished by the same residues.

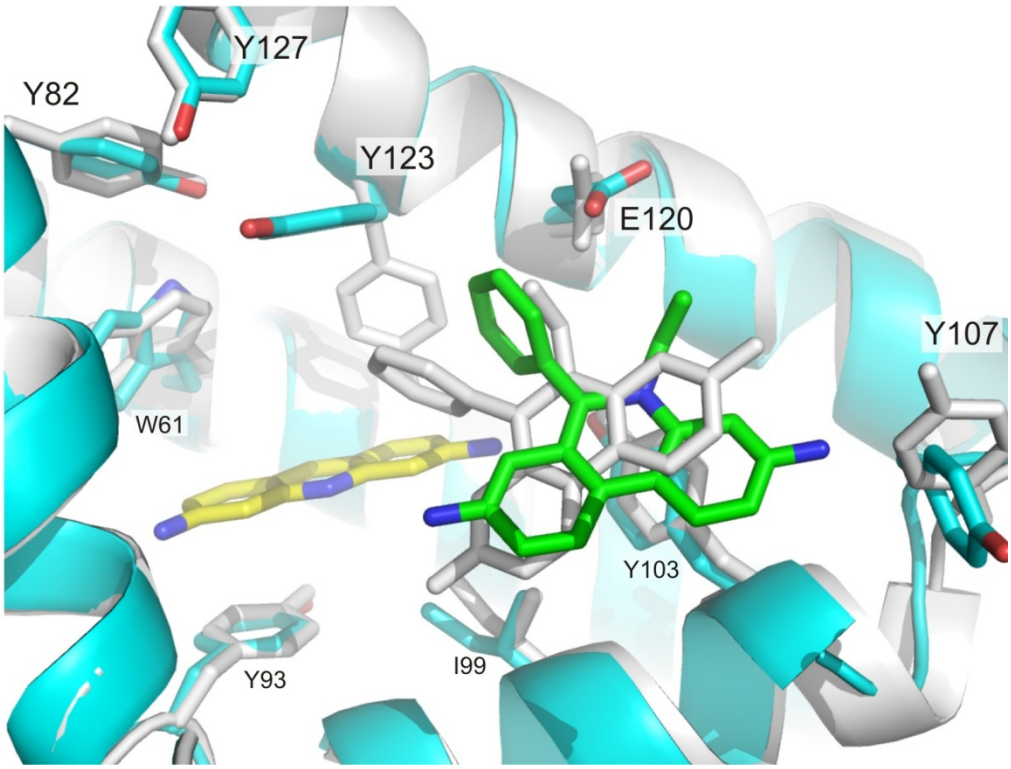

Figure 16: Different orientations of ethidium in the QacR binding pocket. Compared to the binary QacR/ethidium structure, the position of ethidium in the ternary QacR/ethidium/proflavine complex is rotated by approximately 15° along the axis perpendicular to the ring system of ethidium. In this new position, ethidium is engaged in favorable van der Waals interactions with the second substrate proflavine. Ethidium and proflavine of the ternary complex are colored green and yellow, respectively. The binary complex is shown in white. Picture was made using pdb coordinate files 1QVU (QacR/ethidium/proflavine) and 1JTY (QacR/ethidium).

The interatomic distances between ethidium and the binding pocket residues Q96, I100, Y103 and F162 remained constant within ± 0.2 Å, whereas the distance between ethidium and I99 was elongated for 0.8 Å. Y123, which was shown to be involved in binding of proflavine and ethidium in the binary complexes, adopted the conformation observed for the QacR/proflavine binary complex. In this position, it can still form stacking interactions with ethidium. However, the distance between the positive charge of ethidium and the neutralizing E120 was elongated from 4.0 Å to 5.0 Å. Thus, most stacking interactions were maintained, probably at the expense of the

charge-charge interaction. Furthermore, comparison of the ternary and binary complexes demonstrated that by rotation of aromatic side chain residues along their C_α-C_β bonds, substrate can slide inside the pocket while the stacking interactions are maintained (**Figure 16**).

In the same year, Murray *et al.* (157) published the structure of QacR in complex with the bivalent substrates hexamidine and pentamidine. As dequalinium, they belong to the chemical class of diamidines, but differ in the length of the alkyl chain linker (**Figure 19**). Hexamidine binds to QacR in a manner similar to dequalinium, spanning both the R6G- and ethidium pocket and involving a similar set of binding residues. In contrast, pentamidine is twisted and oriented inside the QacR binding pockets in a novel fashion. One benzamidine moiety resides in the R6G pocket, and the charge is neutralized by E63 outside the common binding pocket. The other benzamidine ring protrudes into the core of the protein, interacting with residues which so far were not accounted to be part of the binding pocket.

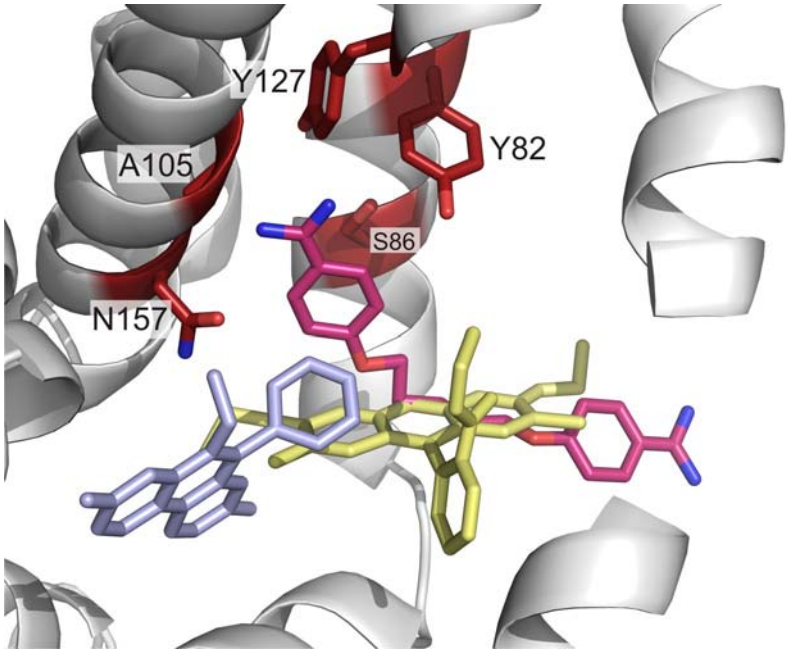

Figure 17: Location of pentamidine in the binding pocket. Pentamidine is twisted inside the QacR binding pocket and one benzamidine ring interacts with residues that neither belong to the R6G- nor the ethidium binding pocket. Remarkably, the positive charge of this moiety is compensated by negative dipoles of polar residues and by cation-π interaction rather than by a formal negative charge. Pentamidine is shown in pink. For comparison, R6G and ethidium are shown in yellow and blue, respectively. Picture was made by using the pdb coordinate files 1RKW (QacR/pentamidine), 1JUS (QacR/R6G) and 1JTY (QacR/ethidium).

Strikingly, the positive charge of the fully buried benzamidine moiety inside this pocket is not compensated by a formal negative charge, but rather by the two negative dipoles of the hydroxyl oxygens of Y127 and S86, the carboxamide oxygen of N157, the carbonyl oxygen of A153 and a cation-π interaction with Y82 (**Figure 17**).

Although E58 compensates the positive charge of berberine in the QacR/berberine structure (39), substitution of E57 or/and E58 in the multidrug binding pocket of QacR counterintuitively increased the binding affinity of QacR for this cationic drug (K_D of wt QacR, QacR_E57Q, QacR_E58Q and QacR_E57Q_E58Q = 2.86 ± 0.62, 1.39 ± 0.15, 0.72 ± 0.08 and 0.32 ± 0.15 μM) (175). The single mutant QacR_E58Q was amenable for crystallization studies and revealed another binding mode for berberine: rather than neutralization of the positive charge of berberine by reorientation of nearby acidic E57, the drug rotates 180° along its long axis (**Figure 18**).

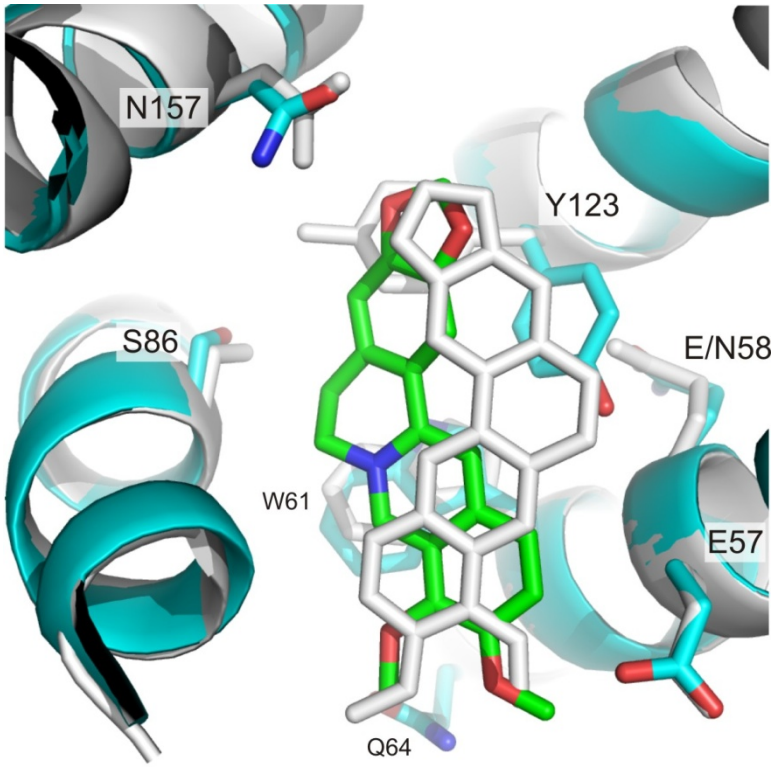

Figure 18: Different location of berberine in the binding pocket of wt and E58N mutant QacR. Compared to the position in the wt protein, berberine is rotate 180° along its long axis in the binding pocket of the QacR_E58N mutant protein. The QacR/berberine complex is shown in cyan and green, respectively. For comparison, the QacR_E58N/berberine complex is shown in white. Picture was made by using the pdb coordinate files 3BTI (QacR_E58N/berberine) and 1JUM (wt QacR/berberine).

In this position, the charge at the pyridinium nitrogen gets compensated by the hydroxyl side chain of S86 (interatomic distance 3.8 Å) and by improved cation-π interactions of the entire molecule with W61 and Y123 (**Figure 18**).

The crystal structures of QacR/drug complexes impressively demonstrated enormous flexibility in ligand binding which might be exemplary for all MDR proteins. So far, densities of ten different compounds could be shown to bind in the extensive QacR binding pocket. The substrates differ in their chemical structure (planar *vs.* propeller-like) as well as in their valence (no charge *vs.* trivalent) (**Figure 19**). A key feature for the vast plasticity of binding pockets of MDR proteins seems to be chemical redundancy. This allows a bound ligand to be shifted or rotated upon binding of additional substrate molecules or mutation of an alleged essential residue. It also may account for the fact that MDR proteins can bind to and transport substrates that the organism has never been exposed to before.

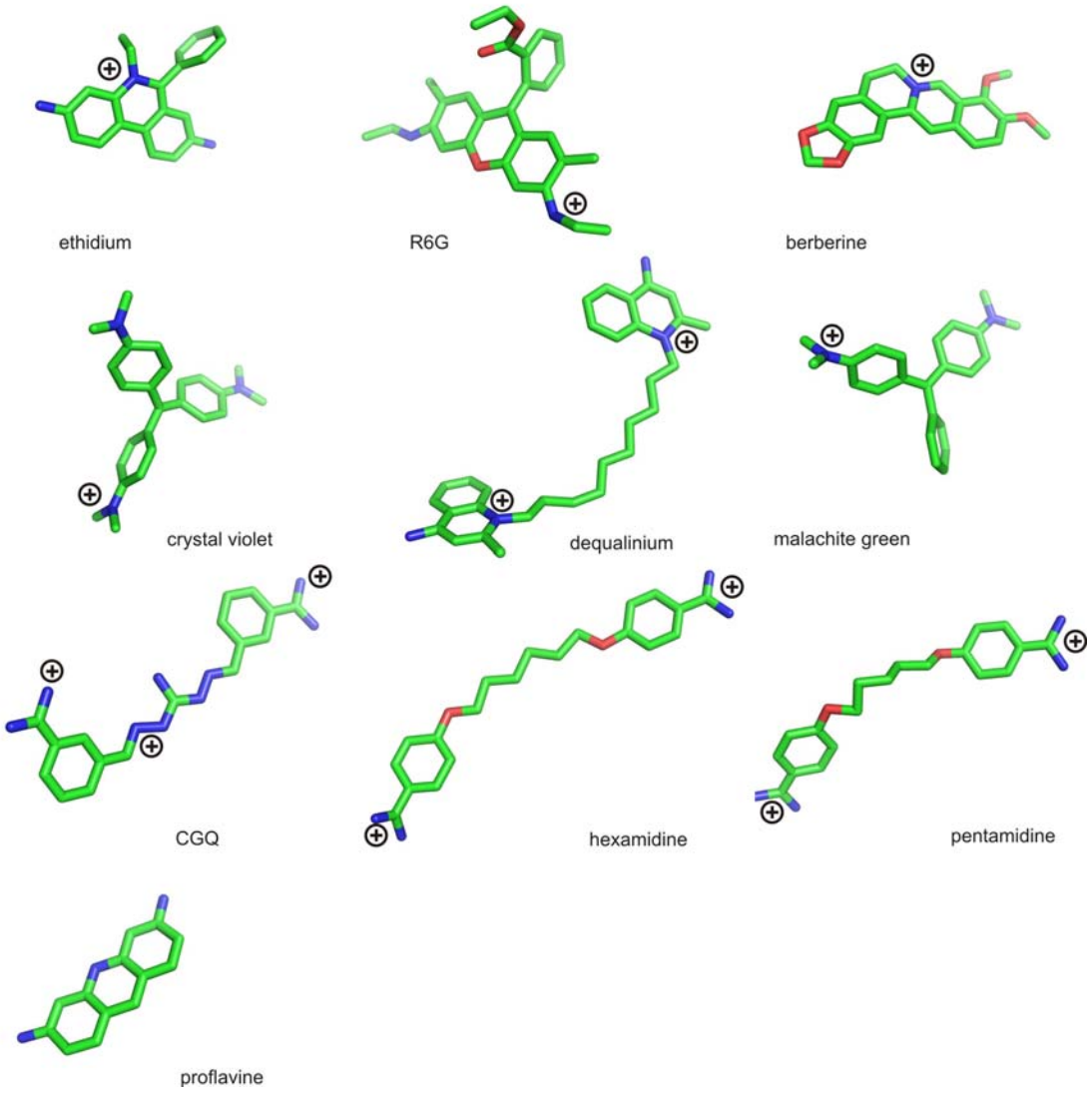

Figure 19: Co-crystallized substrates of QacR. At the moment of writing, QacR was crystallized in the presence of the ten substrates shown above. Note the different valence and geometry of these drugs. CGQ: 3-[C-[N'-(3-carbamimidoyl-benzylidenium)-hydrazino]-[[aminomethylidene]aminium]-iminomethyl]-benzamidium.

2.10 Proton translocation

AcrB utilizes the proton motive force to energize the extrusion of its cognate substrates from the cell into the medium (28,176,177). The transmembrane domain of AcrB harbors four functionally essential charged residues that are conserved throughout the HAE1 family: D407, D408, K940, and R971 (145,146,178). Another highly conserved transmembrane residue, T978, is in hydrogen bonding distance from D407 in the loose and tight monomer and with K940 in the open monomer. However, when T978 was replaced by valine, isoleucin, leucine or asparagine, the relative

activity of these mutants remained 40 to 60% as revealed by drug susceptibility assays (145).

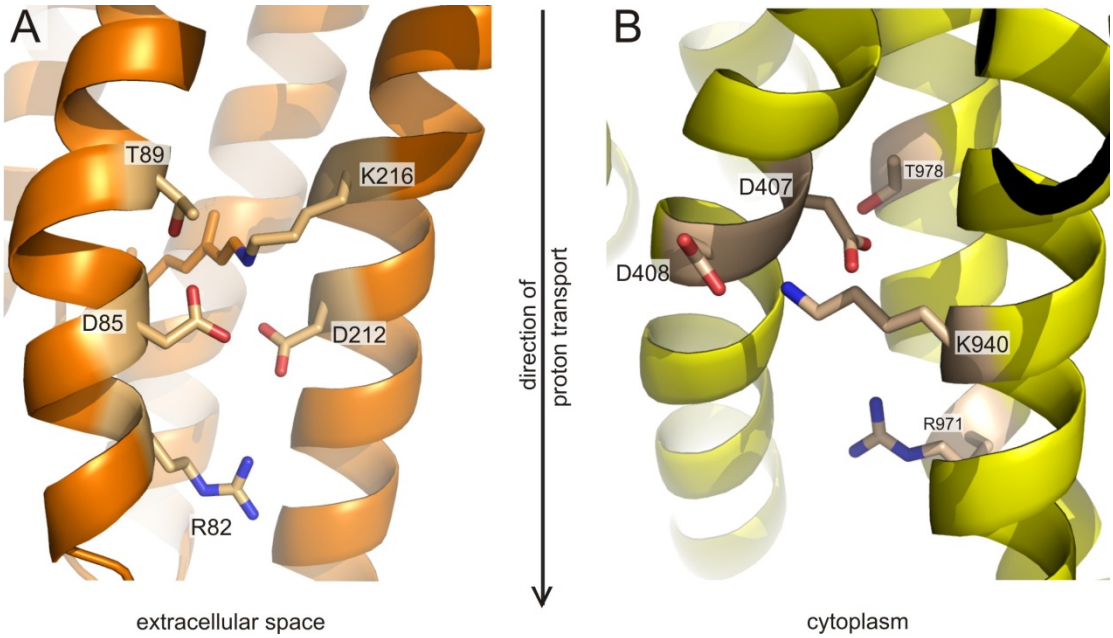

Figure 20: Analogy between the active center of bacteriorhodopsin (BR) and the proton relay of AcrB. **A)** In the ground state of BR, the ε-amino group of K216 (nitrogen atom of the protonated Schiff-base) is located between D212, D85 and in vicinity to T89. Arg82 is located in the hydrated extracellular halfchannel downstream of the proton translocation pathway close to the membrane-extracellular interface. Upon photoisomerisation of the retinal chromophore, the Schiff base becomes deprotonated and the NZ vector bends away from the aspartates. In the M phase of the photocycle, R82 is reoriented away from the Schiff-base towards the membrane-extracellular interface. **B)** In a similar way to K216 in BR, K940 of AcrB is situated between D407 and D408 in the loose and tight state. Protonation and deprotonation events are thought to cause reorientation of K940 towards T978. In analogy to R82 in BR, R971 in AcrB is located in a half-channel close to the membrane-water interface. R971 is oriented towards the proton relay in the tight state and towards the cytoplasm in the loose and tight state. Picture was made using pdb coordinate file 1M0L for BR and unpublished structure for AcrB, respectively.

In the asymmetric structure of AcrB, the four above mentioned essential residues D407, D408 K940 and R971 have distinct different conformations in at least one of the three conformers loose, tight and open (40,41) (**Figure 10**). Mutagenesis and structure suggest that proton translocation is mediated by these titratable residues. Recently, D408 has been shown to be a titratable residue within AcrB with a measured apparent pK_a of 7.4 (179). Up to date, the progression of the protonation and deprotonation events is speculative and awaits further examination. The active

center of the archeal integral membrane protein bacteriorhodopsin (BR), a light driven proton pump intensively studied since its discovery in the early seventies (180), is composed of a set of similar residues (D, K, R) as the proton relay of AcrB (**Figure 20**). Additionally, these residues display an analogous geometry in both proteins. It is therefore tempting to look for structural and functional similarities in the proton transfer pathway between AcrB and the well characterized bacteriorhodopsin.

BR is a rhodopsin-like protein found in the purple membrane of *Halobacterium halobium*. It was shown to be a light-driven proton pump that is not forming functional or structural complexes with other energy-transducing proteins. BR generates an electrochemical gradient of protons resulting in a proton motive force of -250 mV, which corresponds to a difference of four pH units between the intra- and extracellular space (181). BR has seven transmembrane domains and serves as model for the G-protein-coupled receptors (GPCRs). The overall architecture of BR is that of two half-channels, a cytoplasmic and an extracellular one, separated about in the middle of the membrane by the retinal chromophore. The connection between this prosthetic group and the K216 of the (holo) enzyme is accomplished *via* a Schiff base linkage (**Figure 21**).

In the extracellular half-channel, ordered waters and side chain residues form an extensive hydrogen-bonded network, the dynamic properties of which were revealed for many steps of the pumping process by NMR, crystallographic and electron microscope structure analysis.

In contrast to the extracellular half-channel, the cytoplasmic half-channel contains mainly hydrophobic side chain residues and lacks the defined network of ordered waters. Therefore, it remains elusive how the protons are transferred from the cytoplasmic surface to the Schiff base (**Figure 21**).

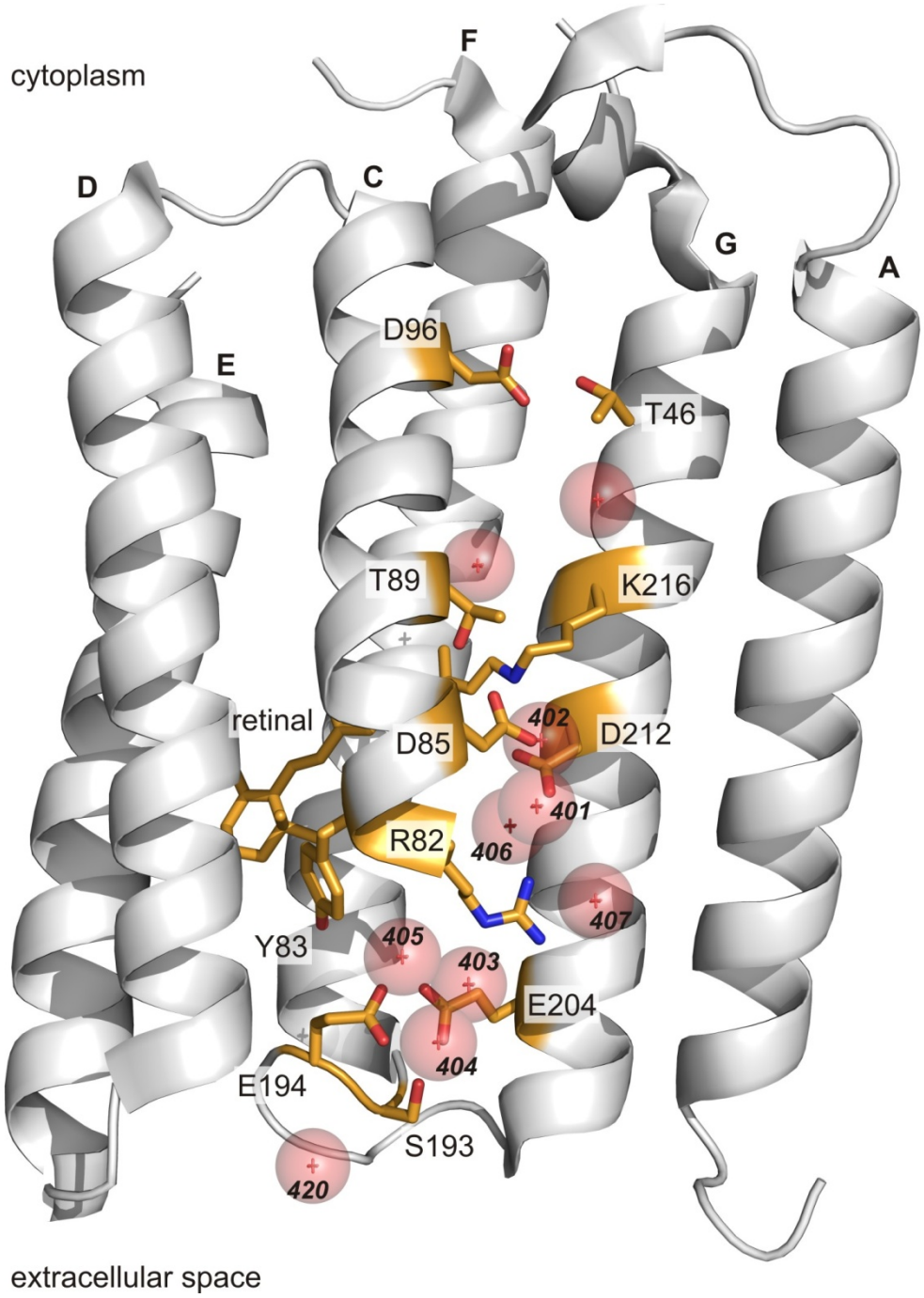

Figure 21: Crystal structure of bacteriorhodopsin in the resting state. The retinal, residues important for proton translocation and structured waters in the extra- and intracellular half-channel are shown. The helices are denoted (A-G). Y185, Y57, helix B and N-terminal part of helix C are omitted for clarity. Drawn from pdb coordinate file 1C3W.

During the transport of a proton across the lipid bilayer, BR adopts the main conformational states denoted as resting state, K-, L-, M-, N- and O- states and numerous substates which were investigated in detail by means of fourier transform

infrared (182-184) and Raman spectroscopy (185,186), solution-state (187) and solid-state (188-190) NMR, X-ray (191-194) and electron spectroscopy (195), using different mutants, varying pH conditions and illumination of BR at different wavelengths.

The interpretation of these data has lead to a model for proton transport by BR (181,196,197). In brief, the energy for the pumping process of a proton against the proton gradient across the lipid bilayer is provided by the absorption of a photon by the chromophore and is initially stored in the strained 13-*cis*,15-*anti* configuration of the retinal in the K intermediate. As the distortion of the retinal and its protein surrounding gradually decreases, the energy is released and transferred in a selective and timed way to the protein, resulting in reorientation of key residues, repositioning of waters and alteration of pK_a of charged residues inside the membrane. This allows the unidirectional transport of protons from the cytoplasm to the extracellular site.

In the resting state (BR), retinal is present in the all-*trans* configuration, the NZ vector[5] of the protonated Schiff base pointing towards the extracellular site. In the extracellular half-channel, the Schiff base donates a hydrogen bond to ordered water W402, which in turn donates a hydrogen bond to ionized D85 and D212. D85, which will be protonated in the first steps of subsequent states, is further hydrogen bonded with T89 and *via* two ordered waters (W401 and W406) with R82. D212, which seems to remain charged throughout the entire cycle, is hydrogen bonded with the phenolic hydroxyl group of Y185 and water W406. A second chain of hydrogen bonds connects D212 to R82 *via* Y57 and water W407 (192,198,199). Finally, E194, E204, S193 and four ordered waters (W403-W405, W420) complete the network of hydrogen bonds towards the extracellular surface (**Figure 21**).

Upon absorption of a photon, the retinal isomerizes in the K (and L) state from all-*trans* to a strained 13-*cis*,15-*anti* configuration, the NZ vector of the Schiff base gradually reorienting towards the cytoplasmic half-channel. This triggers deprotonation of the Schiff base and protonation of D85 during the transition from L to M state. The degree of distortion of the retinal as well as whether W402 is involved in proton transfer from the Schiff base to Asp85 is still debated (200). Protonation of Asp85 leads to disruption of the hydrogen-bonded network of waters in the extracellular half-channel, resulting in the movement of R82 toward the extracellular

[5] the vector originating at the nucleus of the nitrogen atom pointing in the direction of the free electron pair and the proton in the deprotonated and protonated Schiff base, respectively

proton release group (E204, E194 and ordered waters) whereupon a proton is released at the extracellular surface (192,201,202). The biphasic titration behavior of D85 in non-illuminated bacteriorhodopsin indicates that the proton that is released into the extracellular space neither originates from D85 nor from Schiff base directly (201). It is rather assumed that the proton derives from a putative proton release site, probably a $H_5O_2^+$ cluster situated around E204 and E194 (203,204).

Reprotonation of the Schiff base during the transition from the N to O state occurs from the intracellular space and presumably involves the proton donor D96, which is situated approximately in the middle of the inner half-channel. In the resting state, there is no obvious pathway of the proton neither from the cytosol to D96 nor from D96 to the Schiff base due to a lack of polar and charged residues and the absence of a continuous file of waters (**Figure 21**). However, by illumination of a E204N BR mutant crystal, a late M state was simulated in which the Schiff base is deprotonated and D85 is protonated (1.9 Å resolution, nearly full occupancy, i.e. ≥ 93% of all molecules within the crystal adopted the late M state conformation). In this step of the photocycle, electron densities for two additional water molecules could be detected in the surrounding of D96. These are thought to lower the pK_a of D96 due to hydration and partially fill the gap between D96 and the Schiff base (205).

A similar intermediate was observed with an illuminated wt crystal diffracting to 2.25 Å and an observed occupancy of 35% (206). An even larger chain of hydrogen bonded waters could be detected which extends from D96 within 5.8 Å of the Schiff base.

By illumination of the mutant V49A BR crystal (diffracting to 1.62 Å), a late N intermediate could be obtained at 37% occupancy where both the Schiff base and D96 are (re)protonated. This structure revealed a single-file hydrogen bonded chain of waters, extending from D96 to the retinal Schiff base (194). In this intermediate, retinal adopts a relaxed 13-*cis*,15-*anti* configuration and the NZ vector of the Schiff base points towards the cytoplasmic half-channel (**Figure 22**).

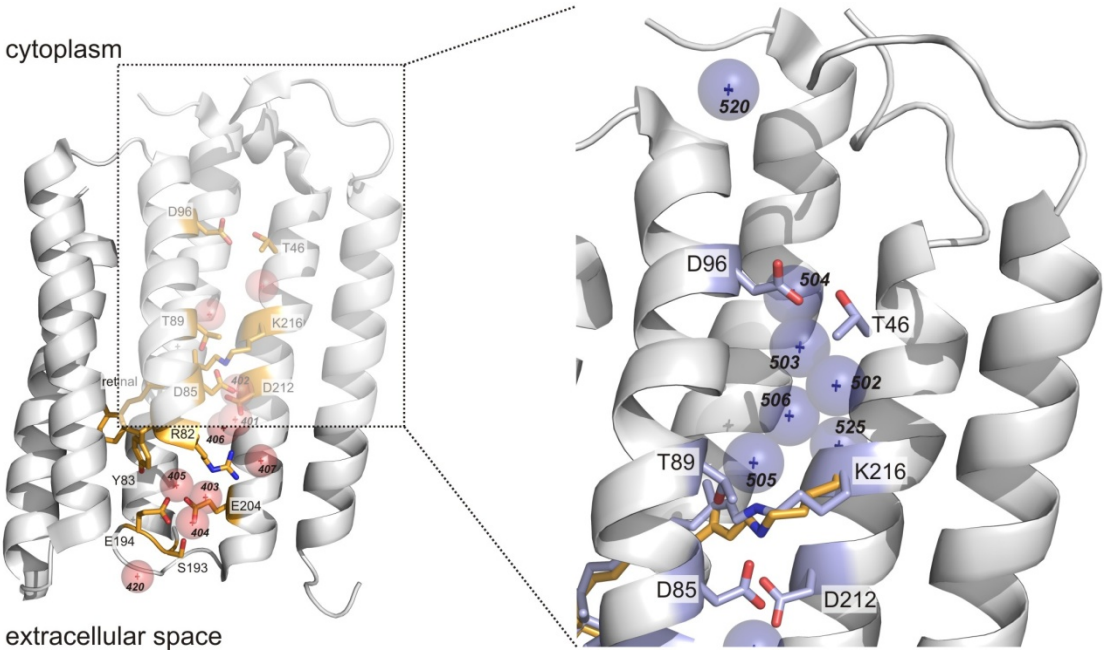

Figure 22: Water molecules in the cytoplasmic half channel of the bacteriorhodopsin V49A mutant. The inset shows the continuous file of water molecules (colored blue) between D96 and the Schiff base in the N state of the photocycle. The structure of the all-*trans* retinal of the resting state is shown in orange. The side chain of mutated V49 would protrude between the water molecules 505 and 506. For comparison, the structure of wt bacteriorhodopsin in the resting state is shown on the left. Figure prepared with pdb coordinate files 1C3W and 1P8H for wt and V49A mutant BR, respectively.

Trials to obtain a crystal structure of an early N intermediate, in which D96 is deprotonated, were unsuccessful. It is also unknown how the cytoplasmic half-channel rearranges to allow for the transfer of the proton from the cytoplasmic surface to D96. However, two water molecules were identified (W520 and W504) at the cytoplasmic surface and close to D96 which might be the first and last members of a continuous chain, formed as a result of protein conformational fluctuation in the N state (194,207).

In the O intermediate, D96 is reprotonated from the cytoplasm and the retinal is reisomerised to a twisted all-*trans* configuration (208).

The resting state of the photocycle is recovered by deprotonation of D85. The proton is thought to be passed on to the empty proton release site. Finally, the negatively charged D85 allows the retinal to adopt a relaxed all-*trans* configuration (202,209,210).

To prevent a futile cycle, it has to be ensured that the Schiff base is reprotonated from the cytoplasmic site and not by D85. This can be accomplished either by physical

separation of the protonated D85 and deprotonated Schiff base or by increasing the pK_a of D85 in the N and O states. The former hypothesis could be accomplished by the reorientation of NZ vector of Schiff base upon deprotonation either due to curvature of the retinal polyene (211) or due to the weak electrostatic interaction between protonated D85 and the Schiff base (189,212). According to Royant *et al*., it is rather D85 that makes the move towards the Schiff base in the L state and then moves again away from the Schiff Base in the M state, induced by bending of helix C (**Figure 21**) (213). The latter hypothesis is based on the assumption that upon proton release to the extracellular side, which happens concomitantly to protonation of D85, the pK_a of D85 rises due to the disrupted extracellular hydrogen-bonded network. This disqualifies D85 as a proton donor for the Schiff base and puts D96 located in the cytoplasmic half-channel forward as candidate proton donor to the Schiff base.

3. The all-tight conformation of AcrB trimer is in support of bi-site activation of drug transport

This section contains a manuscript describing experiments, results and interpretations of the findings obtained for the characterization of the AcrB binding pocket mutants AcrB_F610A, AcrB_V612F and AcrB_F610A_V612F.

My contribution to this work was the construction of the *E. coli* BW25113 Δ*acrB* strain, the production of the plasmids containing mutant AcrB, performing the phenotypical experiments, protein overexpression, purification crystallization and crystallographic data collection.

Processing and refinement of crystallographic data was executed by me with substantial support of Prof. Dr. Klaas Martinus Pos.

The all-tight conformation of AcrB trimer is in support of bi-site activation of drug transport

Thomas Eicher, Lorenz Brandstätter, Jürgen Bohnert, Winfried Kern, Francois Verrey, Markus Grütter, Kay Diederichs, Klaas M. Pos

Abstract

AcrA/AcrB/TolC is the major efflux protein complex in *Escherichia coli* extruding a vast variety of antimicrobial agents from the cell. The asymmetric structure of the trimeric inner membrane component AcrB implies functional rotation in analogy to the functional rotation observed for the F_1F_o ATPase. In one of the monomers, bound substrate could be detected in an internal cavity formed by hydrophobic and aromatic residues. Here we report the phenotypical and structural effect of substituting the binding pocket residues F610 and/or V612 with alanine and phenylalanine, respectively. Except for the antibiotic linezolid, single amino acid exchange generally resulted in reduced growth of bacterial cells. Interestingly, resistance could be partially restored upon introduction of the second mutation. The structure of the AcrB_V612F mutant was solved at 2.2 Å in presence and absence of DARPins. The protein exhibited a novel conformation in which all monomers adopt the tight state presumably representing an intermediate step during functional rotation. Additionally, the location of bound substrate was found to be shifted compared to the wild-type protein, highlighting the remarkable flexibility of AcrB to comply with severe changes in the binding pocket.

Introduction

The three component AcrA/AcrB/TolC multidrug resistance (MDR) pump provides the *E. coli* cell with the necessary means to protect it against a wide range of noxious compounds (1). AcrB resides in the inner membrane and is the energy transducing and substrate specificity determinant (2-6). AcrA is the adapter component which

associates the inner membrane pump with the TolC outer membrane channel (7,8). Importantly, all three components are necessary to obtain the MDR phenotype (3,4,8). Despite its wide range of substrates, which includes dyes, detergents, bile salts, organic solvents and antibiotics of different chemical classes, some restrictive features appear to be size and hydrophobicity. Substrates of AcrB have not been reported to exceed a molecular weight of 10^3 Da or to be more hydrophilic than $\log P_{OW}$ of -0.3[1]. AcrB seems therefore to prefer hydrophobic substrates including polar or charged moieties, but is also able to transport small organic compounds like hexane and octane (9).

Substrate specificity was found to be localized in the periplasmic porter domain of AcrB (6). Both biochemical and structural studies point towards a region consisting of a cluster of phenylalanines responsible for substrate binding (10-14). Recent published structures of AcrB showed an asymmetric homotrimer with the monomers in the distinct states loose (L), tight (T) and open (O). The substrate binding pocket appears to be widened in the tight state where binding of minocycline and doxorubicin was shown (11). In analogy with the functional rotation of the α/β-subunits of the F_1F_o ATPase leading to synthesis of ATP (15,16), a similar catalytic mechanism was postulated for AcrB leading to drug export (11-13). In short, the hypothesis states that within the asymmetric trimer, the monomers can adopt any of the conformational states L, T and O. The process is dependent on the concerted cycling of the monomers through the states L, T, O and back to L, which is the essence of the functional rotation. In the L conformation, substrates are recruited for transport towards the binding pocket from the periplasmic space and/or the membrane. Tunnels lead towards the periplasmic binding site in the T conformation and substrate gets tightly bound. Upon conformational change towards the O state, the substrate is released from the binding pocket and exits AcrB via the trimeric funnel towards the TolC tunnel. The tunnels towards and from the hydrophobic binding pocket are lined with hydrophilic side chains through which hydrophobic substrates are transported (11,12). During a complete functional rotation, occlusions and constrictions inside the dynamic tunnel system seem to propagate from the lateral opening towards the central

[1] P is the partition coefficient of a given solvent in an equimolar octanol-water mixture. $\log P_{OW}$ of -0.3 is the experimental partition coefficient of tetracycline (http://www.drugbank.ca/).

funnel driving the transport of substrate. Hence this mechanism was dubbed "peristaltic pump mechanism" (12,17).

The functional rotation mechanism suggests interdependence of the monomers, which means that if one of the monomers within the trimer has a lethal mutation, the whole trimer is inactive. Recently, this has been impressively shown to be the case by Nikaido and co-workers by the use of a covalently linked AcrB trimer (18). Two crystallographical distinct structures are known up-to-date: the symmetric LLL (all loose) conformation (19) and the asymmetric LTO conformation (11-13). Most of the published structures are in the symmetric conformation but show a marked deviation between each other (19-25). However, it has been discussed whether the symmetry for some of these structures is due to crystallographic "artifacts" like an induced conformation due to crystal contacts or even the presence of twinning inside the crystals (12). On the other hand the LLL conformation might represent the "resting state" e.g. in the absence of substrate (21) with structural flexibility necessary for substrate acquisition. Other structures show the AcrB trimer in the asymmetric LTO state (11-13) with binding of substrates in the T conformer (11). Whether the apparent "substrate-free" preparations are indeed without substrates is ambiguous since the solubilizing and stabilizing detergents used in the preparation of the crystals are all substrates of AcrB. These detergents might not be visible in the electron density maps in or near the minocycline/doxorubicin binding area due to multiple conformational binding of the ligand (11,12,26).

In theory different combinations of the three monomeric states within the AcrB trimer are plausible, especially since the binding change mechanism (15,16) postulates a bi-site activation of the transporter for catalysis (17,27). I.e. before the AcrB substrate can be released from the T monomer by conversion to the O monomer, a second substrate has to be bound to the adjacent monomer. Structural flexibility within the trimer (28,29) suggests that multiple L and T conformational states (LLT or LTT) might be present in the AcrB trimer. Upon high substrate concentration or in the case of altered biophysical properties of the protein, even a TTT (all tight) trimer conformation might be plausible (27). We describe here a structure of AcrB in a novel TTT conformation for the AcrB binding pocket mutant V612F. The latter mutation was previously shown to alter the antibiotic efflux profile for the AcrB homologue YhiV (10).

3. The all-tight conformation of AcrB trimer is in support of bi-site activation of drug transport

AcrB_V612F crystallizes as a symmetric trimer with every monomer in the T conformation. Moreover, this trimeric conformation could be obtained in the presence and absence of the AcrB substrate minocycline. The position of bound minocycline in the binding pocket of the V612F mutant has been shifted compared to the location in the binding pocket of the wild-type (wt) T monomer (11). This highlights the great flexibility of the binding pocket to adapt to severe changes in the ligand-binding side chains, and is reminiscent to the observation made previously for the drug binding protein QacR (30).

Results

A single V610F mutation in the YhiV homologue of AcrB resulted in a 16-fold increase of resistance towards linezolid and a eight-fold increase towards tetracycline, whereas the mutants where more susceptible towards the macrolide antibiotics erythromycin, clarithromycin and azithromycin (10). In AcrB, the corresponding V612 is part of the hydrophobic binding pocket (11-13) of the tight monomer consisting of six phenylalanines, two valines, two isoleucines and a tyrosine. As has been shown recently (11), co-crystallization of the AcrB substrates minocycline and doxorubicin visualized the presence of these substrates inside the binding pocket.

We substituted V612 with phenylalanine in plasmidial encoded AcrB and tested the phenotypic impact of this mutation in an *E. coli* BW25113 *ΔacrB* background (28). A similar change of substrate preference was observed as described for the AcrB homologue YhiV (10) (**Table 1**).

3. The all-tight conformation of AcrB trimer is in support of bi-site activation of drug transport

Table 1: Drug susceptibility of *E. coli* BW25113 *ΔacrB* expressing wt and mutant AcrB

	MIC (μg ml^{-1})						
mutation	R6G	berb	clarithro	oxa	eth	lin	erythro
D407N _D408N	8	64	<4	2	8	8	2-4
wt	128	1024	64	128	128	128	64
V612F	16	128	16	64	32-64	256	16
F610A	16	512	8	32-64	64-128	64-128	8
F610A _V612F	64	512	16-32	64	128	256	16-32

abbreviations: MIC, minimal inhibitory concentration; R6G, rhodamine 6G; berb, berberine; clarithro, clarithromycin; oxa, oxacillin; eth, ethidium; lin, linezolid; erythro, erythromycin

Seven compounds that belong to different chemical classes and that are known AcrB substrates were tested (i.e. the dyes rhodamine 6G (R6G) and ethidium, the plant alkaloid berberine, the macrolides clarithromycin and erythromycin, the β-lactam antibiotic oxacillin and the oxazolidinone antibiotic linezolid). With the exception of linezolid (two-fold increase of the minimal inhibitory concentration (MIC)), AcrB_V612F conferred less drug resistance to the tested compounds than wt AcrB, with oxacillin resistance being least affected. Apart from intrinsic differences between AcrB and YhiV, the reason for the less pronounced effect of the phenylalanine to alanine substitution seen in our measurement could be the mildly decreased expression level of AcrB_V612F compared to the wt protein (**Figure 1**).

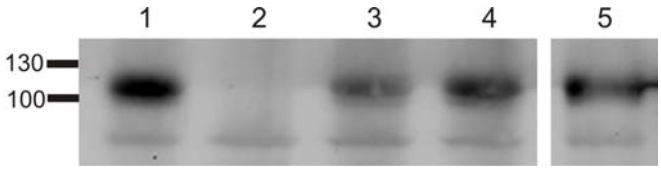

Figure 1: Western blot analysis of cell extracts obtained from *E. coli* BW25113Δ*acrB* cells coding for wt and mutant AcrB. Expression level of AcrB_V612F (lane 3), AcrB_F610A (lane 4) and AcrB_F610A_V612F (lane 5) are mildly decreased compared with wt AcrB (lane 1), As a control, *E. coli* BW25113Δ*acrB* was complemented with the expression vector (lane 2). Molecular size marker is indicated in kDA on the left.

To obtain structural information on the change in substrate specificity, we crystallized an AcrB_V612F/DARPin complex and surprisingly obtained crystals in a hitherto unreported crystal form I23.

Novel all-tight conformation of AcrB

For structure determination of AcrB, we standardly used Designed Ankyrin Repeat Proteins (DARPins) in order to obtain high-resolution AcrB/DARPin co-crystals. DARPins are specific, high-affinity binding proteins selected by *in vitro* ribososome display using a DARPin library (31,32). DARPin clone 1108_19 was shown to bind specifically to the loose and tight monomer (but not to the open monomer) of trimeric AcrB in its asymmetric conformation, yielding a DARPin:AcrB stoichiometry of 2:3 (13). These specific DARPin molecules allowed for new crystal contacts to be formed and appear to stabilize the specific asymmetric conformation of AcrB augmenting the crystallization process.

3. The all-tight conformation of AcrB trimer is in support of bi-site activation of drug transport

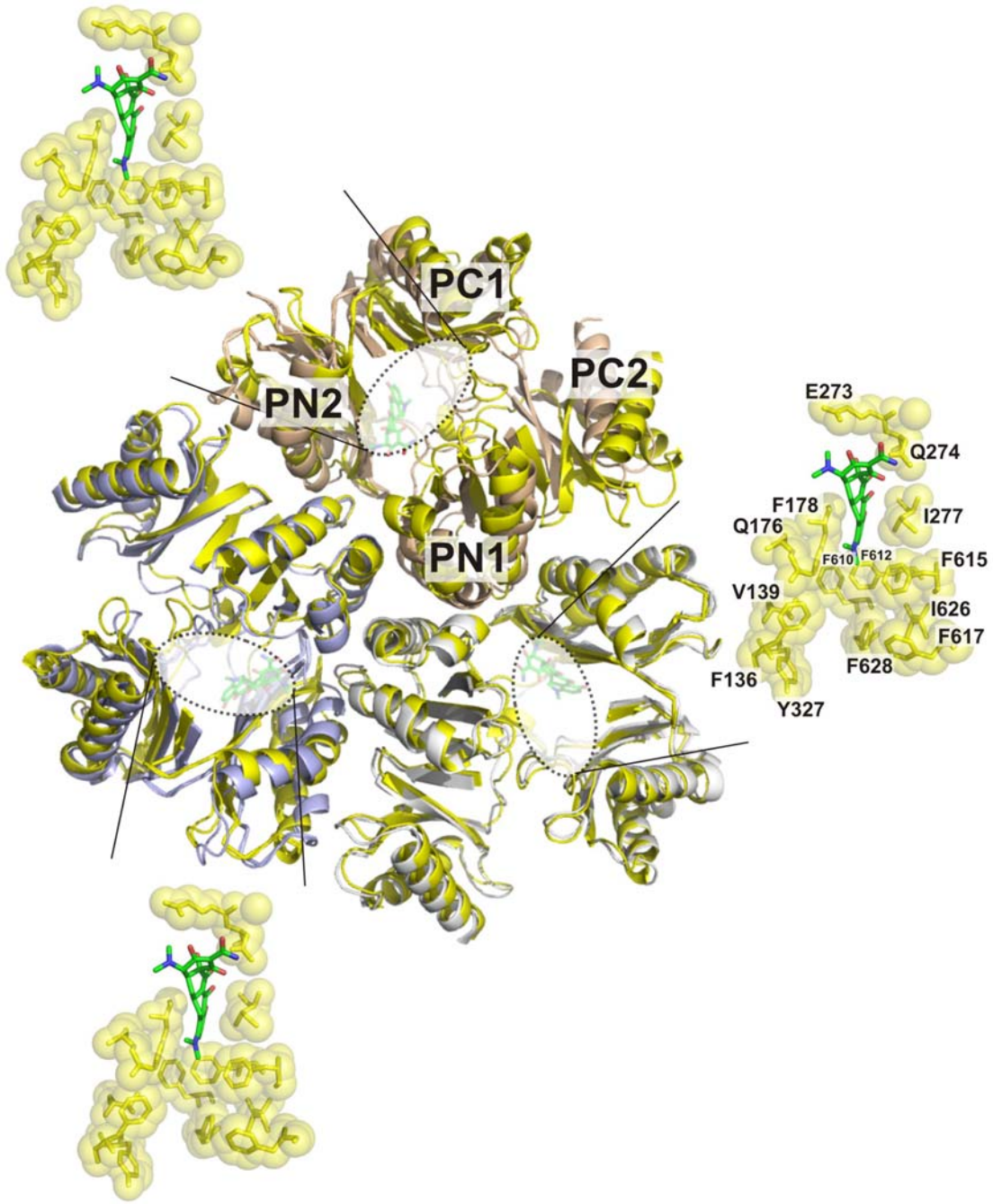

Figure 2: Superimposition of the porter domain of AcrB_V612F (yellow) onto the porter domain of the asymmetric structure of wt AcrB (2GIF). The loose, tight and open monomer of wt AcrB are colored blue, grey and red, respectively. In the AcrB_V612F structure, minocycline (green) is found in the binding pockets between subdomains PN2 and PC1 of each monomer. In the insets, key residues of the binding pocket and residues that help to coordinate minocycline are depicted as spheres.

The structure of the V612F AcrB mutant/DARPin complex was solved at 2.2 Å from cubic crystals (space group I23) grown in presence and absence of the substrate minocycline. A three-fold symmetry axis runs through the center of the AcrB trimer reminiscent to the symmetric AcrB trimer structure derived from the R32 crystal form

3. The all-tight conformation of AcrB trimer is in support of bi-site activation of drug transport

(19,33,34) (**Table S1**). An improved structure of the wt AcrB/DARPin complex (Eicher *et al.*, unpublished data) was used as a search model for molecular replacement. The asymmetric unit of the V612F/DARPin co-crystal consists of a stoichiometric complex. The V612F monomer exhibits the typical features of the AcrB monomer in its tight conformation and includes a bound minocycline molecule in the designated binding pocket (11-13).

This observation is in accordance with the small root mean square deviation (RMSD) between the AcrB_V612F chain and the AcrB wt monomer (pdb entry: 2GIF) in the tight conformation (**Table S1**).

As apparent from the space group symmetry there is one additional DARPin molecule per AcrB_V612F trimer compared to the asymmetric wt AcrB/DARPin $P2_12_12_1$ structure (pdb entry: 2J8S). Although the number of contacts facilitating the single AcrB_V612F/DARPin interaction are maintained by virtually the same side chain residues as in the wt tight monomer AcrB/DARPin complex (**Table S2**), the total number of salt bridges and H-bond interactions in the trimeric AcrB/DARPin assemblies differ substantially due to the unequal AcrB:DARPin stoichiometry in the two structures.

To test whether this novel conformation of AcrB_V612F is an artifact due to binding of the DARPins, we crystallized the protein in the absence of the high affinity binding molecules. Crystals grew in the presence and absence of the substrate minocycline diffracting to 2.8 Å and belonging to the space group P321 (**Table S1**). To solve the structure, the same steps were performed as described for the AcrB_V612F/DARPin complex. The asymmetric unit of the crystal consists of one AcrB monomer in the tight conformation and shows little deviation to the structure obtained in presence of the DARPin molecules (RMSD = 0.43 Å) (**Table S1**). The P321 crystals were grown at the same conditions where wt AcrB forms the asymmetric C2 crystal (12). Surprisingly, no condition was found to promote growth of crystals of AcrB_V612F exhibiting the all loose confirmation, the state that is predominantly found for AcrB wt protein.

Differences between the tight conformer of the wt AcrB and AcrB_V612F

The largest deviations between the tight conformation of the symmetric I23 V612F structure and the asymmetric wt AcrB C2 structure monomer are observed in the loops connecting the PN1 with the PN2 subdomain (RMSD of C_α atoms ≥ 3.5 Å) and the PC1 with the PC2 subdomain (RMSD ≥ 4.7 Å), at the N-terminal end of the cytosolic α-helix (Iα) (RMSD ≥ 6.4 Å) and in the PC1 subdomain (RMSD ≥ 3.2 Å) (**Figure 3**).

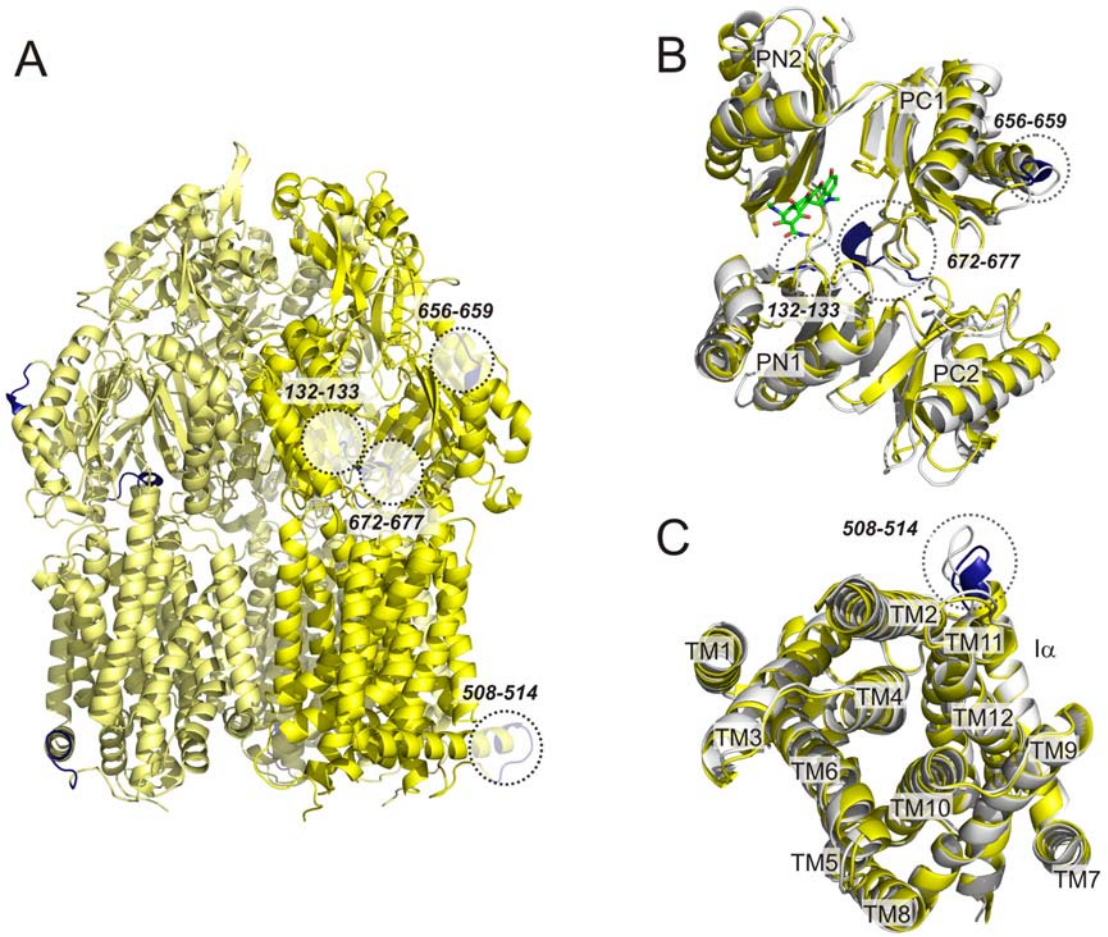

Figure 3: Differences between the tight conformer of wt AcrB and AcrB_V612F. **A)** Side view of the AcrB_V612F trimer. The monomers are colored in different shades of yellow. Stretches which deviate significantly between the wt and AcrB_V612F structure (rmsd ≥ 2.38 Å) are colored blue and highlighted with circles. **B)** Top view onto superposed pore domain of AcrB_V612F (yellow) and tight conformer of wt AcrB (white). Minocycline bound by AcrB_V612F is colored green and F612 is shown in stick representation. Subdomains are indicated. **C)** Superimposition of the transmembrane domain of AcrB_V612F (yellow) and wt AcrB (white). There is little deviation between the two structures in this domain except for the N-terminus of the cytosolic α-helix (Iα). Number of transmembrane helices are indicated. For wt AcrB, the pdb coordinate file 2GIF was used.

The two aforementioned loops are located in the porter domain of AcrB and partially line tunnel 1 in the tight conformer of wt AcrB (**Figure 4**). This tunnel connects the inner membrane with the open binding pocket and is continuous in the structure published by Sennhauser *et al*. (pdb coordinate file 2J8S, (13)), whereas the side chain of F563 protrudes into this tunnel in another structure (17) and was hence postulated to act as a gating residue. In AcrB_V612F, the side chain of F563 adopts the same conformation as in 2J8S, but the tunnel is occluded by the side chains of S561, L674 and T676. The latter two residues are located on the PC1-PC2 connecting loop and seem to be involved in gating of tunnel 1 as well (**Figure 4**).

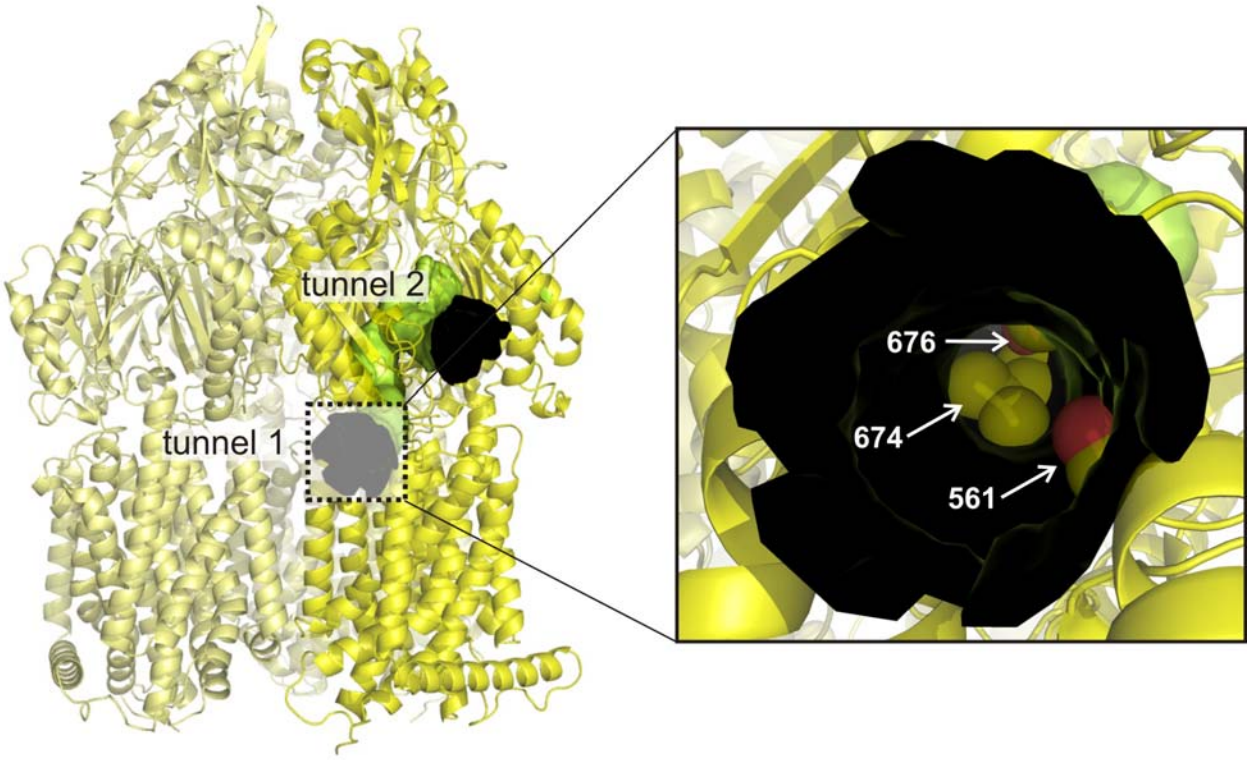

Figure 4: Visualization of the tunnels in the porter domain of AcrB_V612F. In the tight conformer of wt AcrB, occlusions and cavities form tunnel 1 and 2 (green surface) connecting the binding pocket with the inner membrane and the periplasm, respectively. Tunnel 1 is occluded by the residues 561, 674 and 676 in AcrB_V612F as depicted in the inset.

Adaptability of the altered AcrB_V612F binding pocket

AcrB binds and transports a broad spectrum of chemically unrelated compounds. Among the many substrates tested in co-crystallization trials, only doxorubicin and minocycline could be identified in the binding pocket of the tight monomer of the asymmetric AcrB wt structure (11). Structural analysis of the AcrB_V612F/DARPin

complex co-crystallized in the presence of minocycline revealed binding of minocycline by virtually the same side chain residues as observed in the tight monomer of the wt AcrB, but the substrate position has been shifted by approximately 2.1 Å along its longitudinal axis (**Figure 5**).

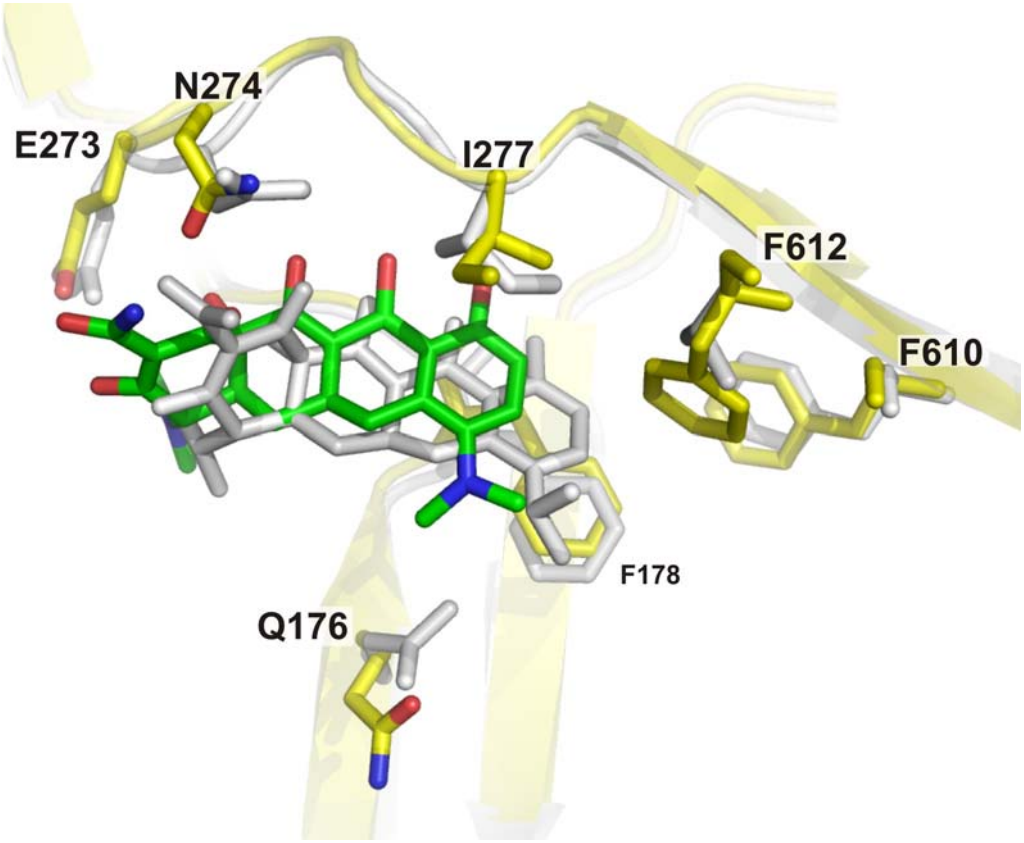

Figure 5: Shifted position of minocycline in the binding pocket of AcrB_V612F compared to its location in the wt AcrB tight monomer binding pocket (pdb entry: 2DRD). The structure of the binding pocket region of AcrB_V612F (yellow) and wt AcrB (grey) co-crystallized with minocycline are superimposed. Residues involved in the binding of minocycline are designated. F615 is omitted for clarity.

In the new substrate location the polar tertiary amine nitrogen (N1) of minocycline is about 0.8 Å nearer to the carboxylate side chain of E273 (new distance of 4.6 Å) and the amide side chain of N274 is approximately 0.6 Å closer to the amide nitrogen (N2) of minocycline, allowing the formation of a hydrogen bond. On the other hand, the ring system of minocycline was 1.5 Å further apart from F178 presumably weakening the π-π interaction (**Table 2**) (**Figure 5**). Despite considerable efforts we were until now not successful in co-crystallization of AcrB_V612F/DARPin with other known AcrB substrates besides minocycline.

3. The all-tight conformation of AcrB trimer is in support of bi-site activation of drug transport

Table 2: Distance between minocycline and binding pocket residues of wt and AcrB_V612F

residues	distance	
	wt AcrB (pdb ID: 2DRD)	AcrB_V612F
E273 (OE1) - MIY (N1)	5.40	4.58
N274 (OD1) – MIY (N2)	3.64	3.08
F178 (CD2) – MIY (C12)	3.10	4.58

Substitution of F610 with alanine rescues the V612F mutant

A systematic alanine scanning approach on the phenylalanine residues inside the AcrB binding pocket revealed the insensitivity of single alanine substitution with regard to the efflux capability of the AcrB pump. Nevertheless, a F610A substitution was shown to have considerable effect on the capacity to confer resistance towards a range of toxic compounds (14). The substituted phenylalanine residue is located in spatial vicinity of the valine at position 612 (**Figure 2** and **Figure 5**). We hypothesized that the bulky F610 side chain might be causing part of the reduced activity observed in the V612F mutant and introduced a F610A substitution in the latter mutant.

Interestingly, the second mutation (F610A in AcrB_V612F or V612F in AcrB_F610A) caused an improvement on the capability to confer drug resistance (**Table 1**). The MIC values for the double mutant were either elevated to the level of the less affected single mutant (i.e. in the case of berberine and oxacillin) or even higher (in the case of R6G, clarithromycin, ethidium, erythromycin). Linezolid resistance, however, remained two-fold elevated compared to wt AcrB, despite introduction of the second (F610A) mutation.

Mutations in the binding pocket inhibit efflux of *N*-phenylnaphthylamine (NPN)

To further investigate the impact of the mutations in the binding pocket on activity of the protein, cells producing AcrB_F610A, AcrB_V612F and AcrB_F610A_V612F were subjected to NPN fluorescence spectroscopy (**Figure 6**). NPN integrates readily in the inner membrane of de-energized bacterial cells where it gives rise to a strong

fluorescent signal. NPN is a cognate substrate of AcrB and its efflux can be followed in real time as quenching of the fluorescence upon re-energization of the cells (35,36). Both the initial efflux rate and steady-state fluorescence quenching for the AcrB_F610A and AcrB_V612F single mutants were considerably diminished as compared to the wild-type. The efflux of NPN was, however, improved upon introduction of the second mutation (yielding AcrB_F610A_V612F), but well below the level observed for the cells expressing wt AcrB. This is in accord to the results obtained with MIC experiments, where the F610A mutation rescues in part the activity of the AcrB_V612F mutant and *vice versa*.

Cells expressing AcrB_D407N_D408N served as negative control. In this mutant, efflux of NPN is completely inhibited as has been shown before (28,36).

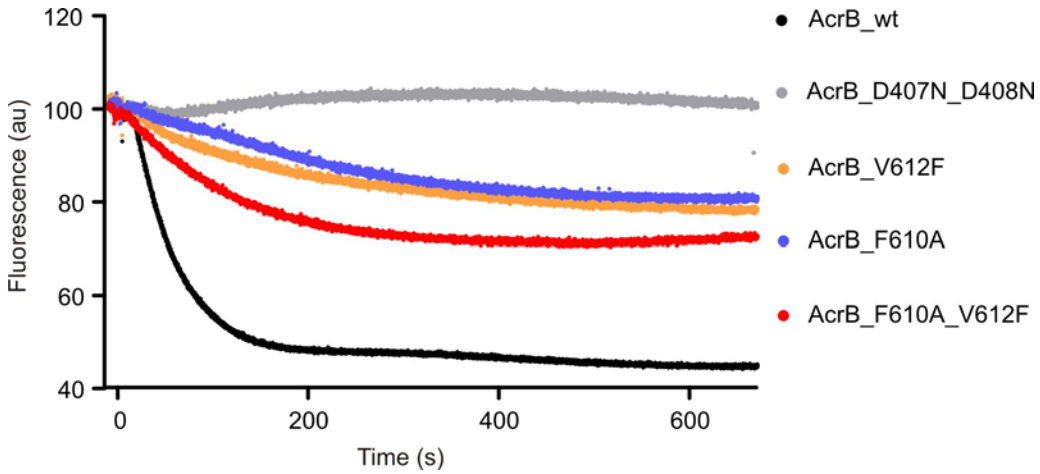

Figure 6: NPN efflux in *E. coli* BW25113 *ΔacrB* harboring plasmid encoding wt and mutant *acrB*. Cells were energized at t=0 and efflux of substrate was followed as decay of the fluorescence signal. Cells producing AcrB_F610A, AcrB_V612F and AcrB_F610A_V612F are still able to accomplish efflux of NPN, although to a lesser degree than cells harboring wt *acrB*. The nonfunctional AcrB_D407N_D408N mutant was used as a negative control. au, arbitrary units.

Discussion

Recent structural studies show that homotrimeric AcrB can adopt different monomer conformations representing the consecutive states L, T and O in an allosteric functional rotation transport cycle. Trimeric AcrB has been crystallized in the symmetric “all loose” (LLL) (19) and the asymmetric LTO state (11-13).

3. The all-tight conformation of AcrB trimer is in support of bi-site activation of drug transport

It has been discussed (17,27) whether the LTO conformation represents the lowest energy form of the AcrB trimer, since *in vivo* cross-link studies (28,37) point towards the presence of this conformation rather than the LLL form. Moreover, addition of DARPins to solubilized AcrB appears to stabilize the asymmetric LTO only while in absence of these ligands, the LLL form can be readily and predominantly crystallized. Additionally, the LTO state seems to be the most abundant conformation of wt AcrB in soluble detergent extracts based on analytical ultracentrifugation experiments in the presence of DARPins (13). However, during functional rotation of the protein, trimeric AcrB is anticipated to exist in intermediate states (17), a hypothesis that is supported by quantitative cysteine cross-link experiments (28).
Here we describe a novel "all tight" (TTT) conformation of trimeric AcrB. This structure was obtained in crystallization trials with AcrB_V612 in the presence and absence of DARPins. Addition of minocycline facilitated crystallization but was not essential to obtain this conformation.

In analogy to the binding change mechanism for the F_1F_o ATPase, conversion of one monomer from the tight to open state and thus release of substrate is thought to be the energy requiring step (15,16). Furthermore, the T to O transition within the LTO trimer is postulated to occur only when a second substrate has bound to the adjacent loose monomer. This in turn promotes conversion of loose to tight conformation, resulting in a TTO intermediate of trimeric AcrB. Then the O monomer would change to the L conformation, resulting in an intermediate TTL state. In the final step, the T monomer would release the bound substrate and change to the O state, which completes the transport cycle and restores the LTO (OLT) state (**Figure 7**).
Based on the observation that AcrB_V612F failed to crystallize in either the LLL or the LTO state, we conclude that this amino acid substitution increases the probability of the monomers to adopt the T conformation. Indeed, when the V612F mutation was introduced *in silico* into the collapsed binding pocket of the loose or open monomer, the side chain of F612 collides in any possible orientation with one or several of the binding pocket residues I626, I276, I277, F610 and F615. However, since the protein is functionally still active and in case of linezolid the MIC was even increased, functional rotation does not seem to be impeded by the V612F mutation. Some structural rearrangements are thus necessary for the AcrB_V612F mutant to adopt L-

3. The all-tight conformation of AcrB trimer is in support of bi-site activation of drug transport

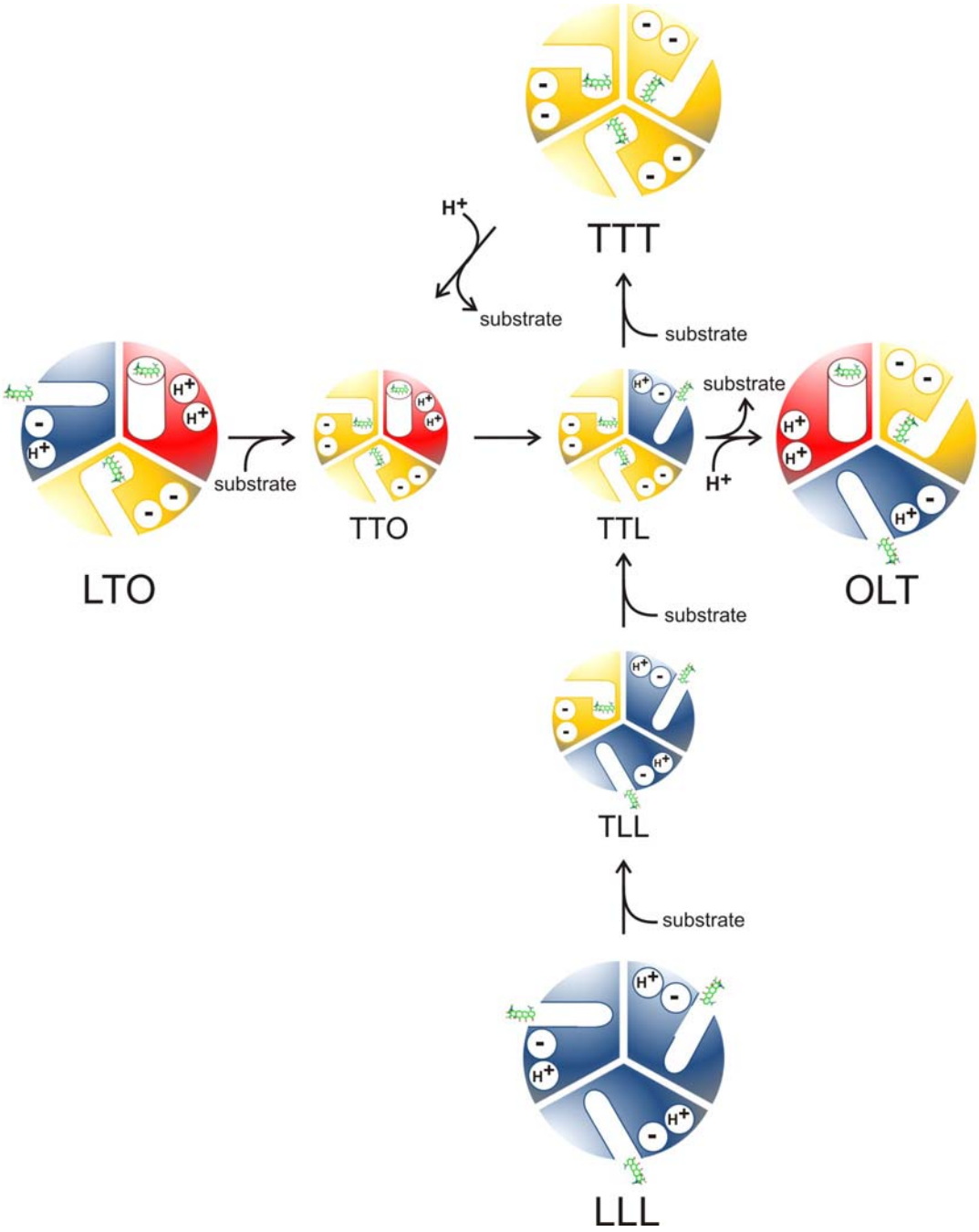

Figure 7: Schematic representation of the AcrB binding change mechanism. The conformational states loose (L), tight (T) and open (O) are colored blue, yellow and red, respectively. Substrate (minocycline) is displayed in green and is located close to the lateral entrance of the tunnel system in the loose monomer, bound tightly in the binding pocket of the tight monomer and is extruded from AcrB in the open monomer. The putative protonation state of D407 and D408 are indicated for the different conformations (H^+ and -, respectively). Structures of conformations which have been crystallized thus far are represented larger than the other putative intermediate states. The TTT state is expected to be predominantly present in the AcrB_V612F mutant.

or O- like states which are probably energetically less favorable than the conformations in wt AcrB. As a consequence, T is the preferred state for AcrB_V612F. Parameters such as high substrate concentration are considered to shift the balance in wt AcrB towards the T state as well, especially since the energy needed for the transition from O to L or L to T presumably is low.

Since there is no structural information on the binary AcrB/drug complexes for the substrates tested in the MIC experiments, it remains speculative whether and how these molecules are adapted in the AcrB binding pocket. However, some interpretation can be done based on the effect of the mutations on the MIC values. For example, the R6G MIC value is decreased severely in the two single mutants F610A and V612F, whereas for other substrates (e.g. oxacillin, ethidium and linezolid) the effects are less severe or even, in the case of linozolid, beneficial. This appears to exclude a general constraint on transport based on hindrance of conformational changes and might be an argument for a specific effect on substrate binding inside the binding pocket. One explanation might be therefore that in the AcrB_V612F mutant, the two bulky phenylalanine residues (F610 and F612) might prohibit access to the entire binding pocket and thereby hinder e.g. R6G to adopt its favored position (**Figure 8**).

The decrease of MIC values in the AcrB_F610A mutant might be explained by the reduced opportunities for substrates to interact via favorable π-π or cation-π interactions. In the AcrB_F610A_V612F double mutant, the access to the entire binding pocket might be re-established due to the F610A mutation and the phenylalanine at position 612 might compensate for the loss of F610. This would allow the altered binding pocket to accommodate e.g. R6G in a similar fashion as the wt protein does. Similar considerations may explain the phenomenon for the other drugs tested by MIC experiments except for linezolid. The MIC of this drug improved upon introduction of phenylalanine at position 612, but hardly changed when the phenylalanine at position 610 was removed. We therefore hypothesize that linezolid is bound differently compared to the other drugs tested and that the interaction of this substrate with the F610 and V612 residues is weak.

3. The all-tight conformation of AcrB trimer is in support of bi-site activation of drug transport

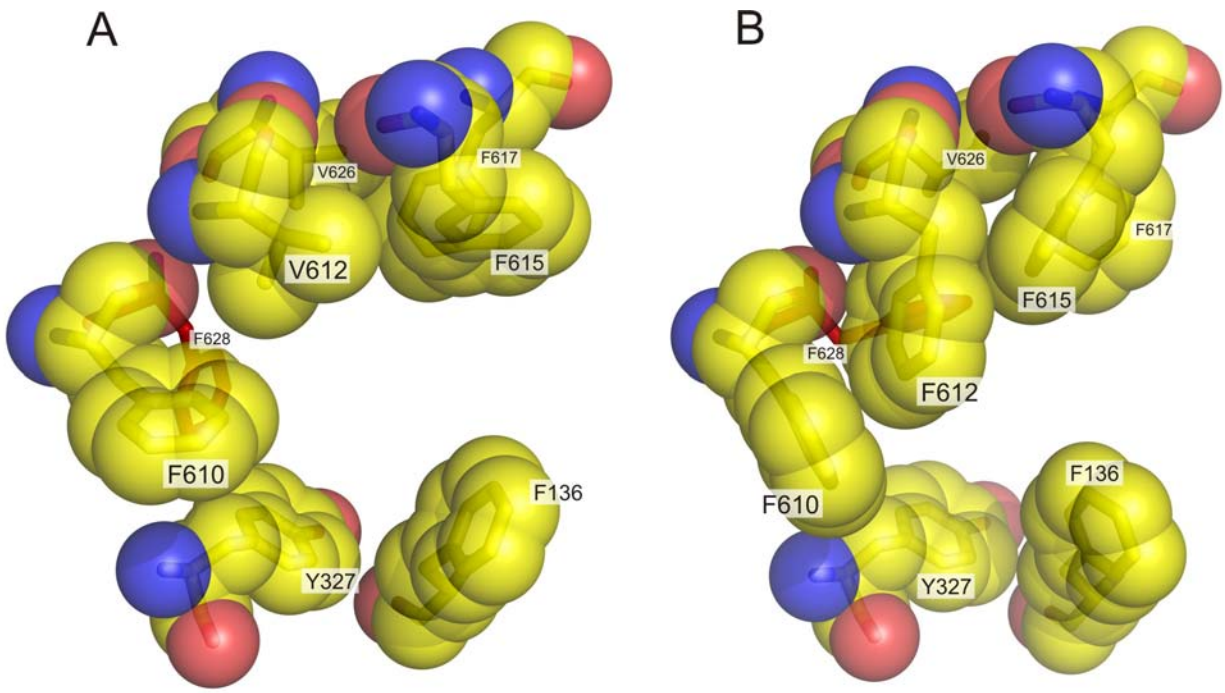

Figure 8: Volume reduction of the AcrB binding pocket by the V612F mutation. The structure of the binding pocket of the tight conformer is shown for wt AcrB (A) and AcrB_V612F (B). Whereas the entire binding pocket of wt AcrB is accessible (A), the bulky side chain of F612 protrudes into the pocket and restricts entry in the mutant protein (B). Note that in AcrB_V612F, the side chains of F628 (colored red) and F615 exhibit different orientations. For wt structure, pdb coordinate file 2GIF was used.

The flexibility of MDR proteins in accommodating different substrates in their binding pockets was impressively demonstrated for the transcription regulator QacR. QacR is a soluble repressor of the TetR family and binds to the same substrate as its target gene *qacA* confers resistance to (38-40). To date, ten crystal structures were published showing QacR in complex with different substrates (41-43). Furthermore, QacR is rather promiscuous and is even capable of binding the same substrate in different positions. QacR was crystallized as binary complex with ethidium (43) and as ternary complex with ethidium and proflavine (42). In the QacR/proflavine/ethidium structure, binding of ethidium is essentially maintained by the same residues as in the binary structure. Rather than to clash with the second substrate, the position of ethidium was rotated approximately 15° along the axis perpendicular to its ring system and the two substrates are now engaged in favorable van der Waals interactions.

In another study, E58 of QacR was mutated to glutamine (30). This residue was shown to compensate for the positive charge of the substrate berberine in the wt structure. However, binding affinity counter intuitively increased for the mutant protein. Structural analysis of this mutant revealed that berberine is bound in an alternative fashion: it was rotated approximately 180° along its longitudinal axis. To avoid steric clash, Y123, which formed van der Waals contacts with the non-aromatic 1,3-dioxolane ring of berberine in the wt structure, rotated along its C_α-C_β bond, to be now engaged in favorable π-π interactions with the aromatic benzene ring of berberine. Furthermore, berberine and W61 are oriented parallel to each other and the overlapping area of the two ring systems has been enlarged due to the new position of the drug molecule. This improves aromatic stacking interactions and allows cation-π interaction with the pyridinium nitrogen of berberine (30).

The situation in AcrB_V612F is quite similar: the position of minocycline within the binding pocket is shifted for about 2.1 Å relative to its location in wt AcrB. The molecule in its original position would have had a distance from the F612 side chain of only 2.0 Å, which would have resulted in a sterical clash between the bulky side chain of F612 and the dimethylamino-phenol ring of minocycline. As mentioned earlier, the polar interactions between the drug and residues E273 and N274 were improved by the dislocation of minocycline, whereas the π-π interaction between the dimethylamino-phenol ring and the aromatic side chain of F178 got impaired (**Table 2**).

These results underline the flexibility of the AcrB binding pocket. Not only is it able to bind a variety of chemically unrelated substrates, but it can also compensate for mutations and – at least in the case of minocycline – accommodate substrate in different locations inside the binding pocket.

The all-tight structure is the second conformational state of trimeric AcrB that was crystallized in the presence of DARPins (13). The asymmetric structure of wt AcrB and the symmetric all-tight conformation of AcrB_V612F were both obtained in the presence and absence of these high affinity binders. Since the deviation between the liganded and unliganded structure is very small for both conformations, the DARPin molecules appear not to impose a non-native confirmation, but rather stabilize an existing conformational state, which helps to improve crystal formation and crystal diffraction.

Materials and methods

Bacterial strains, plasmids and growth conditions

E. coli DH5α (44) was used as host for cloning procedures. *E. coli* BW25113 Δ*acrB* (28) served as background for MIC determination and NPN efflux experiments. *E. coli* C43 (DE3) (45) harboring pET24acrB_V612F was used for protein overexpression. LB medium and LB agar (46) were used for routine bacterial growth at 37°C. Terrific broth (47) was used for protein overexpression. Kanamycin (Applichem) was applied at 50 μg ml^{-1} (Kan^{50}).

Site directed mutagenesis

pET24acrB_{His} (33) served as a template for site-directed mutagenesis. By using the Quikchange protocol (Stratagene), amino acid substitution was achieved with 5' phosphorylated primers. Insertion of mutation was verified by sequencing (Microsynth, Balgach, Switzerland).

Western blot analysis

Cultures of *E. coli* BW25113 Δ*acrB* carrying pET24acrB_{His} with and without additional mutations were grown over night in LB Kan^{50} (5 ml). The pellet of 1.0 ml culture was resuspended in SDS-PAGE loading buffer (0.1 ml * OD_{600} of the harvested culture) supplemented with 2% (v/v) β-mercaptoethanol and boiled for 5 min. The samples (15 μl) were subjected to SDS-PAGE (48) and blotted onto nitrocellulose membrane (49). AcrB and its mutant derivatives were immunodetected with anti-AcrB rabbit antibodies (Neosystem) at a $1:10^4$ dilution. Bound immunoglobulins were probed with mouse anti-rabbit antibody coupled to horseradish peroxidase and visualized using the enhanced chemiluminescence ECL system (Pierce).

Drug susceptibility assays

E. coli BW25113 Δ*acrB* carrying pET24acrB_{His} with and without additional mutations were subjected to MIC experiments as described earlier (28). In brief, 96-well microtiter plates (Thermo-Fisher Scientific) containing LB Kan^{50} and the indicated

drugs were prepared by two-fold serial dilution. The plates were inoculated 1:100 with precultures grown until a cell density of OD_{600} of 0.6. After incubation for 22 hours (37°C, 160 rev min^{-1}) the OD_{600} was determined. The smallest concentration that inhibited growth above the turbidity visual detection limit (OD_{600} of 0.58) was considered to be the MIC.

Each assay was repeated at least twice and in each experiment the plates were prepared in duplicates. On each plate, the strains at any drug concentration were present twice.

N-Phenylnaphthylamine (NPN) efflux assay

The clearance of NPN from the bacterial membrane by the AcrA/AcrB/TolC efflux pump was analyzed by following the decrease in the fluorescence signal (35,36). The same strains and plasmids as described for the MIC experiments were used and the protocol described by Seeger *et al.* (28) was applied.

Crystallization of AcrB_V612F in presence and absence of DARPins

Overexpression and membrane preparation of AcrB_V612F was carried out as described previously (12,33). Overexpression and purification of DARPin clone 1108_19 (13) was accomplished as described by Binz *et al.* (32). For crystallization of AcrB_V612F in absence of DARPins, purification and crystallization was carried out with cyclohexyl-*n*-hexyl-β-D-maltoside as detergent according to Seeger *et al.* (12). Crystals were grown by the hanging drop vapor diffusion method at 0.1 M citrate pH 4.6, 5% polyethylene glycol (PEG) 400, 16-21% PEG 300, 8-11% glycerol. To crystallize the AcrB_V612F/DARPin complex, the method described by Sennhauser *et al.* (13) with *n*-dodecyl-β-D-maltoside as detergent was applied. Unlike the wt protein, AcrB_V612F precipitated during buffer exchange from Tris-HCl to HEPES, which could be avoided when HEPES was replaced by KP_i buffer. Crystals were grown in presence and absence of 2 mM minocycline (Sigma-Aldrich) by the hanging drop vapor diffusion method at 0.1 M acetate buffer pH 4.5, 3-7% PEG 200, 15-25% PEG 400, 0.15 M $MgCl_2$, 0.15 M NaCl.

X-ray diffraction dataset analysis and refinement procedure

Datasets of I23 and P321 crystals were collected at the beamline X06SA of the Swiss Light Source (Paul Scherrer Institut, Villigen, Switzerland) (wavelength 1.0 Å and 0.9762 Å). Data reduction was done with the XDS package (50). The structures were solved by molecular replacement using MOLREP (51) or PHASER (52). Refinement was performed with the program REFMAC5 (53) using rigid body refinement followed by restrained refinement with TLS restraints. Model rebuilding was performed using the program COOT (54), tunnels were calculated using CAVER (55) and MOLE (56). Figures were created using Pymol (http://pymol.sourceforge.net/).

References

1. Sulavik, M. C., Houseweart, C., Cramer, C., Jiwani, N., Murgolo, N., Greene, J., DiDomenico, B., Shaw, K. J., Miller, G. H., Hare, R., and Shimer, G. (2001) *Antimicrob Agents Chemother* **45**, 1126-1136
2. Nakamura, H. (1965) *J Bacteriol* **90**, 8-14
3. Ma, D., Cook, D. N., Alberti, M., Pon, N. G., Nikaido, H., and Hearst, J. E. (1993) *J Bacteriol* **175**, 6299-6313
4. Ma, D., Cook, D. N., Alberti, M., Pon, N. G., Nikaido, H., and Hearst, J. E. (1995) *Mol Microbiol* **16**, 45-55
5. Saier, M. H., Jr., and Paulsen, I. T. (2001) *Semin Cell Dev Biol* **12**, 205-213
6. Elkins, C. A., and Nikaido, H. (2002) *J Bacteriol* **184**, 6490-6498
7. Elkins, C. A., and Nikaido, H. (2003) *J. Bacteriol.* **185**, 5349-5356
8. Fralick, J. A. (1996) *J Bacteriol* **178**, 5803-5805
9. Tsukagoshi, N., and Aono, R. (2000) *J Bacteriol* **182**, 4803-4810
10. Bohnert, J. A., Schuster, S., Fahnrich, E., Trittler, R., and Kern, W. V. (2006) *J Antimicrob Chemother*
11. Murakami, S., Nakashima, R., Yamashita, E., Matsumoto, T., and Yamaguchi, A. (2006) *Nature* **443**, 173-179
12. Seeger, M. A., Schiefner, A., Eicher, T., Verrey, F., Diederichs, K., and Pos, K. M. (2006) *Science* **313**, 1295-1298
13. Sennhauser, G., Amstutz, P., Briand, C., Storchenegger, O., and Grutter, M. G. (2006) *PLoS Biol* **5**, e7
14. Bohnert, J. A., Schuster, S., Seeger, M. A., Fahnrich, E., Pos, K. M., and Kern, W. V. (2008) *J Bacteriol* **190**, 8225-8229
15. Abrahams, J. P., Leslie, A. G., Lutter, R., and Walker, J. E. (1994) *Nature* **370**, 621-628
16. Boyer, P. D. (1997) *Annu. Rev. Biochem.* **66**, 717-749

17. Seeger, M. A., Diederichs, K., Eicher, T., Brandstatter, L., Schiefner, A., Verrey, F., and Pos, K. M. (2008) *Curr Drug Targets* **9**, 729-749
18. Takatsuka, Y., and Nikaido, H. (2009) *J Bacteriol* **191**, 1729-1737
19. Murakami, S., Nakashima, R., Yamashita, E., and Yamaguchi, A. (2002) *Nature* **419**, 587-593
20. Yu, E. W., McDermott, G., Zgurskaya, H. I., Nikaido, H., and Koshland, D. E., Jr. (2003) *Science* **300**, 976-980
21. Su, C. C., Li, M., Gu, R., Takatsuka, Y., McDermott, G., Nikaido, H., and Yu, E. W. (2006) *J Bacteriol* **188**, 7290-7296
22. Tornroth-Horsefield, S., Gourdon, P., Horsefield, R., Brive, L., Yamamoto, N., Mori, H., Snijder, A., and Neutze, R. (2007) *Structure* **15**, 1663-1673
23. Das, D., Xu, Q. S., Lee, J. Y., Ankoudinova, I., Huang, C., Lou, Y., DeGiovanni, A., Kim, R., and Kim, S. H. (2007) *J Struct Biol* **158**, 494-502
24. Drew, D., Klepsch, M. M., Newstead, S., Flaig, R., De Gier, J. W., Iwata, S., and Beis, K. (2008) *Mol Membr Biol* **25**, 677-682
25. Veesler, D., Blangy, S., Cambillau, C., and Sciara, G. (2008) *Acta Crystallogr Sect F Struct Biol Cryst Commun* **64**, 880-885
26. Murakami, S. (2008) *Curr Opin Struct Biol* **18**, 459-465
27. Pos, K. M. (2009) *Biochim Biophys Acta* **1794**, 782-793
28. Seeger, M. A., von Ballmoos, C., Eicher, T., Brandstatter, L., Verrey, F., Diederichs, K., and Pos, K. M. (2008) *Nat Struct Mol Biol* **15**, 199-205
29. Takatsuka, Y., and Nikaido, H. (2007) *J Bacteriol* **189**, 8677-8684
30. Peters, K. M., Schuman, J. T., Skurray, R. A., Brown, M. H., Brennan, R. G., and Schumacher, M. A. (2008) *Biochemistry* **47**, 8122-8129
31. Binz, H. K., Amstutz, P., Kohl, A., Stumpp, M. T., Briand, C., Forrer, P., Grutter, M. G., and Pluckthun, A. (2004) *Nat Biotechnol* **22**, 575-582
32. Binz, H. K., Stumpp, M. T., Forrer, P., Amstutz, P., and Pluckthun, A. (2003) *J Mol Biol* **332**, 489-503
33. Pos, K. M., and Diederichs, K. (2002) *Acta Crystallogr. Biol. Crystallogr.* **D58**, 1865-1867
34. Pos, K. M., Schiefner, A., Seeger, M. A., and Diederichs, K. (2004) *FEBS Lett* **564**, 333-339
35. Nikaido, H. (1996) *J. Bacteriol.* **178**, 5853-5859
36. Lomovskaya, O., Warren, M. S., Lee, A., Galazzo, J., Fronko, R., Lee, M., Blais, J., Cho, D., Chamberland, S., Renau, T., Leger, R., Hecker, S., Watkins, W., Hoshino, K., Ishida, H., and Lee, V. J. (2001) *Antimicrob Agents Chemother* **45**, 105-116
37. Murakami, S., Tamura, N., Saito, A., Hirata, T., and Yamaguchi, A. (2004) *J. Biol. Chem.* **279**, 3743-3748
38. Aramaki, H., Yagi, N., and Suzuki, M. (1995) *Protein Eng* **8**, 1259-1266
39. Grkovic, S., Brown, M. H., Roberts, N. J., Paulsen, I. T., and Skurray, R. A. (1998) *J Biol Chem* **273**, 18665-18673
40. Grkovic, S., Brown, M. H., Schumacher, M. A., Brennan, R. G., and Skurray, R. A. (2001) *J Bacteriol* **183**, 7102-7109
41. Murray, D. S., Schumacher, M. A., and Brennan, R. G. (2004) *J Biol Chem* **279**, 14365-14371
42. Schumacher, M. A., Miller, M. C., and Brennan, R. G. (2004) *EMBO J* **23**, 2923-2930
43. Schumacher, M. A., Miller, M. C., Grkovic, S., Brown, M. H., Skurray, R. A., and Brennan, R. G. (2001) *Science* **294**, 2158-2163

44. Woodcock, D. M., Crowther, P. J., Doherty, J., Jefferson, S., DeCruz, E., Noyer-Weidner, M., Smith, S. S., Michael, M. Z., and Graham, M. W. (1989) *Nucleic Acids Res* **17**, 3469-3478
45. Miroux, B., and Walker, J. E. (1996) *J Mol Biol* **260**, 289-298
46. Sambrook, J., Fritsch, E. F., and Maniatis, T. (1989) *Molecular cloning: a laboratory manual*, Cold Spring Harbor Laboratory Press, Cold Spring Harbor, N.Y.
47. Tartof, K. D., and Hobbs, C. A. (1987) *Bethesda Research Laboratories Focus* **9**, 12
48. Schagger, H., and von Jagow, G. (1987) *Anal Biochem* **166**, 368-379
49. Kyhse-Andersen, J. (1984) *J. Biochem. Biophys. Methods* **10**, 203-209
50. Kabsch, W. (1993) *J. Appl. Cryst.*, 795-800
51. Vagin, A. A., Teplyakov, A. (1997) *J Appl. Cryst.*, 1022-1025
52. Storoni, L. C., McCoy, A. J., and Read, R. J. (2004) *Acta Crystallogr. Biol. Crystallogr.* **D60**, 432-438
53. Murshudov, G. N., Vagin, A. A., Dodson, E. J. (1997) *Acta Crystallogr. Biol. Crystallogr.* **D53**, 240-255
54. Emsley, P., and Cowtan, K. (2004) *Acta Crystallogr. Biol. Crystallogr.* **D60**, 2126-2132
55. Petrek M., O. M., Banas P., Koca J., Damborsky J. (2006)
56. Petrek, M., Kosinova, P., Koca, J., and Otyepka, M. (2007) *Structure* **15**, 1357-1363

Supplementary materials for:

The all-tight conformation of AcrB trimer is in support of bi-site activation of drug transport

Thomas Eicher, Lorenz Brandstätter, Jürgen Bohnert, Winfried Kern, Francois Verrey, Markus Grütter, Kay Diederichs, Klaas M. Pos

Table S1 and Table S2
References

Table S1: Crystallographic data and refinement

	AcrB_V612F/DARPin & minocycline	**AcrB_V612F**
Data collection		
space group	I23	P321
Cell dimensions		
a (Å)	227.46	134.41
b (Å)	227.46	134.41
c (Å)	227.46	190.97
α (°)	90.00	90.00
β (°)	90.00	90.00
γ (°)	90.00	120
Resolution (Å)	2.20	2.80
R_{meas} (%)	116.9	143.5
I/σ_I	3.97	1.87
Completeness (%)	79.1	97.8
redundancy	22.82	10.62
Refinement		
trimer model	unpublished	AcrB_V612F/DARPin & minocycline
program	PHENIX[a,b] & REFMAC5[c]	PHENIX[a,b] & REFMAC5[c]
Resolution (Å)	29.87 - 2.20	49.69 - 2.80
No. of reflection	98553	49614
R_{work}	18.97	25.85
R_{free}	22.17	28.26
No. atoms		
macromolecule residues	9152	7937
solvent residues	1013	
B-factors		
macromolecule	39.3	56.9
solvent	43.5	
overall	39.7	56.9
RMS deviations		
bond length (°)	0.007	0.007
bond angles (Å)	1.1	1.0
RMS deviation to 2J8S (Å)[d]		
loose	2.34	2.32
tight	1.11	1.07
open	2.77	2.80
RMS deviation between AcrB_V612F/DARPin and AcrB_V612F (Å)[d]	0.43	

a: (1)
b: (2)
c: (3)
d: calculated with the program superpose (3)

Table S2: Distance between AcrB monomer and DARPin molecule in wild-type (wt) AcrB and AcrB_V612F[a]

AcrB_V612F / DARPin complex			**wt AcrB/DARPin complex** (pdb ID: 2J8S)	
chain D[b]	chain B[c]	dist. (Å)	distance (Å) between corresponding atoms of chain D[b] and B[c], resp.	distance (Å) between corresponding atoms of chain E[b] and A[c], resp.
ARG 23 (NH2)	ASP 723 (O)	2.94	3.24	3.16
TYR 56 (OH)	TYR 811 (O)	3.52	3.71	3.54
ASN 112 (ND2)	SER 807 (O)	2.73	2.66	2.55
LYS 144 (NZ)	SER 805 (O)	2.83	3.14	2.97
LYS 144 (NZ)	SER 802 (O)	2.75	2.64	2.58
LYS 147 (NZ)	GLU 734 (OE2)	2.62	3.69	2.76
TYR 56 (OH)	TYR 811 (N)	2.97	3.08	3.00
THR 78 (OG1)	TRP 809 (NE1)	2.91	n.a.	2.83
ASN 112 (OD1)	SER 807 (N)	3.17	3.28	n.a.
LYS 147 (NZ)	GLU 734 (OE1)	3.57	n.a.	3.73
ASP 13 (OD2)	LYS 659 (NZ)	n.a	3.23	n.a.
ARG 23 (NH2)	GLU 722 (OE2)	n.a.	3.94	n.a.
VAL 46 (O)	TRP 809 (NE1)	n.a.	n.a.	3.27
ASP 44 (OD2)	TYR 811 (OH)	n.a.	3.03	n.a
chain D[b]	chain B'[d]	dist. (Å)	distance (Å) between corresponding atoms of chain D[b] and A[c], resp.	distance (Å) between corresponding atoms of chain E[b] and C[c], resp.
ILE 154 (O)	ARG 263 (NH2)	2.85	3.61	3.2
ASN 155 (O)	ARG 263 (NH1)	2.78	n.a.	2.76
ASN 155 (O)	ARG 263 (NH2)	3.01	2.8	n.a.
ASN 156 (OD1)	LYS 248 (NZ)	2.79	2.62	n.a.
# of contacts		14	14	12
Δ^iG^e (kcal/mol)		-6.1	-5.7	-3.5
total # of contacts		42	26	
total Δ^iG^e (kcal/mol)		-18.3	-9.2	

[a]: calculated at PISA webservice (http://www.ebi.ac.uk/msd-srv/prot_int/pistart.html), (4)
[b]: DARPin molecule
[c]: AcrB molecule
[d]: B' is the symmetry related protomer of B, corresponds to A in 2J8S
[e]: solvation free energy upon formation of interface

References

1. Adams, P. D., Grosse-Kunstleve, R. W., Hung, L. W., Ioerger, T. R., McCoy, A. J., Moriarty, N. W., Read, R. J., Sacchettini, J. C., Sauter, N. K., and Terwilliger, T. C. (2002) *Acta Crystallogr D Biol Crystallogr* **58**, 1948-1954
2. Afonine, P. V., Grosse-Kunstleve, R. W., and Adams, P. D. (2005) *Acta Crystallogr D Biol Crystallogr* **61**, 850-855
3. Murshudov, G. N., Vagin, A. A., Dodson, E. J. (1997) *Acta Crystallogr. Biol. Crystallogr.* **D53**, 240-255
4. Krissinel, E., and Henrick, K. (2007) *J Mol Biol* **372**, 774-797

4. The AcrB proton pathway

The manuscript describes the experiments, results and interpretations of the crystallographic data of wt AcrB and the proton translocation variants AcrB_D407N, AcrB_D408N, AcrB_K940A, AcrB_R971A and AcrB_T978.

My share to this work was overexpression, purification, crystallization and collection of crystallographic data of the mutant proteins as well as of wt AcrB crystallized in presence of doxorubicin.

Processing and refinement of crystallographic data was performed by me with substantial support of Prof. Dr. Klaas Martinus Pos.

Dr. Markus Seeger purified and crystallized the protein for the AcrB/minocycline dataset.

The AcrB proton pathway

Thomas Eicher, Markus A. Seeger, Lorenz Brandstätter, Francois Verrey, Markus Grütter, Kay Diederichs, Klaas M. Pos

Abstract

The tripartite AcrA/AcrB/TolC complex extrudes structurally and functionally diverse chemical compounds and is the major multidrug efflux pump in *Escherichia coli*. AcrB is a trimeric integral inner membrane protein and is both the substrate specificity and energy module of the complex. The recently published asymmetric structure of AcrB implies transport of substrate in the soluble domain by functional rotation of the monomers in a connected and concerted fashion through the three different conformations loose, tight and open. The rather large conformational changes in the porter domain are thought to be energized by protonation and deprotonation of four essential charged residues that form the proton relay network and reside in the transmembrane domain. To gain insight into the functional rotation mechanism, we crystallized wild-type and proton relay network mutants of AcrB in the presence of Designed Ankyrin Repeat Proteins (DARPins) and solved the structures at resolutions of 2.0 - 3.0 Å. The presence of ordered waters exhibited by the high resolution structures allowed us to deduce a pathway for proton-transfer from the periplasm to the cytoplasm. Based on the different orientations of the proton relay network residues and dynamic conformational changes of the transmembrane helices in the different monomers of wild-type and mutant AcrB, we propose a detailed model for protonation and deprotonation events during functional rotation.

Introduction

Organisms of all phyla express genes encoding multidrug-resistance (MDR) pumps to clear the cell interior from noxious compounds. For some bacteria, up to 18% of all the transport proteins encoded are putative MDR transporters, which can be classified on basis of their sequence homology to five families (1,2). ATP binding cassette (ABC) transporters are predominantly found in eukaryotes, whereas putative MDR transporters from major facilitator (MF) and resistance-nodulation-cell division (RND) superfamilies are mainly found in firmicutes and proteobacteria, respectively (3). The acriflavine resistance transporter B (AcrB) from *E. coli* is a member of the RND superfamily and functions in conjunction with the periplasmic adaptor protein AcrA and the outer membrane channel TolC. The components form a trimeric complex which enables the *E. coli* cell to extrude a broad spectrum of substrates directly from the outer leaflet of the inner membrane into the media, bypassing both periplasm and outer membrane. AcrB is both the substrate specificity determinant and the energy module of this tripartite complex. Functional AcrB forms a trimer, and each monomer constitutes of twelve transmembrane helices (TM) and two periplasmic loops which protrude 70 Å into the periplasmic space (reviewed in (4-6)).
AcrB was shown to crystallize in symmetric (7) and asymmetric conformation (8-10). Transport of substrate was suggested to be accomplished by a cyclic functional rotation of the monomers adapting three different conformations loose, tight and open as observed in the asymmetric structure (4-6,11). The AcrB trimer was found to contain a dynamic tunnel system within its periplasmic domain through which substrates are thought to be guided towards and away from a hydrophobic binding pocket. This pocket is present only in the tight conformer, where bound substrate (minocycline) could unambiguously be identified (8). Upon conformational change from the tight to the open state, the tunnels system changes its appearance so that the lateral entry tunnels are closed and instead a new tunnel leading from the collapsed binding pocket to the funnel in the centre of the trimer is formed. From here, substrate is thought to move into the extracellular space *via* TolC.
According to reconstitution assays (12,13) and phylogenetic analysis (1), AcrB is a drug/proton antiporter energized by the proton motive force and protons are

anticipated to be transferred through the transmembrane domain driven by the electrochemical gradient from the periplasm to the cytoplasm. Of the approximately 330 residues forming the twelve transmembrane helices of the AcrB monomer, 30 polar and charged residues could be putatively involved in proton translocation. Site-directed mutagenesis studies revealed that only four of them, D407, D408, K940, and R971 are essential for AcrB function (14-16). D408 was identified by DCCD labeling studies to be protonated at one or more monomer conformations during the transport cycle and is a likely candidate for protonation/deprotonation events at physiological pH as is apparent from its deduced pK_a of 7.4 (16). T978, first thought to be an essential hydroxyl group carrier, showed almost no activity when changed to alanine; however, when mutated to valine, AcrB retains 64% of its activity (15).

The putatively titratable side chains of residues D407, D408 and K940, also referred to as triad, are located on TM 4 and 10 at approximately 2/3 of the distance from the periplasmic membrane plane to the membrane-cytoplasm boundary. These helices are situated in the middle of an oval bundle formed by the twelve helices of each monomer. T978 is situated on neighboring TM 11. In the loose and tight monomer, these four residues are situated within hydrogen bond interaction distance of each other. The functionally essential R971 is situated close to the membrane-cytoplasmic border and is considered a key residue in proton transfer. Together these four residues, D407, D408, K940, and R971 constitute a putative proton relay network.

In the loose and tight monomer, K940 is situated on the same parallel plane within the transmembrane domain in almost equal distance from the side chains D408 and D407. Upon conformational change from tight to open, K940 reorients from D407 and D408 towards the polar residues T978, S979 and N941 (residing on TM 11 and TM 10, respectively). In addition, a coil-to-helix transition at the periplasmic end of TM 8 as well as a bulging of TM 5 towards TM 4 and 10 can be observed (8-10). These subtle conformational changes might trigger the much larger conformational rearrangements observed in the periplasmic domain, which ultimately lead to the extrusion of substrate. Despite this structural detail on the molecular level, it is still beyond understanding how the events in the transmembrane domain are linked to those in the periplasmic domain. Moreover, it remains ambiguous how protons move from the bulk solvent of the periplasm to the triad residing in the transmembrane domain. Crystallization of mutant AcrB resulted in symmetric crystals growing in the H32

space group ((17) and results not shown). In this report we successfully co-crystallized AcrB mutants D407N, D408N, K940A, T978A and R971A in presence of Designed Ankyrin Repeat Proteins (DARPins) (10,18,19) and resolved the asymmetric structures using X-ray diffraction data with a resolution of 2.2 Å (AcrB_R971A) to 3.0 Å (AcrB_T978A). Wild-type (wt) AcrB/DARPin co-crystals with bound doxorubicin and minocycline diffracted to 2.0 Å and the structures provided molecular details on drug binding. Interestingly, only two AcrB mutants, D407N and R971A, show apparent different conformations in the transmembrane domain compared to the wt protein, whereas the other mutants, AcrB_D408N, AcrB_K940A, AcrB_T978A retained essentially the same conformation as shown for the wt AcrB structure.

On the basis of these high resolution structures, we suggest a proton pathway through the transmembrane domain *via* the proton relay network.

Results

Binding of minocycline and doxorubicin by the AcrB wild-type protein

The Protein Data Bank (www.pdb.org) contains at the moment of writing 24 AcrB structures. The first AcrB structure (year 2002, PDB entry: 1IWG) was based on 3.5 Å X-ray diffraction data from R32 crystals containing one unliganded AcrB monomer in the asymmetric unit i.e. it describes a symmetric AcrB trimer (7). In the following years, other groups deposited symmetric (wt and mutant) AcrB X-ray structures (based on 3.1 - 3.8 Å data) with and without ligands (17,20-27). With one exception (27), most of these structures were derived from the first structure (PDB entry: 1IWG) taken as a template. Recently, six structures describing an asymmetric AcrB trimer were published (PDB entries: 2DHH, 2DR6, 2DRD, 2GIF, 2HRT, 2J8S) (8-10) with the best resolution structure (2.5 Å, PDB entry 2J8S) obtained with AcrB/DARPins co-crystals (10). Two of the deposited asymmetric structures were derived from 3.1 and 3.3 Å data of AcrB/minocycline and AcrB/doxorubicin co-crystals, respectively (8).

We describe here the crystallization and structural elucidation of wt AcrB/DARPin complexes in the presence of minocycline and doxorubicin based on 2.0 Å and 2.25 Å diffraction data (**Table S1**). AcrB/DARPin complexes were co-crystallized in the presence of 2.0 mM and 0.4 mM minocycline and doxorubicin, respectively, yielding crystals in an orthorhombic space group. The structures were refined to an R_{free} of 24.11% and 22.82%, respectively. Electron densities for substrates could be clearly identified near the hydrophobic binding pocket of the tight monomer. Moreover, clear densities for ordered waters were identified, including in the transmembrane domain.

Binding of minocycline is accomplished by residues F178, G179, N274, I277, V612 and F615 (**Table S2**). The dimethylamino moiety of the drug is sandwiched by the aromatic side chains of F178 and F615. V612 and I277 make stacking contacts with the D and C rings, respectively. The carboxamid group of minocycline interacts with the polar side chain of N274 and the amido nitrogen of G179 is in 3.3 Å distance of the B ring (**Figure 1**).

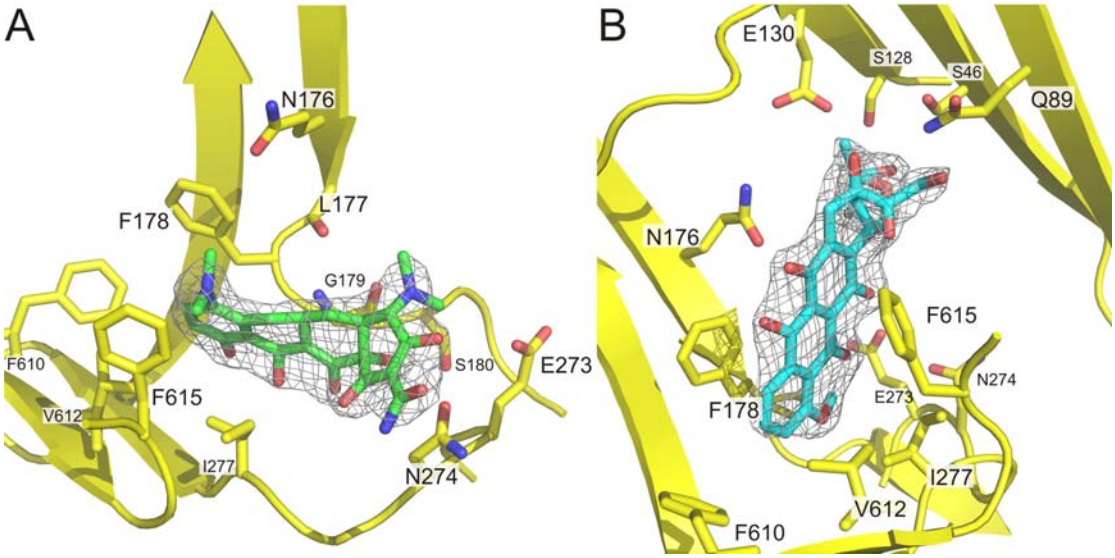

Figure 1: Binding of minocycline and doxorubicin in the binding pocket of the tight monomer of the AcrB trimer. Binding of the substrate molecules is achieved by aromatic stacking interactions, van der Waals contacts and polar interactions by both protein side chain and main chain atoms. The mesh represents the 2Fo-Fc electron density map contoured at 1.3 σ. **A)** AcrB/minocycline complex. **B)** AcrB/doxorubicin complex.

The ring system of doxorubicin is situated in the same plane as minocycline; however, the positions of the two substrate molecules differ by an angle of approximately 60°.

F178 and F615 wedge the C and D rings of doxorubicin. At the other end of the molecule, Q89 interacts with the hydroxyl group of the dihydroxypropanone moiety and together with the side chains of S46, S128 and E130 with the daunosamine sugar moiety

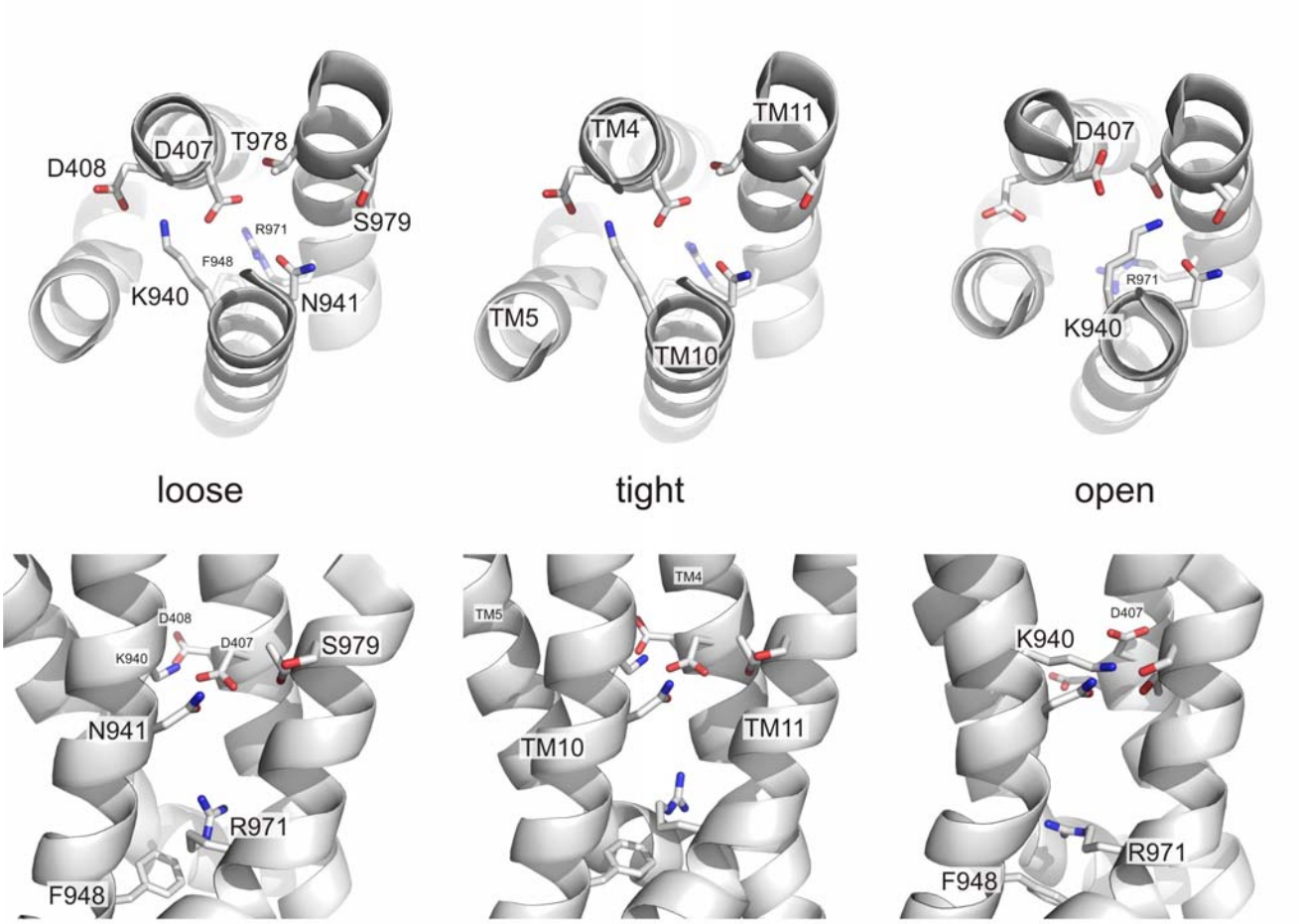

Figure 2: Proton relay and associated residues in different states of the functional rotation of AcrB. Most apparent differences between the three monomers are the reorientation of D407, K940 and R971 as well as bulging of TM 5 upon transition from tight to open. A section of the transmembrane domain viewed from the periplasm and viewed from the side is shown in the upper and lower row, respectively.

Ordered water molecules in the transmembrane domain of wt AcrB

AcrB is a secondary active transporter catalyzing the exchange of protons and drugs. While drug binding and transport is primarily localized in the periplasmic domain proton transport occurs through the transmembrane domain and putatively involves four conserved charged and polar residues that form the proton relay network. The high resolution structure shows the exact geometry of these residues inside the transmembrane domain (**Figure 2**, **Table 1**). In the loose monomer, K940 is situated exactly parallel at equidistance (2.7 Å) to the carboxyl groups of D407 and D408.

Additionally, D407 is within hydrogen bonding distance (2.8 Å) to the hydroxyl group of T978. R971, with its guanidinium side chain residing approximately 6.7 Å from D407 is located further towards the cytoplasm on TM 11. The aromatic side chain of F948 is within close proximity to R971 (3.8 Å).

Upon transition to the tight conformer, TM 4 harboring D407 and D408 displays a kinked conformation at position 400 to 403 (**Figure 3**). The geometry of the residues of the proton relay is hardly affected and the distances between the side chains of these residues remain constant.

Table 1: Distance between residues of the proton relay network in wt AcrB

residues	distance (Å)[a]		
	loose	tight	open
D408-K940	2.7	2.5	8.8
D407-K940	2.7	2.8	3.9
D407-T978	2.8	2.6	4.4
D407-R971	6.7	6.6	10.6

[a]: shortest interatomic distance

In the open monomer, D407 adopts a more tilted conformation towards the periplasm (**Figure 2**). K940 reorients in the direction of TM 11, which in turn shortens its distance to TM 10 at this level by approximately 2.3 Å. In this new position, K940 is likely engaged in polar interactions with T978, S979 and N941. At the same positional height, TM 5 shifts approximately 2.3 Å towards TM 4 and TM 10, into the space formerly occupied by K940. Thus a convergence of TM 4 and 5 as well as of TM 10 and TM 11 can be observed (**Table 2**). Intriguingly, these pairs of α-helices seem to be symmetry related since AcrB is considered to have evolved by a gene duplication event of an ancient protein consisting of six transmembrane helices and one soluble loop (28,29). Further towards the cytoplasm, R971 reorients away from the D407/D408/K940 triad and a concomitant movement of the bulky side chain of F948 can be observed.

Table 2: distance between symmetry related transmembrane helices in different conformations

helices	distance (Å)[a]		
	loose wt/R971A/D407N[b]	tight wt/R971A/D407N[b]	open wt/R971A/D407N[b]
TM4 - TM5 D408 - L442	7.6 / 6.9 / 7.3	8.5 / 6.8 / 8.5	5.3 / 5.6 / 5.5
TM10 - TM11 K940 - S979	11.9 / 10.3 / 10.9	12.5 / 10.4 / 11.5	9.5 / 9.4 / 9.7

[a]: shortest interatomic distances between C_α atoms
[b]: wt: wild-type AcrB; R971A: AcrB_R971A; D407N: AcrB_D407N

The high resolution structure reveals electron density of ordered water molecules in the transmembrane domain in proximity to the proton relay (**Figure 3**). In two of the three monomers, clustering of water molecules is evident. In the loose monomer groups (clusters) of three to five water molecules are apparent. Cluster 1 is situated at the interface of TM 10 and TM 12 and within hydrogen bonding distance of T934 situated on TM 10. The other clusters are localized at the lower 1/3 of the transmembrane domain relatively close to the D407/D408/K940 triad. Cluster 2 resides between TM 10 and TM 11 and is coordinated by D407 and T978. Another cluster (cluster 3) is located between K940 and D408 and includes water molecules occupying the space between TM 4 and TM 6. A fourth cluster (cluster 4) appears to be strategically positioned between D407 and R971. Since the water molecules of cluster 4 are in ideal hydrogen bond of each other, D407 is continuously H-bond connected to R971. Proton transport between D407 (and other residues of the triad) to R971 and further *via* E414 and R418 (not shown) to the bulk solvent of the cytoplasm is therefore theoretically possible.

Cluster 2 and 3 are connected by the side chains of D407, K940 and D408 and are located within hydrogen bonding distance from each other. Cluster 1, however, appears to be isolated and not in direct hydrogen bond contact with either the periplasm or the proton relay network (**Figure 3**).

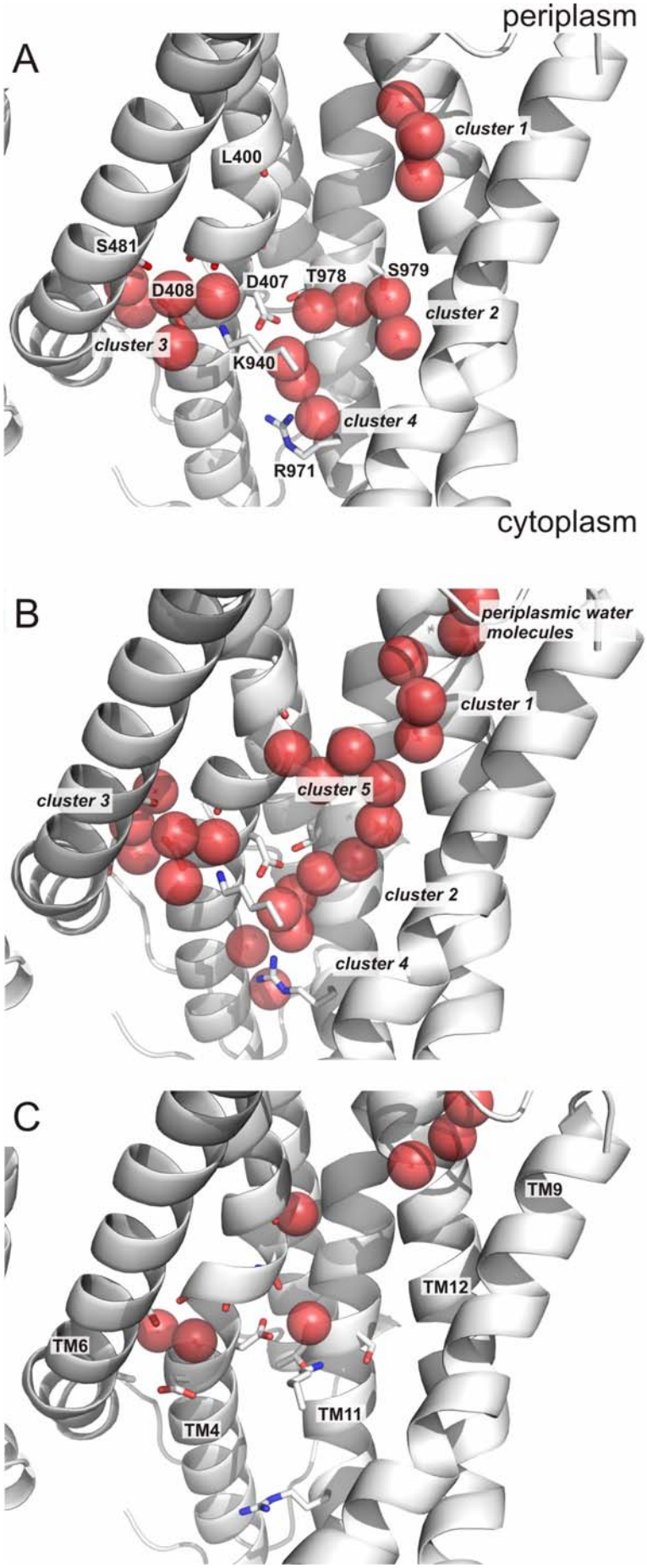

Figure 3: The presence of water and water clusters in the transmembrane domains of the AcrB monomers loose (A), tight (B) and open (C). Residues of the putative proton relay, T978 and S979 are depicted. Residues S481 and T489 situated on TM6 as well as the carbonyl oxygens of residues L400, G403, L404 and L405 are shown in stick presentation. The water clusters 1 to 5 and transmembrane helices 4, 6, 9, 11, 12 are indicated. To increase clarity, only K940 and not the entire TM 10 is shown. **A)** In the loose monomer, residues of the proton relay network are amply hydrated by clusters 2 to 4. A continuous hydrogen bonded network is formed by water molecules of clusters 2, 3 and 4, between residues of the proton relay and the polar side chain of S481 extending from the interspace of TM 4 and TM 6 towards R971. A gap of 9.6 Å is present between cluster 1 and cluster 2.

B) In the tight monomer, the carbonyl oxygen of L400 is exposed due to the kink in TM 4, coordinating one water molecule (C5W1) within the newly formed cluster 5. These water molecules partially fill the gap between cluster 1 and 2. Between cluster 1 and cluster 5 a gap of 4.8 Å is present.

C) The number of water molecules in the transmembrane domain of the open monomer is drastically reduced compared to the hydration in the loose and tight monomer. Only three water molecules in vicinity of the triad are observed. They seem to stabilize the strained TM 4, interacting with the exposed carbonyl oxygens of L404 and L405. Additionally, the carboxyl oxygen of D407 is within hydrogen bonding distance of carbonyl oxygen G403, indicating that D407 might be protonated in the open conformer.

This is in quite a contrast to the water clustering in the tight monomer where cluster 1 is neighbored by another cluster (cluster 5) made out of five water molecules. Cluster 5 is situated in the space defined by TM 4, TM 10 and TM 11. Starting with water molecule C5W1, this cluster propagates from the kink in TM 4 at first laterally towards cluster 1 and then towards the triad. The waters of cluster 5 are separated by a small gap of 4.8 Å from cluster 1 and by 5.4 Å from cluster 2. In addition, water molecules are apparent in the structure that protrude deeper from the periplasm towards cluster 1 in the tight monomer compared to the situation found in the loose monomer. The nearest water from the periplasm is now separated from cluster 1 by only 4.0 Å (**Figure 3**).

The number of water molecules of the transmembrane core domain of the open monomer is dramatically reduced compared to the hydration of the loose and tight monomer. From clusters 1, 2, 3 and 5, only few molecules are left. Cluster 4, which connects D407 with R971 in the loose and tight monomer is absent. However, two water molecules located just above cluster 1 are situated at analogous positions compared to the tight conformer.

The water molecules in the transmembrane domain might not only be directly involved in proton translocation, but are also most likely engaged in the stabilization of the conformation in the transmembrane domain. During the conformational changes, the TM 4 backbone deviates from the typical α-helical constraints at various positions. In the tight conformation, the carbonyl oxygen of L400 is not in hydrogen bonding distance to the amido nitrogen of 404. Apparently, water molecule C5W1 of cluster 5 is situated within a distance of 2.8 Å, which allows the formation of a stabilizing hydrogen bond. In the open conformer, TM 4 is mainly distorted towards the N-terminal region just above D407. The exposed carbonyl oxygens of G403 and L405 appear to undergo stabilizing interactions with two water molecules of cluster 3. In addition, due to reorientation of D407, the carbonyl oxygen of G403 and the hydroxyl proton of D407 carboxylate side chain are within a distance of 2.7 Å in the open monomer (**Figure 3**).

Crystal structure of AcrB proton translocation mutants

We determined the structure of five proton translocation mutants i.e. AcrB_D407N, AcrB_D408N, AcrB_K940A, AcrB_R971A and AcrB_T978A at a resolution of 2.2

to 3.0 Å (**Table S1**). Visual inspection revealed that the asymmetric structures of AcrB_D408N, AcrB_K940A, and AcrB_T978A are very similar compared to the wt structure, whereas the loose and tight monomer of AcrB_D407N and AcrB_R971A show significant deviations. This observation is in accordance with the calculated root mean square deviation (rmsd) between these mutant structures and the wt (**Table S1**).

R971A mutant

The structure of the AcrB_R971A mutant was determined from 2.2 Å resolution diffraction data and after refinement resulted in an R/R_{free} of 24.70/27.70%. The transmembrane domain of either the loose and tight conformer deviate by 1.08 and 1.01 Å rmsd from the corresponding monomer in the wt structure (**Table S1**).

In the loose monomer, the cytoplasmic end of TM 4 and TM 5 are shifted in direction of TM 11 for 2.0 and 1.6 Å, respectively. The position of the TM 4 backbone differs between residues L400 and D407 compared to the wt structure. This change includes a mild reorientation of D407 and the exposure of carbonyl oxygen of L400 (**Figure 4**).

In the tight conformation of the R971A mutant, the C-terminal periplasmic end of TM 2 bends 1.9 Å towards TM 1. TM 4 and TM 5 also differ from the wt structure, but this deviation is apparent further towards the periplasm: TM 4 is relaxed between the residues G397 and D407 and lacks the pronounced kink at L400 as seen in the wt structure (**Figure 5**). TM 5 bulges towards TM 4 and TM 10 at the level of the D407/D408/K940 triad and occupies a position commensurable with the one in the open conformer of the wt structure (**Figure 6**). Similarly, D407 and K940 exhibit in the R971A tight monomer orientations that are characteristic for the open conformation of the wt structure: The D407 side chain is directed towards the periplasm and K940 is reoriented away from D408 and D407 towards TM 11. Furthermore, a coil-to-helix transition at the periplasmic end of TM 8 is apparent, much like the wt conformation in the open monomer (**Figure 6**). Compared to TM 8 in the tight conformation of the wt protein, the periplasmic end is also shifted 1.7 Å towards the position it occupies in the open conformer (C_α of L868).

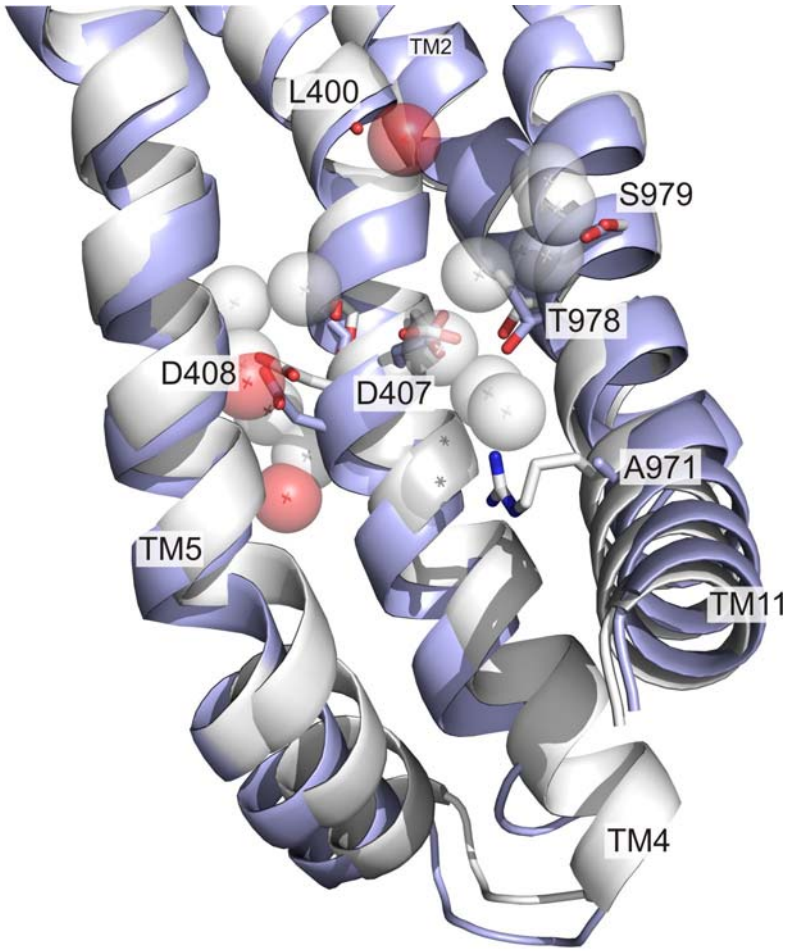

Figure 4: Differences between the loose monomer of wt AcrB and AcrB_R971A. Compared to the wt protein, the cytoplasmic end of TM 4 and TM 5 in the loose conformer of AcrB_R971A are shifted towards TM 11. The intrinsical kink in TM 4 just below residue L400 is also more pronounced in the AcrB_R971A structure. The transmembrane domain is, compared to the wt structure (grey spheres), poorly hydrated (red spheres). Similar observations apply to the AcrB_D407N mutant. AcrB_R971A and wt AcrB are colored blue and white, respectively. Ordered water molecules of the mutant and wt protein are indicated with red and white spheres, respectively. All residues of TM 10 are removed for enhanced visibility of TM 4 and TM 5 and the ordered water molecules.

The hydration of the putative proton translocation channel is also different in the mutant compared to the wt. Most obvious is the absence of ordered water molecules in the lower halfchannel (cluster 4) in all the three conformers. Whereas the proton relay in the loose conformer of wt AcrB is hydrated by waters of cluster 2 - 4, only two water molecules were detected near D408 in the R971A mutant. On the other hand, the exposed carbonyl oxygen of L400 on TM 4 is stabilized by a water molecule that is not present in the wt structure.

Unlike in the wt protein tight monomer, K940 repositions itself from D407 and D408 in the tight conformation of the R971A mutant AcrB (**Figure 6**). However, in the open conformer of the wild-type, the entire TM 11 bulges towards TM 10, which allows K940 to tightly interact with the polar side chains of T978 and S979. This shift of TM 11 is not present in the tight conformation of the R971A mutant structure. Instead, K940 points towards a chain of ordered water molecules (cluster 6) that are not present in any conformation of the wt structure, hydrating the space defined by TM 2, TM 4 and TM 11 (**Figure 5**). On the other hand, cluster 5 of the tight conformation of wt AcrB is not present in the R971A mutant.

D407N mutant

The structure of the AcrB_D407N mutant was determined using data diffracting to a resolution of 2.35 Å and was refined yielding an R/R_{free} of 22.78/25.51%. The transmembrane domain of the loose and tight conformer deviate by 0.63 and 0.80 Å from the corresponding monomer in the wt structure, respectively (**Table S1**).

The AcrB_D407N mutant deviates from the wt protein in a similar manner as the R971A mutant, although to a lesser extent. In the loose conformation, the C_α trace of TM 4 and the N-terminal cytoplasmic end of TM 5 of the D407N mutant lies in between R971A and the wt (**Figure 4**). In the tight conformer, the same shift of the periplasmic end of TM 8 is observed as in R971A, although the coil-to-helix transition is not as extensive. TM 2 and TM 4 are reminiscent to the tight conformer of the R971A mutant and TM 5 bulges towards TM 4 and TM 10 by 1.1 Å compared to a shift of 2.3 Å in the tight to open transition in the wt protein. The side chain of K940, however, exhibits the same orientation as seen in the wt structure (**Figure 6**). As a peculiarity of the D407N mutant, the side chain orientation of N407 is the same in all three conformers.

The putative proton translocation pathway in the loose conformer of D407N is hydrated even more sparsely than the corresponding monomer in the R971A mutant and lacks any apparent ordered water molecule.

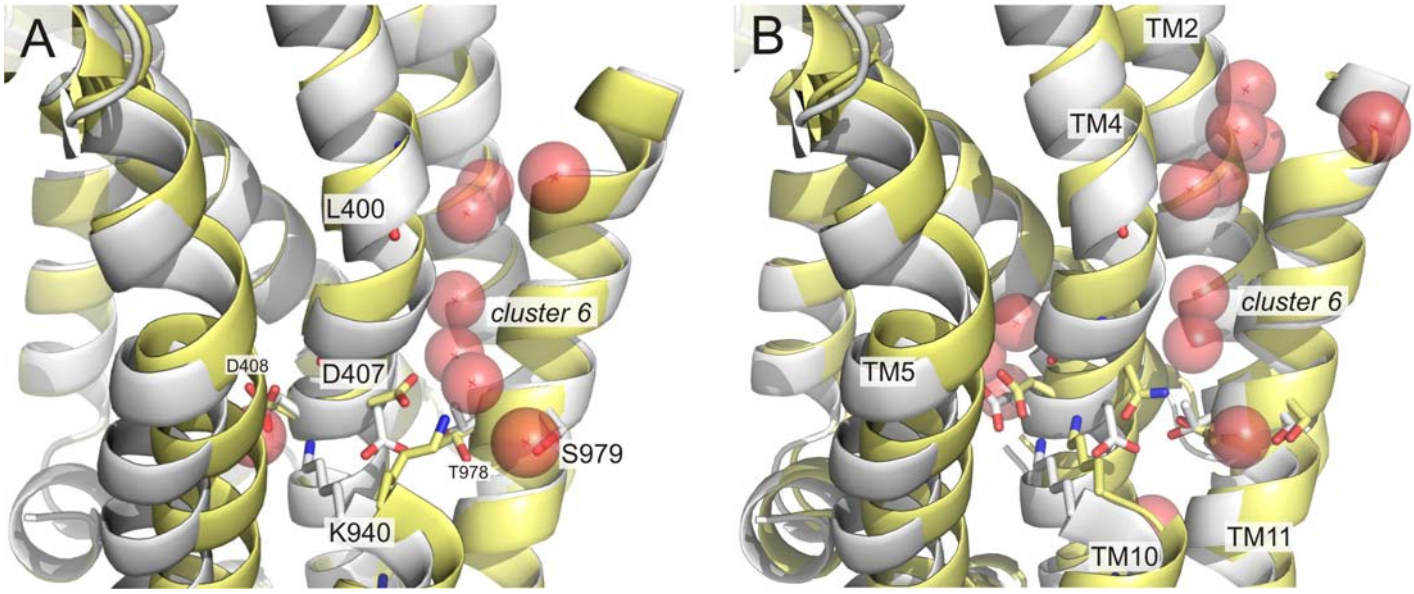

Figure 5: Transmembrane domain of R971A and D407N mutant protein in tight state. **A)** Tight conformer of AcrB_R971A. In comparison to the wt protein, TM 4 in the R971A mutant is less strained between L400 and L404. TM5 and D407 exhibit positions that are typical for the open monomer in the AcrB wt structure. Similarly, K940 is oriented towards TM 11, but unlike to the open monomer of the wt protein, the amino group is orienting a novel cluster (6) of water molecules. **B)** Tight conformer of AcrB_D407N. The transmembrane domain of the tight conformer in AcrB_D407N is similar to the tight monomer in the R971A mutant. Cluster 6 is not contacted by K940, but by the carboxamide group of N407. Structure of AcrB_R971A and AcrB_D407N are colored yellow, AcrB wt structure is shown in grey. Water molecules of the proton translocation mutants are shown as red spheres.

The tight conformation harbors a chain of waters that is reminiscent to cluster 6 in the R971A mutant (**Figure 5**). However, the water molecule that is coordinated by the repositioned K940 in the R971A mutant is lacking in the D407N mutant. At the opposite end of cluster 6, there are three additional water molecules extending 4 Å in the periplasmic direction. In comparison to the wild-type, however, the numbers of waters in each cluster is drastically reduced and the hydrogen bond connection between the triad and R971 is interrupted.

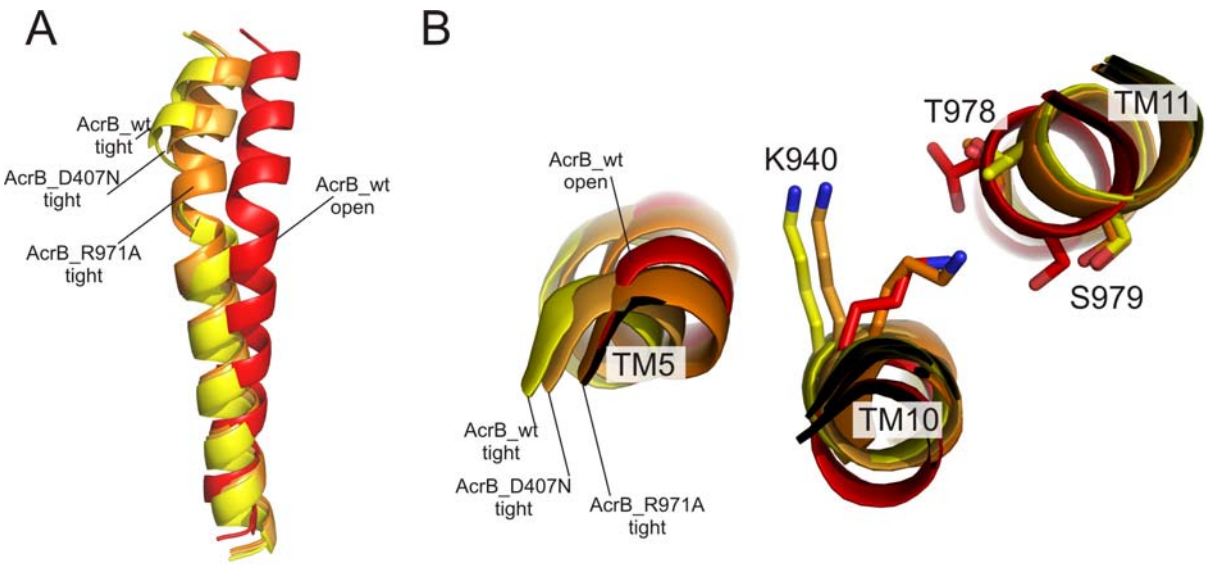

Figure 6: Differences between tight (yellow) and open (red) monomer of wt AcrB and tight momomer of AcrB_R971A (orange) and AcrB_D407N (bright orange). **A)** Periplasmic (N-terminal) end of TM 8. Upon conformational change from tight to open, the periplasmic end of TM 8 in wt AcrB undergoes a coil-to-helix transition, which leads to a relocation of the C_α atom of L868 by 7.8 Å. TM 8 in the tight monomer of the R971A and D407N mutant adopts an intermediate conformation between the two states tight and open described for the wt protein (C_α L868 shift = 2.0 and 1.6 Å in AcrB_R971A and AcrB_D407N, respectively).
B) Reorientation of K940. In the wt protein, K940 reorients towards T978 and S979 of TM 11 during the transition from tight to open. This conformational change is concomitant with TM 11 approaching TM 10 and a bulging of TM 5 towards TM 4 and 10. This bulging can also be observed in the tight conformation of the R971A mutant and, to a lesser extent, in the D407N mutant. Whereas the orientation of K940 in the D407N mutant is comparable to the tight conformer of the wt protein, this residue is repositioned towards TM 11 in the R971A mutant, adopting a similar conformation as observed in the open conformer of wt AcrB. However, the amino group of K940 is not in hydrogen bond contact with T978 or S979, but rather with water molecules of cluster 6 (see **Figure 5**). Structure of the tight and open monomer of AcrB wt is shown in yellow and red, respectively. The tight conformer of AcrB_D407N and AcrB_R971A are shown in bright and dark orange, respectively.

Discussion

Residues D407 and D408 on TM 4 play a crucial role in the transfer of protons from the periplasm to the cytoplasm (14-16). Whereas the cytoplasmic half of TM 4 is a straight α-helix with regular hydrogen bonding interactions, the periplasmic end of TM 4 (residues 392 to 409) is strained at various degrees in the symmetric structure of

AcrB (1IWG) and in all the conformers of the high resolution structures we present here. The periplasmic half of TM 4 contains two aspartate, two glycine and one threonine side chain, all of which have intrinsically low propensity for α-helix formation (30). TM 4 exhibits two major kinks at positions A409 and G403. The latter kink is most distinct in the tight conformer, where as a consequence the carbonyl oxygen of L400 gets exposed. Water molecule C5W1 of cluster 5 (**Figure 3**) is coordinated by this oxygen and marks the starting point of a chain of waters in the upper halfchannel that expands towards the triad. This water file is separated by a gap of 5.3 Å from the solvent network (cluster 2 to 4) hydrating the proton relay.

Upon conformational change from the tight to the open, the kink at G403 becomes less pronounced. As a consequence, water C5W1 is dislocated which disrupts the file of waters in the upper halfchannel. On the other hand, TM 4 is in the open conformation severely distorted between D408 and G403, which results in exposure of the carbonyl oxygens of L405, L404 and G403. The carbonyl oxygen of L405 is stabilized by a water molecule of cluster 3 located in the interspace of TM 4 and TM 6. Another water molecule is sandwiched by the side chain of D408 and the carbonyl oxygen of L405. Computational pK_a calculation of the titratable residues of the transmembrane domain using the PROPKA appoach (31,32) suggest that in the open monomer D407 is protonated. In this state, D407 orients towards the periplasm and its putatively protonated side chain is situated within a distance of 2.7 Å to the exposed carbonyl oxygen of G403, forming a hydrogen bond (**Figure 3**).

In the transmembrane domain region of wt AcrB, the loose conformation is similar to the tight conformation. However, in the loose TM domain the helical kink at position G403 is less pronounced. Consequently no water molecule is present at an appropriate position to start the file of water (cluster 5) of the upper halfchannel as observed in the tight conformation (**Figure 3**).

Open state K940 is surrounded by the polar side chains of residues N941, T978 and S979. The latter two residues reside on TM 11 which shifts towards TM 10 upon the tight to open transition and thereby improves the polar interaction of K940 with T978 and S979 (**Figure 6**). As a consequence, the open conformation does not provide sufficient space between TM 4 and TM 11 to adapt water molecules. Therefore, proton movement *via* a water network does not appear to be feasible in the open monomer.

Out of the five crystallized AcrB proton translocation mutants, only two of them - AcrB_D407N and AcrB_R971A - differ significantly from the wt structure. Our interpretation is that these mutants represent intermediary conformations in the tight conformer, and for both mutants at different stages of the transition from tight to open like those observed in the wt protein. In this light, the D407N structure might represent an early intermediate where the coil-to-helix transition of the periplasmic end of TM 8 and the bulging of TM 5 is only slightly visible as a structural deviation from the wt tight conformation, whereas the R971A structure might be an intermediate of the tight to open transition at a more advanced state. In the latter mutant, the bulging of TM 5 is clearly observable and might be responsible for the reorientation of K940 towards T978 and S979 (**Figure 6**). However, instead of interacting with these polar side chains, like in the open monomer in the wt protein, the ε-amino group of K940 is within hydrogen bonding distance to a water molecule of water cluster 6, which is not present in the open monomer of the wt structure (F**igure 5**).

Based on the high resolution structures of wt and mutant D407N and R971A AcrB, we propose the following order of protonation and deprotonation events during functional rotation from loose to tight to open and back to loose (**Figure 7**): the transmembrane domain of the loose monomer is amply hydrated. D407 is protonated, whereas D408 bears a negative charge. Together, they compensate for the positive charge of the protonated K940, which is situated at equidistance between the two aspartates. The proton relay residue closest to the membrane/cytoplasm interface, R971, might be deprotonated in order to have a charge balance in this region. A similar deprotonation has been postulated for the bacteriorhodopsin R82 (33,34). The transition from loose to tight is induced by the transfer of the proton from D407 to R971. As a result, TM 4 becomes distorted at G403, leading to exposure of the carbonyl oxygen of L400. This carbonyl oxygen is involved in the stabilization of a newly recruited cluster of water molecules (cluster 5) that is separated by approximately 5 Å from waters of cluster 1 situated close to the periplasm and from water cluster 2 which is hydrating the D407/D408/K940 proton relay. Simultaneously, an almost uninterrupted file of ordered water molecules projects from the bulk solvent of the periplasm towards water cluster 1 (**Figure 3**). A small 4.0 Å gap separates the bulk water from cluster 1 and it is hypothesized that due to protein conformational

fluctuation, these clusters converge and form a transient continuous file of water molecules from the bulk solvent of the periplasm to the triad.

On the other hand, in order to avoid a continuous proton pathway through the AcrB transmembrane domain from the periplasm to the cytoplasm and therefore dissipation of the proton motive force, the pathway from the triad to the cytoplasm has to be non-continuous before the triad is in contact with the bulk solvent of the periplasm. This could be accomplished by extrusion of water molecules of cluster 4 present between D407 and R971. Diminishing the number of water molecules would also increase the hydrophobicity in this part of the transmembrane domain and might facilitate lysine deprotonation as well as shift the pK_a of D407 and D408 in order to accept protons from the periplasm. We propose that the open conformer is the result of protonation of D407 by a periplasmic proton. Concomitantly, K940 donates its proton to D408 and reorients towards TM 11. The protonated R971 might keep its positive charge and reorients from the now dehydrated and rather hydrophobic region of the transmembrane domain towards the cytoplasm (as observable in the open monomer conformation). This R971 side chain conformation might be stabilized by cation-π interaction with the aromatic side chain of F948 (**Figure 7**).

The transition from the now open state conformation into the loose conformation might involve the release of a proton from R971 to the cytoplasm. Subsequently, water molecules might re-enter the region between R971 and D407, as observed in the wt loose monomer conformation. K940 would be recharged by the acceptance of a proton from D407 and repositions to its initial position between the D407 and D408 side chains, allowing the exchange of protons between these two aspartates (**Figure 7**).

In short, the protonation scheme depicted in **Figure 7** describes one complete functional rotation cycle of AcrB energized by the flow of one proton from the periplasm to the cytoplasm following its electrochemical gradient. This theoretically enables AcrB to establish a maximal substrate gradient of approximately 1:1000 between the cytoplasm and the cell exterior given the typical value of the proton motive force of -180 mV. To our knowledge, there is no report where the ratio of $[substrate]_{in}/[substrate]_{out}$ was described to be smaller than 1/1000.

The amino acid substitutions at D407 and R971 apparently severely affect the proton pathway presumably due to the shifts in pK_a of the other residues of the proton relay network and due to the effect on water cluster formation and disintegration.

In the loose conformation of AcrB_R971A mutant, the orientation of the residues of the triad is similar to the wt structure and we therefore assume that the protonation state of these residues is the same as in the wt protein. However, the proton transfer from the triad in the direction of the cytoplasm, which is expected to happen during the loose to tight transition in wt AcrB, is interrupted due to the lack of the R971 proton acceptor (**Figure 7**). Considering the sparse hydration of the transmembrane domain in the tight conformer of the R971A mutant, it is likely that the isolated D408 is protonated in the tight monomer of this mutant. Some conformational change might still be feasible and we postulate that during transition from loose to tight, D408 accepts a proton of K940. K940 reorients towards TM 11 and shares a proton with D407 in this observed position. D407 reorients slightly towards the periplasm and would be able to accept a proton from the periplasm (necessary to establish the open conformation), but cannot release the shared proton of D407 and K940 *via* R971. Due to the lack of the R971 side chain, the functional rotation would be interrupted at this point.

In order to explain the conformational intermediate state observed in the D407N mutant, we assume that D407 is essential for the transfer of a proton from the triad to R971 and also presumably is the first residue of the proton relay that gets protonated by a periplasmic proton. Both events are abolished due to the D407N mutation, rendering the AcrB_D407N non-functional. Again some conformational flexibility is apparent and we suggest that in the loose monomer of the D407N mutant, K940 is protonated and shares its proton with the negatively charged D408 (**Figure 7**). Due to the isolation of the triad from the periplasm as a consequence of the loss of the D407 carboxylic group, there is no proton redistribution during the loose to tight conversion. The intermediate state observed in the tight conformation of this mutant describes the inability of N407 to donate a proton to R971. The open conformer of this mutant might be a result of proton transfer from K940 to D408, and subsequent reorientation of the lysine side chain towards TM 11. Interestingly, the carboxyl group of N407 would be logically involved in hydrogen bond formation with the ε-amino group of K940. The oppositely oriented amino group of N407 is, however, not

capable of hydrogen bonding to the carbonyl group in this conformation due to the planar orientation of the sp^2 orbitals. The protonation state of R971 might be the same in all three monomers. Alternatively, R971 accepts and donates protons from and to the cytoplasm, which however does not lead to a net influx of protons from the periplasm to the cytoplasm and hence prevents energization of the entire efflux pump leading to the inactive pump phenotype.

In the AcrB_R971A and D407N mutant, it is mainly the loose and tight monomer that are different compared to the wt structure, whereas the open monomer hardly deviates. We hypothesize that substitution of a formal charged residue by a more hydrophobic amino acid severely disturbs the charge distribution between the proton relay residues in the loose and tight conformation, which can be expected to also affect the structure. In the open monomer, the residues of the triad are postulated to be neutral and R971 is isolated from the triad by reorientation towards the cytoplasm. Therefore, the structure of the open monomer is probably unaffected by the R971A substitution and even stabilised by the D407N exchange.

Recently, structures of the proton translocation mutants D407A, D408A, K940A and T978A crystallized in the symmetric space group H32 were published. The crystals diffracted to a maximum resolution in the range of 3.38 to 3.65 Å (17). All of these mutants showed the following differences compared to the symmetric structure of AcrB, the only conformation known at that time: (i) distortion of the N-terminal portion of TM 4 with major kinks at G403 and A409, (ii) unwinding of TM 5 at the height of the triad and (iii) a shift of F386 and F388 located on the loop between TM 4 and TM 5 towards the centre of the AcrB trimer. The authors attributed these changes to the disrupted salt bridge interactions of the proton translocation mutants. Remarkably, the kink on TM 4 at G403 and A409 were later shown to be features of the tight and open conformer in the asymmetric structure, respectively (8-10). In addition, TM 5 was shown to be flexible and to adopt different conformations during functional rotation. In the wt structure and the proton translocation mutants we present here, a bulging of TM 5 rather than unwinding (as described by (17)) can be observed, which might be explained by the increased resolution and the improved model. Our structures are, however, not indicative for a shift of residues F386 and F388 towards the central cavity.

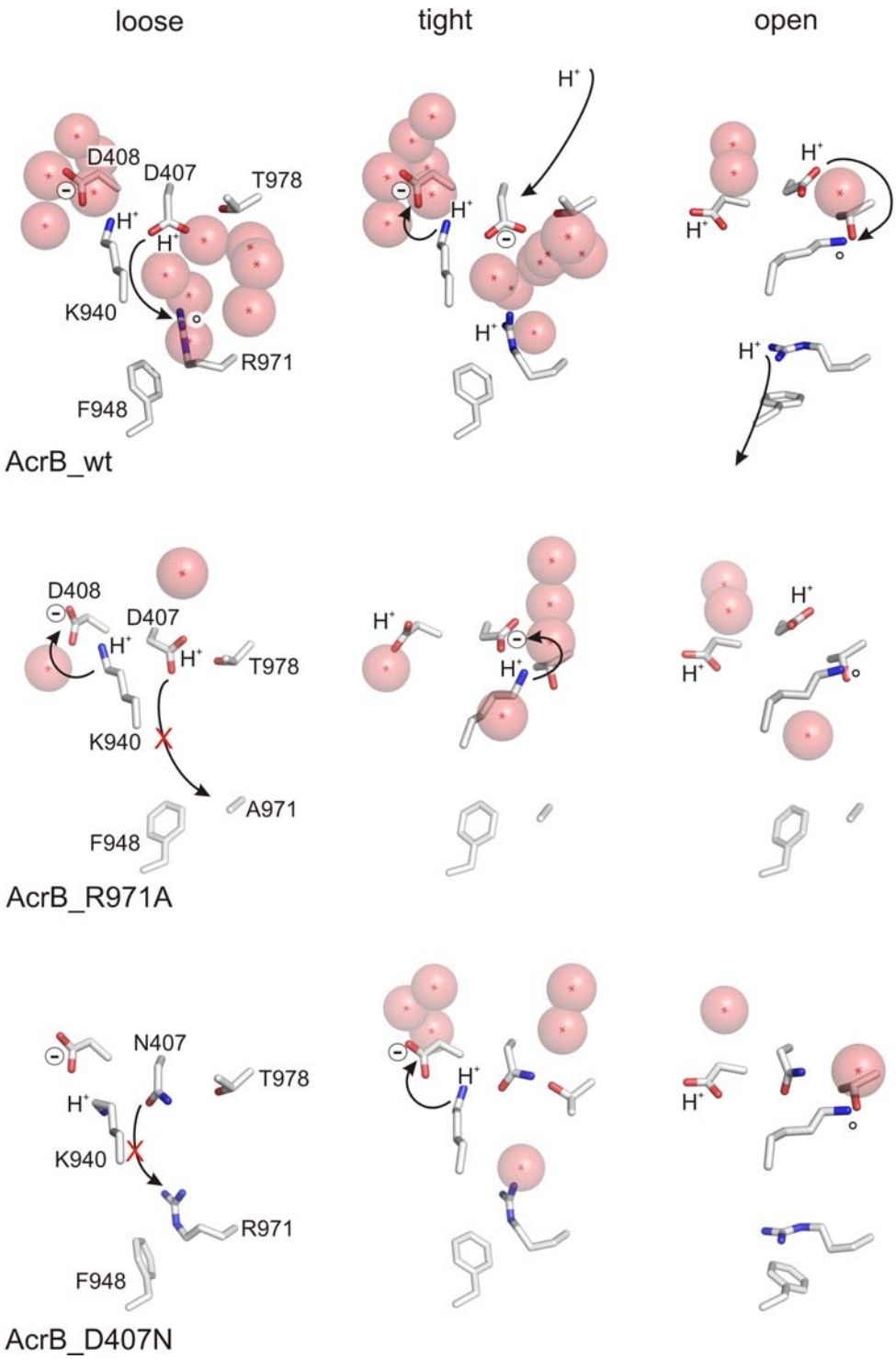

Figure 7: Schematic representation of hypothetical protonation and deprotonation events in the transmembrane domain of wt AcrB, AcrB_R971A or AcrB_D407N during functional rotation. Key residues are denoted and water molecules of cluster 2, 3, 4 and 6 (AcrB_R971 and AcrB_D407N) close to proton relay residues are shown in red spheres. The arrows indicate redistribution of protons. The protonation states of the arginine, lysine and aspartate residues are indicated. R971 in the AcrB_D407N mutant might be either charged or neutral during the entire functional rotation. See *Discussion* for detailed description.

Of all the different substrates we crystallized in presence of AcrB, we could only identify minocycline and doxorubicin in the binding pocket. Whereas the position of minocycline is congruent with the structure of Murakami *et al*. (8), the orientation of doxorubicin is quite different (**Figure 8**). Superimposition of the two structures reveals that the core ring systems of the doxorubicin molecules partially overlap, but that they are oriented in opposite directions. Therefore, F178 of our high resolution structure interacts with the aromatic D ring rather than with the non-aromatic A ring. In the structure of Murakami *et al.*, F617 seems to interact with the D ring, whereas in our structure doxorubicin and F617 are separated by 5.3 Å and the side chain of F617 exhibits a different orientation. It has to be emphasized that only for the AcrB/minocyline complex the position of the substrate was confirmed by using a brominated derivative (8).

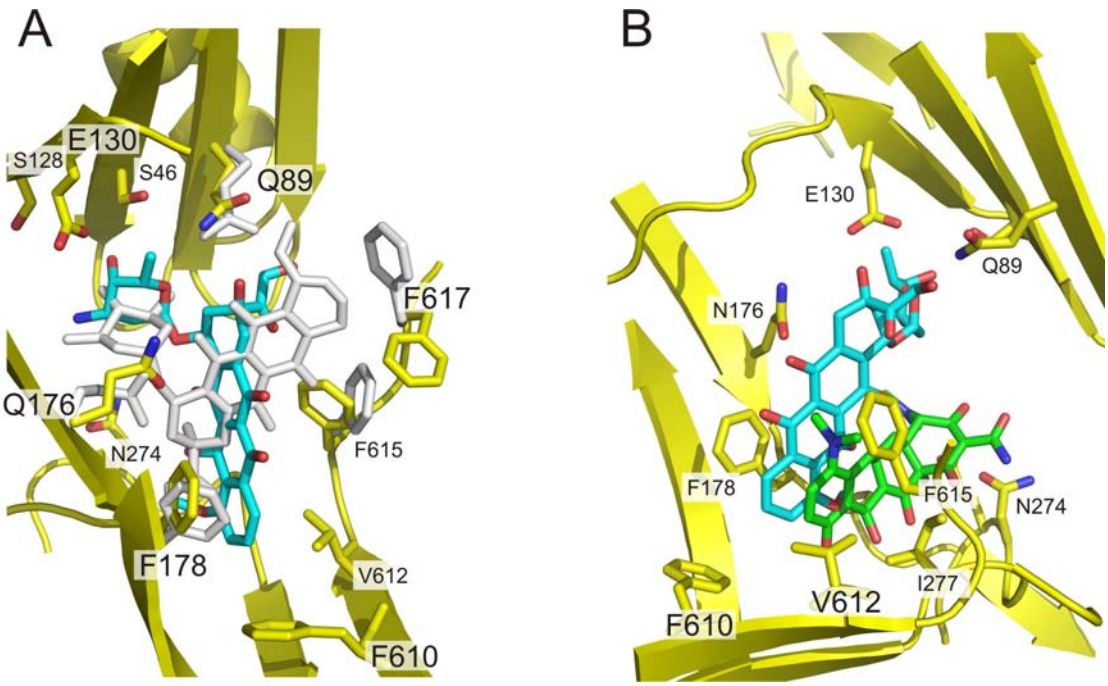

Figure 8: Superimposition of bound substrate in the AcrB binding pocket. **A)** Comparison of doxorubicin binding in 2DR6 and in recent structure. The new AcrB/doxorubicin complex is shown in yellow and cyan, respectively. Doxorubicin and binding pocket residues of 2DR6 that differ significantly are shown in grey. **B)** Comparison of position of minocycline and doxorubicin in the binding pocket. Doxorubicin and minocycline are shown in cyan and green, respectively. The depicted side chains derive from the AcrB/minocycline structure, but are congruent with the orientation observed for the AcrB/doxorubicin complex.

In summary, the high resolution crystal structures described in this report reveal a hitherto unprecedented molecular detail of substrate binding and transmembrane hydration allowing to propose a detailed molecular mechanism for proton transfer in accordance with the observed properties of the multidrug/proton antiporter AcrB.

Materials and Methods

Bacterial strains, plasmids and growth conditions

E. coli C43 (DE3) (35) harboring pET24acrB$_{His}$ (26) and mutant derivatives (16) were used for protein overexpression. LB medium and LB agar (36) were used for routine bacterial growth at 37°C. Terrific broth (37) was used for protein overexpression. Kanamycin (Applichem) was applied at 50 μg ml^{-1} (Kan^{50}).

Crystallization of wt and mutant AcrB in presence of DARPins

Overexpression and membrane preparation of wt and mutant AcrB was carried out as described previously (9,26). DARPin clone 1108_19 (10) was overexpressed and purified according to Binz *et al.* (19). To crystallize the AcrB/DARPin complex, the method described by Sennhauser *et al.* (10) with *n*-dodecyl-β-D-maltoside as detergent was applied. For the AcrB_T978A variant, buffer exchange was from Tris-HCl to KP$_i$ buffer, instead of HEPES (pH 7.5), due to precipitation problems. Substrate was added prior to crystallization at a concentration of 2 mM and 0.4 mM for minocycline and doxorubicine (Sigma-Aldrich), respectively. Formation of crystals for the AcrB_T978A/DARPin complex was only observed in the absence of substrate. Crystals were grown by the hanging drop vapor diffusion method at 0.05 M ADA buffer pH 6.5, 7-9% polyethylene glycol (PEG) 4000, 6-10% glycerol, 0.2 M $(NH_4)SO_4$.

X-ray diffraction dataset analysis and refinement procedure

Datasets of $P2_12_12_1$ crystals were collected at the beamline X06SA of the Swiss Light Source (Paul Scherrer Institut, Villigen, Switzerland) (wavelength 0.80-1.0 Å). Data reduction was done with the XDS package (38). Refinement was performed with the program PHENIX (39) and REFMAC5 (40). Model rebuilding was performed using

the program COOT (41). In later stages, bulk solvent correction was applied using phenix.refine (42) and additional water molecules were appended and analyzed employing COOT. Figures were created using Pymol (http://pymol.sourceforge.net/).

References

1. Saier, M. H., Jr., and Paulsen, I. T. (2001) *Semin Cell Dev Biol* **12**, 205-213
2. Lorca, G. L., Barabote, R. D., Zlotopolski, V., Tran, C., Winnen, B., Hvorup, R. N., Stonestrom, A. J., Nguyen, E., Huang, L. W., Kim, D. S., and Saier, M. H., Jr. (2007) *Biochim Biophys Acta* **1768**, 1342-1366
3. Ren, Q., and Paulsen, I. T. (2005) *PLoS Comput Biol* **1**, e27
4. Seeger, M. A., Diederichs, K., Eicher, T., Brandstatter, L., Schiefner, A., Verrey, F., and Pos, K. M. (2008) *Curr Drug Targets* **9**, 729-749
5. Pos, K. M. (2009) *Biochim Biophys Acta* **1794**, 782-793
6. Murakami, S. (2008) *Curr Opin Struct Biol* **18**, 459-465
7. Murakami, S., Nakashima, R., Yamashita, E., and Yamaguchi, A. (2002) *Nature* **419**, 587-593
8. Murakami, S., Nakashima, R., Yamashita, E., Matsumoto, T., and Yamaguchi, A. (2006) *Nature* **443**, 173-179
9. Seeger, M. A., Schiefner, A., Eicher, T., Verrey, F., Diederichs, K., and Pos, K. M. (2006) *Science* **313**, 1295-1298
10. Sennhauser, G., Amstutz, P., Briand, C., Storchenegger, O., and Grutter, M. G. (2006) *PLoS Biol* **5**, e7
11. Eicher, T., Brandstatter, L., and Pos, K. M. (2009) *Biol Chem*
12. Goldberg, M., Pribyl, T., Juhnke, S., and Nies, D. H. (1999) *J Biol Chem* **274**, 26065-26070
13. Zgurskaya, H. I., and Nikaido, H. (1999) *Proc Natl Acad Sci U S A* **96**, 7190-7195
14. Guan, L., and Nakae, T. (2001) *J. Bacteriol.* **183**, 1734-1739
15. Takatsuka, Y., and Nikaido, H. (2006) *J Bacteriol* **188**, 7284-7289
16. Seeger, M. A., von Ballmoos, C., Verrey, F., and Pos, K. M. (2009) *Biochemistry*
17. Su, C. C., Li, M., Gu, R., Takatsuka, Y., McDermott, G., Nikaido, H., and Yu, E. W. (2006) *J Bacteriol* **188**, 7290-7296
18. Binz, H. K., Amstutz, P., Kohl, A., Stumpp, M. T., Briand, C., Forrer, P., Grutter, M. G., and Pluckthun, A. (2004) *Nat Biotechnol* **22**, 575-582
19. Binz, H. K., Stumpp, M. T., Forrer, P., Amstutz, P., and Pluckthun, A. (2003) *J Mol Biol* **332**, 489-503
20. Yu, E. W., McDermott, G., Zgurskaya, H. I., Nikaido, H., and Koshland, D. E., Jr. (2003) *Science* **300**, 976-980
21. Yu, E. W., Aires, J. R., McDermott, G., and Nikaido, H. (2005) *J. Bacteriol.* **187**, 6804-6815
22. Tornroth-Horsefield, S., Gourdon, P., Horsefield, R., Brive, L., Yamamoto, N., Mori, H., Snijder, A., and Neutze, R. (2007) *Structure* **15**, 1663-1673

23. Das, D., Xu, Q. S., Lee, J. Y., Ankoudinova, I., Huang, C., Lou, Y., DeGiovanni, A., Kim, R., and Kim, S. H. (2007) *J Struct Biol* **158**, 494-502
24. Drew, D., Klepsch, M. M., Newstead, S., Flaig, R., De Gier, J. W., Iwata, S., and Beis, K. (2008) *Mol Membr Biol* **25**, 677-682
25. Veesler, D., Blangy, S., Cambillau, C., and Sciara, G. (2008) *Acta Crystallogr Sect F Struct Biol Cryst Commun* **64**, 880-885
26. Pos, K. M., and Diederichs, K. (2002) *Acta Crystallogr. Biol. Crystallogr.* **D58**, 1865-1867
27. Pos, K. M., Schiefner, A., Seeger, M. A., and Diederichs, K. (2004) *FEBS Lett* **564**, 333-339
28. Paulsen, I. T., Brown, M. H., and Skurray, R. A. (1996) *Microbiol Rev* **60**, 575-608
29. Guan, L., Ehrmann, M., Yoneyama, H., and Nakae, T. (1999) *J Biol Chem* **274**, 10517-10522
30. Pace, C. N., and Scholtz, J. M. (1998) *Biophys J* **75**, 422-427
31. Li, H., Robertson, A. D., and Jensen, J. H. (2005) *Proteins* **61**, 704-721
32. Bas, D. C., Rogers, D. M., and Jensen, J. H. (2008) *Proteins* **73**, 765-783
33. Xiao, Y., Hutson, M. S., Belenky, M., Herzfeld, J., and Braiman, M. S. (2004) *Biochemistry* **43**, 12809-12818
34. Hutson, M. S., Alexiev, U., Shilov, S. V., Wise, K. J., and Braiman, M. S. (2000) *Biochemistry* **39**, 13189-13200
35. Miroux, B., and Walker, J. E. (1996) *J Mol Biol* **260**, 289-298
36. Sambrook, J., Fritsch, E. F., and Maniatis, T. (1989) *Molecular cloning: a laboratory manual*, Cold Spring Harbor Laboratory Press, Cold Spring Harbor, N.Y.
37. Tartof, K. D., and Hobbs, C. A. (1987) *Bethesda Research Laboratories Focus* **9**, 12
38. Kabsch, W. (1993) *J. Appl. Cryst.*, 795-800
39. Adams, P. D., Grosse-Kunstleve, R. W., Hung, L. W., Ioerger, T. R., McCoy, A. J., Moriarty, N. W., Read, R. J., Sacchettini, J. C., Sauter, N. K., and Terwilliger, T. C. (2002) *Acta Crystallogr D Biol Crystallogr* **58**, 1948-1954
40. Murshudov, G. N., Vagin, A. A., Dodson, E. J. (1997) *Acta Crystallogr. Biol. Crystallogr.* **D53**, 240-255
41. Emsley, P., and Cowtan, K. (2004) *Acta Crystallogr. Biol. Crystallogr.* **D60**, 2126-2132
42. Afonine, P. V., Grosse-Kunstleve, R. W., and Adams, P. D. (2005) *Acta Crystallogr D Biol Crystallogr* **61**, 850-855

Supplementary materials for:

The AcrB proton pathway

Thomas Eicher, Markus A. Seeger, Lorenz Brandstätter, Francois Verrey, Markus Grütter, Kay Diederichs, Klaas M. Pos

Supplementary tables S1 and S2
References

Table S1: Crystallographic data and refinement

	AcrB_wt/ DARPin & minocycline	**AcrB_wt/ DARPin & doxorubicin**	**AcrB_D407N/ DARPin & minocycline**	**AcrB_D408N/ DARPin & minocycline**	**AcrB_K940A/ DARPin & minocycline**	**AcrB_R971A/ DARPin**	**AcrB_T978A/ DARPin**
Data collection							
space group	$P2_12_12_1$	$P2_12_12_1$	$P2_12_12_1$	$P2_12_12_1$	$P2_12_12_1$	$P2_12_12_1$	$P2_12_12_1$
Cell dimensions							
a (Å)	145.99	145.85	145.59	145.88	145.91	145.79	146.01
b (Å)	161.72	161.60	161.59	161.16	162.32	160.77	164.05
c (Å)	245.97	245.70	245.97	245.29	245.81	246.45	245.58
α (°)	90.00	90.00	90.00	90.00	90.00	90.00	90.00
β (°)	90.00	90.00	90.00	90.00	90.00	90.00	90.00
γ (°)	90.00	90.00	90.00	90.00	90.00	90.00	90.00
Resolution (Å)	2.00	2.26	2.35	2.40	2.35	2.20	3.00
R_{meas} (%)	166.8[a]	73.1	218.9[c]	59.1	122.6	83.8	119.7
I/σ_I	1.38[b]	2.37	1.26[d]	3.37	2.66	2.39	2.22
Completeness (%)	97.9	93.4	98.3	96.0%	97.7	94.2%	97.8
redundancy	6.23	5.15	7.15	6.87	7.49	7.42	8.31
Refinement							
Trimer model	2J8S	2J8S	2J8S	2J8S	2J8S	2J8S	2J8S
Program	PHENIX[e,f] & REFMAC5 [g]	PHENIX[e,f] & REFMAC5 [c]	PHENIX[e,f] & REFMAC5 [c]	PHENIX[e,f] & REFMAC5 [c]	PHENIX[e,f] & REFMAC5 [c]	PHENIX[e,f] & REFMAC5 [c]	PHENIX[e,f] & REFMAC5 [c]
Resolution (Å)	39.47 - 2.00	38.45 - 2.25	49.34 - 2.35	44.80 - 2.40	45.78 - 2.35	48.90 - 2.20	47.74 - 3.00
No. of reflections	389310	275152	240370	225098	241893	288958	118297
R_{work}	22.07	19.84	22.78	18.89	19.04	24.70	24.62
R_{free}	24.11	22.82	25.51	23.41	22.70	27.70	27.16

	AcrB_wt/ DARPin & minocycline	AcrB_wt/ DARPin & doxorubicin	AcrB_D407N/ DARPin & minocycline	AcrB_D408N/ DARPin & minocycline	AcrB_K940A/ DARPin & minocycline	AcrB_R971A/ DARPin	AcrB_T978A/ DARPin
No. atoms							
macromolecule	26118	26124	26153	26105	26071	26164	26079
residues							
solvent residues	3929	2293	2153	2112	2358	2244	
B-factors							
macromolecule	30.6	45.8	39.0	43.4	43.6	28.6	37.1
solvent	50.0	49.9	45.8	43.1	45.5	34.6	
overall	33.12	46.1	39.5	43.4	43.8	29.1	37.1
RMS deviations							
bond length (Å)	0.006	0.006	0.006	0.006	0.006	0.006	0.007
bond angles (°)	0.962	1.045	0.956	1.010	1.028	0.963	1.032
RMS deviation of transmembrane							
domain of mutant	loose		0.63	0.36	0.37	1.08	0.27
protein compared	tight		0.80	0.44	0.27	1.01	0.26
to wt (Å)[h]	open		0.40	0.22	0.24	0.32	0.25

[a]: 102.7% at 2.12 Å
[b]: 2.64 at 2.12 Å
[c]: 179.6% at 2.45 Å
[d]: 1.58 at 2.45 Å
[e]: (1)
[f]: (2)
[g]: (3)
[h]: calculated with program superpose (3). Selected residues (main chain atoms): 8-29, 330-558, 862-1029.

Table S2: Distance between binding pocket residues and AcrB substrates minocycline and doxorubicin

residues	distance (Å)[a]	residues	distance (Å)[a]
Doxorubicin (DM2)		Minocycline (MIY)	
S46 (CB) - DM2 (O4')	3.1		
Q89 (NE2) - DM2 (O5')	3.3		
S128 (OG) - DM2 (O4')	4.7		
E130 (OE1) - DM2 (C6')	3.2		
Q176 (OE1) - DM2 (C16)	4.0	Q176 (OE1) - MIY (C71)	4.7
		L177 (O) - MIY (C7)	4.2
F178 (CD1) - DM2 (C20)	3.4	F178 (CE1) - MIY (C71)	3.5
G179 (N) - DM2 (C21)	3.0	G179 (N) - MIY (C16)	3.3
		S180 (CB) - MIY (O7)	3.8
		E273 (OE1) - MIY (C19)	4.0
		N274 (OD1) - MIY (O7)	3.1
I277 (CB) - DM2 (O4)	4.1	I277 (CB) - MIY (O5)	3.3
F610 (CZ) - DM2 (C2)	4.6		
V612 (CG2) - DM2 (C2)	3.8	V612 (CE2) - MIY (C12)	4.0
F615 (CE1) - DM2 (O13)	3.1	F615 (CD1) - MIY (CN7)	3.2

[a]: shortest interatomic distance

References

1. Adams, P. D., Grosse-Kunstleve, R. W., Hung, L. W., Ioerger, T. R., McCoy, A. J., Moriarty, N. W., Read, R. J., Sacchettini, J. C., Sauter, N. K., and Terwilliger, T. C. (2002) *Acta Crystallogr D Biol Crystallogr* **58**, 1948-1954
2. Afonine, P. V., Grosse-Kunstleve, R. W., and Adams, P. D. (2005) *Acta Crystallogr D Biol Crystallogr* **61**, 850-855
3. Murshudov, G. N., Vagin, A. A., Dodson, E. J. (1997) *Acta Crystallogr. Biol. Crystallogr.* **D53**, 240-255

5. Structural and functional aspects of the multidrug efflux pump AcrB

This section contains a Minireview that was accepted for publication in Biological Chemistry and published online on May 20th 2009.

The article essentially consists of excerpts of the introduction of this thesis providing a brief overview of the different mechanisms leading to antibiotic resistance and summarizes genetic and biochemical experiments on AcrB performed by various groups.
Additionally, the different structures and conformations of AcrB are recapitulated and the current understanding of substrate transport and energization is presented.

Biol. Chem., Vol. 390, pp. xxx-xxx, August 2009 • Copyright © by Walter de Gruyter • Berlin • New York. DOI 10.1515/BC.2009.XXX

Review

Structural and functional aspects of the multidrug efflux pump AcrB

Thomas Eicher[1], Lorenz Brandstätter[1] and Klaas M. Pos[2,*]

[1] Institute of Physiology and Zurich Center for Integrative Human Physiology (ZIHP), University of Zurich, Winterthurerstrasse 190, CH-8057 Zurich, Switzerland

[2] Cluster of Excellence Frankfurt – Macromolecular Complexes and Institute of Biochemistry, Goethe University Frankfurt, Max-von-Laue-Str. 9, D-60438 Frankfurt/Main, Germany

* Corresponding author
e-mail: pos@em.uni-frankfurt.de

Abstract

The tripartite efflux system AcrA/AcrB/TolC is the main pump in *Escherichia coli* for the efflux of multiple antibiotics, dyes, bile salts and detergents. The inner membrane component AcrB is central to substrate recognition and energy transduction and acts as a proton/drug antiporter. Recent structural studies show that homotrimeric AcrB can adopt different monomer conformations representing consecutive states in an allosteric functional rotation transport cycle. The conformational changes create an alternate access drug transport tunnel including a hydrophobic substrate binding pocket in one of the cycle intermediates.

Keywords: AcrB; alternate access transport mechanism; antibiotic resistance; binding change mechanism; drug transport; membrane protein structure; multiple drug efflux pump.

Introduction

Resistance of bacteria towards antibiotics is known to be evoked by at least three different mechanisms: (i) target modification [e.g., resistance against macrolides mediated by methylation of the ribosome (Skinner et al., 1983; Zalacain and Cundliffe, 1989, 1990) or resistance against fluoroquinolones by mutations in DNA gyrase (Yoshida et al., 1990; Hooper, 1995)]; (ii) antibiotic modification (e.g., hydrolysis of β-lactam ring by β-lactamase; Thomson and Smith Moland, 2000) or phosphorylation, adenylation or acetylation of aminoglycosides (Wright, 1999); and (iii) reduced accumulation of antibiotics in the target compartments (periplasm, cytoplasm) through suppression of porin synthesis (Hancock and Brinkman, 2002) and/or overproduction of efflux pumps (Nikaido, 1998, 2009; Lomovskaya et al., 1999; Li and Nikaido, 2004; Lomovskaya and Totrov, 2005; Nikaido and Takatsuka, 2008).

Resistance conferred by antibiotic and target modification is often restricted to a single class of antibiotics or even a single compound. In contrast, multidrug resistance (MDR) transporters enable the bacteria to efflux a broad range of substances and hence confer simultaneous resistance to unrelated compounds. The central role of MDR transporters as a primary line of defense and, intriguingly, as mediators for the acquisition of other resistance mechanisms have been shown in several cases (Lomovskaya et al., 1999; Mazzariol et al., 2000; Mahamoud et al., 2007).

Proteins of the Resistance-Nodulation-Division (RND) superfamily (TC#2.A.6) are ubiquitous in all phyla. In prokaryotes, their main physiological function seems to be associated with the extrusion of noxious substrates, with notable exceptions such as the secretory accessory proteins SecDF (Gardel et al., 1987; Pogliano and Beckwith, 1994), lipid exporter MmpL7 (Camacho et al., 2001; Domenech et al., 2005) and the putative lipooligosaccharide nodulation factor exporter NolG (Baev et al., 1991). In Eukarya, however, the functionally characterized RND proteins seem to be involved in lipid homeostasis (Davies et al., 2000; Davies and Ioannou, 2000; Sleat et al., 2004; Infante et al., 2008a,b) and cell morphogenesis (Taipale et al., 2002; Nakano et al., 2004). As phylogenetic analyses suggest, energization via the proton (or sodium ion) motive force might be a common feature for all RND proteins (Saier and Paulsen, 2001).

Resistance nodulation division (RND) efflux pump AcrB

Proteobacterial members of the RND superfamily are located in the inner membrane. They typically assemble with two accessory proteins, a membrane fusion protein (MFP; TC#8.A.1) and an outer membrane factor (OMF; TC#1.B.17). The so-formed tripartite MFP/RND/OMF complex spans the inner membrane, the periplasm as well as the outer membrane of the Gram-negative bacterium. Most extensively studied examples of these three component systems are MexA/MexB/OprM of *Pseudomonas aeruginosa* or AcrA/AcrB/TolC of *Escherichia coli* (Figure 1A). Both outer membrane and tripartite efflux pumps are considered to be the main barrier for drugs on their way to the inside of the bacterial cell (Plesiat and Nikaido, 1992; Nikaido, 2003, 2009). It is this combination of the intrinsic impermeability of the outer membrane, reduction of the number of outer membrane pores and upregulation of multidrug efflux pumps which enables effective synergistic drug resistance (Nikaido,

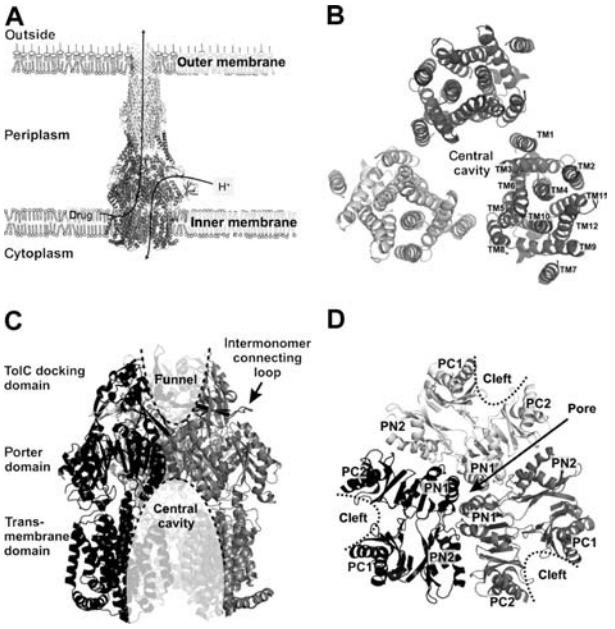

Figure 1 Schematic drawing of the tripartite multidrug efflux system AcrAB-TolC of Gram-negative *E. coli* and AcrB structural features.
(A) Inner membrane component AcrB (RND component) accounts for substrate recognition/selection and energy transduction. Drugs might be captured from the outer leaflet of the inner membrane and are extruded in a coupled exchange with protons. The TolC channel (OMF component) mediates the exit through the outer membrane and connects to AcrB via a long periplasmic conduit. AcrA (MFP component) connects AcrB and TolC. The presence of all three components is essential for the MDR phenotype. (B) Topological view of the transmembrane (TM) domain perpendicular to the membrane plane. TM4 and TM10 are surrounded by the other 10 TM helices. The TM domains of the three monomers confine a large central cavity. (C) Side view of trimeric AcrB. A central pore located in the porter domain separates a funnel-like structure in the TolC-docking domain from the central cavity located in the TM domain. The central pore, however, does not appear to allow direct passage of drugs. The trimeric state of AcrB is mainly stabilized by the intermonomer connecting loops. (D) Top view of the porter domain with its subdomains PN1, PN2, PC1 and PC2 perpendicular to the membrane plane. The central pore is formed by three α-helices, donated by the PN1 subdomains of each AcrB monomer. A cleft is apparent between the PC1 and PC2 subdomains of each monomer.

1996). Strikingly, dysfunction of only one component of the tripartite system results in a complete drug-sensitive phenotype.

RND proteins, such as MexB (Mex: multiple efflux) and AcrB (Acr: acriflavine resistance), represent the energy module and the substrate specificity determinant of the tripartite RND/MFP/OMF efflux system. The substrate variety of MexB or AcrB, compared to the many other MDR proteins, is staggering. It includes dyes, bile salts, organic solvents and antibiotics of different chemical classes; molecules that are anionic, cationic, zwitterionic, aromatic or just aliphatic; chemicals of bulky or planar geometry. However, since export of membrane lipids and co-factors, such as flavins, is expected to be detrimental for bacterial cells, additional criteria to discriminate between noxious compounds and vital cell constituents must exist, a matter of ongoing research. Like most proteobacterial RND proteins, AcrB consists of 12 transmembrane (TM) α-helices and two extensive periplasmic loops which account for approximately half of the 1049 amino acids of the protein. The loops connect TM1 with TM2 and TM7 with TM8, respectively. The topology of the TM domain – five-plus-one-TM helices, repeated twice – is also referred to as RND signature (Ioannou, 2001). The repetition of the motif suggests that RND transporters arose as a result of an intragenic tandem duplication event.

It appears that the substrate specificity determination is residing in the periplasmic loops, which was shown through the design of chimeric proteins. Specifically, the two extracellular loops of the *Escherichia coli* aminoglycoside exporter AcrD were replaced by the periplasmic loops of AcrB (Elkins and Nikaido, 2002). The resulting transporter exhibited a resistance pattern that was typical for AcrB. Conversely, when the periplasmic loops of AcrB were replaced by the corresponding domains of AcrD, the chimeric protein lost the ability to confer resistance towards substrates of AcrB, but the resistance towards aminoglycosides was enhanced. Domain swapping experiments between MexB and MexY led to similar results (Eda et al., 2003). Here, the periplasmic loops of MexB were combined with the TM domain of MexY. Again, the resulting protein conferred resistance towards typical MexB substrates, while the cells were susceptible towards MexY specific drugs. Additional evidence on the role of the periplasmic domain in substrate specificity determination came from a study where six single site mutations causing altered substrate specificity were all found to be located on the extracellular loops (Mao et al., 2002). Crystallographic studies provided further insights on the role of the periplasmic loops in substrate recognition and transport (Murakami et al., 2006; Seeger et al., 2006; Sennhauser et al., 2007).

Structure of AcrB

The first AcrB structure (Murakami et al., 2002) was based on 3.5 Å X-ray diffraction data from crystals containing one unliganded AcrB monomer in the asymmetric unit and for which the trimer is generated by exact crystallographic symmetry. Each monomer contains a TM domain with 12 TM helices which form a bundle with two central helices (TM4 and TM10) in its topological core. On these central α-helices, three titratable residues, Asp407, Asp408 and Lys940, were found to be essential for protein function (Guan and Nakae, 2001; Su et al., 2006; Takatsuka and Nikaido, 2006; see Figure 1B).

The periplasmic part – formed by the periplasmic loops described above – extends 70 Å into the periplasm. It can be further divided into a TolC docking domain which is most distal from the membrane plane and a porter domain, formerly known as pore domain (Figure 1C).

The TolC-docking domain is the expected interaction site of the outer membrane channel TolC (Tikhonova and Zgurskaya, 2004; Tamura et al., 2005; Bavro et al., 2008; Pietras et al., 2008). The TolC docking domain of each monomer furthermore exhibits a hairpin-like loop that protrudes into the neighboring monomer, which appears

to be the main stabilizing factor for the trimeric AcrB complex.

The porter domain is divided into subdomains PN1, PN2, PC1 and PC2, which are coupled by sequential proximity (PN1–PN2, PC1–PC2) or by sharing β-strands to form common β-sheets (PN2–PC1, PC2–PN1; see Figure 1D). The PN1 subdomains are located in the center of the trimer, surrounded by the PN2, PC1 and PC2 subdomains towards the periphery. A cleft is apparent between the PC1 and PC2 subdomains, which is approximately perpendicular to the membrane plane. In the center of the trimer, the TolC docking domain exhibits a funnel-like structure narrowing to a central pore, defined by α-helices (designated pore helices) of the PN1 subdomains of each monomer. This pore has a small diameter and therefore does not allow drug passage in this conformation. Towards the membrane plane, the central pore leads to a central cavity and further to a 30–35 Å wide, presumably lipid-filled TM hole defined by the ring-like arrangement of the TM helices of the trimer. Three vestibules at the monomer interface located just above the membrane plane lead towards the central cavity. It is postulated that substrate might access the central cavity via these vestibules (Murakami et al., 2002). Indeed, there have been several reports on AcrB/substrate co-crystals with positive densities in the electron density maps derived from (symmetric) R32 crystals that have been interpreted as substrate molecules bound to the inner wall of the AcrB central cavity (Yu et al., 2003a,b, 2005; Pos et al., 2004; Tornroth-Horsefield et al., 2007; see Figure 1B, C).

In 2006 and 2007, three groups independently published an asymmetric structure of AcrB grown in the monoclinic space group C2 (2.8–2.9 Å; Murakami et al., 2006; Seeger et al., 2006), triclinic space group P1 (3.0 Å; Seeger et al., 2006) and an AcrB structure including bound designed ankyrin repeat proteins (DARPins) grown in orthorhombic space group $P2_12_12_1$ (2.5 Å; Sennhauser et al., 2007). The DARPin bound AcrB structure was almost identical with the AcrB structures crystallized without binder with root mean square deviation (rmsd) of the superimposed trimeric structures $\leq$1 Å. The DARPin molecules only bind to the loose and the tight conformers, resulting in a ratio of two DARPin molecules per AcrB trimer. This stoichiometry was verified by sedimentation velocity experiments, suggesting that in solution and probably also *in vivo* AcrB adopts mainly the asymmetric conformation (Sennhauser et al., 2007).

Within the asymmetric AcrB trimer, each monomer has a different conformation denoted as loose, tight and open (access, binding and extrusion, respectively; Murakami et al., 2006; Seeger et al., 2006), while the loose state is closest to the conformation of the monomers in the symmetric structure (Murakami et al., 2002). Although the pore helices are differently oriented in the asymmetric structure as compared to the symmetric structure, the pore diameter is similar and hence there does not appear to be a substrate export pathway through the pore. Instead, conformer specific cavities and tunnels could be identified in the porter domain (Murakami et al., 2006; Seeger et al., 2006; Sennhauser et al., 2007; see Figure 2). In the loose conformer, a tunnel (tunnel 2) starts in the PC1/PC2 subdomain cleft approximately 15 Å above the membrane plane and protrudes in the direction of the pore. In the tight conformer, an additional new tunnel (tunnel 1) with an entrance situated in a groove formed by TM8 and TM9 at the height of the membrane plane is apparent. Due to reorientation of the PN2 subdomain in the tight monomer, a hydrophobic pocket at the interface of PN2 and PC1 subdomains is created (Figure 2). This pocket is situated close to the end of tunnels 1 and 2 in the tight conformer (defined by the PN1 subdomain of the adjacent open monomer) and is rich in aromatic amino acids (Bohnert et al., 2008), a feature that is often observed for binding pockets of MDR proteins (Zheleznova et al., 1999; Schumacher et al., 2001, 2004; Murray et al., 2004; see Figure 2, inset). Indeed, Murakami et al. (2006) detected electron densities for the AcrB substrates minocycline and doxorubicin in the hydrophobic pocket. By using a brominated derivative of the former

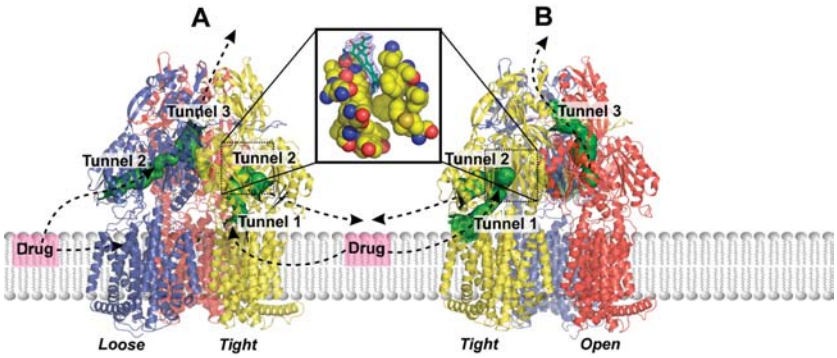

Figure 2 Tunnels in the porter domain of trimeric AcrB peristaltic drug efflux pump.
The AcrB monomers are presented in blue (loose), yellow (tight) and red (open). The tunnels are highlighted as green surfaces in a ribbon model of the AcrB trimer and might function as transport paths of drugs. Tunnel 1 might serve as entrance for drugs from the outer leaflet of the inner membrane towards the hydrophobic substrate binding pocket. Tunnel 2 might serve as an alternative entrance for substrates entering via the periplasm or as an exit duct for non-substrates. Tunnel 3 in the *open* monomer is the exit pathway for substrates towards TolC and the outside medium. Inset: in the T monomer (yellow), a hydrophobic pocket is defined by phenylalanine, valine, isoleucine and tyrosine side chains at the PN2/PC1 interface. Bound minocycline is depicted with the observed electron density in a $2F_o$-F_c electron density map contoured 1 σ (T. Eicher, M. Seeger, K.M. Pos and colleagues, unpublished data). Panels (A) and (B) represent in each case a one-third conversion of a full L→T→O→L cycle [adapted from Pos (2009) and modified].

compound (9-bromo-minocyclin), they unambiguously could assign the position of this substrate within the binding pocket. In the open monomer, the lateral periplasmic entrance of the tunnel observed in the loose and tight conformation is now closed owing to coil-to-helix transition of TM8, whereas another tunnel (tunnel 3) is created due to tilting of the pore helix (PN1 subdomain). The latter tunnel leads from the now collapsed binding pocket to the funnel located in the center of the AcrB trimer (Figure 2).

Transport mechanism

It is postulated (Murakami et al., 2006; Seeger et al., 2006, 2008b; Sennhauser et al., 2007; Murakami, 2008; Pos, 2009) that substrate transport by AcrB is accomplished via functional rotation in which each monomer changes its conformation in a concerted fashion (Figure 3). The mechanism resembles that of Boyer's binding change mechanism of the F_1F_o ATPase, where conformational cycling of the (α and) β subunits through the states loose, tight and open leads to the synthesis of ATP (Hackney et al., 1979; Hutton and Boyer, 1979; Boyer, 1997).

One transport hypothesis assumes the substrates to be garnered from the outer leaflet of the inner membrane (Figure 2). Substrate might enter the loose monomer via the TM8/TM9 groove (Murakami et al., 2002; Seeger et al., 2008a; Pos, 2009) or via tunnel 2 approximately 15 Å above the membrane plane. While it is not clear how hydrophobic compounds might enter tunnel 2 once these have been partitioned in the inner membrane, several groups provided structural data of symmetric AcrB (where all the monomers adopt the loose conformation) based on 3.2–3.8 Å data with presumably bound AcrB substrates in the tunnel 2 region (Yu et al., 2005; Drew et al., 2008). High resolution (2.5 Å) data describing the asymmetric trimer show clear densities in the TM8/TM9 groove of the loose monomer, which has been attributed to the highly concentrated detergent and AcrB substrate n-dodecyl-β-D-maltoside (Sennhauser et al., 2007). Upon conformational change from the loose to the tight state, tunnel 1 appears and might provide one of the pathways for substrates towards the hydrophobic pocket which accommodates the substrate molecule. Structural flexibility within the trimer (Takatsuka and Nikaido, 2007; Seeger et al., 2008b) suggests that the loose and even tight conformational states might be adoptable in the absence of substrates and that substrate binding to the hydrophobic pocket specifically stabilizes the tight conformation. This might also present an alternative role for tunnel 2 in these conformations as an exit pathway for compounds which are not substrates of the pump (Figure 2). In analogy with the binding change mechanism (Milgrom et al., 1998), the conversion of the tight monomer to the open monomer is energy-consuming and subject to bi-site activation, i.e., only occurs upon binding of substrate to the neighboring monomer (Figure 3). Upon transition from the tight to the open state, the binding pocket closes again; substrate is squeezed out and follows a newly formed tunnel (tunnel 3) to the TolC-docking domain funnel, and is from there finally extruded into the media via TolC.

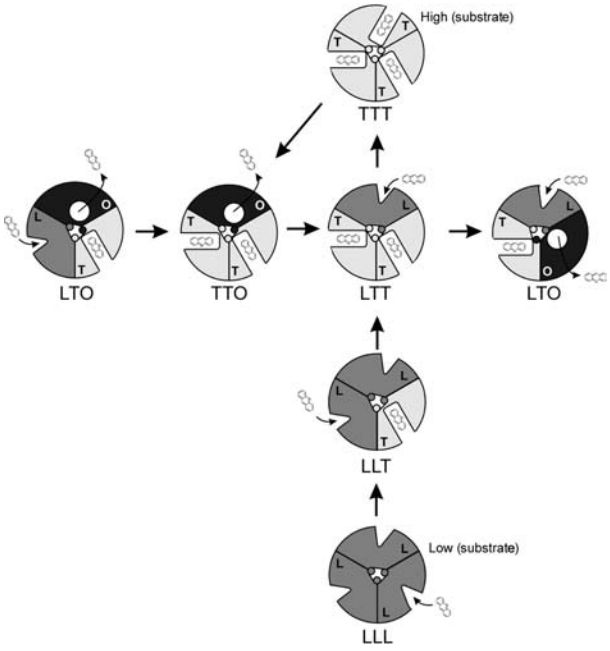

Figure 3 Schematic representation of the AcrB binding change functional rotation transport mechanism.
The conformational states loose (L), tight (T) and open (O) are indicated in different levels of gray. The lateral grooves in the L and T monomer indicate the substrate binding sites. The different geometric forms reflect low (triangle), high (rectangle) or no (circle) binding affinity for the transported substrates. State TTT is postulated to occur at high substrate concentration. The states LLL and LLT are postulated to occur in the absence or at low substrate concentrations. In this model, bi-site activation is essential for the complete transport cycle [adapted from Pos (2009) and modified].

In summary, upon conformational change from loose to tight to open and back to loose, an alternating access tunnel is formed through which substrates are transported from the outer leaflet of the inner membrane towards the outside medium. The mode of action is suggested to be based on occlusions migrating from the lateral entrance(s) to the central funnel and is reminiscent of a peristaltic pump.

To test the proposed conformational cycling *in vivo*, subdomains that undergo substantial rearrangement during cycling were locked by the introduction of disulfide bonds (Takatsuka and Nikaido, 2007; Seeger et al., 2008b). As could be demonstrated by tracing the efflux of a fluorescent substrate, formation of disulfide bonds significantly decreased AcrB mediated transport. When the disulfide bonds were broken by the addition of the reducing reagent dithiothreitol, transport activity was restored, which was in strong support of the functional rotation mechanism. Even more convincing, Takatsuka and Nikaido designed a functional covalently linked AcrB trimer, which could be inactivated by the introduction of a mutation in the proton relay network (D407A) or by disulfide formation in only *one* of the protomers (Takatsuka and Nikaido, 2009). These results are in accordance with the proposed functional rotation mechanism. Moreover, using quantitative measurements using β-lactams as substrates, Nagano and Nikaido (2009) found positive cooperativity for cephalosporins with low apparent affinity to AcrB (but not for nitrocefin, a cephalosporin with

high affinity), which might indicate bi-site activation as postulated (Seeger et al., 2008a; Pos, 2009).

The interaction between each AcrB monomer and its affiliated AcrA molecule has been investigated very recently (Symmons et al., 2009) and might suggest that during functional rotation of AcrB subtle conformational changes are transmitted towards AcrA. Rather than just being a rigid adapter, AcrA might actively transduce energy generated by AcrB and induce subtle peristaltic motions in the TolC channel. Similar to the tunnels observed in a single AcrB protomer during functional rotation (Murakami et al., 2006; Seeger et al., 2006; Sennhauser et al., 2007), TolC is possibly not a rigid hollow cylinder but changes its diameter by conformational change of each monomer, thereby pushing substrate unidirectionally from the closing aperture into the media (Vaccaro et al., 2006, 2008; Seeger et al., 2008a; Pos, 2009).

Proton transport and energy transduction

AcrB utilizes the proton motive force to energize the extrusion of its cognate substrates from the cell into the medium (Zgurskaya and Nikaido, 1999; Saier and Paulsen, 2001). The TM domain of AcrB harbors four functionally essential charged residues that are conserved throughout the HAE-1 family: Asp407, Asp408, Lys940 and Arg971 (Su et al., 2006; Takatsuka and Nikaido, 2006). Another highly conserved TM residue, Thr978, is in hydrogen bonding distance from Asp407 in the loose and tight monomer and with Lys940 in the open monomer. However, when Thr978 was replaced by valine, isoleucine, leucine or asparagine, the relative activity of these mutants remained 40% to 60% as revealed by drug susceptibility assays (Takatsuka and Nikaido, 2006).

In the asymmetric structure of AcrB, the four above-mentioned essential residues Asp407, Asp408, Lys940 and Arg971 have distinct different conformations in at least one of the three conformers loose, tight and open (Murakami et al., 2006; Seeger et al., 2006; Sennhauser et al., 2007). Both structural and mutagenesis studies suggest that proton translocation is mediated by these titratable residues. The conformational changes during the putative conformational cycling in the TM domain are much more subtle compared to the porter domain: Lys940 is sandwiched between Asp407 and Asp408 in the loose and tight states, but becomes reoriented towards Thr978 in the open state; the N-terminal end of TM8 in the loose and tight monomers is marked by Pro874, but becomes elongated by four full turns in the open monomer, whereas TM5 bulges towards TM4 and TM10 in the open conformation. These conformational changes are thought to be the result of protonation and deprotonation events on these titratable, membrane embedded residues. The geometry of the titratable residues is reminiscent to the situation observed in bacteriorhodopsin, an archaeal integral membrane protein intensively studied since its discovery in the early seventies (Oesterhelt and Stoeckenius, 1973). It is therefore tempting to look for analogies between AcrB and the well-characterized bacteriorhodopsin. How these conformational changes are levered to the porter domain and cause the large conformational changes observed there is subject to ongoing investigation.

Acknowledgments

I would like to thank Markus Seeger and my collaborators at the University of Konstanz, Kay Diederichs and André Schiefner, for their indispensable efforts on this work.

References

Baev, N., Endre, G., Petrovics, G., Banfalvi, Z., and Kondorosi, A. (1991). Six nodulation genes of nod box locus 4 in *Rhizobium meliloti* are involved in nodulation signal production: nodM codes for D-glucosamine synthetase. Mol. Gen. Genet. *228*, 113–124.

Bavro, V.N., Pietras, Z., Furnham, N., Perez-Cano, L., Fernandez-Recio, J., Pei, X.Y., Misra, R., and Luisi, B. (2008). Assembly and channel opening in a bacterial drug efflux machine. Mol. Cell *30*, 114–121.

Bohnert, J.A., Schuster, S., Seeger, M.A., Fahnrich, E., Pos, K.M., and Kern, W.V. (2008). Site-directed mutagenesis reveals putative substrate binding residues in the *Escherichia coli* RND efflux pump AcrB. J. Bacteriol. ●●, ●●●–●●●.

Boyer, P.D. (1997). The ATP synthase – a splendid molecular machine. Annu. Rev. Biochem. *66*, 717–749.

Camacho, L.R., Constant, P., Raynaud, C., Laneelle, M.A., Triccas, J.A., Gicquel, B., Daffe, M., and Guilhot, C. (2001). Analysis of the phthiocerol dimycocerosate locus of *Mycobacterium tuberculosis*. Evidence that this lipid is involved in the cell wall permeability barrier. J. Biol. Chem. *276*, 19845–19854.

Davies, J.P. and Ioannou, Y.A. (2000). Topological analysis of Niemann-Pick C1 protein reveals that the membrane orientation of the putative sterol-sensing domain is identical to those of 3-hydroxy-3-methylglutaryl-CoA reductase and sterol regulatory element binding protein cleavage-activating protein. J. Biol. Chem. *275*, 24367–24374.

Davies, J.P., Chen, F.W., and Ioannou, Y.A. (2000). Transmembrane molecular pump activity of Niemann-Pick C1 protein. Science *290*, 2295–2298.

Domenech, P., Reed, M.B., and Barry, C.E., III. (2005). Contribution of the *Mycobacterium tuberculosis* MmpL protein family to virulence and drug resistance. Infect. Immun. *73*, 3492–3501.

Drew, D., Klepsch, M.M., Newstead, S., Flaig, R., De Gier, J.W., Iwata, S., and Beis, K. (2008). The structure of the efflux pump AcrB in complex with bile acid. Mol. Membr. Biol. *25*, 677–682.

Eda, S., Maseda, H., and Nakae, T. (2003). An elegant means of self-protection in Gram-negative bacteria by recognizing and extruding xenobiotics from the periplasmic space. J. Biol. Chem. *278*, 2085–2088.

Elkins, C.A. and Nikaido, H. (2002). Substrate specificity of the RND-type multidrug efflux pumps AcrB and AcrD of *Escherichia coli* is determined predominantly by two large periplasmic loops. J. Bacteriol. *184*, 6490–6498.

Gardel, C., Benson, S., Hunt, J., Michaelis, S., and Beckwith, J. (1987). secD, a new gene involved in protein export in *Escherichia coli*. J. Bacteriol. *169*, 1286–1290.

Guan, L. and Nakae, T. (2001). Identification of essential charged residues in transmembrane segments of the multidrug transporter MexB of *Pseudomonas aeruginosa*. J. Bacteriol. *183*, 1734–1739.

Hackney, D.D., Rosen, G., and Boyer, P.D. (1979). Subunit interaction during catalysis: alternating site cooperativity in photophosphorylation shown by substrate modulation of [^{18}O]ATP species formation. Proc. Natl. Acad. Sci. USA *76*, 3646–3650.

Hancock, R.E. and Brinkman, F.S. (2002). Function of pseudomonas porins in uptake and efflux. Annu. Rev. Microbiol. *56*, 17–38.

Hooper, D.C. (1995). Bacterial resistance to fluoroquinolones: mechanisms and patterns. Adv. Exp. Med. Biol. *390*, 49–57.

Hutton, R.L. and Boyer, P.D. (1979). Subunit interaction during catalysis. Alternating site cooperativity of mitochondrial adenosine triphosphatase. J. Biol. Chem. *254*, 9990–9993.

Infante, R.E., Abi-Mosleh, L., Radhakrishnan, A., Dale, J.D., Brown, M.S., and Goldstein, J.L. (2008a). Purified NPC1 protein. I. Binding of cholesterol and oxysterols to a 1278-amino acid membrane protein. J. Biol. Chem. *283*, 1052–1063.

Infante, R.E., Radhakrishnan, A., Abi-Mosleh, L., Kinch, L.N., Wang, M.L., Grishin, N.V., Goldstein, J.L., and Brown, M.S. (2008b). Purified NPC1 protein: II. Localization of sterol binding to a 240-amino acid soluble luminal loop. J. Biol. Chem. *283*, 1064–1075.

Ioannou, Y.A. (2001). Multidrug permeases and subcellular cholesterol transport. Nat. Rev. Mol. Cell Biol. *2*, 657–668.

Li, X.Z. and Nikaido, H. (2004). Efflux-mediated drug resistance in bacteria. Drugs *64*, 159–204.

Lomovskaya, O. and Totrov, M. (2005). Vacuuming the periplasm. J. Bacteriol. *187*, 1879–1883.

Lomovskaya, O., Lee, A., Hoshino, K., Ishida, H., Mistry, A., Warren, M.S., Boyer, E., Chamberland, S., and Lee, V.J. (1999). Use of a genetic approach to evaluate the consequences of inhibition of efflux pumps in *Pseudomonas aeruginosa*. Antimicrob. Agents Chemother. *43*, 1340–1346.

Mahamoud, A., Chevalier, J., Alibert-Franco, S., Kern, W.V., and Pages, J.M. (2007). Antibiotic efflux pumps in Gram-negative bacteria: the inhibitor response strategy. J. Antimicrob. Chemother. *59*, 1223–1229.

Mao, W., Warren, M.S., Black, D.S., Satou, T., Murata, T., Nishino, T., Gotoh, N., and Lomovskaya, O. (2002). On the mechanism of substrate specificity by resistance nodulation division (RND)-type multidrug resistance pumps: the large periplasmic loops of MexD from *Pseudomonas aeruginosa* are involved in substrate recognition. Mol. Microbiol. *46*, 889–901.

Mazzariol, A., Tokue, Y., Kanegawa, T.M., Cornaglia, G., and Nikaido, H. (2000). High-level fluoroquinolone-resistant clinical isolates of *Escherichia coli* overproduce multidrug efflux protein AcrA. Antimicrob. Agents Chemother. *44*, 3441–3443.

Milgrom, Y.M., Murataliev, M.B., and Boyer, P.D. (1998). Bi-site activation occurs with the native and nucleotide-depleted mitochondrial F1-ATPase. Biochem. J. *330*, 1037–1043.

Murakami, S. (2008). Multidrug efflux transporter, AcrB – the pumping mechanism. Curr. Opin. Struct. Biol. *18*, 459–465.

Murakami, S., Nakashima, R., Yamashita, E., and Yamaguchi, A. (2002). Crystal structure of bacterial multidrug efflux transporter AcrB. Nature *419*, 587–593.

Murakami, S., Nakashima, R., Yamashita, E., Matsumoto, T., and Yamaguchi, A. (2006). Crystal structures of a multidrug transporter reveal a functionally rotating mechanism. Nature *443*, 173–179.

Murray, D.S., Schumacher, M.A., and Brennan, R.G. (2004). Crystal structures of QacR-diamidine complexes reveal additional multidrug-binding modes and a novel mechanism of drug charge neutralization. J. Biol. Chem. *279*, 14365–14371.

Nagano, K. and Nikaido, H. (2009). Kinetic behavior of the major multidrug efflux pump AcrB of *Escherichia coli*. Proc. Natl. Acad. Sci. USA *106*, 5854–5858.

Nakano, Y., Kim, H.R., Kawakami, A., Roy, S., Schier, A.F., and Ingham, P.W. (2004). Inactivation of dispatched 1 by the chameleon mutation disrupts Hedgehog signalling in the zebrafish embryo. Dev. Biol. *269*, 381–392.

Nikaido, H. (1996). Multidrug efflux pumps of Gram-negative bacteria. J. Bacteriol. *178*, 5853–5859.

Nikaido, H. (1998). Multiple antibiotic resistance and efflux. Curr. Opin. Microbiol. *1*, 516–523.

Nikaido, H. (2003). Molecular basis of bacterial outer membrane permeability revisited. Microbiol. Mol. Biol. Rev. *67*, 593–656.

Nikaido, H. (2009). Multidrug resistance in bacteria. Annu. Rev. Biochem., in press ●●, ●●●–●●●.

Nikaido, H. and Takatsuka, Y. (2008). Mechanisms of RND multidrug efflux pumps. Biochim. Biophys. Acta ●●, ●●●–●●●.

Oesterhelt, D. and Stoeckenius, W. (1973). Functions of a new photoreceptor membrane. Proc. Natl. Acad. Sci. USA *70*, 2853–2857.

Pietras, Z., Bavro, V.N., Furnham, N., Pellegrini-Calace, M., Milner-White, E.J., and Luisi, B.F. (2008). Structure and mechanism of drug efflux machinery in Gram-negative bacteria. Curr. Drug Targets *9*, 719–728.

Plesiat, P. and Nikaido, H. (1992). Outer membranes of Gram-negative bacteria are permeable to steroid probes. Mol. Microbiol. *6*, 1323–1333.

Pogliano, J.A. and Beckwith, J. (1994). SecD and SecF facilitate protein export in *Escherichia coli*. EMBO J. *13*, 554–561.

Pos, K.M. (2009). Drug transport mechanism of the AcrB efflux pump. Biochim. Biophys. Acta, in press ●●, ●●●–●●●.

Pos, K.M., Schiefner, A., Seeger, M.A., and Diederichs, K. (2004). Crystallographic analysis of AcrB. FEBS Lett. *564*, 333–339.

Saier, M.H., Jr. and Paulsen, I.T. (2001). Phylogeny of multidrug transporters. Semin. Cell Dev. Biol. *12*, 205–213.

Schumacher, M.A., Miller, M.C., Grkovic, S., Brown, M.H., Skurray, R.A., and Brennan, R.G. (2001). Structural mechanisms of QacR induction and multidrug recognition. Science *294*, 2158–2163.

Schumacher, M.A., Miller, M.C., and Brennan, R.G. (2004). Structural mechanism of the simultaneous binding of two drugs to a multidrug-binding protein. EMBO J. *23*, 2923–2930.

Seeger, M.A., Schiefner, A., Eicher, T., Verrey, F., Diederichs, K., and Pos, K.M. (2006). Structural asymmetry of AcrB trimer suggests a peristaltic pump mechanism. Science *313*, 1295–1298.

Seeger, M.A., Diederichs, K., Eicher, T., Brandstatter, L., Schiefner, A., Verrey, F., and Pos, K.M. (2008a). The AcrB efflux pump: conformational cycling and peristalsis lead to multidrug resistance. Curr. Drug Targets *9*, 729–749.

Seeger, M.A., von Ballmoos, C., Eicher, T., Brandstatter, L., Verrey, F., Diederichs, K., and Pos, K.M. (2008b). Engineered disulfide bonds support the functional rotation mechanism of multidrug efflux pump AcrB. Nat. Struct. Mol. Biol. *15*, 199–205.

Sennhauser, G., Amstutz, P., Briand, C., Storchenegger, O., and Grutter, M.G. (2007). Drug export pathway of multidrug exporter AcrB revealed by DARPin inhibitors. PLoS Biol. *5*, e7.

Skinner, R., Cundliffe, E., and Schmidt, F.J. (1983). Site of action of a ribosomal RNA methylase responsible for resistance to erythromycin and other antibiotics. J. Biol. Chem. *258*, 12702–12706.

Sleat, D.E., Wiseman, J.A., El-Banna, M., Price, S.M., Verot, L., Shen, M.M., Tint, G.S., Vanier, M.T., Walkley, S.U., and Lobel, P. (2004). Genetic evidence for nonredundant functional cooperativity between NPC1 and NPC2 in lipid transport. Proc. Natl. Acad. Sci. USA *101*, 5886–5891.

Su, C.C., Li, M., Gu, R., Takatsuka, Y., McDermott, G., Nikaido, H., and Yu, E.W. (2006). Conformation of the AcrB multidrug efflux pump in mutants of the putative proton relay pathway. J. Bacteriol. *188*, 7290–7296.

Symmons, M.F., Bokma, E., Koronakis, E., Hughes, C., and Koronakis, V. (2009). The assembled structure of a complete tripartite bacterial multidrug efflux pump. Proc. Natl. Acad. Sci. USA, in press ●●, ●●●–●●●.

Taipale, J., Cooper, M.K., Maiti, T., and Beachy, P.A. (2002). Patched acts catalytically to suppress the activity of Smoothened. Nature *418*, 892–897.

Takatsuka, Y. and Nikaido, H. (2006). Threonine-978 in the transmembrane segment of the multidrug efflux pump AcrB of *Escherichia coli* is crucial for drug transport as a probable component of the proton relay network. J. Bacteriol. *188*, 7284–7289.

Takatsuka, Y. and Nikaido, H. (2007). Site-directed disulfide cross-linking shows that cleft flexibility in the periplasmic domain is needed for the multidrug efflux pump AcrB of *Escherichia coli*. J. Bacteriol. *189*, 8677–8684.

Takatsuka, Y. and Nikaido, H. (2009). Covalently linked trimer of the AcrB multidrug efflux pump provides support for the functional rotating mechanism. J. Bacteriol. *191*, 1729–1737.

Tamura, N., Murakami, S., Oyama, Y., Ishiguro, M., and Yamaguchi, A. (2005). Direct interaction of multidrug efflux transporter AcrB and outer membrane channel TolC detected via site-directed disulfide cross-linking. Biochemistry *44*, 11115–11121.

Thomson, K.S. and Smith Moland, E. (2000). Version 2000: the new β-lactamases of Gram-negative bacteria at the dawn of the new millennium. Microbes Infect. *2*, 1225–1235.

Tikhonova, E.B. and Zgurskaya, H.I. (2004). AcrA, AcrB, and TolC of *Escherichia coli* form a stable intermembrane multidrug efflux complex. J. Biol. Chem. *279*, 32116–32124.

Tornroth-Horsefield, S., Gourdon, P., Horsefield, R., Brive, L., Yamamoto, N., Mori, H., Snijder, A., and Neutze, R. (2007). Crystal structure of AcrB in complex with a single transmembrane subunit reveals another twist. Structure *15*, 1663–1673.

Vaccaro, L., Koronakis, V., and Sansom, M.S. (2006). Flexibility in a drug transport accessory protein: molecular dynamics simulations of MexA. Biophys. J. *91*, 558–564.

Vaccaro, L., Scott, K.A., and Sansom, M.S. (2008). Gating at both ends and breathing in the middle: conformational dynamics of TolC. Biophys. J. *95*, 5681–5691.

Wright, G.D. (1999). Aminoglycoside-modifying enzymes. Curr. Opin. Microbiol. *2*, 499–503.

Yoshida, H., Bogaki, M., Nakamura, M., and Nakamura, S. (1990). Quinolone resistance-determining region in the DNA gyrase gyrA gene of *Escherichia coli*. Antimicrob. Agents Chemother. *34*, 1271–1272.

Yu, E.W., Aires, J.R., and Nikaido, H. (2003a). AcrB multidrug efflux pump of *Escherichia coli*: composite substrate-binding cavity of exceptional flexibility generates its extremely wide substrate specificity. J. Bacteriol. *185*, 5657–5664.

Yu, E.W., McDermott, G., Zgurskaya, H.I., Nikaido, H., and Koshland, D.E., Jr. (2003b). Structural basis of multiple drug-binding capacity of the AcrB multidrug efflux pump. Science *300*, 976–980.

Yu, E.W., Aires, J.R., McDermott, G., and Nikaido, H. (2005). A periplasmic drug-binding site of the AcrB multidrug efflux pump: a crystallographic and site-directed mutagenesis study. J. Bacteriol. *187*, 6804–6815.

Zalacain, M. and Cundliffe, E. (1989). Methylation of 23S rRNA caused by tlrA (ermSF), a tylosin resistance determinant from *Streptomyces fradiae*. J. Bacteriol. *171*, 4254–4260.

Zalacain, M. and Cundliffe, E. (1990). Methylation of 23S ribosomal RNA due to carB, an antibiotic-resistance determinant from the carbomycin producer, *Streptomyces thermotolerans*. Eur. J. Biochem. *189*, 67–72.

Zgurskaya, H.I. and Nikaido, H. (1999). Bypassing the periplasm: reconstitution of the AcrAB multidrug efflux pump of *Escherichia coli*. Proc. Natl. Acad. Sci. USA *96*, 7190–7195.

Zheleznova, E.E., Markham, P.N., Neyfakh, A.A., and Brennan, R.G. (1999). Structural basis of multidrug recognition by BmrR, a transcription activator of a multidrug transporter. Cell *96*, 353–362.

Received March 1, 2009; accepted April 29, 2009

6. Discussion

6.1 Proton relay network: VexF vs. HAE1 superfamily consensus sequence

An examination of all 31 HAE1 members present in the Transport Classification Database (http://www.tcdb.org/, autumn 2008) revealed that the percentage of identical and similar amino acid residues in this subfamily ranges from 17% (MexY and TriC from *P. aeruginosa*) to 99% (SrpB and TtgH from *P. putida*). However, in the transmembrane domain, there are stretches where conservation is strong for all the listed HAE1 members. The longest stretches comprise up to 30 amino acids and reside on TM4, TM10 and TM11. These regions comprise the essential residues D407, D408, K940, and R971[6] (**Figure 23**) (145,146,178,179). In 30 out of the 31 HAE1 transporters listed in the transport classification database, D407, D408, R971, K940 and also T978 are highly conserved, with only MexK and TriC (both from *P. aeruginosa*) showing an arginine substitution for the corresponding K940. A striking difference, however, can be found for VexF of *Vibrio cholerae*: D408, is substituted by a glycine, and the positively charged K940 is exchanged for a polar glutamine (**Figure 23**). Interestingly, Rahman *et al.* (214) reported that heterologously expressed VexF transports ethidium and R6G out of *E. coli* cells only when Na^+ is present. It is therefore tempting to speculate that VexF is driven by the electrochemical gradient of Na^+ and not of protons like the hitherto characterized RND transporters.

[6] AcrB numbering is used throughout unless indicated differently.

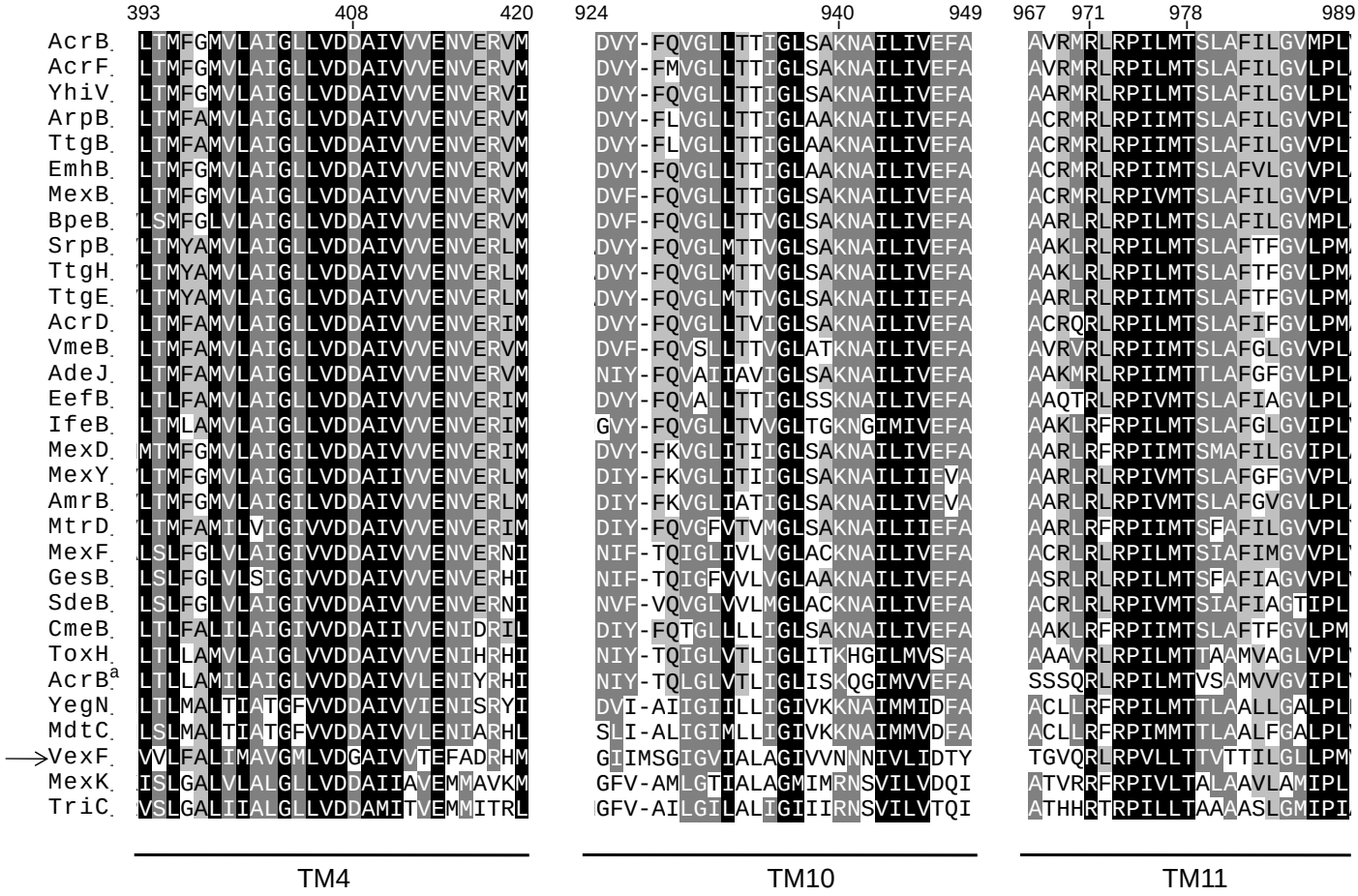

Figure 23: Conserved stretches among HAE1 transporters listed at Membrane Transport Protein Classification Database (http://www.tcdb.org/, autumn 2008). The most conserved stretches comprise almost the entire transmembrane helices 4, 10 and 11. Note that VexF (arrow) has different residues at the highly conserved positions 408 and 940. AcrB numbering is used throughout. Multiple sequence alignment was performed using the program Mafft (67).

[a]: AcrB of *Francisella tularensis*

6.2 The putative sodium binding site of VexF

The fact that electrochemical gradients of both H^+ or Na^+ can be used as secondary driving force has been known since the establishment of Na^+ energetics by the characterization of the oxaloacetate decarboxylase and the methylmalonyl-CoA decarboxylase (215,216). For MDR proteins belonging to the MATE family, both proton motive force (PMF) (for example PmpM of *P. aeruginosa*, He 2004 (51)) and sodium-ion motive force (SMF) (for example NorM of *V. parahaemolyticus* (50,217)) are known to energize the transport of substrates. The differences between the consensus sequence of the putative proton translocation pathway in HAE1

transporters and VexF might account for the changed preference of the coupling ion. A comparative analysis of the Na^+ binding sites of known Na^+ transporting membrane proteins like the c subunit of the F_1F_o ATPase (*Ilyobacter tartaricus*, (218)) as well as of the Na^+ driven transporters LeuT (*Aquifex aeolicus* (219)), Glt_{Ph} (*Pyrococcus horikoshii* (220)) and vSGLT (*V. parahaemolyticus* (221)) described here evaluates the possibility whether VexF from *V. cholerae* might use Na^+ as coupling ion.

LeuT is a Na^+ coupled leucine transporter. The crystal structure (219) was solved at 1.65 Å and showed the membrane protein in complex with two Na^+ ions and its cognate substrate leucine. LeuT revealed two Na^+ binding sites which differ in the number of coordinating oxygen atoms as well as in charge. The Na^+ ion in binding site 1 is coordinated by two carbonyl oxygen atoms of a partly unwound α-helix (A22 and T254), a hydroxyl oxygen of T254, two side chain carbonyl oxygen atoms of N27 and N286 and one carboxyl oxygen of the substrate leucine. At Na^+ binding site 2, the ion is bound by three carbonyl oxygen atoms located on partially unwound α-helices (G20, V23, A351) and two hydroxyl oxygens of T354 and S355 (**Figure 24**).

The structure of the galactose/ Na^+ cotransporter vSGLT was solved at 2.7 Å (221). At this resolution, electron densities from water molecules and Na^+ cannot be distinguished. However, comparison between the putative Na^+ binding site of vSGLT and the Na^+ binding site 2 of LeuT revealed that they are very analogous. The coordination of Na^+ was postulated to be accomplished by three carbonyl oxygen atoms that are located on a partially unwound α-helix (A62, I65 and A361) as well as by the two hydroxyl oxygens of T364 and S365 (**Figure 24**).

Glt_{Ph} is a Na^+ coupled aspartate transporter (220). The two Na^+ binding sites are again very similar to those observed in LeuT. The Na^+ ion in binding site 1 is coordinated by two main chain carbonyl oxygen atoms of a partly unwound α-helix (G306 and N310), the main chain carbonyl oxygen of N401, a hydroxyl oxygen of S278 and a carboxy oxygen of D405. At Na^+ binding site 2, the ion is bound by one carbonyl oxygen atom of the same partly unwound α-helix (T308) and by the three carbonyl oxygens of S349, I350 and T352 that reside at the C-terminus of an α-helical hairpin. Stabilizing coordination might be accomplished by the dipole moments of the C-termini of the α-helical hairpin and the partly unwound α-helix (**Figure 24**).

Although LeuT, Glt_{Ph} and vSGLT do not share similarities on the amino acid sequence level , the three dimensional architecture of the Na^+ binding sites exhibit

significant analogy with some of the coordinating oxygen atoms at equivalent positions. Most prominent are the unwound regions within transmembrane α-helices (one region for vSGLT and two regions for LeuT and Glt_{Ph}). These regions provide main chain carbonyl atoms which appear to be essential for Na^+ binding.

The crystal structure of the undecameric c ring of the Na^+ coupled F_1F_o ATPase was solved at 2.4 Å by Meier *et al.* (218). The Na^+ ions are coordinated by the hydroxyl oxygen of S66, the carboxyl group of E65, the carboxamide oxygen of Q32 and the backbone carbonyl oxygen of V63 located at the bend of transmembrane helix A (**Figure 24**).

The coordinating oxygen atoms involved in Na^+ binding derive from hydroxyl groups, carboxamide oxygens, carboxyl groups and backbone carbonyl oxygens of unwound or kinked α-helices. The number of oxygen atoms coordinating one Na^+ ion is four (F_1F_o ATPase, binding site 2 of Glt_{Ph}), five (binding site 2 of LeuT, vSGLT, binding site 2 of Glt_{Ph}) and six (binding site 1 of substrate loaded LeuT) and the formal over all charge of the polar binding pocket is either 0 (binding site 2 of LeuT and GltPh, vSGLT) or -1 (binding site 1 of Glt_{Ph} and substrate loaded LeuT, c ring of F_1F_o ATPase).

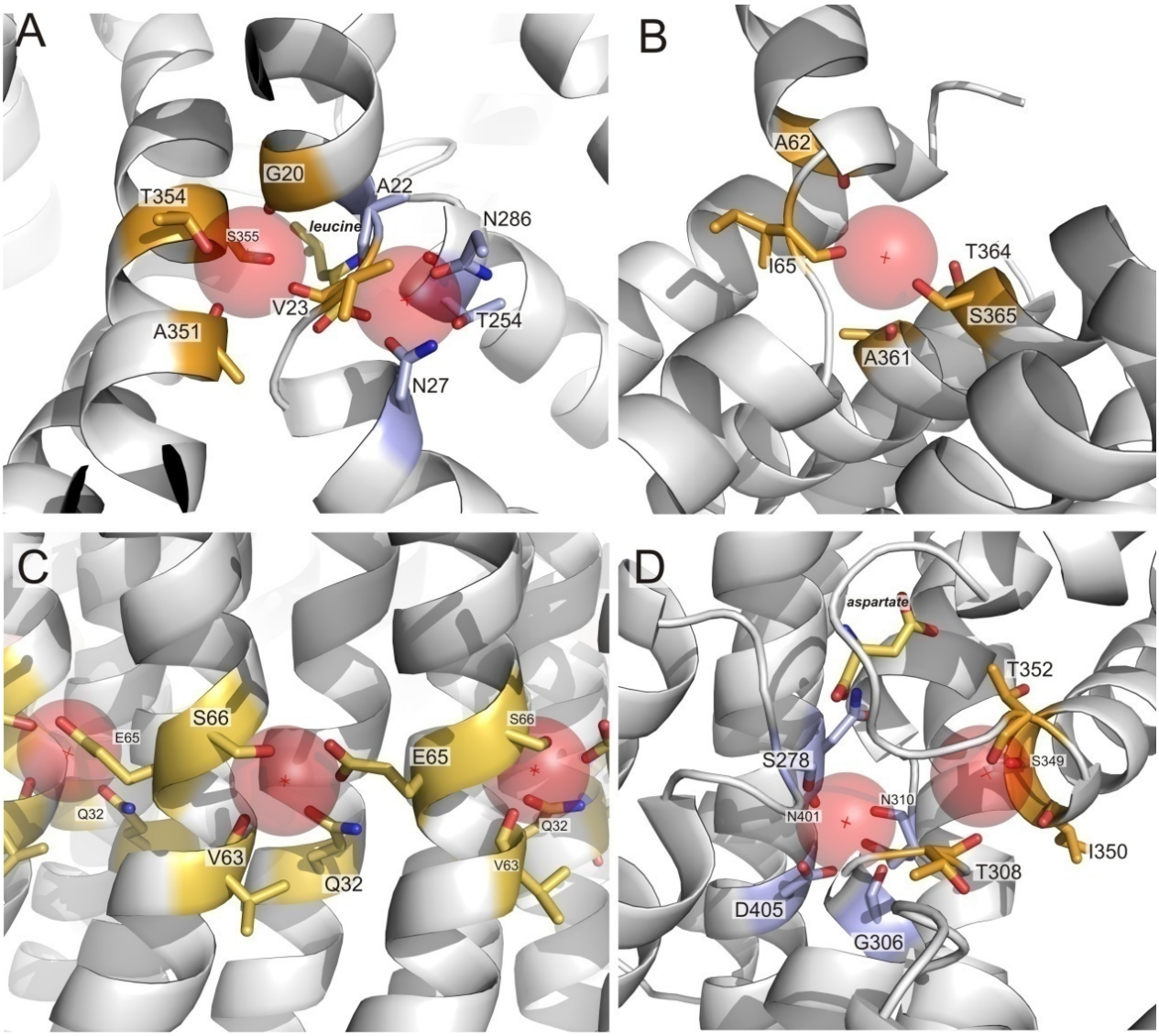

Figure 24: Na^+ binding sites in Na^+ coupled primary and secondary active transporters. Na^+ ion are shown as red spheres. **A)** Residues forming Na^+ binding site 1 (blue) and 2 (orange) of LeuT are shown as sticks. The substrate leucine which is part of binding site 1 is colored yellow. **B)** The Na^+ binding site in vSGLT was found by structural alignment with LeuT (221). Note that this putative Na^+ binding site is composed of a very similar set of amino acid residues as Na^+ binding site 2 of LeuT and exhibits essentially the same geometry (Na^+ coordinating carbonyl oxygens of residues in vSGLT: A_n – I_{n+3}, T_m – S_{m+1}, A; Na^+ coordinating carbonyl oxygens of residues of Na^+ binding site 2 of LeuT: G_n – V_{n+3}, T_m – S_{m+1}, A). **C)** In the undecameric ring of the F_1F_o ATPase, the Na^+ ion is bound at the interface of $monomer_n$ (V63 and S66) and $monomer_{n+1}$ (Q32 and E65). **D)** Residues forming Na^+ binding site 1 (blue) and 2 (orange) of Glt_{Ph}. Glt_{Ph} exhibits a similar Na^+ binding motif as LeuT: a break in the geometry of a core α-helix of three to five residues results in an opened up, non-α-helical peptide chain. The exposed carbonyl atoms of the first and fifth residue in Glt_{Ph} (G306 and N310) or the first and forth residues of the Na^+ binding motif in LeuT (G20 and V23) are part of Na^+ binding site 1 (blue). In both proteins, the third residue of this motif (T308 and A22 in Glt_{Ph} and LeuT, respectively) participate in forming Na^+ binding site 2 (orange). Pictures prepared with pdb coordinate files 3F3E (LeuT), 3DH4 (vSGLT), 1YCE (F_1F_o ATPase) and 2NWX (Glt_{Ph}).

By taking the structure of asymmetric AcrB (pdb-ID: 2GIF) as a template and aligning the amino acid sequence of VexF with AcrB, a homology model of the VexF structure was built by using SWISS-MODEL workspace (222-226) (**Figure 25**).
The model suggests that in VexF D401, N922 and T959 are located in spatial vicinity and oriented towards each other as this is the case for the analogous residues D407, K940 and T978 in AcrB. The hydroxyl oxygens of T960 and T959, the carboxamide oxygens of N922 and N923 and the carboxyl oxygen of D401 all point towards a center defined by TM4, TM5, TM10 and TM11. Based on genetic experiments (144,179) and considering the asymmetric structure of AcrB (40,41,142), exchange of the essential residues D408 and K940 in conventional HAE1 transporters are expect to render the proteins functionally inactive due to impairment of protonation and deprotonation of the proton relay and impairment of the transfer of protons from the periplasm to the cytoplasm.
In light of the reported Na^+ dependence of VexF function (214) however, the altered amino acid composition in the transmembrane domain could indeed indicate an altered cation specificity: (i) as in Na^+ coupled transporters mentioned above, the putative Na^+ binding site in VexF is devoid of any formally positively charged residue due to the exchange of lysine to asparigine. (ii) By the replacement of aspartate by glycine, the second formally negative charge is omitted. As from the known cases discussed above, the Na^+ binding site harbors one (c ring of F_1F_o ATPase, binding site 1 of Glt_{Ph} and the Na^+ binding site 1 of substrate loaded LeuT) or none (vSGLT, binding Na^+ binding site 2 of GltPh, Na^+ binding site 2 of LeuT) negatively charged residue. (iii) Exchange of the highly conserved D408 and K940 by amino acids with considerably smaller side chains enlarges the space between charged and polar residues, makes this region more flexible and may facilitate binding of (a) Na^+ ion(s). The potential Na^+ binding site in VexF is shown in **Figure 25**.

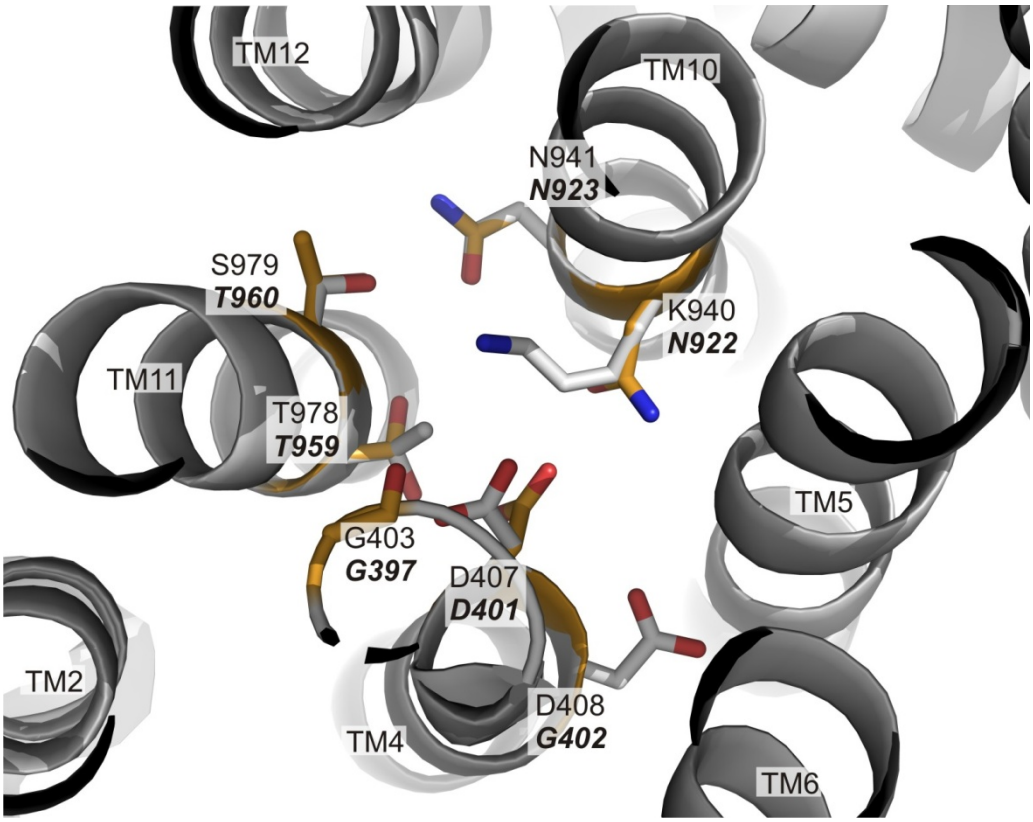

Figure 25: Superimposition of transmembrane domain of the open monomer of AcrB (pdb-ID: 2GIF) and the homology model of VexF. D408 and K940, both highly conserved within HAE1 transporters are substituted in VexF by a glycine and a asparagine residue, respectively. A putative Na^+ binding site is created in VexF by the hydroxyl oxygens of T959 and T960, the carboxamide oxygen of N922 and N923 and the carboxyl oxygen of D401. In the open monomer, TM4 is considerably tilted, which opens up the peptide chain and may allow the carbonyl oxygen of G397 to contribute in coordinating Na^+ (orange sticks, residues are indicated in italics). For comparison, the analogous residues in AcrB are shown as white sticks. Residues of VexF and AcrB are indicated in italics and regular, respectively. The transmembrane helices are denoted.

6.3 Composition of putative proton relay network in HME vs. HAE1 superfamily

The Heavy Metal Extrusion (HME) family members are proteobacterial transporters of the RND superfamily that extrude heavy metal ions in exchange with cations. Prominent members of this family are listed in **Table 1** according to the transport classification database (www.tcdb.org). HME transporters share between 20% and 22% identical residues with AcrB and accomplish transport of monovalent (2.A.6.1.3, 2.A.6.1.4) or divalent (2.A.6.1.1, 2.A.6.1.2, 2.A.6.1.5) heavy metal ions, respectively. To check whether the proposed protonation and deprotonation mechanism in the

transmembrane domain of AcrB may also apply for HME transporters, SilA, CusA, CnrA, CzcA, CzcA1 and further 76 homologous proteins identified by a blast search (227) were analyzed (**Table 2**).

Table 1: Prominent HME proteins transporting monovalent and divalent HM

HME protein	organism	substrate
SilA	*S. typhimurium*	Ag^{+} [a]
CusA	*E. coli*	Ag^{+}/Cu^{+} [b]
CnrA	*Ralstonia metallidurans*	Ni^{2+}/Co^{2+} [c]
CzcA	*Alcaligenes eutrophus*	$Co^{2+}/Zn^{2+}/Cd^{2+}$ [d]
CzcA1	*P. putida*	$Zn^{2+}/Cd^{2+}/Pb^{2+}$ [e]

[a]: (228)
[b]: (229-231)
[c]: (232)
[d]: (62)
[e]: (233)

Intriguingly, some of the conserved stretches among the members of the HAE1 family are also similar in the HME family. These include TM4, TM11 and to a lesser extend TM10 which harbor the essential residues D407, D408, R971, T978 and K940 in AcrB. At the corresponding position of D408 however, there is an alanine residue in the HME members transporting monovalent heavy metal ions and their homologs[7] and a glycine residue in case of HME proteins transporting divalent heavy metal ions[8] as reported by Franke *et al.* (230). Moreover, the corresponding position to K940 of AcrB is substituted by glutamate in case of the monovalent HMEs and by leucine in the divalent HMEs (**Tabel 2**). This observation questions the AcrB paradigm, as K940 and D408 are essential residues for function in AcrB and central to the proton translocation hypothesis. Moreover, striking differences between HME members seem to correlate with the substrate specificity of the transporters, questioning the exclusive role of the periplasmic domain in substrate transport and the spatial separation of energy transduction and substrate transport as has been postulated for AcrB (40,41,139).

[7] hereafter referred to as monovalent HMEs
[8] hereafter referred to as divalent HMEs

Table 2: Putative proton translocating residues in HAE1[a] and HME proteins

		monovalent HMEs		divalent HMEs		
position	HAE1[a]	SilA	CusA	CzcA	CzcA1	CnrA
407	D	D	D	D	D	D
408	D[b]	**A**	**A**	**G**	**G**	**G**
940	K[c]	**E**	**E**	**L**	**L**	**L**
971	R	R	R	R	R	R[d]
978	T	T	T	T	T	T[e]

76 Homologous proteins of the HME transporters SilA, CusA, CzcA, CzcA1 and CnrA were identified by a blast search at the Swiss Institute of Bioinformatics using the BLAST network service (http://www.expasy.ch/tools/blast/, (227)). The proteins were aligned with AcrB using the program Mafft (67). Residues putatively involved in proton translocation in HAE1 proteins (40,41,144,145) were compared with the analogous residues in the HME proteins.
[a]: 31 HAE1 proteins listed in tcdb (autumn 2008)
Homologous proteins having different amino acids at the indicated position (name of protein and/or UniProtKB/Swiss-Prot accession number) are indicated:
[b]: VexF (A6P7H3): G
[c]: MexK (Q9HXW4) and TriC (Q9I6X4): R; VexF (A6P7H3): Q
[d]: A9IF41 and Q1GPY7: K
[e]: B3PGJ3: V

6.4 Substrate specificity determinants in HAE1 vs. HME superfamily

In AcrB, a hydrophobic binding pocket is formed by the residues F136, V139, Q176, F178, N274, I277, Y327, F610, V612, F615, F617, I626, F628 (**Figure 12**) exclusively in the tight monomer (40,41). Densities for the AcrB substrates minocycline and doxorubicin could be identified in respective co-crystallized crystals ((40), Eicher unpublished). Since similarity in amino acid sequence often coincides with similar structure and might be an indication for a similar catalytic mechanism, the binding pocket residues at the corresponding positions in HME proteins might be involved in binding of their substrates (heavy metal ions).

These putative HME binding pocket residues were analyzed in 76 homologous proteins of SilA, CusA, CzcA, CzcA1 and CnrA and compared with the residues in AcrB (**Table 3**).

Table 3: Putative binding pocket residues in AcrB and HME proteins

		monovalent HMEs		divalent HMEs		
position	AcrB	SilA	CusA	CzcA	CzcA1	CnrA
136	F	W	W	I	I	V/I
139	V	E/Q	E	W	W[f]	Y/F
176	Q	A	A	N	N	G
178	F	V/I/L	V/I/L	I	I	Y/F[i]
274	N	M/I/A/L[a]	M/I/A/L[a]	L[c]	L[c]	L/V/I/[j]
277	I	G	G	G	G	G
327	Y	Y	Y	Y	Y	L/Y
610	F	-	-	F[d]	F[g]	Y/F[k]
612	V	-	-	R/K	R/K	R/K
615	F	F/Y[b]	F/Y[b]	T	T	T[l]
617	F	K	K	E	E	S/E/D
626	I	I/V	I/V	D	D	D
628	F	L/F	L/F	Y/F[e]	Y/F[h]	Y/F[m]

76 Homologous proteins of the HME transporters SilA, CusA, CzcA, CzcA1 and CnrA were identified and aligned as described before. Residues forming the binding pocket in AcrB (40,41) were compared with the analogous residues in the HME proteins.
Homologous proteins having different amino acids at the indicated position (UniProtKB/Swiss-Prot accession number) are indicated:
[a]: B3IK35 and Q1GQC4: T; A6V8I4: V
[b]: Q1LD81: Q
[c]: Q88AL5, Q4ZLZ2 and Q48CG6: M
[d]: A6SYY5 and Q3JB89: V
[e]: A6SYY5 and Q3JB89: L; Q1GY56: T
[f]: A7ICX5: Y
[g]: A6SYY5: V
[h]: A6SYY5: L; Q1GY56: T
[i]: B3RCX3 and Q0JYI5: H; A6SYW2: Q
[j]: B4W715, B2FNF1, B4WBU0, B4SNN7: P
[k]: A6SYY5 and Q9A5Q7: V
[l]: Q1NFT2: Q
[m]: B4W715, B2FNF1, B4WBU0, B4SNN7: V; Q134C4: I; A6SYY5: L

The residues that form the putative binding pocket of HMEs are considerably different from AcrB. G277 is conserved amongst all the HME transporters analyzed. For almost all the other investigated residues of the putative binding pocket, there is a clear distinction between monovalent and divalent HMEs. At position 617, lysine is conserved in monovalent HMEs, whereas the divalent HMEs have a negatively charged residue or a polar serine. The divalent HMEs all have an aspartate at position 626, whereas the monovalent HMEs exhibit an isoleucine or a valine. Tryptophane at

position 136 is 100% conserved amongst the monovalent HMEs, whereas divalent HMEs all have isoleucine or valine. Position 139 is occupied with glutamate or glutamine in monovalent HMEs, while there are exclusively aromatic residues in divalent HMEs.

Unlike monovalent HMEs, divalent HMEs have conserved polar residues in the putative binding pocket. Most prominent is threonine at position 615. This position is occupied by aromatic phenylalanines and tyrosines in monovalent HMEs.

In the monovalent HMEs, there are some profound differences in the PC1 domain compared to AcrB. According to the alignment, there is an insertion of eleven conserved residues between Q622 and N623 which might therefore be important for substrate binding. This hypothesis is supported by mutational analysis of CusA (230). Upon mutation of M623 to isoleucine (CusA numbering), sensitivity towards copper was increased as was shown by MIC experiments. Additionally, there is a gap between residues 609 and 615. This missing stretch includes V610 and F612, residues that are directly involved in binding of minocycline in AcrB ((40), Eicher unpublished). In divalent HMEs, these positions are occupied by conserved aromatic phenylalanines and tyrosines and with formally positive charged arginines and lysines, respectively (**Figure 26**).

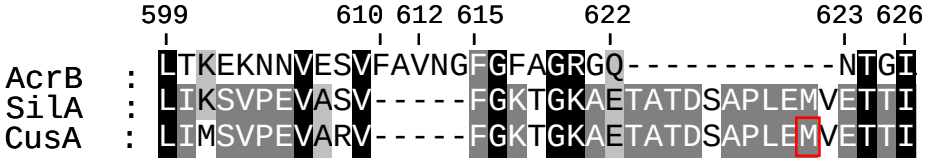

Figure 26: Excerpt of alignment of AcrB with SilA, CusA and homologous proteins identified by a blast search. Compared to AcrB, SilA, CusA and their homologous proteins lack residues 610 - 614. Instead, they have an insertion of eleven amino acids between Q622 and N623, most of which are conserved. M623 (CusA numbering), which is important for copper resistance in *E. coli* (230) is highlighted.

Alignment of AcrB with divalent HMEs revealed that their PN2 domain is elongated (**Figure 27**): homologues of CzcA and CzcA1 have an insertion of five amino acid residues at position 140, whereas homologues of CnrA have an insertion of five to 18 residues at the same position and four to 16 residues at position 148. This statement can be extended from AcrB to all the 31 members of the HAE1 family.

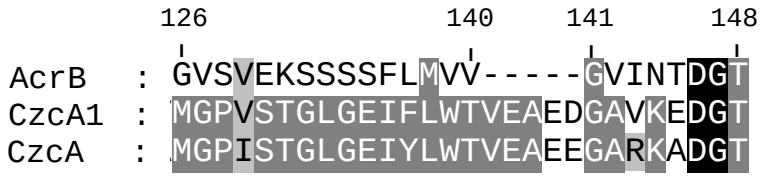

Figure 27: Excerpt of alignment of AcrB with CzcA, CzcA1 and homologous proteins identified by a blast search. Compared to AcrB, CzcA, CzcA1 and their homologous proteins have an insertion of five amino acids between V140 and G141, some of which are conserved.

Apart from different residues in the putative binding pocket, the monovalent HMEs show an insertion of 10 amino acids at position 422 and up to twelve amino acids at position 956. This corresponds to the C-terminal end of TM4 and TM10, respectively, both residing in the cytoplasm. Hence, the cytoplasmic loop connecting TM4 with TM5 and TM10 with TM11 is longer in SilA and CusA and their homologues. This observation is a general difference between monovalent HMEs and all the HAE1 listed in tcdb.

6.5 Substrate specificity determinants within HAE1 superfamily

AcrB is known to confer resistance towards a broad spectrum of unrelated noxious compounds. One criteria that distinguishes substrates from non-substrates might be the overall hydrophobicity, since AcrB does not transport hydrophilic substances like aminoglycosides.

The composition of the binding pocket might correlate with the substrate range, especially regarding the hydrophobicity of the substrates. In this light, AcrB and 15 homologues whose substrates are known were analyzed. These transporters are AcrF (*E. coli*), AdeJ (*Acinetobacter baumanii*), YhiV (*E. coli*), ArpB (*P.* putida), MexB, MexD and MexF (*P. aeruginosa*) (24,234-240), which are known to transport substrates with similar hydrophobicity as AcrB; AcrD (*E. coli*) (139,241,242), MexY (*P. aeruginosa)* (243-245) and AmrB (*P. pseudomallei*) (246) transport the more hydrophilic aminoglycosides; and EmhB (*P. fluorescens*), SrpB, TtgH, TtgE and TtgB (*P. putida*) (247-249) which are classical organic solvent transporters.

At a first glance (**Table 4**), many residues are quite conserved in most selected HAE1 transporters (V139, F178, Y327, F617), whereas others are more variable (N274, I277).

Of all the selected transporters, AcrD, which is capable of exporting hydrophilic aminoglycosides ($logP_{OW}$ of kanamycin = -6.30), deviates most from the consensus binding pocket of AcrB-like transporters. At positions 139 and 612, aliphatic valines are substituted by polar threonines and aromatic phenylalanines are exchanged for polar serines at positions 615 and 617. At position 176, AcrD bears an acidic aspartate whereas the AcrB-like transporters all have glutamine. The binding pockets of the selected AcrB-like transporters are devoid of formal positive charges while AcrD features basic amino acids at positions 274 and 626.

The deviations observed in MexY and AmrB from the common AcrB-like binding pockets are less dramatic: MexY features an acidic glutamate at position 176 (AcrB-like transporters have N176), it has a tryptophan residue at position 178 (AcrB-like transporters have F178) and at position 610 a hydrophilic tyrosine is observed compared to F610 in AcrB-like transporters. As MexY, AmrB features a tryptophan at position 178, an acidic aspartate at position 274 where most AcrB-like transporters have a polar residue and an aromatic tyrosine at position 277 where most AcrB-like transporters have an aliphatic residue.

The amino acid residues forming the putative binding pocket in organic solvent transporters are conserved and correspond to the residues of AcrB-like transporters with the following exceptions: TtgH, TtgE and SrpB exhibit a methionine at position 610 and a leucine at position 628, whereas TtgB and EmhB – as the AcrB-like transporters – have phenylalanines at the corresponding positions. Interestingly, TtgB and EmhB were shown to confer resistance towards a variety of antibiotics and dyes[9], whereas for TtgH, TtgE and SrpB, the only substrates reported up to date are organic solvents.

There appears to be a coupled variation of residues 610 and 612 with respect to substrate specificity. In HMEs transporting divalent HM ions, a basic amino acid goes with an aromatic residue and in HAE1 transporters that exclusively transport organic

[9] carbenicillin, nalidixic acid, chloramphenicol, tetracycline and ampicillin for TtgB and chloramphenicol, nalidixic acid, R6G, dequalinium, ciprofloxacin and streptomycin for EmhB (247,249)

solvents, the aliphatic methionine 610 pairs with aliphatic valine 612. The aminoglycoside transporters AcrD shows coupling of a polar with an aromatic residue, whereas in AcrB-like transporters, pairing of an aliphatic with an aromatic residue seems to be conserved. In most AcrB-like transporters, aromatic and aliphatic residues are located at positions 610 and 612, respectively, except for MexF, where the aromatic and aliphatic side chains are positionally exchanged. Interestingly, the similar observations was made in MIC experiments with *acrB*, *acrB_F610A*, *acrB_V612F* and the *acrB_F610A_V612F* double mutant: resistance towards most antibiotics was reduced when 610/612 pairing was of aliphatic-aliphatic or aromatic-aromatic nature, but could be restored to almost wt levels by re-establishing a random aliphatic-aromatic pairing (Eicher, unpublished).

Table 4: Residues of the putative binding pocket in selected HAE1 transporters

	AcrB-like transporters												
residue	136	139	176	178	274	277	327	610	612	615	617	626	628
AcrB	F	V	Q	F	N	I	Y	F	V	F	F	I	F
AcrF	Y	V	Q	F	N	V	Y	F	V	F	F	M	F
AdeJ	F	V	Q	F	N	F	Y	F	V	F	F	I	F
MexB	F	V	Q	F	D	I	Y	F	V	F	F	M	F
ArpB	F	V	Q	F	N	V	Y	F	V	F	F	M	F
YhiV	I	V	Q	F	D	T	Y	F	V	F	F	L	F
MexD	F	I	Q	F	S	I	Y	F	I	F	F	L	F
MexF	L	V	Q	F	Q	L	Y	V	F	L	I	I	F
	aminoglycoside transporters												
residue	136	139	176	178	274	277	327	610	612	615	617	626	628
AcrD	N	T	D	Y	K	Y	Y	F	T	S	P	R	F
MexY	I	I	E	W	E	F	Y	Y	V	F	L	M	F
AmrB	A	I	Q	W	D	Y	Y	F	L	Y	L	M	F
	solvent transporters												
residue	136	139	176	178	274	277	327	610	612	615	617	626	628
TtgB	F	V	Q	F	N	V	Y	F	V	F	F	M	F
TtgH	F	V	Q	F	S	I	Y	M	V	F	F	L	L
TtgE	F	V	L	F	N	I	Y	M	V	F	F	L	L
EmhB	F	V	Q	F	N	I	Y	F	V	F	F	L	F
SrpB	F	V	Q	F	S	I	Y	M	V	F	F	L	L

7. Conclusions and outlook

AcrB is the most potent MDR transport protein in *E. coli* and probably one of the most intensively studied bacterial multidrug transporters. This integral membrane protein associates with the accessory proteins AcrA and TolC and forms a tripartite complex which allows the extrusion of noxious substrates from the inner membrane directly into the extracellular space. The clinical importance of AcrB and its intrinsic properties – high recombinant overproduction potential and the presence of a large soluble domain – makes it an attractive candidate for structural analysis by X-ray crystallography. The high affinity Designed Akyrin Repeat Proteins (DARPins) are an excellent tool to improve on crystallizability of recalcitrant mutants and to enhance resolution. The results presented in this thesis initiate the understanding of the molecular mechanism of substrate transport and energization by AcrB and might be valid for other members of the RND superfamily as well.

7.1 Energization of AcrB

One of the obstacles in generating a model for energization of the AcrB efflux pump was the lack of essential polar or charged residues between the periplasm and the proton relay residues D407/D408/K940/R971 and postulating a proton transfer pathway. The problem was reminiscent to the situation observed in bacteriorhodopsin. In this light-driven archeal proton pump, the prosthetic group retinal is situated in the middle of the membrane and deprotonates upon photoisomerization. While the extracellular halfchannel is lined with polar and charged amino acids, the cytoplasmic halfchannel is very hydrophobic and contains only one aspartate and two threonines (**Figure 21**) thus representing a hydrophobic barrier between the cytoplasm and the prosthetic group. Due to insertion of mutations, illumination at different wavelengths and improving on resolution, electron densities for ordered water molecules inside the cytoplasmic halfchannel could be identified. According to the current hypothesis, these water molecules join due to protein conformational fluctuation and form a transient continuous water file at a given step of the photocycle connecting the cytoplasm with the chromophore. It therefore seems that the hydrophobic barrier

prevents the backflow of protons from the extracellular space to the cytosol along their electrochemical gradient (reviewed in (181,196,197)).

Our high resolution structures of wt and mutant AcrB/DARPin complexes show the position of waters during different stages of the pumping process. Water molecules are coordinated by polar side chains and backbone atoms of flexible transmembrane helices. It is most probably along these intermediary files of ordered waters that the proton travels from the bulk solvent of the periplasm to the D407/D408/K940 triad penetrating the hydrophobic barrier during functional rotation. The hydrophobic barrier ensures that the inflow of protons is coupled to the conformational changes in the transmembrane domain, which ultimately trigger the large conformational changes seen in the porter domain and hence energize the transport of substrate against their concentration gradient. In order to elucidate how reorientation of D407, K940 and R971, the bulging of TM5 and the distortion of TM4 are linked to the coil-to-helix transition of TM8 and the movement of the subdomains of the porter domain, more structural information might be required.

7.2 Substrate binding by AcrB

Commensurable to the MDR binding protein QacR of *S. aureus*, binding of drugs to the AcrB binding pocket is promiscuous (39,156,157). Upon mutation of V612 to phenylalanine, substrate transport and binding was not abolished, but only mildly decreased for most substrates tested and even improved for linezolid. For the substrate minocycline, we could show that the position inside the binding pocket is shifted by 2.1 Å, which leads to improved interactions with the polar side chains of E273 and N274, whereas π-stacking with F178 seems to have weakened. Regarding the multitude of substrates transported by AcrB, it is rather remarkable that in the numerous AcrB/substrate co-crystallization trials, only in two cases positive difference electron density peaks were observed, i. e. for minocycline and doxorubicin. These drugs both belong to the tetracycline class of antibiotics and are hence structurally very similar. Both are composed of a planar ring system which is substituted by different functional groups. If the resistance to the other compounds is due to the recognition and binding of the substrate to the observed hydrophobic

pocket, the following might account for lack of their electron densities in the measured crystal diffraction data:

(i) AcrB might bind the compounds tested in co-crystallization experiments, but at different locations inside the binding pocket and hence not in a single, discrete binding mode. In this case, the electron density of the bound ligand is expected to be weak and spread according to the multiple conformation adapted inside the binding pocket. This phenomenon has been described for the MDR binding protein QacR in complex with the bivalent aromatic diamidines DB75 and DB359 (250). In these structures, the coil-to-helix transition of the DNA binding domain, the extrusion of Y92 from the binding pocket and the fact that QacR does not form crystals in the absence of substrate was indicative for ligand binding. However, the positive difference electron densities inside the binding pocket were not continuous and therefore could not be attributed to a bound ligand.

(ii) Binding of substrates added in co-crystallization experiments might be competed by other substances present in the crystallization set up such as polyethyleneglycol (PEG) or detergent. In fact, the detergents used in our crystallization studies, *n*-dodecyl-β-D-maltoside (DDM) and cyclohexyl-*n*-hexyl-β-D-maltoside (CHM) are substrates of AcrB. Their concentration in the protein crystal is estimated to be approximately 400 mM and may therefore interfere with the added drug molecules.

(iii) Binding of substrates might be impeded by the putative non-native conformations of AcrB inside the crystal lattice. The non-physiological crystal contacts are of special concern. In any of the asymmetric structures as well as in the symmetric all-tight conformation of AcrB_V612F, the protein-protein contacts at the surface of the PC1 and/or PN2 subdomais of the tight monomer are extensive and might account for the allegedly reduced movement of the PC1 subdomain during conformational cycling. To analyze the distances between different AcrB subdomains *in vivo*, we introduced pairs of cysteines and investigated the extent of cross-link formation by mass spectrometric means (160). Interestingly, we found strong cross-link formation between Q229C and E585C located on the intermonomer connecting loop and the PC1 subdomain, respectively (unpublished data), although the minimal distance measured in the AcrB 3D-structure is 8.9 Å and thus exceeds the threshold for cross-link formation by far (6.4 Å). We therefore hypothesize that the crystal contacts might impose a constraint for further opening of the binding pocket, which is situated at the

interface of the PN2 and PC1 subdomain. As a consequence, the range of substrates that are able to bind to AcrB in the 3D crystal might be narrowed to relatively small planar compounds such as antibiotics of the tetracycline class. Recent structure and cross-link driven docking approach experiments suggest that the surface of the PN2 and to a lesser extent of the PC1 subdomain are involved in contact formation with AcrA (121). Additionally, MFPs are known to influence the substrate specificity of the trimeric MFP/RND/OMF complex (132,133), indicating that probably also *in vivo* protein-protein contact at the PN2 and PC1 subdomains affect binding of substrate by the binding pocket.

7.3 Methods to obtain structural information on AcrB in additional conformations

Additional structural information of AcrB in alternative conformations is crucial to deepen our understanding of the working mechanism of this important MDR protein. Since formation of crystal contacts is one of the major bottlenecks in 3D crystallization, chances for the protein to crystallize in a novel conformation are improved when the crystal contacts are tackled specifically. Therefore, several methods were developed aiming to allow formation of new crystal contacts. Besides co-crystallization of the target protein with high affinity binding proteins such as fragments of monoclonal antibodies (251,252) or DARPins (142), an approach termed Rational Surface Engineering proved to be successful in improving crystallization behavior of some proteins (253). This method is based on the observation that residues with large polar side chains located on the surface of proteins are disadvantageous for the crystallization process. Glutamates and lysines are particularly unfavorable since integration of the protein into the crystal and especially the formation of crystal contacts involves the ordering of surface side chains which is affiliated with a loss of entropy. We therefore mutated subsequently four clusters containing nine lysine and glutamate residues located on flexible loops at the surface of AcrB to alanine. Since the R32 crystal forms were still predominant, we specifically mutated nine formally charged residues involved in the R32 crystal contacts in a later step. With this method, we were able to crystallize AcrB in the space group C2 with novel cell parameters diffracting up to 3.3 Å.

One method that not only circumvents the issue of crystal contacts in part but allows addressing the conformational state of AcrB in absence of substrate is 2D crystallography. To obtain 2D crystals, detergent solubilized membrane proteins are supplemented with membrane lipids. Detergent molecules are then removed by dialysis, which drives integration of the membrane protein into the planar lipid bilayer. If reconstitution is successful, the protein molecules might arrange in a regular 2D lattice and the structure of the protein in its native environment can be analyzed by electron transmission microscopy (TEM). Furthermore, 2D crystallography seems to be well suited to crystallize AcrB in presence of its accessory proteins AcrA and TolC, both of which are essential for substrate transport *in vivo*. We therefore established collaboration with Prof. Dr. Alok Mitra from the University of Auckland, who is well known internationally for his work in high-resolution electron crystallography of membrane proteins (254,255).

Purified AcrB was successfully integrated into the lipid bilayer by slow detergent removal using standard protocols (256). As shown in **Figure 28**, the AcrB 2D crystals exhibited tubular geometry. As a consequence, the electron beam is scattered by two layers of 2D crystals, which severely exacerbates data processing. However, upon addition of 3-[(3-Cholamidopropyl)dimethylammonio]-1-propanesulfonate (CHAPS) to preformed tubular AcrB 2D crystals, the tubules got partially dissolved and were present as single layered sheets. 2D crystals were negative-stained or cryo-protected and analyzed by TEM. The diffraction limit of the negative-stained specimen was found to be 20.6 Å and of the cryo-EM sample 18.5 Å, respectively. A 2D projection map of the crystal was generated after data processing. In the case of negative-stained AcrB crystals, the monomers of trimeric AcrB can be clearly distinguished. For vitrified AcrB crystals, the preliminary data did not indicate clear subunit morphology. Interestingly, both sample preparation methods resulted in a lattice with two-fold, but no three-fold symmetry. Attempts to improve resolution and reconstitution of AcrB with its accessory proteins AcrA and TolC are subject of current research in the laboratory of Prof. Dr. Alok Mitra.

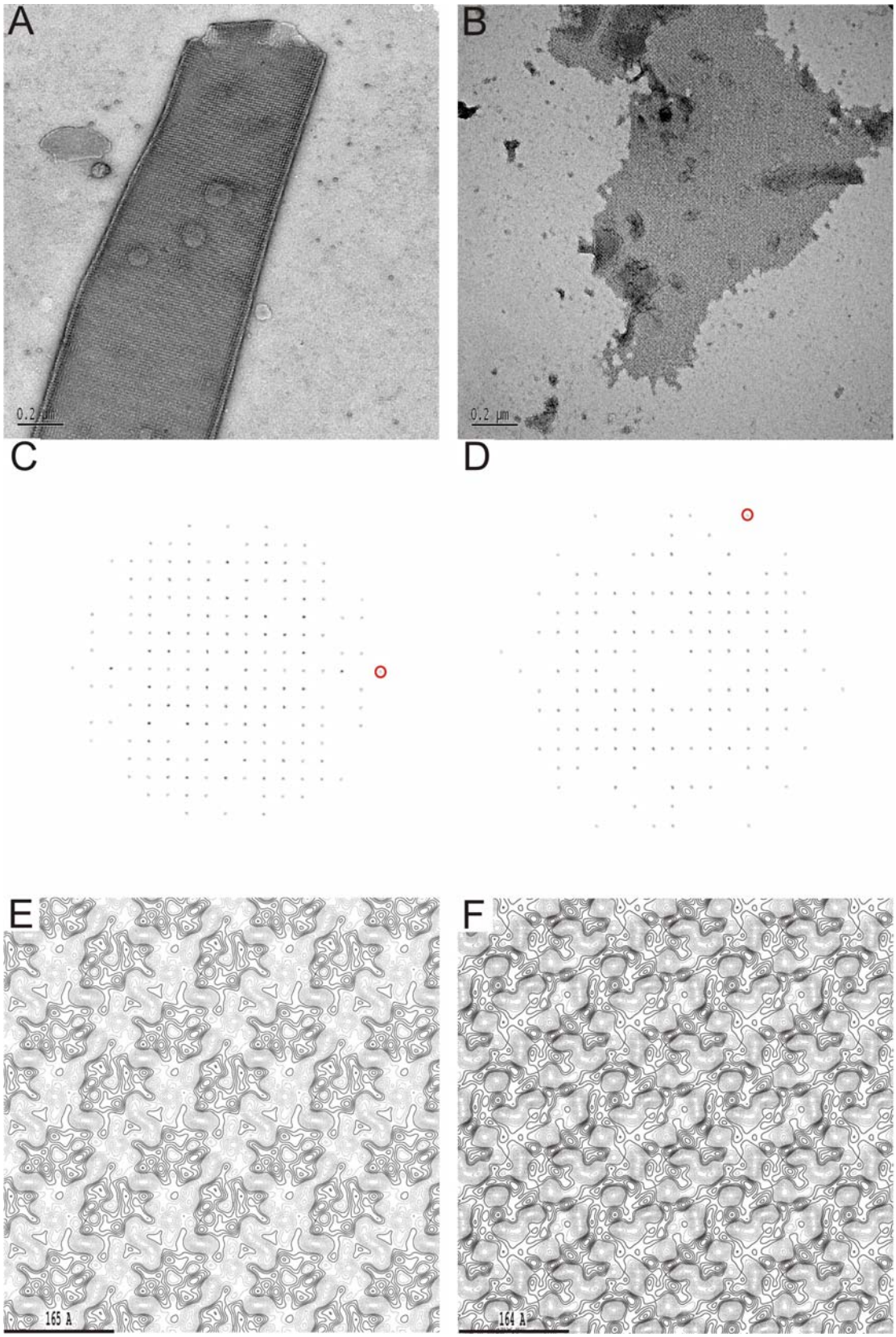

Figure 28: 2D crystallization of AcrB - preliminary data. **A)** Representative picture of negative stained AcrB 2D crystals. Upon integration into the lipid bilayer, AcrB mainly forms crystals with tubular geometry. The suspension containing 2D crystals of AcrB was placed on a glow-discharged EM grid covered with a continuous carbon film and stained with 1.5% uranyl acetate.

B) Single layered AcrB 2D crystal obtained after treatment of preformed crystals with 0.2 – 0.3% CHAPS.
C) Fourier transform (diffraction) of negative stained AcrB 2D crystal after masking of noise. Red circle indicates resolution limit (20.6 Å). The unit cell dimensions of the negative stained specimen were a = 165 Å, b = 177 Å, $\gamma = 90°$.
D) Diffraction of vitrified AcrB 2D crystal after masking of noise. Resolution limit was found to be 18.5 Å (red circle) and the unit cell dimensions were a = 164 Å, b = 168 Å, $\gamma = 90°$. After applying AcrB 2D crystals onto the EM grids, the samples were vitrified by snap-freezing in liquid ethane using Vitrobot Mark IV (FEI Company)
E) and **F)** 2D projection map of negative stained and cryo-EM AcrB 2D crystals, respectively. The continuous lines represent protein. Length of the a- axis is indicated.
Negative-stained and cryo-EM grids were examined at 120kV in a low-dose mode using Philips CM12 and Philips Tecnai12, respectively. The images of the 2D crystals were recorded at a nominal magnification of 42'000 and at 0.8 μm to 1.0 μm underfocus.
Images of 2D crystals of AcrB were processed by using the MRC program suite for 2D crystallography (195,257). The unit cell dimensions of the crystal lattice were determined and the amplitudes and phases were extracted after two rounds of lattice unbending procedure (as for example in (258)). At the defocus used, the highest resolution spot was located within the first node of contrast transfer function, and thus no correction for the phase reversal was applied. The extracted phases and amplitudes for the image were queried using the program ALLSPACE to determine the most likely plane group of symmetry. Extracted phase and amplitude were used to create 2D projection maps without imposing any symmetry

8. References

1. Garrett, L. (1994) *Newly Emerging Diseases in a World Out of Balance*, Penguin Books, New York
2. (WHO), W. H. O. (2002) *Deaths by cause, sex and mortality stratum in WHO Regions, estimates for 2001*, WHO, Geneva
3. Avorn, J. L., Barrett, J. F., Davey, P. G., McEwen, S. A., O'Brien, T. F., and Levy, S. B. (2001) *Antibiotic resistance: synthesis of recommendations by expert policy groups*, World Health Organization, Boston
4. Butler, M. S., and Buss, A. D. (2006) *Biochem Pharmacol* **71**, 919-929
5. Barrett, C. T., and Barrett, J. F. (2003) *Curr Opin Biotechnol* **14**, 621-626
6. Projan, S. J. (2003) *Curr Opin Microbiol* **6**, 427-430
7. Projan, S. J. (2002) *Curr Opin Pharmacol* **2**, 513-522
8. Shlaes, D. M., Proja, S.J., Edwards, J.E. (2004) *ASM News* **70**, 275-281
9. Bush, K. (2004) *ASM News* **70**, 282-287
10. Overbye, K. M., and Barrett, J. F. (2005) *Drug Discov Today* **10**, 45-52
11. Walsh, C. (2003) *Antibiotics: Actions, origins, resistance*, ASM Press, Washington, DC
12. Palumbi, S. R. (2001) *Science* **293**, 1786-1790
13. Tsiodras, S., Gold, H. S., Sakoulas, G., Eliopoulos, G. M., Wennersten, C., Venkataraman, L., Moellering, R. C., and Ferraro, M. J. (2001) *Lancet* **358**, 207-208
14. Skinner, R., Cundliffe, E., and Schmidt, F. J. (1983) *J Biol Chem* **258**, 12702-12706
15. Zalacain, M., and Cundliffe, E. (1989) *J Bacteriol* **171**, 4254-4260
16. Zalacain, M., and Cundliffe, E. (1990) *Eur J Biochem* **189**, 67-72
17. Yoshida, H., Bogaki, M., Nakamura, M., and Nakamura, S. (1990) *Antimicrob Agents Chemother* **34**, 1271-1272
18. Hooper, D. C. (2001) *Emerg Infect Dis* **7**, 337-341
19. Thomson, K. S., and Smith Moland, E. (2000) *Microbes Infect* **2**, 1225-1235
20. Wright, G. D. (1999) *Curr Opin Microbiol* **2**, 499-503
21. Hancock, R. E., and Brinkman, F. S. (2002) *Annu Rev Microbiol* **56**, 17-38
22. Nikaido, H. (1998) *Curr Opin Microbiol* **1**, 516-523
23. Lomovskaya, O., Lee, A., Hoshino, K., Ishida, H., Mistry, A., Warren, M. S., Boyer, E., Chamberland, S., and Lee, V. J. (1999) *Antimicrob Agents Chemother* **43**, 1340-1346
24. Li, X. Z., and Nikaido, H. (2004) *Drugs* **64**, 159-204
25. Lomovskaya, O., and Totrov, M. (2005) *J Bacteriol* **187**, 1879-1883
26. Nikaido, H. (2009) *Annu Rev Biochem*
27. Nikaido, H., and Takatsuka, Y. (2008) *Biochim Biophys Acta*
28. Saier, M. H., Jr., and Paulsen, I. T. (2001) *Semin Cell Dev Biol* **12**, 205-213
29. Higgins, C. F. (2007) *Nature* **446**, 749-757
30. Gottesman, M. M., Pastan, I., and Ambudkar, S. V. (1996) *Curr Opin Genet Dev* **6**, 610-617
31. Zaman, G. J., Flens, M. J., van Leusden, M. R., de Haas, M., Mulder, H. S., Lankelma, J., Pinedo, H. M., Scheper, R. J., Baas, F., Broxterman, H. J., and et al. (1994) *Proc Natl Acad Sci U S A* **91**, 8822-8826

32. Hipfner, D. R., Deeley, R. G., and Cole, S. P. (1999) *Biochim Biophys Acta* **1461**, 359-376
33. Sheppard, D. N., and Welsh, M. J. (1999) *Physiol Rev* **79**, S23-45
34. van Veen, H. W., Venema, K., Bolhuis, H., Oussenko, I., Kok, J., Poolman, B., Driessen, A. J., and Konings, W. N. (1996) *Proc Natl Acad Sci U S A* **93**, 10668-10672
35. Dawson, R. J., and Locher, K. P. (2007) *FEBS Lett* **581**, 935-938
36. Mirza, O., Guan, L., Verner, G., Iwata, S., and Kaback, H. R. (2006) *Embo J* **25**, 1177-1183
37. Guan, L., Mirza, O., Verner, G., Iwata, S., and Kaback, H. R. (2007) *Proc Natl Acad Sci U S A* **104**, 15294-15298
38. Huang, Y., Lemieux, M. J., Song, J., Auer, M., and Wang, D. N. (2003) *Science* **301**, 616-620
39. Schumacher, M. A., Miller, M. C., Grkovic, S., Brown, M. H., Skurray, R. A., and Brennan, R. G. (2001) *Science* **294**, 2158-2163
40. Murakami, S., Nakashima, R., Yamashita, E., Matsumoto, T., and Yamaguchi, A. (2006) *Nature* **443**, 173-179
41. Seeger, M. A., Schiefner, A., Eicher, T., Verrey, F., Diederichs, K., and Pos, K. M. (2006) *Science* **313**, 1295-1298
42. Ninio, S., Elbaz, Y., and Schuldiner, S. (2004) *FEBS Lett* **562**, 193-196
43. Soskine, M., Adam, Y., and Schuldiner, S. (2004) *J Biol Chem* **279**, 9951-9955
44. Daley, D. O., Rapp, M., Granseth, E., Melen, K., Drew, D., and von Heijne, G. (2005) *Science* **308**, 1321-1323
45. Granseth, E., Daley, D. O., Rapp, M., Melen, K., and von Heijne, G. (2005) *J Mol Biol* **352**, 489-494
46. Rapp, M., Seppala, S., Granseth, E., and von Heijne, G. (2007) *Science* **315**, 1282-1284
47. Chen, Y. J., Pornillos, O., Lieu, S., Ma, C., Chen, A. P., and Chang, G. (2007) *Proc Natl Acad Sci U S A* **104**, 18999-19004
48. Muth, T. R., and Schuldiner, S. (2000) *EMBO J* **19**, 234-240
49. Yerushalmi, H., and Schuldiner, S. (2000) *J Biol Chem* **275**, 5264-5269
50. Morita, Y., Kodama, K., Shiota, S., Mine, T., Kataoka, A., Mizushima, T., and Tsuchiya, T. (1998) *Antimicrob Agents Chemother* **42**, 1778-1782
51. He, G. X., Kuroda, T., Mima, T., Morita, Y., Mizushima, T., and Tsuchiya, T. (2004) *J Bacteriol* **186**, 262-265
52. Pogliano, J. A., and Beckwith, J. (1994) *EMBO J* **13**, 554-561
53. Gardel, C., Benson, S., Hunt, J., Michaelis, S., and Beckwith, J. (1987) *J Bacteriol* **169**, 1286-1290
54. Camacho, L. R., Constant, P., Raynaud, C., Laneelle, M. A., Triccas, J. A., Gicquel, B., Daffe, M., and Guilhot, C. (2001) *J Biol Chem* **276**, 19845-19854
55. Domenech, P., Reed, M. B., and Barry, C. E., 3rd. (2005) *Infect Immun* **73**, 3492-3501
56. Baev, N., Endre, G., Petrovics, G., Banfalvi, Z., and Kondorosi, A. (1991) *Mol Gen Genet* **228**, 113-124
57. Sleat, D. E., Wiseman, J. A., El-Banna, M., Price, S. M., Verot, L., Shen, M. M., Tint, G. S., Vanier, M. T., Walkley, S. U., and Lobel, P. (2004) *Proc Natl Acad Sci U S A* **101**, 5886-5891
58. Infante, R. E., Wang, M. L., Radhakrishnan, A., Kwon, H. J., Brown, M. S., and Goldstein, J. L. (2008) *Proc Natl Acad Sci U S A* **105**, 15287-15292

59. Infante, R. E., Abi-Mosleh, L., Radhakrishnan, A., Dale, J. D., Brown, M. S., and Goldstein, J. L. (2008) *J Biol Chem* **283**, 1052-1063
60. Taipale, J., Cooper, M. K., Maiti, T., and Beachy, P. A. (2002) *Nature* **418**, 892-897
61. Nakano, Y., Kim, H. R., Kawakami, A., Roy, S., Schier, A. F., and Ingham, P. W. (2004) *Dev Biol* **269**, 381-392
62. Goldberg, M., Pribyl, T., Juhnke, S., and Nies, D. H. (1999) *J Biol Chem* **274**, 26065-26070
63. Nikaido, H. (2003) *Microbiol Mol Biol Rev* **67**, 593-656
64. Plesiat, P., and Nikaido, H. (1992) *Mol Microbiol* **6**, 1323-1333
65. Nikaido, H. (1996) *J. Bacteriol.* **178**, 5853-5859
66. Davies, J. P., Chen, F. W., and Ioannou, Y. A. (2000) *Science* **290**, 2295-2298
67. Katoh, K., and Toh, H. (2008) *Brief Bioinform* **9**, 286-298
68. Guindon, S., and Gascuel, O. (2003) *Syst Biol* **52**, 696-704
69. Jones, D. T., Taylor, W. R., and Thornton, J. M. (1992) *Comput Appl Biosci* **8**, 275-282
70. Davies, J. P., and Ioannou, Y. A. (2000) *J Biol Chem* **275**, 24367-24374
71. Vanier, M. T., Pentchev, P., Rodriguez-Lafrasse, C., and Rousson, R. (1991) *J Inherit Metab Dis* **14**, 580-595
72. Pentchev, P. G., Comly, M. E., Kruth, H. S., Vanier, M. T., Wenger, D. A., Patel, S., and Brady, R. O. (1985) *Proc Natl Acad Sci U S A* **82**, 8247-8251
73. Scott, C., Higgins, M. E., Davies, J. P., and Ioannou, Y. A. (2004) *J Biol Chem* **279**, 48214-48223
74. Naureckiene, S., Sleat, D. E., Lackland, H., Fensom, A., Vanier, M. T., Wattiaux, R., Jadot, M., and Lobel, P. (2000) *Science* **290**, 2298-2301
75. Liou, H. L., Dixit, S. S., Xu, S., Tint, G. S., Stock, A. M., and Lobel, P. (2006) *J Biol Chem* **281**, 36710-36723
76. Xu, S., Benoff, B., Liou, H. L., Lobel, P., and Stock, A. M. (2007) *J Biol Chem* **282**, 23525-23531
77. Voght, S. P., Fluegel, M. L., Andrews, L. A., and Pallanck, L. J. (2007) *Cell Metab* **5**, 195-205
78. Malathi, K., Higaki, K., Tinkelenberg, A. H., Balderes, D. A., Almanzar-Paramio, D., Wilcox, L. J., Erdeniz, N., Redican, F., Padamsee, M., Liu, Y., Khan, S., Alcantara, F., Carstea, E. D., Morris, J. A., and Sturley, S. L. (2004) *J Cell Biol* **164**, 547-556
79. Altmann, S. W., Davis, H. R., Jr., Zhu, L. J., Yao, X., Hoos, L. M., Tetzloff, G., Iyer, S. P., Maguire, M., Golovko, A., Zeng, M., Wang, L., Murgolo, N., and Graziano, M. P. (2004) *Science* **303**, 1201-1204
80. Davis, H. R., Jr., Zhu, L. J., Hoos, L. M., Tetzloff, G., Maguire, M., Liu, J., Yao, X., Iyer, S. P., Lam, M. H., Lund, E. G., Detmers, P. A., Graziano, M. P., and Altmann, S. W. (2004) *J Biol Chem* **279**, 33586-33592
81. Rosenblum, S. B., Huynh, T., Afonso, A., Davis, H. R., Jr., Yumibe, N., Clader, J. W., and Burnett, D. A. (1998) *J Med Chem* **41**, 973-980
82. Chang, T. Y., Reid, P. C., Sugii, S., Ohgami, N., Cruz, J. C., and Chang, C. C. (2005) *J Biol Chem* **280**, 20917-20920
83. Radhakrishnan, A., Sun, L. P., Kwon, H. J., Brown, M. S., and Goldstein, J. L. (2004) *Mol Cell* **15**, 259-268
84. Radhakrishnan, A., Ikeda, Y., Kwon, H. J., Brown, M. S., and Goldstein, J. L. (2007) *Proc Natl Acad Sci U S A* **104**, 6511-6518

85. Nohturfft, A., Brown, M. S., and Goldstein, J. L. (1998) *Proc Natl Acad Sci U S A* **95**, 12848-12853
86. Nohturfft, A., Brown, M. S., and Goldstein, J. L. (1998) *J Biol Chem* **273**, 17243-17250
87. Hua, X., Nohturfft, A., Goldstein, J. L., and Brown, M. S. (1996) *Cell* **87**, 415-426
88. Yang, T., Espenshade, P. J., Wright, M. E., Yabe, D., Gong, Y., Aebersold, R., Goldstein, J. L., and Brown, M. S. (2002) *Cell* **110**, 489-500
89. Sun, L. P., Li, L., Goldstein, J. L., and Brown, M. S. (2005) *J Biol Chem* **280**, 26483-26490
90. Brown, M. S., and Goldstein, J. L. (1997) *Cell* **89**, 331-340
91. Goldstein, J. L., DeBose-Boyd, R. A., and Brown, M. S. (2006) *Cell* **124**, 35-46
92. Gil, G., Faust, J. R., Chin, D. J., Goldstein, J. L., and Brown, M. S. (1985) *Cell* **41**, 249-258
93. Liscum, L., Finer-Moore, J., Stroud, R. M., Luskey, K. L., Brown, M. S., and Goldstein, J. L. (1985) *J Biol Chem* **260**, 522-530
94. Roitelman, J., Olender, E. H., Bar-Nun, S., Dunn, W. A., Jr., and Simoni, R. D. (1992) *J Cell Biol* **117**, 959-973
95. Sever, N., Song, B. L., Yabe, D., Goldstein, J. L., Brown, M. S., and DeBose-Boyd, R. A. (2003) *J Biol Chem* **278**, 52479-52490
96. Song, B. L., Sever, N., and DeBose-Boyd, R. A. (2005) *Mol Cell* **19**, 829-840
97. McMahon, A. P., Ingham, P. W., and Tabin, C. J. (2003) *Curr Top Dev Biol* **53**, 1-114
98. Varjosalo, M., and Taipale, J. (2007) *J Cell Sci* **120**, 3-6
99. Johnson, R. L., Rothman, A. L., Xie, J., Goodrich, L. V., Bare, J. W., Bonifas, J. M., Quinn, A. G., Myers, R. M., Cox, D. R., Epstein, E. H., Jr., and Scott, M. P. (1996) *Science* **272**, 1668-1671
100. Corcoran, R. B., and Scott, M. P. (2006) *Proc Natl Acad Sci U S A* **103**, 8408-8413
101. Lum, L., and Beachy, P. A. (2004) *Science* **304**, 1755-1759
102. Matise, M. P., and Joyner, A. L. (1999) *Oncogene* **18**, 7852-7859
103. Methot, N., and Basler, K. (2001) *Development* **128**, 733-742
104. Taipale, J., and Beachy, P. A. (2001) *Nature* **411**, 349-354
105. Sulavik, M. C., Houseweart, C., Cramer, C., Jiwani, N., Murgolo, N., Greene, J., DiDomenico, B., Shaw, K. J., Miller, G. H., Hare, R., and Shimer, G. (2001) *Antimicrob Agents Chemother* **45**, 1126-1136
106. Kobayashi, N., Nishino, K., and Yamaguchi, A. (2001) *J Bacteriol* **183**, 5639-5644
107. Nagel de Zwaig, R., and Luria, S. E. (1967) *J Bacteriol* **94**, 1112-1123
108. Piddock, L. J. (2006) *Nat Rev Microbiol* **4**, 629-636
109. Koronakis, V., Sharff, A., Koronakis, E., Luisi, B., and Hughes, C. (2000) *Nature* **405**, 914-919
110. Akama, H., Matsuura, T., Kashiwagi, S., Yoneyama, H., Narita, S., Tsukihara, T., Nakagawa, A., and Nakae, T. (2004) *J. Biol. Chem.* **279**, 25939-25942
111. Federici, L., Du, D., Walas, F., Matsumura, H., Fernandez-Recio, J., McKeegan, K. S., Borges-Walmsley, M. I., Luisi, B. F., and Walmsley, A. R. (2005) *J Biol Chem* **280**, 15307-15314
112. Bavro, V. N., Pietras, Z., Furnham, N., Perez-Cano, L., Fernandez-Recio, J., Pei, X. Y., Misra, R., and Luisi, B. (2008) *Mol Cell* **30**, 114-121

113. Thanabalu, T., Koronakis, E., Hughes, C., and Koronakis, V. (1998) *EMBO J* **17**, 6487-6496
114. Andersen, C., Koronakis, E., Bokma, E., Eswaran, J., Humphreys, D., Hughes, C., and Koronakis, V. (2002) *Proc Natl Acad Sci U S A* **99**, 11103-11108
115. Augustus, A. M., Celaya, T., Husain, F., Humbard, M., and Misra, R. (2004) *J Bacteriol* **186**, 1851-1860
116. Dinh, T., Paulsen, I. T., and Saier, M. H., Jr. (1994) *J Bacteriol* **176**, 3825-3831
117. Johnson, J. M., and Church, G. M. (1999) *J Mol Biol* **287**, 695-715
118. Zgurskaya, H. I., and Nikaido, H. (1999) *J Mol Biol* **285**, 409-420
119. Mikolosko, J., Bobyk, K., Zgurskaya, H. I., and Ghosh, P. (2006) *Structure* **14**, 577-587
120. Higgins, M. K., Bokma, E., Koronakis, E., Hughes, C., and Koronakis, V. (2004) *Proc. Natl. Acad. Sc.i U. S. A.* **101**, 9994-9999
121. Symmons, M. F., Bokma, E., Koronakis, E., Hughes, C., and Koronakis, V. (2009) *Proc Natl Acad Sci U S A* **106**, 7173-7178
122. Yoneyama, H., Maseda, H., Yamabayashi Ta, T. A., Izumi, S., and Nakae, T. (2002) *Biochem Biophys Res Commun* **292**, 513-518
123. Lomovskaya, O., and Lewis, K. (1992) *Proc Natl Acad Sci U S A* **89**, 8938-8942
124. Lee, E. H., and Shafer, W. M. (1999) *Mol Microbiol* **33**, 839-845
125. Colmer, J. A., Fralick, J. A., and Hamood, A. N. (1998) *Mol Microbiol* **27**, 63-72
126. Gilson, L., Mahanty, H. K., and Kolter, R. (1990) *EMBO J* **9**, 3875-3884
127. Tikhonova, E. B., Devroy, V. K., Lau, S. Y., and Zgurskaya, H. I. (2007) *Mol Microbiol* **63**, 895-910
128. Nikaido, H., and Hall, J. A. (1998) *Methods Enzymol* **292**, 3-20
129. Davidson, A. L., Shuman, H. A., and Nikaido, H. (1992) *Proc Natl Acad Sci U S A* **89**, 2360-2364
130. Liu, C. E., Liu, P. Q., Wolf, A., Lin, E., and Ames, G. F. (1999) *J Biol Chem* **274**, 739-747
131. Harley, K. T., Djordjevic, G. M., Tseng, T. T., and Saier, M. H. (2000) *Mol Microbiol* **36**, 516-517
132. Elkins, C. A., and Nikaido, H. (2003) *J. Bacteriol.* **185**, 5349-5356
133. Krishnamoorthy, G., Tikhonova, E. B., and Zgurskaya, H. I. (2008) *J Bacteriol* **190**, 691-698
134. Nakamura, H. (1965) *J Bacteriol* **90**, 8-14
135. Ioannou, Y. A. (2007) *Dev Cell* **12**, 481-483
136. Paulsen, I. T., Brown, M. H., and Skurray, R. A. (1996) *Microbiol Rev* **60**, 575-608
137. Guan, L., Ehrmann, M., Yoneyama, H., and Nakae, T. (1999) *J Biol Chem* **274**, 10517-10522
138. Eda, S., Yoneyama, H., and Nakae, T. (2003) *Biochemistry* **42**, 7238-7244
139. Elkins, C. A., and Nikaido, H. (2002) *J Bacteriol* **184**, 6490-6498
140. Eda, S., Maseda, H., and Nakae, T. (2003) *J Biol Chem* **278**, 2085-2088
141. Mao, W., Warren, M. S., Black, D. S., Satou, T., Murata, T., Nishino, T., Gotoh, N., and Lomovskaya, O. (2002) *Mol Microbiol* **46**, 889-901
142. Sennhauser, G., Amstutz, P., Briand, C., Storchenegger, O., and Grutter, M. G. (2006) *PLoS Biol* **5**, e7

143. Murakami, S., Nakashima, R., Yamashita, E., and Yamaguchi, A. (2002) *Nature* **419**, 587-593
144. Guan, L., and Nakae, T. (2001) *J. Bacteriol.* **183**, 1734-1739
145. Takatsuka, Y., and Nikaido, H. (2006) *J Bacteriol* **188**, 7284-7289
146. Su, C. C., Li, M., Gu, R., Takatsuka, Y., McDermott, G., Nikaido, H., and Yu, E. W. (2006) *J Bacteriol* **188**, 7290-7296
147. Pietras, Z., Bavro, V. N., Furnham, N., Pellegrini-Calace, M., Milner-White, E. J., and Luisi, B. F. (2008) *Curr Drug Targets* **9**, 719-728
148. Tamura, N., Murakami, S., Oyama, Y., Ishiguro, M., and Yamaguchi, A. (2005) *Biochemistry* **44**, 11115-11121
149. Tikhonova, E. B., and Zgurskaya, H. I. (2004) *J Biol Chem* **279**, 32116-32124
150. Tornroth-Horsefield, S., Gourdon, P., Horsefield, R., Brive, L., Yamamoto, N., Mori, H., Snijder, A., and Neutze, R. (2007) *Structure* **15**, 1663-1673
151. Yu, E. W., Aires, J. R., McDermott, G., and Nikaido, H. (2005) *J. Bacteriol.* **187**, 6804-6815
152. Pos, K. M., Schiefner, A., Seeger, M. A., and Diederichs, K. (2004) *FEBS Lett* **564**, 333-339
153. Yu, E. W., Aires, J. R., and Nikaido, H. (2003) *J Bacteriol* **185**, 5657-5664
154. Yu, E. W., McDermott, G., Zgurskaya, H. I., Nikaido, H., and Koshland, D. E., Jr. (2003) *Science* **300**, 976-980
155. Zheleznova, E. E., Markham, P. N., Neyfakh, A. A., and Brennan, R. G. (1999) *Cell* **96**, 353-362
156. Schumacher, M. A., Miller, M. C., and Brennan, R. G. (2004) *EMBO J* **23**, 2923-2930
157. Murray, D. S., Schumacher, M. A., and Brennan, R. G. (2004) *J Biol Chem* **279**, 14365-14371
158. Petrek, M., Kosinova, P., Koca, J., and Otyepka, M. (2007) *Structure* **15**, 1357-1363
159. Drew, D., Klepsch, M. M., Newstead, S., Flaig, R., De Gier, J. W., Iwata, S., and Beis, K. (2008) *Mol Membr Biol* **25**, 677-682
160. Seeger, M. A., von Ballmoos, C., Eicher, T., Brandstatter, L., Verrey, F., Diederichs, K., and Pos, K. M. (2008) *Nat Struct Mol Biol* **15**, 199-205
161. Takatsuka, Y., and Nikaido, H. (2007) *J Bacteriol* **189**, 8677-8684
162. Milgrom, Y. M., Murataliev, M. B., and Boyer, P. D. (1998) *Biochem J* **330 (Pt 2)**, 1037-1043
163. Pos, K. M. (2009) *Biochim Biophys Acta* **1794**, 782-793
164. Takatsuka, Y., and Nikaido, H. (2009) *J Bacteriol* **191**, 1729-1737
165. Mokhonov, V. V., Mokhonova, E. I., Akama, H., and Nakae, T. (2004) *Biochem Biophys Res Commun* **322**, 483-489
166. Touze, T., Eswaran, J., Bokma, E., Koronakis, E., Hughes, C., and Koronakis, V. (2004) *Mol. Microbiol.* **53**, 697-706
167. Zgurskaya, H. I., and Nikaido, H. (2000) *J Bacteriol* **182**, 4264-4267
168. Eda, S., Maseda, H., Yoshihara, E., and Nakae, T. (2006) *FEMS Microbiol Lett* **254**, 101-107
169. Stegmeier, J. F., Polleichtner, G., Brandes, N., Hotz, C., and Andersen, C. (2006) *Biochemistry* **45**, 10303-10312
170. Lobedanz, S., Bokma, E., Symmons, M. F., Koronakis, E., Hughes, C., and Koronakis, V. (2007) *Proc Natl Acad Sci U S A* **104**, 4612-4617
171. Vaccaro, L., Scott, K. A., and Sansom, M. S. (2008) *Biophys J* **95**, 5681-5691
172. Pos, K. M. (2009) *Proc Natl Acad Sci U S A* **106**, 6893-6894

173. Ahmed, M., Borsch, C. M., Taylor, S. S., Vazquez-Laslop, N., and Neyfakh, A. A. (1994) *J Biol Chem* **269**, 28506-28513
174. Aramaki, H., Yagi, N., and Suzuki, M. (1995) *Protein Eng* **8**, 1259-1266
175. Peters, K. M., Schuman, J. T., Skurray, R. A., Brown, M. H., Brennan, R. G., and Schumacher, M. A. (2008) *Biochemistry* **47**, 8122-8129
176. Seeger, M. A., Diederichs, K., Eicher, T., Brandstatter, L., Schiefner, A., Verrey, F., and Pos, K. M. (2008) *Curr Drug Targets* **9**, 729-749
177. Zgurskaya, H. I., and Nikaido, H. (1999) *Proc Natl Acad Sci U S A* **96**, 7190-7195
178. Murakami, S., and Yamaguchi, A. (2003) *Curr Opin Struct Biol* **13**, 443-452
179. Seeger, M. A., von Ballmoos, C., Verrey, F., and Pos, K. M. (2009) *Biochemistry*
180. Oesterhelt, D., and Stoeckenius, W. (1973) *Proc Natl Acad Sci U S A* **70**, 2853-2857
181. Kuhlbrandt, W. (2000) *Nature* **406**, 569-570
182. Szaraz, S., Oesterhelt, D., and Ormos, P. (1994) *Biophys J* **67**, 1706-1712
183. Zscherp, C., Schlesinger, R., Tittor, J., Oesterhelt, D., and Heberle, J. (1999) *Proc Natl Acad Sci U S A* **96**, 5498-5503
184. Dioumaev, A. K., Brown, L. S., Needleman, R., and Lanyi, J. K. (1999) *Biochemistry* **38**, 10070-10078
185. Pande, J., Callender, R. H., and Ebrey, T. G. (1981) *Proc Natl Acad Sci U S A* **78**, 7379-7382
186. Braiman, M., and Mathies, R. (1982) *Proc Natl Acad Sci U S A* **79**, 403-407
187. Patzelt, H., Simon, B., terLaak, A., Kessler, B., Kuhne, R., Schmieder, P., Oesterhelt, D., and Oschkinat, H. (2002) *Proc Natl Acad Sci U S A* **99**, 9765-9770
188. Herzfeld, J., and Lansing, J. C. (2002) *Annu Rev Biophys Biomol Struct* **31**, 73-95
189. Herzfeld, J., and Tounge, B. (2000) *Biochim Biophys Acta* **1460**, 95-105
190. Hatcher, M. E., Hu, J. G., Belenky, M., Verdegem, P., Lugtenburg, J., Griffin, R. G., and Herzfeld, J. (2002) *Biophys J* **82**, 1017-1029
191. Pebay-Peyroula, E., Rummel, G., Rosenbusch, J. P., and Landau, E. M. (1997) *Science* **277**, 1676-1681
192. Luecke, H., Schobert, B., Richter, H. T., Cartailler, J. P., and Lanyi, J. K. (1999) *J Mol Biol* **291**, 899-911
193. Royant, A., Edman, K., Ursby, T., Pebay-Peyroula, E., Landau, E. M., and Neutze, R. (2001) *Photochem Photobiol* **74**, 794-804
194. Schobert, B., Brown, L. S., and Lanyi, J. K. (2003) *J Mol Biol* **330**, 553-570
195. Henderson, R., Baldwin, J. M., Ceska, T. A., Zemlin, F., Beckmann, E., and Downing, K. H. (1990) *J Mol Biol* **213**, 899-929
196. Lanyi, J. K. (2004) *Annu Rev Physiol* **66**, 665-688
197. Hirai, T., and Subramaniam, S. (2003) *FEBS Lett* **545**, 2-8
198. Edmonds, B. W., and Luecke, H. (2004) *Front. Biosci.* **9**, 1556-1566
199. Belrhali, H., Nollert, P., Royant, A., Menzel, C., Rosenbusch, J. P., Landau, E. M., and Pebay-Peyroula, E. (1999) *Structure* **7**, 909-917
200. Luecke, H. (2000) *Biochim. Biophys. Acta* **1460**, 133-156
201. Balashov, S. P., Imasheva, E. S., Govindjee, R., and Ebrey, T. G. (1996) *Biophys J* **70**, 473-481
202. Richter, H. T., Needleman, R., Kandori, H., Maeda, A., and Lanyi, J. K. (1996) *Biochemistry* **35**, 15461-15466

203. Rammelsberg, R., Huhn, G., Lubben, M., and Gerwert, K. (1998) *Biochemistry* **37**, 5001-5009
204. Spassov, V. Z., Luecke, H., Gerwert, K., and Bashford, D. (2001) *J Mol Biol* **312**, 203-219
205. Luecke, H., Schobert, B., Cartailler, J. P., Richter, H. T., Rosengarth, A., Needleman, R., and Lanyi, J. K. (2000) *J Mol Biol* **300**, 1237-1255
206. Sass, H. J., Buldt, G., Gessenich, R., Hehn, D., Neff, D., Schlesinger, R., Berendzen, J., and Ormos, P. (2000) *Nature* **406**, 649-653
207. Lanyi, J. K. (2004) *Mol. Membr. Biol.* **21**, 143-150
208. Rouhani, S., Cartailler, J. P., Facciotti, M. T., Walian, P., Needleman, R., Lanyi, J. K., Glaeser, R. M., and Luecke, H. (2001) *J Mol Biol* **313**, 615-628
209. Bousche, O., Sonar, S., Krebs, M. P., Khorana, H. G., and Rothschild, K. J. (1992) *Photochem Photobiol* **56**, 1085-1095
210. Hessling, B., Souvignier, G., and Gerwert, K. (1993) *Biophys J* **65**, 1929-1941
211. Subramaniam, S., and Henderson, R. (2000) *Nature* **406**, 653-657
212. Lanyi, J., and Schobert, B. (2002) *J Mol Biol* **321**, 727-737
213. Royant, A., Edman, K., Ursby, T., Pebay-Peyroula, E., Landau, E. M., and Neutze, R. (2000) *Nature* **406**, 645-648
214. Rahman, M. M., Matsuo, T., Ogawa, W., Koterasawa, M., Kuroda, T., and Tsuchiya, T. (2007) *Microbiol Immunol* **51**, 1061-1070
215. Dimroth, P. (1980) *FEBS Lett* **122**, 234-236
216. Hilpert, W., and Dimroth, P. (1982) *Nature* **296**, 584-585
217. Morita, Y., Kataoka, A., Shiota, S., Mizushima, T., and Tsuchiya, T. (2000) *J Bacteriol* **182**, 6694-6697
218. Meier, T., Yu, J., Raschle, T., Henzen, F., Dimroth, P., and Muller, D. J. (2005) *FEBS J* **272**, 5474-5483
219. Yamashita, A., Singh, S. K., Kawate, T., Jin, Y., and Gouaux, E. (2005) *Nature* **437**, 215-223
220. Boudker, O., Ryan, R. M., Yernool, D., Shimamoto, K., and Gouaux, E. (2007) *Nature* **445**, 387-393
221. Faham, S., Watanabe, A., Besserer, G. M., Cascio, D., Specht, A., Hirayama, B. A., Wright, E. M., and Abramson, J. (2008) *Science* **321**, 810-814
222. Arnold, K., Bordoli, L., Kopp, J., and Schwede, T. (2006) *Bioinformatics* **22**, 195-201
223. Kopp, J., and Schwede, T. (2004) *Nucleic Acids Res* **32**, D230-234
224. Schwede, T., Kopp, J., Guex, N., and Peitsch, M. C. (2003) *Nucleic Acids Res* **31**, 3381-3385
225. Guex, N., and Peitsch, M. C. (1997) *Electrophoresis* **18**, 2714-2723
226. Peitsch, M. C., Wells, T. N., Stampf, D. R., and Sussman, J. L. (1995) *Trends Biochem Sci* **20**, 82-84
227. Altschul, S. F., Madden, T. L., Schaffer, A. A., Zhang, J., Zhang, Z., Miller, W., and Lipman, D. J. (1997) *Nucleic Acids Res* **25**, 3389-3402
228. Gupta, A., Matsui, K., Lo, J. F., and Silver, S. (1999) *Nat Med* **5**, 183-188
229. Franke, S., Grass, G., and Nies, D. H. (2001) *Microbiology* **147**, 965-972
230. Franke, S., Grass, G., Rensing, C., and Nies, D. H. (2003) *J Bacteriol* **185**, 3804-3812
231. Outten, F. W., Huffman, D. L., Hale, J. A., and O'Halloran, T. V. (2001) *J Biol Chem* **276**, 30670-30677
232. Liesegang, H., Lemke, K., Siddiqui, R. A., and Schlegel, H. G. (1993) *J Bacteriol* **175**, 767-778

233. Leedjarv, A., Ivask, A., and Virta, M. (2008) *J Bacteriol* **190**, 2680-2689
234. Ma, D., Cook, D. N., Hearst, J. E., and Nikaido, H. (1994) *Trends Microbiol* **2**, 489-493
235. Damier-Piolle, L., Magnet, S., Bremont, S., Lambert, T., and Courvalin, P. (2008) *Antimicrob Agents Chemother* **52**, 557-562
236. Nishino, K., Nikaido, E., and Yamaguchi, A. (2007) *J Bacteriol* **189**, 9066-9075
237. Kieboom, J., and de Bont, J. (2001) *Microbiology* **147**, 43-51
238. Poole, K., Gotoh, N., Tsujimoto, H., Zhao, Q., Wada, A., Yamasaki, T., Neshat, S., Yamagishi, J., Li, X. Z., and Nishino, T. (1996) *Mol Microbiol* **21**, 713-724
239. Poole, K., Krebes, K., McNally, C., and Neshat, S. (1993) *J Bacteriol* **175**, 7363-7372
240. Kohler, T., Michea-Hamzehpour, M., Henze, U., Gotoh, N., Curty, L. K., and Pechere, J. C. (1997) *Mol Microbiol* **23**, 345-354
241. Rosenberg, E. Y., Ma, D., and Nikaido, H. (2000) *J Bacteriol* **182**, 1754-1756
242. Nishino, K., and Yamaguchi, A. (2001) *J Bacteriol* **183**, 5803-5812
243. Aires, J. R., Kohler, T., Nikaido, H., and Plesiat, P. (1999) *Antimicrob Agents Chemother* **43**, 2624-2628
244. Mine, T., Morita, Y., Kataoka, A., Mizushima, T., and Tsuchiya, T. (1999) *Antimicrob Agents Chemother* **43**, 415-417
245. Westbrock-Wadman, S., Sherman, D. R., Hickey, M. J., Coulter, S. N., Zhu, Y. Q., Warrener, P., Nguyen, L. Y., Shawar, R. M., Folger, K. R., and Stover, C. K. (1999) *Antimicrob Agents Chemother* **43**, 2975-2983
246. Moore, R. A., DeShazer, D., Reckseidler, S., Weissman, A., and Woods, D. E. (1999) *Antimicrob Agents Chemother* **43**, 465-470
247. Hearn, E. M., Gray, M. R., and Foght, J. M. (2006) *J Bacteriol* **188**, 115-123
248. Kieboom, J., Dennis, J. J., de Bont, J. A., and Zylstra, G. J. (1998) *J Biol Chem* **273**, 85-91
249. Rojas, A., Duque, E., Mosqueda, G., Golden, G., Hurtado, A., Ramos, J. L., and Segura, A. (2001) *J Bacteriol* **183**, 3967-3973
250. Brooks, B. E., Piro, K. M., and Brennan, R. G. (2007) *J Am Chem Soc* **129**, 8389-8395
251. Zhou, Y., Morais-Cabral, J. H., Kaufman, A., and MacKinnon, R. (2001) *Nature* **414**, 43-48
252. Dutzler, R., Campbell, E. B., and MacKinnon, R. (2003) *Science* **300**, 108-112
253. Derewenda, Z. S. (2004) *Structure (Camb)* **12**, 529-535
254. Ren, G., Cheng, A., Melnyk, P., and Mitra, A. K. (2000) *J Struct Biol* **130**, 45-53
255. Ren, G., Cheng, A., Reddy, V., Melnyk, P., and Mitra, A. K. (2000) *J Mol Biol* **301**, 369-387
256. Mosser, G. (2001) *Micron* **32**, 517-540
257. Crowther, R. A., Henderson, R., and Smith, J. M. (1996) *J Struct Biol* **116**, 9-16
258. Hyun, J. K., Coulibaly, F., Turner, A. P., Baker, E. N., Mercer, A. A., and Mitra, A. K. (2007) *J Virol* **81**, 11075-11083

Publications

Seeger MA, Schiefner A, Eicher T, Verrey F, Diederichs K, Pos KM (2006) Structural asymmetry of AcrB trimer suggests a peristaltic pump mechanism. *Science* **313**(5791)**:** 1295-1298

Seeger MA, von Ballmoos C, Eicher T, Brandstatter L, Verrey F, Diederichs K, Pos KM (2008b) Engineered disulfide bonds support the functional rotation mechanism of multidrug efflux pump AcrB. *Nat Struct Mol Biol* **15**(2)**:** 199-205

Seeger MA, Diederichs K, Eicher T, Brandstatter L, Schiefner A, Verrey F, Pos KM (2008a) The AcrB efflux pump: conformational cycling and peristalsis lead to multidrug resistance. *Curr Drug Targets* **9**(9)**:** 729-749

Eicher T, Brandstatter L, Pos KM (2009) Structural and functional aspects of the multidrug efflux pump AcrB. *Biol Chem*

10. Acknowledgements

To complete this thesis, I would like to acknowledge the people that contributed to the success of this project either directly, indirectly or even involuntarily.

Firstly, I would like to express my thanks to Martin, my boss and supervisor who gave me the opportunity to work on this exciting project. I highly appreciated the scientific talks, our semi-scientific meetings and the truly unscientific conversations we had in- and outside of the laboratory. Even in hard times (severe time constraints, competition from over the ocean or over the hallway etc.) you held your spirits high and were a reliable source for good advice and lend a sympathetic ear for our problems.

Special thanks goes to my doctor father François, who gave valuable advice and feedback during lab-meetings, provided our subgroup with the infrastructure and gave us a lot of freedom in pursuing our aims. Although our little subgroup was dealing with organisms lacking kidneys, a digestive tract or any decent kind of proximal or distal tubules, I always felt part of this really integrative group.

Raimund Dutzler for accompanying me during my PhD thesis as the external expert of my thesis committee. Your critical questions and helpful advice in the tough business of crystallography was highly appreciated.

Kay Diederichs from the University of Konstanz for his indispensable help with words and deeds in the unbiological process of crystallographic data processing and his readiness to write an expertise for this work.

Our collaborators from the Department of Biochemistry, Markus Grütter, Gabi Sennhauser and Patrick Amstutz. Our beloved AcrB wouldn’t have disrobed so much without the help of the nifty DARPin molecules.

Alok Mitra and the people of his lab in Auckland, New Zealand. Especially Jae Hyun, who spent a vast amount of time and effort with explaining me the secrets of 2D crystallography during and after my stay at the University of Auckland. At this point I

would also like to thank the Boehringer-Ingelheim fonds who generously supported my stay in New Zealand.

And of course all the J-floor people who were always cooperative and created such a pleasant atmosphere inexorably spreading from the coffee corner into each lab and office.
My closest combatant Lorenz. I really enjoyed working with you; in the end, I had the feeling that we were completely synchronized, culminating in the fact that I even didn't have to remove my earplugs while talking to you, isn't that great? May your experiments flourish and spread the glory of AcrB all around the world or even into space (if you finally decide to become an astronaut).
My former collaborator Markus, whose enthusiasm for proteins, poisonous chemicals and bad music is legendary. I wish you all the best in your future scientific endeavors.
Beni who was the place to go for all biological, chemical, physical, mathematical, experimental and other questions and never missed a meal at mensa. Thank you very much for your constant professional advice and input!
Simone who keeps on contributing so much to the lively atmosphere on the J-floor. I will hear the ringing of your bell and smell the scent of pão de queijo till the end of time...
Dustin, one of the very pleasant inmates of our office. Thank you for sharing breaking news of any kind with me and for giving valuable advice concerning administrative proceedings and stumbling blocks.
Nadine and Brigitte for supplying me with nutrition and for keeping my blood glucose level at a constant high level; Vicky for her valuable scientific and linguistic input; Toni for giving me a brush-up in *E. coli* stochastics; and all the other people who are not mentioned individually.

My friends outside the lab, who distracted me from recalcitrant mutant proteins and from the global threat of antibiotic resistance.

My parents and family, who always backed and encouraged me during my long education and scientific career.

And of course Viola for supporting me during all these years so passionately and wholeheartedly. Thank you so much!